THE UNIVERSITY
of LIVERPOOL

CHROMATIC IDENTIFICATION OF INCIPIENT TRANSFORMER FAILURES DUE TO PARTIAL DISCHARGES

Thesis submitted in accordance with the requirements of
the University of Liverpool for the degree of Doctor in Philosophy by

Jinghua Zhang

October 2003

Dedicated to: My Love

My Beloved Family

My Teachers & Friends

Abstract

The thesis describes research into the application of chromatic tristimulus processing for four purposes (dissolved gas analysis (DGA), temperature, acoustic and electrical/radio frequency (RF) signals analyses) in relation to electric power transformer partial-discharge (PD) failure prognosis, as well as PD detection, location, classification and characterisation.

Chromatic application of PD failure prognosis has originality. For each purpose, different chromatic signatures have been observed leading to the possibility of chromatically fingerprinting a transformer and identifying the extent of PD activity.

Chromatic DGA signatures have been established using results from 50 transformer tanks. Three categories of transformer working conditions (safe, alert and faulty) have been classified from the DGA database. As one of the project objectives, an original method for calculating the probability of transformer failure based on DGA signatures has been achieved. Such quantification can provide a cost-effective and practice-efficient online monitoring package. The sensitivity of chromatic maps has been investigated on one transformer by using temperature factors. Chromatic electrical/RF PD signatures have been derived from a number of results obtained during two sets of site tests. As a second project objective, the chromatic numerical classification of PD pulses identified in electrical/RF signals indicates the possibility of differentiating various PD sources within a transformer (air corona, PD inside the tank but outside the windings and PD inside the windings). Acoustic chromatic signatures have been derived from a more limited number of results obtained during one set of site tests. An innovative chromatic approach for combining the signals from three acoustic transducers has been developed theoretically and implemented practically. It has not only provided a constructive means to further compress the acoustic information but also explored the extent of the chromatic methodology.

Acknowledgements

Contents

List of Figures

List of Tables

Glossary

AC	alternating current
BSI	British Standards Institution
CIE	Commission Internationale de l'Eclairage (International Commission on Illumination)
CIMS	the Centre for Intelligent Monitoring Systems
CT	current transformer
CRT	cathode ray tube
DC	direct current
DGA	dissolved gas analysis
FFT	fast Fourier transform
GIS	gas insulated substations
GLHS	generalised lightness, hue and saturation
HLS	hue-lightness-saturation
HV	high voltage
IEC	International Electrotechnical Commission
NGC	National Grid Company
NGT	National Grid Transco
pC	pico Coulomb
PD	partial discharge
p.d.f.	probability density function
RF	radio frequency
RFCT	radio frequency current transformer
RMS	root-mean-square
SF_6	sulphur hexafluoride gas
TTD	three-transducer detector
UHF	ultra high frequency
UMIST	University of Manchester Institute of Science and Technology

Chapter 1

Introduction

This introductive chapter commences with a description of background knowledge relating to power system structures, transformers in power systems, types of power transformers, oil-immersed power transformers, transformer faults of various kinds, partial discharges (PD) and their impacts etc. This is followed by a discussion of current research about transformer PD failure worldwide, and the objectives and benefits of this project. Finally there is an outline of the thesis contents.

1.1 Background Knowledge

1.1.1 Transformers in Power Systems

In electric power systems the power-generation equipment is usually located at some distance from the points of consumption of the power **[Miller, 1970]** for economic, environmental and reliability reasons **[Allan, 1994; Erinmez et al., 1994]**. Electrical power is transferred from generation to load by means of transmission and distribution lines **[McPherson et al., 1990]**. Consequently a power system consists of networks of generation, transmission and distribution with each part having its most suitable voltages **[Elgerd, 1977, Fitzgerald, et al., 2003]**.

In a generation system, normally generators generate electricity at voltages in the region of 11kV~25kV **[Erinmez et al., 1994; Tyler, 1997; Weedy et al., 1998]**. If this level of voltage were directly used for transmission, the energy wasted would be high. It is because that for a fixed power $P = VI$ to be transmitted, the lower the voltage V, the greater the current I. Thus the losses during transmission, mainly ohmic losses in the form of heat power ($P_\Omega = I^2R$) **[Miller, 1970; Elgerd, 1977; Rolls, 1982]** would be higher (R, transmission line resistance). In order to reduce losses of power during transmission, the voltage from the generator is then increased in magnitude to an efficient transmission voltage **[Weedy et al., 1998]**.

The transmission voltages are 220kV and above with other standard voltages of 275kV, 330kV, 400kV, 500kV and 765kV **[Weedy et al., 1998]**. In the UK, 400kV is in the main voltage with 275kV also used **[Tyler, 1997]** in large conurbations (e.g. London, Manchester etc.) **[Erinmez et al., 1994]**. These high voltages are decreased in level in step with the power supplied via the distribution system, since consumer equipment is operated with low voltages (typically, factories several kV, residences 240V).

The distribution system is built in a layered structure, with the primary distribution layer usually operated at 132kV and other standard distribution voltages at 66kV, 33kV (towns or section of cities); 11kV, 6.6kV, 3.3 kV (actual load centres, housing estates, office blocks or factories) and 240/110V at the customer terminals **[Erinmez et al., 1994; Tyler, 1997; Weedy et al., 1998]**. The main differences between a transmission line and a distribution line are the voltage levels and power-handling capabilities **[Miller, 1970]**.

This linking of generation, transmission and distribution systems at different voltages has relied upon a simple, convenient and reliable device **[White, 1994]** - the power transformer. A transformer is a device that transfers energy from one AC system to another **[BSI, 1970; McPherson et al., 1990; Fitzgerald, et al., 2003]**. It can accept electrical energy at one voltage and deliver it at another voltage, permitting electrical energy to be generated at relatively low voltages, transmitted at high voltages and to be used at safer voltages. In other words, connecting a step-up transformer between the generator and a transmission line, as the power transformer steps up the voltage, it

reduces the current proportionately thus reducing line losses and making long-distance transmission possible. Step-down transformers connected between the transmission line and the various electrical loads forming a distribution structure permit the transmitted power to be used by customers at various safe voltages **[Richardson, 1978]**.

In the words of White:

> The tremendous development and progress in the transmission and distribution of electrical energy during the past 100 years may not have been possible but for the capability of linking the generator, the transmission line, the secondary distribution system and a great variety of loads, each part operating at its most suitable voltage **[White, 1994]**.

Thus the extensive power systems existing today could not have been developed without power transformers **[Allan, 1991]**.

1.1.2   Oil-immersed Transformers

Power transformer designs involve oil-immersed, air-cooled "dry-type" and gas-filled types **[Flux, 1993]**. For high voltage applications, oil-immersed designs are generally preferred **[Ashton et al., 1981]** and most power transformers are immersed in a tank of oil unlike "dry-type" transformers operating in air, since oil is a better insulator than air **[Naidu et al., 1995]**. On the other hand, the paper and pressboard insulation employed in transformers when dried and impregnated with oil, often under vacuum, is capable of withstanding high stresses and provides an extremely reliable insulation at low cost **[Ashton et al., 1981]**. This is the important advantage when compared to gas-filled transformers, which use electronegative sulphur hexafluoride gas (SF_6) at a pressure of about 1 atm to eliminate fire risk and requiring complicated force-cooled heat exchangers **[Flux, 1993]** and high cost **[Naidu et al., 1995]**.

Thus the transformer oil is encapsulated by a tank with other principal features (e.g. core, windings etc. **[BSI, 1970; Flux, 1993]**) of the transformer as well. With such a design, the transformer oil is also used as a heat transfer medium for the cooling system **[Richardson, 1978]** (to remove the heat generated in the transformer windings and core due to the passage of electric current), by oil circulation **[White, 1994]**.

1.1.3 Partial Discharges within Transformers and the Impact

However, failure of a transformer, no matter how reliable, especially after a long period usage, may ultimately be unavoidable **[Davies, 1984]**. This includes faults within the transformer tank, faults on transformer connections, overheating, faults external to the transformer zone and so on **[Rushton et al., 1981; Davies, 1984]**. The most severe faults are caused by partial discharges (PD), which occur within the transformer and may lead to insulation breakdown and catastrophic failure. This is because a PD is a discharge **[Haydon, 1964]**, which only partially bridges the insulation between conductors **[BSI, 1999]**. It may occur inside the insulation or adjacent to a conductor.

Generally there are three types of partial discharges **[Kreuger, 1992]**:
1) Internal discharges, including those in electrical treeing **[Pearmain et al., 1993; Naidu et al., 1995]**;
2) Surface discharges;
3) Corona discharges.

All are accompanied by chemical breakdown products, light/heat from excited molecules, radio frequency (RF) emissions and acoustic pressure waves **[Pearson et al., 1995]**.

The impact of such failures may be substantial both in safety and financial terms **[NGT, 2000]**. This is because utility personnel working in substations are often exposed to dangerous environments and may be required unknowingly to work in the vicinity of suspect equipment. For a utility, large power transformers are major capital items with each one costing up to £2 M and construction lead times up to 18 months **[Lapworth, 1994]**. When problems occur they are often difficult to diagnose and expensive to correct. For example, handling the oil alone from a transformer to allow an internal inspection, which very often can be inconclusive, can cost over £100,000 for a large transformer **[Lapworth, 1994]**.

1.2   Current Researches

A significant proportion of the power transformers used currently in the UK were installed during the 1950s and 1960s **[Domun, 1990]**. For such transformers with long period usage, failure is unavoidable as indicated above. Naylor expressed that:

> The analysis of faults in machine and transformer windings presents particular difficulty in that the effective impedances of the affected windings under internal fault conditions are not normally known. The methods of analysis which may be employed are, therefore, severely limited and are usually concerned with obtaining a reasonable estimate based on certain simplifying assumptions **[Naylor, 1981]**.

However, since the PD has many effects, as mentioned above (physical, chemical and electrical), in principle any of these effects could be used to detect the presence of the discharges. For many years, researches have been performed in these fields.

Since all faults within the transformer tank give rise to the generation of gas, which may be slow for minor or incipient faults or violent in the case of heavy faults **[Rushton et al., 1981]**, the generation of gas may be used as a means of fault detection. Transformer oil dissolved gas analysis (DGA) has been considered as an important indication for PD production and development **[Glass, 1977; Kelly, 1980; Oommen et al. 1982; Cardwell, 1989; Domun, 1990]**. With the evolution of applications, new techniques such as fuzzy logic, neural networks etc. attempts have been made to improve DGA in recent years **[Cao et al., 1993; Su et al., 2000; Guardado et al., 2001; Yang et al., 2001; Ahmad et al., 2002]**. Good progress has been made and encouraging results obtained.

Due to the large size of a transformer tank, the temperature rise produced by a PD within the tank would only be small. Thus at present, temperature parameters have not been taken into account for PD investigations. However detection of light is applicable to external discharges. An effective method is photography **[Kreuger, 1992]**.

Regarding radio frequency emissions, signal acquisition using RF, especially ultra high frequency (UHF), has been proved successfully in related areas such as gas insulated

substations (GIS) **[Hampton et al., 1988; Bargigia et al., 1992; Pearson et al., 1995]** and this area **[Kemp, 1995; Rutgers et al., 1997; Judd et al., 2000; Russwurm, 2000]**. Researches of PD classification and pattern recognition using neural network **[Hamilton et al., 1997]** and wavelet **[Weiss, 1994; Ma et al., 2002a; Ma et al., 2002b]** etc. techniques have been undertaken.

It is commonly believed **[Ogihara, 1964; Lundgaard, 1992a; Bozzo et al. 1995]** that PD acoustics detection is a suitable method for locating the PD source, since compared to UHF emissions, acoustic waves have lower frequency, longer wavelength and lower propagation speed, resulting in less attenuation when the signal passes through the tank wall. This makes detection possible outside the tank yielding less onerous equipment demands. Thus the use of acoustic transducers to detect sound waves from the discharge has been widely demonstrated **[Lundgaard, 1992b; Eleftherion, 1995; Bengtsson et al., 1997]**.

In the recent years the National Grid Company (NGC, merged as National Grid Transco, NGT, from November 2002) as well as other organisations has sought with the above advanced technology in signal acquisition and processing, to develop devices to detect, classify, locate and characterise PD **[NGT, 2000]**.

1.3   Project Objectives and Benefits

Thus as a NGT sponsored project, this project was to develop a methodology to give a direct indication of incipient failure and expected failure mode to avoid unnecessary damage and to minimize impact both in safety and finance **[NGT, 2000]**. This is the objective of the NGT PD project, which aligns with the drive to evolve transformer failure prognosis.

The problem is to combine various data sets (dissolved gases, temperature, RF and acoustic signals), which will be monitored on a transformer, to yield an overall degradation signature for the transformer. The approach to achieve this will utilize novel chromatic processing techniques, which will identify trends to failure at an early

stage via loci of points on a chromatic map and classify PD patterns via the layout of points on the map. Early diagnosis of such events can lead to the prognosis of transformer failure with a consequent significant economic gain.

The benefits of the investigations are self-evident. On the one hand in terms of safety, changes in PD activity, which may signify an imminent problem if easily and instantly detectable, could be the best early warning of personnel safety and equipment condition.

On the other hand in terms of finance, for example, a 750MVA unit, which showed PD through DGA; the inability to return to service quickly meant loss of availability and constraint costs in excess of £1 M **[NGT, 2000]**. There were several examples where a defect was only confirmed through back energisation, a costly and time consuming process, to detect and locate the PD. If an early identification of PD was possible those costs could be avoided.

1.4   Outline of Thesis

This thesis has been organised into seven chapters. The next chapter, **Chapter 2** Chromatic Methodology, provides a theoretical introduction to this relatively new technique. **Chapter 3** Review of Transformer PD Diagnosis Methods, starting with physical and chemical characteristics of PD, includes almost all the possible categories of the transformer diagnosis methods being utilized currently worldwide. Site-test results from each of the reviewed categories of methods (DGA, temperature, electrical/RF and acoustic signal analysis) have been investigated in the subsequent chapters using the chromatic methodology. Therefore the **subsequent three chapters** describe the results from site tests, analysis of results and discussion of results. The final chapter, **Chapter 7** Conclusions and Further Work, summarises the work that has been undertaken to date and the research outcomes. It also suggests some further development work.

Chapter 2

Chromatic Methodology

2.1 Introduction

In signal processing, one purpose is to attempt to identify general signals in terms of some fundamental signal properties. Such useful properties include signal energy content (E_f), average frequency (ω_c) and RMS bandwidth (B). They can be defined respectively as follows [Weiss, 1994].

$$E_f = \int_{-\infty}^{\infty} |f(t)|^2 \, dt = \frac{1}{2\pi} \int_{-\infty}^{\infty} |F(\omega)|^2 \, d\omega \qquad (2.1)$$

$$\omega_c = \frac{\int_{-\infty}^{\infty} \omega |F(\omega)|^2 \, d\omega}{E_f} \qquad (2.2)$$

$$B^2 = \frac{1}{E_f} \int_{-\infty}^{\infty} (\omega - \omega_c)^2 |F(\omega)|^2 \, d\omega \qquad (2.3)$$

where

$F(\omega)$ is the Fourier transform [Papoulis et al., 2002] of $f(t)$.

ω is the frequency and t is the time.

The same requirements apply in system monitoring applications. With signals detected or data sampled from a monitoring system, signal processing or data analysis needs to be performed for information extraction. These are signal identification, classification and characterisation etc. Due to the complexity of the signals/data measured online, the direct information, which may be obtained is often limited. An advanced and tested technique is needed for information extracting purpose. In this chapter, one such technique, the chromatic methodology, is introduced and its application for continuous signal processing and discrete data analysis considered.

2.2   Chromatic Methodology Generality

The chromatic method was initially derived from photic field concepts by Moon and Spencer **[Moon et al., 1981]**. Further evolution of the chromatic methodology has been advanced in parallel to and arguably separately from other signal processing techniques **[Weiss, 1994]**. With numerous examples of generically different practical implementations of the chromatic methodology for a range of different monitoring situations already examined, it is appropriate that the deployment of the chromatic methodology for even further monitoring be more widely explored **[Jones et al., 2000; Brazier et al., 2001]**. Thus such an innovative methodology has been applied as the main processing technique for this transformer PD failure prognosis project. Consequently it is useful to have some knowledge of the chromatic methodology.

2.2.1   The Gabor Transform Based Chromaticity Theory

The chromatic methodology provides a means of signal recognition for system monitoring applications in terms of parameters which are analogues to those defined by Equations (2.1) ~ (2.3) **[Jones et al., 2000]**.

It is known that an arbitrary signal can be represented in terms of a set of Gaussian signals **[Gabor, 1946; Weiss, 1994; Stergioulas, 1997]**. This stable expansion is called the Gabor transform of the signal.

Assuming a real signal $u(t)$, the corresponding normalized analytic signal is defined by **[Stergioulas et al., 1998]**

$$s(t) = u(t) + j \cdot v(t) \qquad (2.4)$$

Considering Gaussian signals

$$r(t; A, \rho) = (2\rho)^{1/4} e^{[-\pi\rho t^2 + 2\pi^{1/2}(\rho A_R + jA_I)t - \rho A_R^2 - jA_R A_I]} \qquad (2.5)$$

Where t is the time, $A = A_R + jA_I$ defines the average location of the signal in the time-frequency plane ($\langle t \rangle = \pi^{-1/2} A_R$, $\langle f \rangle = \pi^{-1/2} A_I$) and ρ defines the width of the Gaussian in time $\Delta t = (4\pi\rho)^{-1/2}$ and frequency $\Delta f = (4\pi\rho^{-1})^{-1/2}$ (Figure 2.1).
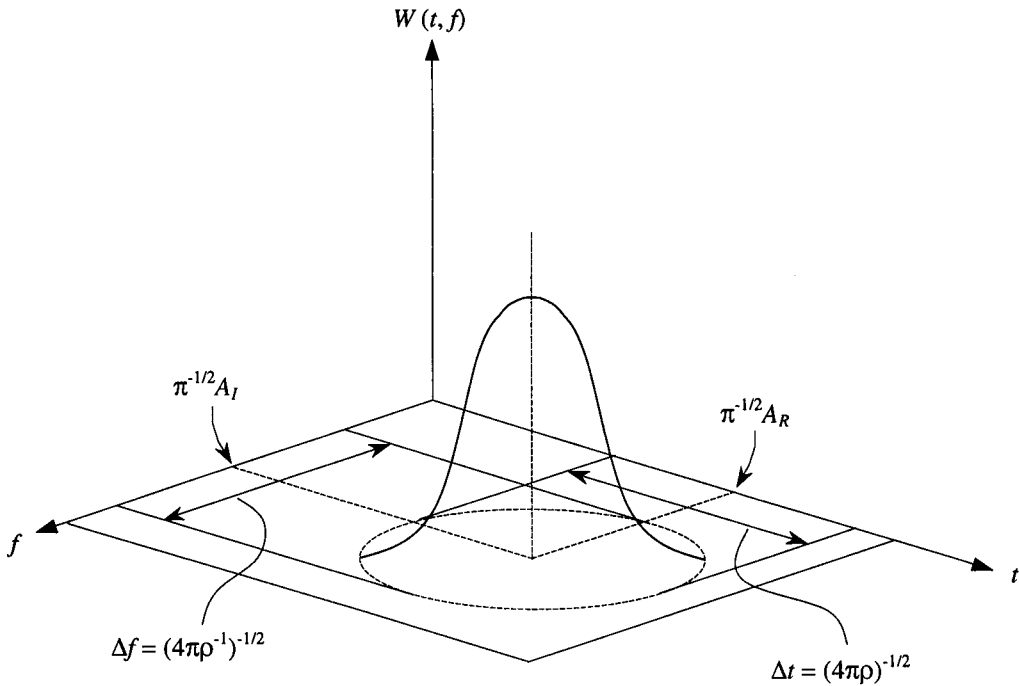
Figure 2.1 A Gaussian signal in time-frequency space
[Jones et al., 2000]

It can be proved that **[Stergioulas, 1997; Stergioulas et al., 2000]**

$$s(t) = \iint \frac{1}{\pi} S(A, \rho) \cdot r(t; A, \rho) d^2 A \qquad (2.6)$$

where

$$S(A,\rho) = \int_{-\infty}^{\infty} r^*(\tau; A, \rho) \cdot s(\tau) d\tau \qquad (2.7)$$

The asterisk indicates the complex conjugate and $S(A, \rho)$ are the coefficients in the expansion.

Thus any signal $s(t)$ can be expanded exactly in terms of an infinite number of Gaussian components (the Gabor expansion), but for practical applications it is advantageous to use only a finite number of Gaussian components **[Jones et al., 2000]**. That is for the time-frequency complex plane A to take only values in an $M \times N$ lattice, which is known as a von Neumann lattice **[von Neumann, 1955; Russell et al., 1998]**.

$$A = m\alpha_1 + jn\alpha_2 \qquad (2.8)$$

where

$m = 1, ..., M;\ n = 1, ..., N;\ \alpha_1$ and α_2 are the lattice constants.

Therefore the reconstructed signal is given approximately by

$$s_{rec}(t) = \sum_{m,n} \frac{1}{\pi} S_{mn}(\rho) \cdot r(t; m\alpha_1 + jn\alpha_2, \rho) \approx s(t) \qquad (2.9)$$

where

$$S_{mn}(\rho) = \int_{-\infty}^{+\infty} r^*(\tau; m\alpha_1 + jn\alpha_2, \rho) \cdot s(\tau) d\tau \qquad (2.10)$$

are the Gabor coefficients.

This compresses data in the time and frequency domains without loss of significant information **[Stergioulas, 1997; Stergioulas et al., 2000]** even if M and N take a small number of integer values. Thus information contained within a time-varying signal can be approximated by a limited number (e.g. $N = 2, 3, 6$ or 16) of Gaussians located on the frequency axis ($M = 1$) **[Jones et al., 2000]**. The optimum number of Gaussians (N) will depend upon the accuracy of signal representation required. If a large number of Gaussians terms were used, they would overlap significantly – mathematically this is

the over-completeness of the Gaussian basis. This allows a further reduction in the value of N without a corresponding proportional loss in the information contained in the signal. This non-orthogonality of the terms represents a significant and important advantage of the Gabor expansion over the Fourier series insofar as the sinusoidal basis used in the Fourier series is orthogonal and complete **[Kufner et al., 1971; Tolstov, 1976]**.

It has been shown **[Jones et al., 2000]** that with a distimulus system ($N = 2$), a broad indication of the overall signal profile can be obtained; a tristimulus system ($N = 3$) provides in addition a reasonable approximation to some of the finer details of the signal; a $N = 6$ system produces a good signal replica (better than 95% signal reproducibility) whilst $N = 16$ gives little improvement over the $N = 6$ case. Therefore, a tristimulus system gives an acceptable performance for many applications and is consistent with the usefulness of colour vision.

Such a tristimulus system may be considered as quantifying complex optical spectra by using three photo-detectors to define the chromaticities **[Jones et al., 1994]**. If the spectrum is denoted by $s(\lambda)$ and the response of the detectors $H(\lambda)$, where λ is the optical wavelength; then the output currents from each of the three optical detectors take the form **[Jones et al., 2000]**

$$I_n = \int s(\lambda) H_n(\lambda) d\lambda \qquad (2.11)$$

where

$$n = 1, 2 \text{ and } 3$$

When these correspond to the responsivities of the human vision system the signal is manifested as colour, e.g. red (R) (with the longest wavelength, i.e. lowest frequency), green (G) and blue (B).

2.2.2 Practical Chromatic Signal Processing

In order to describe complex signals in a simple perspicuous form, the procedures evolved by the colour science community may be adopted. Via a number of algorithms,

the chromatic detector outputs can be made to form two dimensional chromaticity maps with intensity as a third dimension. A number of colour models (also colour solids, colour spaces **[Munsell, 1946; Birren et al., 1969]**) have been considered, such as *xy* (sometimes named as *xyY* or *Lxy*) chromaticity from the Commission Internationale de l'Eclairage (CIE, International Commission on Illumination) XYZ **[CIE, 1932; Judd, 1933]**, CIE LAB (or Lab, L*a*b* recommended in 1976) **[Wyszecki et al., 1982; Schwarz et al., 1987]** and the generalised lightness, hue and saturation (GLHS) colour models that are most commonly used in computer graphics **[Levkowitz et al., 1993]** etc.

Of these models the most well known, and useful for subjective colour mixing evaluations is the CIE *xy* horseshoe locus diagram (Figure 2.2) **[CIE, 1932; Wyszecki et al., 1967]**.

2.2.2.1 CIE *xy* Chromaticity

As mentioned above, the *xy* chromaticity is evolved from XYZ chromaticity. The three coordinate parameters x, y, and z are defined by calculating the fractional components of the tristimulus values.

$$x = \frac{I_1}{I_1 + I_2 + I_3} \qquad y = \frac{I_2}{I_1 + I_2 + I_3} \qquad z = \frac{I_3}{I_1 + I_2 + I_3}$$

(2.12)

Equation (2.12) shows that the three parameters x, y and z are normalized by the sum of intensities $(I_1 + I_2 + I_3)$ received by the three detectors, which are called the normalized colour coordinates. It is obvious that:

$$x + y + z = 1$$

(2.13)

Therefore, it is apparent that only two of the chromaticity coordinates are required, and the third coordinate can be calculated using Equation (2.13).

$$x = \frac{I_1}{\sum\limits_{m=1}^{3} I_m} \qquad\qquad y = \frac{I_2}{\sum\limits_{m=1}^{3} I_m}$$

(2.14)

The chromaticity diagram can be produced using the normalized colour coordinates of x and y as shown in Figure 2.2, within which chromaticities of all possible colours viewed by the three detectors exist. The colour values governed by the coordinates of x and y produce a horseshoe shaped colour locus, in which each point corresponds to a particular wavelength of a visible spectrum.
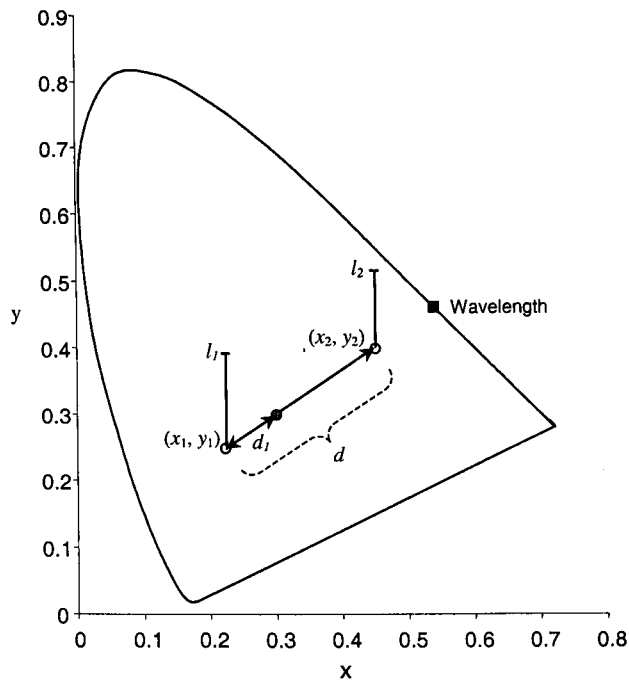
Figure 2.2 CIE xy chromaticity diagram
[CIE, 1932; Wyszecki et al., 1967; Jones et al., 2000]

The significance of the two-dimensional mapping described above is that it allows complex signals to be represented as a single point in two-dimensional space. As a result the relationship between two signals is easily visualized and the complex signals can be conveniently determined. For instance the signal obtained by superimposing two signals (x_1, y_1) and (x_2, y_2) of strengths I_1 and I_2 respectively and separated on a

chromatic map by a distance *d* (Figure 2.2) is located at a point governed by the moment equation.

$$l_1 d_1 = l_2 (d - d_1)$$

(2.15)

However, the non-uniform distribution **[Foley et al., 1995]** of colour along the spectral locus appears to be one of the major disadvantages of the CIE *xy* colour mapping system. Therefore, alternative systems that use extensions of *xy* was introduced by the CIE, which stretch the chromaticity diagram to provide a more uniform mapping that can be seen in Luv (or CIE-UCS for uniform chromaticity scale) and Lu'v' **[Wyszecki et al., 1982]**. Although these representations provide improvements, problems relating to the extraction of dominant wavelength and saturation can still be seen in this representation. The new concept of colour mapping named CIE LAB, which was introduced by the CIE in 1976, provides a uniform space for colour mapping but with a global visualisation in 3D space **[Hill et al., 1997]**.

2.2.2.2 GLHS Model

For signal processing applications, the hue-lightness-saturation (HLS) system, which belongs to the colour models that are most commonly used in computer graphics, provides a particularly useful bridge between colour concepts and spectral signal forms **[Jones et al., 2000]**. The computer graphics colour models includes the RGB model and the lightness-hue-saturation (LHS) family of models.

The RGB model is used in CRT colour monitor modelling **[Schwarz et al., 1987]**. A major disadvantage of this concept is that the information relating to hue, saturation and brightness of the colour cannot be traced directly. Also, as the RGB colour space lies within the human perceptual space, it represents fewer colours than those, which can be seen. Fortunately, alternative colour concepts can be used to transform the colour representations on a RGB cube **[Smith, 1978; Deng, 2000]** into more satisfactory colour representations as discussed in the following.

The LHS family is considered to be better suited for human interaction. In the LHS family of models, there are HSV (V for value; also called HSB with B for brightness) hexcone [Smith, 1978; Foley et al., 1995], HSL triangle [Smith, 1978], LHS triangle [Levkowitz et al., 1993] and HLS double hexcone [Foley et al., 1995] etc. colour spaces, which all are special cases of the generalized lightness, hue and saturation (GLHS) colour model [Levkowitz et al., 1993].

The generalisation uses piecewise planar constant lightness surfaces with three non-negative weights w_{min}, w_{mid} and w_{max} defined. Such that

$$w_{max} > 0 \qquad (2.16)$$

$$w_{min} + w_{mid} + w_{max} = 1 \qquad (2.17)$$

The lightness function is defined as

$$l(c) = w_{min} \cdot \min(c) + w_{mid} \cdot mid(c) + w_{max} \cdot \max(c) \qquad (2.18)$$

where

$$\begin{aligned}
c &= (R, G, B) \\
\min(c) &= MINIMUM\{R, G, B\} \\
mid(c) &= MID\_VALUE\{R, G, B\} \\
\max(c) &= MAXIMUM\{R, G, B\}
\end{aligned} \qquad (2.19)$$

The hue $h(c)$ ($0 \le h(c) < 360$) of a chromatic colour is defined as

$$h(c) = 60 \cdot (k(c) + f(c)) \qquad (2.20)$$

where $k(c)$ is the number of the sector defined by the order of the magnitudes of the R, G and B values,

$$k(c) = \begin{cases} 0, & if \quad R > G \geq B; \\ 1, & if \quad G \geq R > B; \\ 2, & if \quad G > B \geq R; \\ 3, & if \quad B \geq G > R; \\ 4, & if \quad B > R \geq G; \\ 5, & if \quad R \geq B > G. \end{cases} \tag{2.21}$$

and the hue faction $f(c) \in [0, 1)$, is calculated as follows:

$$f(c) = \begin{cases} \dfrac{mid(c) - \min(c)}{\max(c) - \min(c)}, & if \quad k(c) \quad is \quad even, \\[4mm] \dfrac{\max(c) - mid(c)}{\max(c) - \min(c)}, & if \quad k(c) \quad is \quad odd. \end{cases} \tag{2.22}$$

The saturation $s(c)$ of a chromatic colour is defined as

$$s(c) = \begin{cases} \dfrac{l(c) - \min(c)}{l(c)}, & if \quad l(c) \leq l(q(c)), \\[4mm] \dfrac{\max(c) - l(c)}{M - l(c)}, & if \quad l(c) > l(q(c)). \end{cases} \tag{2.23}$$

where

$$l(q(c)) = w_{mid} \frac{mid(c) - \min(c)}{\max(c) - \min(c)} M + w_{max} M \tag{2.24}$$

and M is a maximum coordinate attached to white colour.

For an achromatic colour with $\max(c) = \min(c)$, the hue, lightness and saturation can be defined as

$$\begin{aligned} l(c) &= \max(c) \\ h(c) &= undefined, \quad (e.g.-1) \\ s(c) &= 0 \end{aligned} \tag{2.25}$$

Different values of w_{min}, w_{mid} and w_{max} derive different LHS colour models. Thus the essential choice in selecting a particular model within the LHS family of models is made in the definition of the lightness function, which in turn determines the constant-lightness surfaces and hence the shape of the colour solid that represents the model (triangle, hexcone or double hexcone etc.). The values of the weights for the three example models are given in Table 2.1. Considering the three detectors' outputs R, G and B (Section 2.2.1, Page 12), for different LHS colour models the lightness function definitions are summarized in Table 2.2.

Table 2.1 Values of the three weights for various LHS colour models

GLHS colour model	w_{min}	w_{mid}	w_{max}
LHS/HSL triangle	1/3	1/3	1/3
HSV hexcone	0	0	1
HLS double hexcone	1/2	0	1/2

Table 2.2 Summary of lightness definitions for various LHS colour models

GLHS colour model	Lightness definition
LHS/HSL triangle	$L = \dfrac{R+G+B}{3}$
HSV hexcone	$L = \max(R, G, B)$
HLS double hexcone	$L = \dfrac{\max(R, G, B) + \min(R, G, B)}{2}$

As mentioned at the beginning of this subsection, the useful bridge between colour concepts and spectral signal forms for signal processing applications is the HLS double hexcone model (Table 2.2) **[Jones et al., 2000]**.

2.2.2.3 The HLS Chromaticity

Figure 2.3 shows the HLS double hexcone colour model: hue axis is along the boundary of the horizontal plane, whilst lightness axis is vertical to the plane and the

saturation axis has the origin at the central point of the plane extending radially outwards.
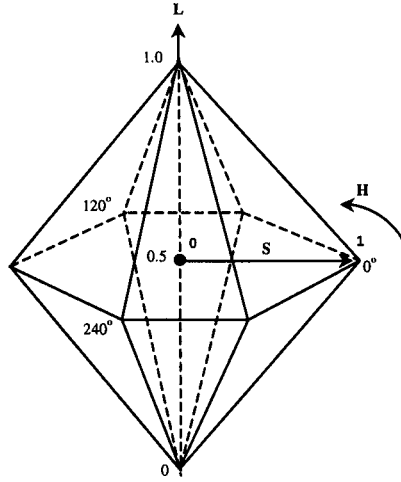
Figure 2.3 HLS double-hexcone colour model
[Foley et al., 1995; Deng, 2000]

With the lightness function determined, the transformation from the three detectors' outputs *R*, *G* and *B* to the three parameters of HLS system may be obtained by simplifying Equations (2.18), (2.20) and (2.23) **[Brazier et al., 2001]**. Hence

$$L = \frac{\max(RGB) + \min(RGB)}{2} \qquad (2.26)$$

$$H = \begin{cases} 60 \cdot \dfrac{G-B}{\max(R,G,B) - \min(R,G,B)}, & if \quad R = \max(R,G,B) \\[3mm] 60 \cdot [2 + \dfrac{B-R}{\max(R,G,B) - \min(R,G,B)}], & if \quad G = \max(R,G,B) \\[3mm] 60 \cdot [4 + \dfrac{R-G}{\max(R,G,B) - \min(R,G,B)}], & if \quad B = \max(R,G,B) \end{cases}$$

$$\qquad (2.27)$$

$$S = \begin{cases} \dfrac{\max(RGB) - \min(RGB)}{\max(RGB) + \min(RGB)} & if \quad L \le 0.5 \\[4mm] \dfrac{\max(RGB) - \min(RGB)}{2 - \max(RGB) - \min(RGB)} & otherwise \end{cases}$$

$$\qquad (2.28)$$

Based on the above HLS equations ($H \in [0, 360)$, $L \in [0, 1]$, $S \in [0, 1]$), a HLS double-cone model (Figure 2.4) is usually used for chromatic signal processing application.
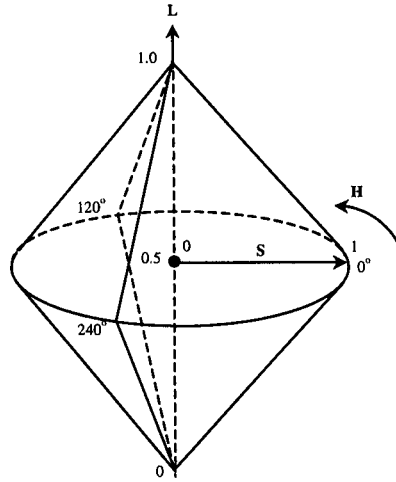
Figure 2.4 HLS double-cone colour model
[Jones et al., 2000; Brazier et al., 2001]

In this case the two-dimensional chromatic map may be formed from the cylindrical coordinates ($0 \leq (\theta = H) < 360°$, $0 \leq (r = L) \leq 1$ or $0 \leq (r = S) \leq 1$) and the chromatic boundary encompassing all signals now remains fixed as a circle of unity radius (Figure 2.5).
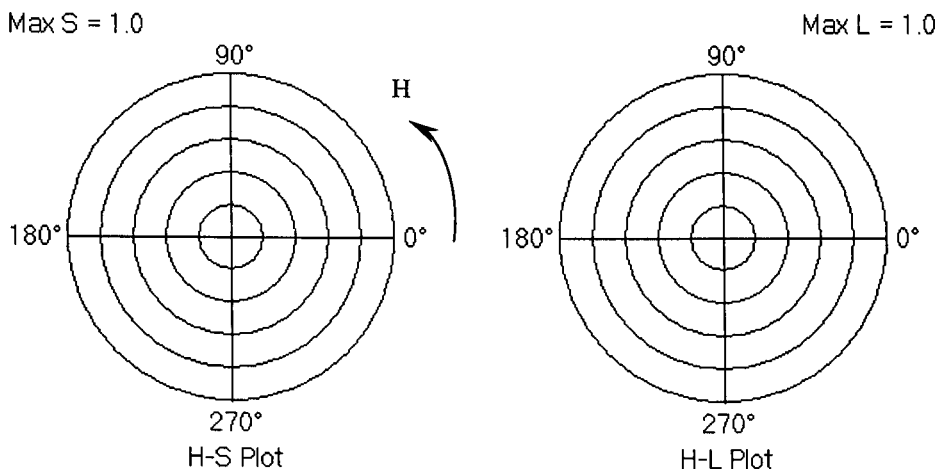
Figure 2.5 Chromatic map basic components: H-S and H-L polar plots

Therefore the two-dimensional mapping allows complex signals to be represented as a single point in a polar plot. As a result the relationship between two signals is easily visualized and the complex signals can be conveniently determined. Furthermore, through the use of the well-established algorithms, the signals resulting from the superposition of a multiplicity of separate signals and the uniform distribution of this mapping system cover the disadvantages of the xy chromaticity system.

2.3   Chromatic Methodology Applications

With the chromatic methodology theory introduced, it is useful to explore its applications for signal processing in system monitoring. This includes the application of the chromatic methodology for continuous signal processing and for discrete data analysis.

2.3.1   Continuous Signal Processing

The chromatic methodology as deployed for continuous signal analysis may be briefly explained by reference to Figure 2.6. This shows a time-frequency map of the continuous signals i.e. it shows how the frequency components of a signal vary with time t_1, t_2, and t_3. The chromatic approach involves passing the time varying signal through three filters (R, G and B) in parallel, the frequency responses of the filters being non-orthogonal. The implication is that the filter responses overlap to provide cross correlation between the subdivided signals on each channel. In this manner a signal having a complex structure can be conveniently defined by only three parameters calculated from the three channels (R, G and B, Figure 2.6).

An alternative approach is to use Fast Fourier Transform (FFT) **[Jennison, 1961; Champeney, 1973; Bracewell, 1978; Marshall et al., 1990]** within a time window (e.g. t_2-t_1 = t_3-t_2 Figure 2.6) to produce time segmented spectra which are then addressed by the non-orthogonal filters R, G and B. A root-mean-square (RMS) algorithm (window size could be specified as preferred) is then performed on the outputs of the tristimulus

filters. For smooth effect and fast processing, an average calculation with preferred window size can be implemented.
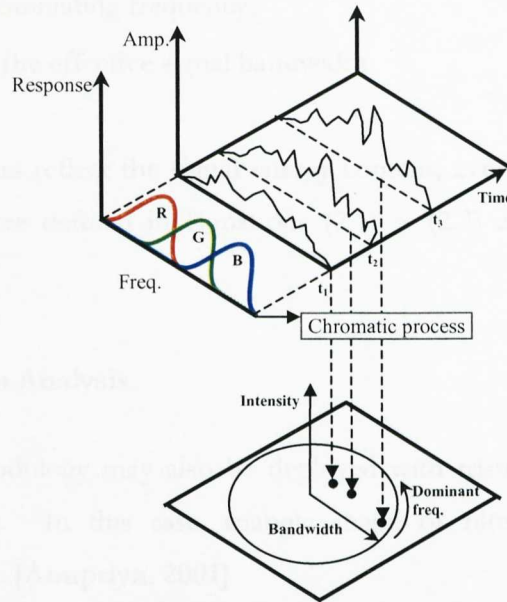
Figure 2.6 Schematics of chromatic processing for continuous signals

A further enhancement of these schemes is possible and is used in this thesis. An **option** of normalization might be performed based on the maximum value recorded on each R, G and B channel (i.e. $R_{average-max}$, $G_{average-max}$ and $B_{average-max}$). Averaged results or normalized results are then mathematically processed to yield three chromatic parameters in HLS space as stated in Equations (2.26) ~ (2.28). Thus the whole processing scheme is as shown in Figure 2.7.
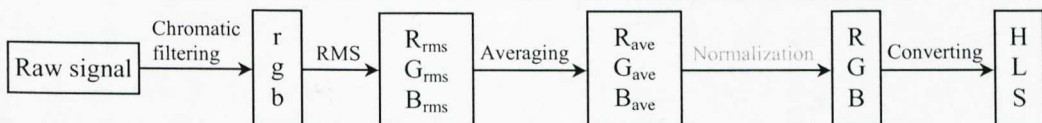
Figure 2.7 Flow diagram of chromatic processing for continuous signals

For the purpose of the present investigations the three signal parameters are chosen to be

- L (lightness), the nominal signal strength;
- H (hue), the dominating frequency;
- S (saturation), the effective signal bandwidth.

These three parameters reflect the signal energy content, average frequency and RMS bandwidth, which were defined in Equations (2.1) ~ (2.3) at the beginning of this chapter.

2.3.2 Discrete Data Analysis

The chromatic methodology may also be deployed with tristimulus filters to analyse discrete data records. In this case, triangle shape of filters may be applied for simplification purpose **[Anupriya, 2001]**.

This approach has been extended in this thesis in the following manner. Figure 2.8 shows a particular configuration of the three processors, which might be used and are denoted by R, G and B. It shows how these three non-orthogonal processors may be applied to an array of data $(D_1 \sim D_{10})$. The output of each processor constitutes the integrated product of the data and the gradient of the processor response.
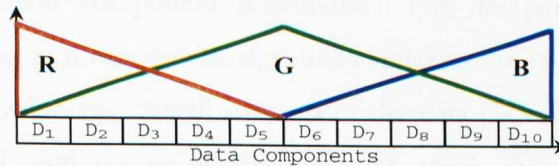
Figure 2.8 Schematics of chromatic processing for discrete data

The outputs of the tristimulus filters (R, G and B) are then mathematically processed via Equations (2.26) ~ (2.28) to yield the three chromatic parameters H, L and S.

Based on the data arrangement shown in Figure 2.8, the relationship between the dominant products $(D_1 \sim D_{10})$ and hue angles is shown in Figure 2.9. The hue angle of a dominant product is calculated as follows. By setting all the data values of the products to be zero except for D_1, applying the chromatic processing described above, the calculated hue angle of D_1 is 15° with a saturation value equalling 1. Similarly the hue angles of all the other dominant products can be calculated in this manner. Their juxtaposition is shown on the polar plots (Figure 2.9).
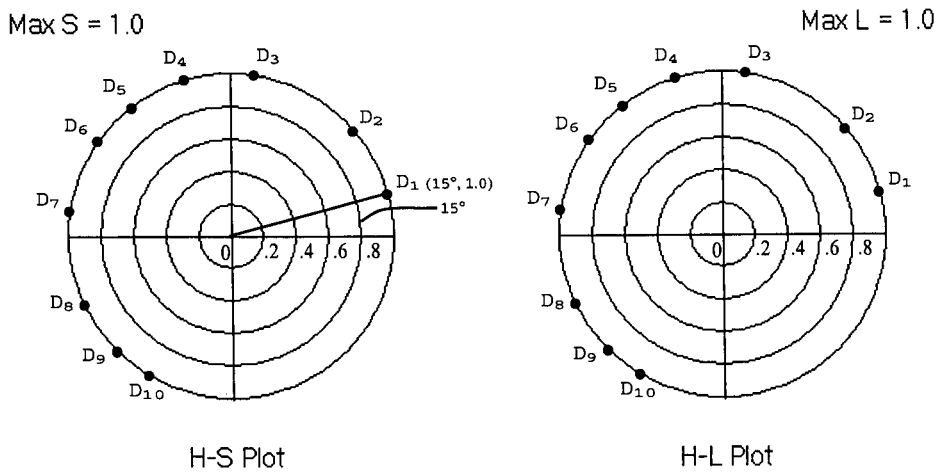
Figure 2.9 Dominant discrete product represented by hue angle

To utilise this representation in practice, the dominant datum $D_{\#}$ is indicated by the H value (i.e. the polar coordinate $D_{\#}$ on the H-S plot), the value of S indicates the extent to which the dominant component dominates. For the parameters of hue and lightness, a H-L polar plot can also be sketched similar to the H-S plot. The H-L plot indicates, via the L value, the overall strength of the data $(D_1 \sim D_{10})$. The stronger the data, the larger is L and the larger the radius at which the experimental point is registered. A point with polar coordinates H, L, S (i.e. θ, r_L, r_S) having values (15°, 1, 1) indicates that there is only a single component (S=1), which is D_1 (H=15°) and that it has a relatively high strength (L=1). Coordinates (15°, 0.1, 0.1) indicate that D_1 marginally dominates a low strength data set (L=0.1) with contributions from several datum points (S=0.1).

2.4   Summary

This chapter starting with the need for signal processing and system monitoring has provided a theoretical introduction to the chromatic methodology, and its relationship to the Gabor transform. It has been shown how the sophisticated GLHS colour model evolved by the colour science community can be adapted for more general signal processing applications. A brief introduction to the application of the chromatic methodology for continuous signal processing and discrete data analysis has been given along with indications of how the approach may be further evolved for extracting information from monitoring signal/data for prognosis purposes.

Chapter **3**

Review of Transformer PD Diagnosis Methods

3.1   Introduction

A PD is the localised breakdown of gas over a distance of usually <1mm **[Pearson et al., 1995]**. Corona discharges **[Kreuger, 1992]** occurred at surface defects such as small protrusions, sharp metallic points, take the form of corona streamers which give rise to current pulses with very short rise times (<1ns). Plus surface discharges and internal discharges, characterised by high rates of change of current such as discharges in voids, and micro-sparks associated with poor contacts or with the transport of conducting particles, are all examples of partial discharges. In all cases, the PD pulse causes electromagnetic energy to be radiated. In micro-sparks and intense coronas the discharge is followed by a rapid expansion of the ionised gas channel, and an acoustic pressure wave is generated **[Pearson et al., 1995]**. A PD is also accompanied by the emission of light from excited atoms, and by the creation of breakdown products **[Cobine, 1941; Kreuger, 1992]**.

This chapter describes the various diagnosis methods available for detecting different PDs. These are, as summarised in Figure 3.1, DGA, oil/tank temperature, electrical/RF emissions and acoustic emissions analyses.
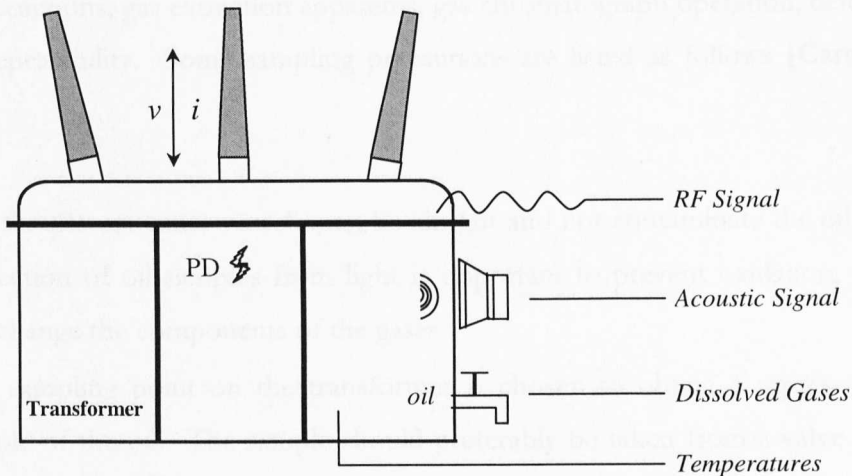
Figure 3.1 Possible information sources for transformer failure prognosis

3.2 Dissolved Gas Analysis

3.2.1 DGA Generality

The oil inside a transformer is used to provide electrical insulation to prevent sparking occurring **[Tyler, 1997; Weedy et al., 1998]**. It is also used as a heat transfer medium to remove the heat generated in the transformer windings and core by the passage of electric current **[White, 1994]**. Due to electrical activity within the transformer, many gases such as H_2, CO, CO_2, CH_4, C_2H_2, C_2H_4, C_2H_6 etc. may be produced from the transformer oil **[BSI, 1999]** by associated chemical reactions and may be dissolved in the oil thereafter **[Cardwell, 1989]**. Since each product is produced by one or several specific decomposition reactions, various gas statuses are associated with different conditions of the transformer **[Glass, 1977]**. Hence oil sampling is the fundamental task in DGA diagnosis; its accuracy is significant and will affect the interpretation of the final diagnosis result directly.

3.2.2 Oil Sampling

The oil samples are taken from the drain valve of the transformer. There are a number of factors which influence the accuracy of the dissolved gas analysis results, such as sampling precautions, gas extraction apparatus, gas chromatograph operation, detection limits and repeatability. Some sampling precautions are listed as follows **[Cardwell, 1989]**:

- The sample container vessel must be airtight and not contaminate the oil. The protection of oil samples from light is important to prevent oxidation, which can change the components of the gases.

- The sampling point on the transformer is chosen to obtain a representative sample of the oil. The sample should preferably be taken from a valve where the oil takes part in the normal circulation.

- The sampling method is important and only a trained technician should take samples to ensure consistent results. Samples must obviously be clean and free of any contamination from the valve or sampling tube and should be analysed within one week after being taken.

The remaining factors, gas extraction apparatus, gas chromatograph operation, detection limits and repeatability are detailed in IEC 567 of 1977 and IEC 599 of 1978.

Most of the NGT DGA data were sampled and identified on a regular monthly basis. This has made the condition monitoring tracking possible and the following diagnosis method effective. However, it should be noted that a number of different organisations would have been involved in acquiring and analysing the gas samples during the 20-year period, over which records are available.

3.2.3 DGA Diagnosis Method

It is known that analysis of hydrocarbon gases dissolved in the transformer oil is an especially important part of such condition monitoring **[Glass, 1977; White, 1994]**.

Table 3.1 summarises the key gases **[Kelly, 1980]** produced by various decomposition mechanisms found in transformers during service.

Table 3.1 **[Cardwell, 1989]** indicates that, if cellulose is overheated to around 150 Celsius, carbon monoxide (CO) and carbon dioxide (CO_2) will be produced. Oil at such a temperature will produce methane (CH_4), ethane (C_2H_6) and ethylene (C_2H_4). Under electrical stress condition (with a temperature greater than 1000 Celsius), the transformer oil will decompose into hydrogen (H_2) and acetylene (C_2H_2); at 1000 Celsius cellulose will still produce carbon monoxide and carbon dioxide, but extra products produced would change the output from water to carbon/tar.

Table 3.1 Sources of "key gases" from decomposition of cellulose and oil

Material	Condition & temperature	Key gases
Cellulose	Overheated > 150 ºC	CO CO_2 (water)
Cellulose	Excessive Heat >1000 ºC	CO CO_2 (carbon/tar)
Oil	Overheated > 150 ºC	CH_4 C_2H_6 C_2H_4 (organic acids)
Oil	Electrical Stress (partial discharges and arcing to 1000 ºC)	H_2 C_2H_2 (waxes & water)

3.3   Temperature Monitoring

Partial discharges occurring within a transformer can produce localised temperature variations within the transformer. Consequently temperature should be an important indirect indicator of the extent of PD activity within a transformer, similar to DGA (Section 3.2), not only for thermal aging diagnosis **[Pagan, 1998]**.

By monitoring the transformer oil temperature at various locations in a transformer, the extent of PD activities as well as their locations may be determined. The measured temperatures need to be related to other factors than simply PD, which may affect the temperature values. For instance, the changes in ambient temperature, the variation in the electrical load of the transformer and the rate at which the oil is circulated will all have an effect. The various locations at which the temperature may be monitored along with other factors affecting the temperature are listed in Table 3.2.

Table 3.2 Temperature factors available for diagnosis

Temperature factors	Meaning
Ambient °C	Ambient temperature in Celsius
Bot. Tank °C	Bottom tank temperature in Celsius
Top Tank1 °C	Top tank1 temperature in Celsius
Top Tank2 °C	Top tank2 temperature in Celsius
Oil in	A raw value from the sensor
Oil out	A raw value from the sensor
Load (scaled)	A scaled load value
Load (MVA)	Calculated value based on "Load (scaled)"
Oil in °C	Calculated temperature in Celsius based on "Oil in"
Oil out °C	Calculated temperature in Celsius based on "Oil out"

3.4   Electrical/RF Emissions

3.4.1   Electrical/RF Emissions Generality

When a partial discharge occurs within a transformer, it results in the production of individual electric pulses due to the movement of charge. The pulses propagate through the windings of the transformer and its connections to the bushings, with attenuation by the impedance of the winding and connections. On arrival at the bushing, which can be regarded as a high-pass filter, the high frequency component of the signal passes without further significant attenuation to the bushing tap. This signal may then be captured either electrically by a direct connection to the bushing tap **[Kemp, 2001; Kemp et al., 2002]**, which would need to have been disconnected from earth or by a current transformer inserted in the test tapping to earth circuit **[Tu et al., 2001; Golubev, 2002; Han, 2002]**.

Also, radio frequency signals are produced when a partial discharge occurs **[Furlong, 1999]**. In order to capture the signals, on the one hand, specially designed and manufactured sensors may be inserted into the transformer either via specially designed flanges or through the drain valves **[Rutgers et al., 1997; Rutgers et al., 2001; Unsworth et al., 2002]**; on the other hand, antennae may be placed around a transformer to detect the signals generated **[Babnik, 2001; Babnik et al., 2002; Moore et al., 2002]**. Signals received by the sensors/antennae are then recorded,

transmitted and processed in different ways according to the methods employed. The electrical and RF methods mentioned are summarised in Table 3.3.

Table 3.3 Diagnosis methods via electrical pulses and RF emissions

Method		Brief description	Freq. range
1. Direct pulse detection	A	Bushing test tapping, by direct connection to the bushing tap	40k~30MHz
	B	Bushing test tapping, by current transformer	10k~200MHz
2. Internal RF probes	A	Sensors inserted, via specially designed flanges	10M~100MHz
	B	Sensors inserted, via drain valves	0~1.8GHz
3. External RF probes		Antennae application	0~1GHz

The above diagnosis methods, except Method 2A (explained in Section 3.4.2.5), were used on the NGT site test by several organisations and institutions respectively. Some of them such as Glasgow Caledonian University (Method 1A), University of Southampton (Method 1B), UMIST (Methods 1A and 1B), KEMA (Method 2B) and University of Bath (Method 3) provided a substantial number of captured signals for processing and analysis. Furthermore some signals were obtained based on a sensor-shared method. For example, UMIST used both KEMA and Siemens sensors to capture signals for comparison purposes; University of Bath used signals from a KEMA probe to act as a reference etc. These aspects are discussed in the following chapters. It is helpful to briefly describe in more detail the methods utilised by each participant.

3.4.2   Electrical/RF Signal Capturing and Diagnosis Methods

3.4.2.1   Glasgow Caledonian University Method

The technique used by Glasgow Caledonian University was Method 1A (Table 3.3). The test tappings were disconnected from earth before connection of the detection and pre processing circuitry. Discharge signals coupled electrically via the bushing capacitance to the test tap could be monitored. Connection to the test tappings was made using die cast watertight boxes, with detection and pre-processing circuitry housed within each box. With the test tap unearthed it is possible for the bushing test tapping voltage to rise to significant levels, and therefore both spark gaps and zener

diodes were incorporated at the front end of the electronic circuitry. Any rise of voltage on the test tapping could be hazardous to the monitoring equipment and personnel so fibre optic connecting cables were used to provide galvanic isolation. Two fibre-optic cables (bandwidth 65MHz ~ 125MHz) were used to transmit the PD signals from the test tapping boxes to the measurement equipment where they were stored and processed. The fibre optic transmitters were housed within the same die cast boxes and powered from 12-volt batteries, which were re-charged nightly. The pre processing of the discharge signal at the bushing test tap split the individual discharge pulses from the AC 50 Hz that was used as the power reference.

Wavelet analysis **[Kemp, 2001; Kemp et al., 2002; Ma et al., 2002a; Ma et al., 2002b]** was used to both de-noise and categorise the individual pulses. 3D plots (Φ-q-n) showing the phase relationship to the AC signal, the magnitude of the pulses and their repetition rate were produced. These were then used to aid interpretation of the signals captured.

3.4.2.2 Southampton University Method

The system used by University of Southampton utilised Radio Frequency Current Transformers (RFCT) **[Jenkins, 1967; BSI, 1973; Cunningham et al., 1993]** to capture signals from both bushings and the neutral, Method 1B (Table 3.3). The received signals with a frequency range of 10kHz to 200MHz were then processed by a spectrum analyser and a computer. Figure 3.2 shows the connections to the bushings and the processing circuitry used.
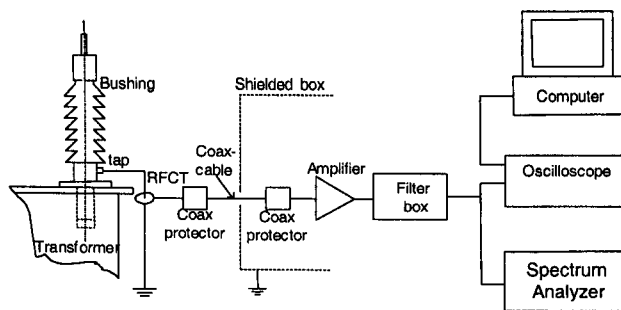
Figure 3.2 Southampton University measurement system schematics
[Han, 2002]

3.4.2.3   UMIST Method

The UMIST measurement system was a wide-band data acquisition system utilising a multi-channel electrical measurement technique (Method 1B & 1A Table 3.3). It used all six HV bushings and the neutral connection to acquire the signals. Small toroidal 50kHz - 30MHz sensors were placed around the bushing tap to earth connection and a large split CT **[Jenkins, 1967; BSI, 1973; Cunningham et al., 1993]** with an effective bandwidth of 170kHz to 10MHz was used to detect current in the neutral connection. That is both methods of Method 1 in Table 3.3 were utilised. The sample rate was 100MHz with 50kHz to 10MHz effective bandwidth. For signal processing, pre-amplifiers and signal-conditioning units were used. Figure 3.3 shows the measurement system.
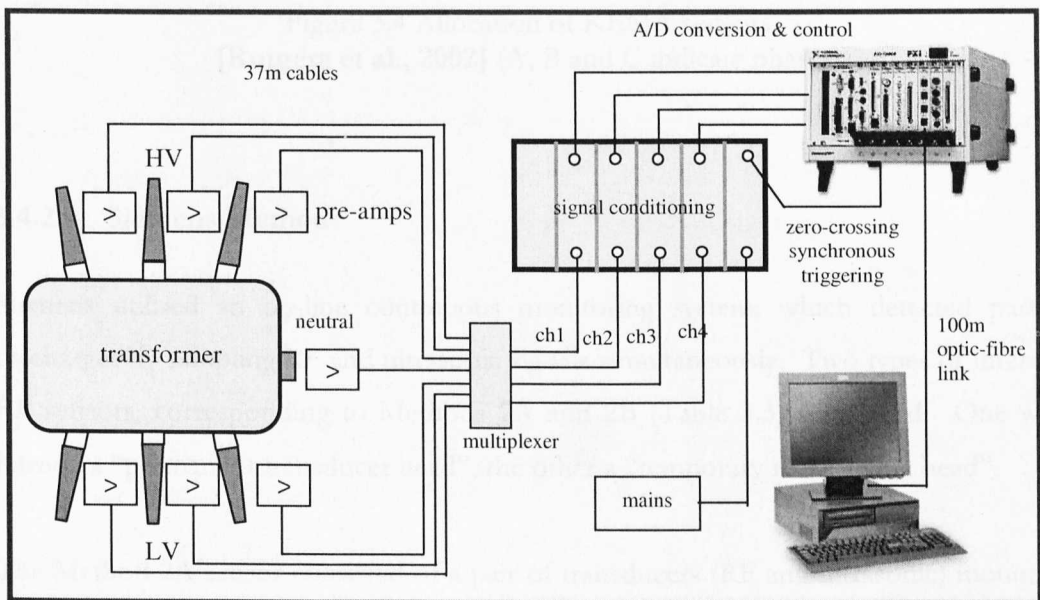
Figure 3.3 UMIST measurement system schematics
[Tu et al., 2002]

3.4.2.4   KEMA Method

KEMA utilised Method 2B (Table 3.3) for PD measurement. The KEMA probe, a patented UHF partial discharge detection technique, was used to detect and characterise the PD signals by being installed via the transformer drain valve. A

spectrum analyser, a fast A/D converter, a peak detector and a data logger were used to measure the UHF signals. On the Northfleet site test, two KEMA UHF sensors were installed as shown in Figure 3.4.

400 kV side

UHF INJECTION

UHF
SENSOR

C   B   A

COOLER
SIDE

Ac.sensor 2   Ac. sensor 3   Ac. sensor 1

275 kV side
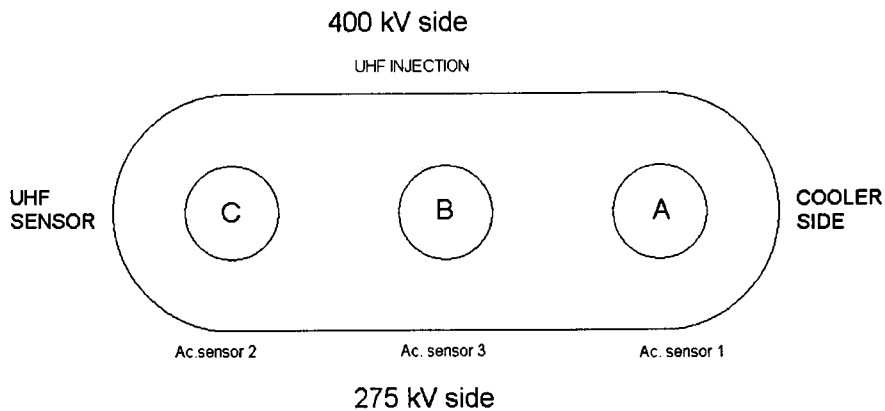
Figure 3.4 Allocation of KEMA sensors
[Rutgers et al., 2002] (A, B and C indicate phases)

3.4.2.5   Siemens Method

Siemens utilised an on-line continuous monitoring system, which detected partial discharges by sampling RF and ultrasonic signals simultaneously. Two types of internal RF sensors, corresponding to Methods 2A and 2B (Table 3.3) were used. One was termed a "permanent transducer head", the other a "temporary re-locatable head".

The Method 2A sensor consisted of a pair of transducers (RF and ultrasonic) mounted on a sealed lead through a plate covered by a noise shield. The lead through plate and electronics was contained in a steel enclosure that was mounted on a flange welded to the transformer wall or an existing inspection plate, so that the transducers were immersed in the mineral oil flush with the internal wall. The advantage of this was that the noisy signals from other parts of the substation were eliminated by the shielding. Since in the NGT site tests none of the sensors were permitted to enter further than the tank wall inner surface, this "permanent transducer head" could not be installed.

The Method 2B sensor ("temporary re-locatable head") is shown in Figure 3.5. It has size-reduced RF and ultrasonic transducers, connected through the drain valve of the transformer. This was utilised in the NGT site tests although the re-locatable head is not as effective as using the permanent head as stated by Siemens.
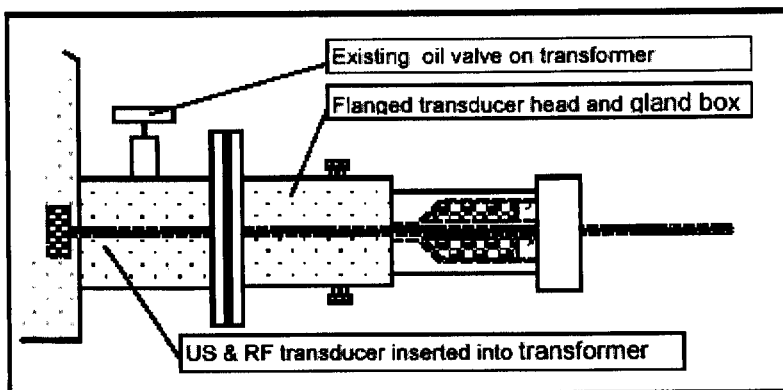
Figure 3.5 Siemens re-locatable transducer head
[Unsworth et al., 2002]

The signals captured by the transducers were passed to two separate processors – ultrasonic processor and RF processor, which were of the form shown in Figure 3.6. The ultrasonic processing channel consisted of an ultrasonic pre-amplifier, a 125kHz high pass filter, a precision rectifier, a 1kHz low pass filter, an amplifier and buffer. The RF processor consisted of a RF pre-amplifier operating in the range 1 ~70 MHz, a PF precision rectifier, a 1MHz low pass filter, a high-speed comparator and a digital mono-shot. For analysis, the system measured the time delay between the arrival of the ultrasonic and RF signals generated by the PD source.

a) ultrasonic processor
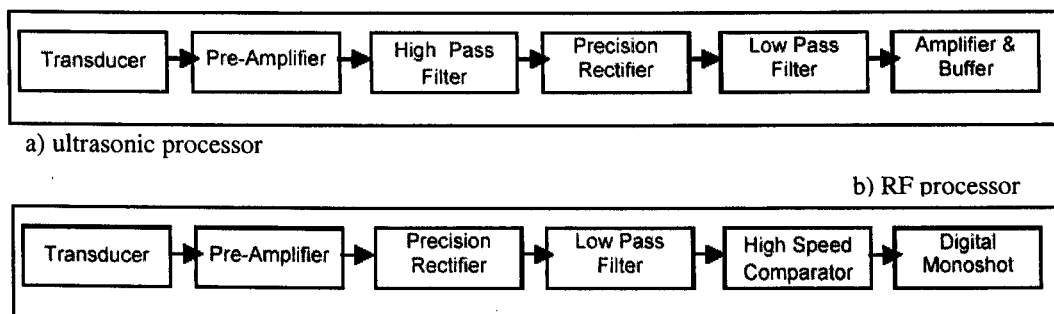
b) RF processor

Figure 3.6 Siemens ultrasonic and RF processors
[Unsworth et al., 2002]

3.4.2.6   Bath University Method

The University of Bath used two separate non-invasive techniques, both techniques were used simultaneously, and neither required connection to the test tappings or insertion through drain valves **[Babnik, 2001; Babnik et al., 2002]**.

Technique 1, Radiometric Measurements, TV YAGI antennae were used for Remote Radiometric measurement of the PD signals. These antennae, having a frequency range of 470MHz to 850MHz, were positioned around the transformer. A KEMA probe had previously been inserted in the oil drain valve at the end of the transformer, as mentioned in Section 3.4.2.4. Signals were acquired from the antennae and also from the KEMA probe to act as a reference. These were analysed using a phosphor screen oscilloscope and a laptop computer.

Technique 2, Impulse Noise Locating System, was used to determine if partial discharges were present within the transformer, and involved the application of an impulse noise locating system. Antennae were placed on the concrete plinth adjacent to the transformer, positioned so that they were in direct line of site to all of the 400kV and 275kV bushings. Sampling equipment and a PC were situated in a van adjacent to the transformer. The coordinates of each of the antennae relative to the corner of the transformer bund wall were measured and recorded.

3.5   Acoustic Emissions

3.5.1   Acoustic Emissions Generality

As mentioned in Section 3.1, with partial discharge occurring within a transformer, electrical and RF emissions are generated accompanied by acoustic emissions. In order to capture the acoustic signals, specially designed and manufactured sensors may be inserted into the transformer in a similar manner to the RF probe Methods 2A/B (Table 3.3). The Siemens sensor, which embodied both RF and ultrasonic transducers inside the transformer tank (Section 3.4.2.5), is a good example of this. An optical fibre acoustic sensor **[Culshaw et al., 1997; Granttan et al., 1998]** could also be deployed.

The field test undertaken by Virginia Tech **[Yu et al., 2002; Tsai et al., 2002]** proved that fibre optic sensors could be packaged and installed in transformer drain valves.

But more commonly, acoustic sensors may be mounted on the transformer tank wall. Organisation such as IPEC **[Smith, 2001; Smith, 2002]**, Alstom **[Raja et al., 2002]**, Electricity de France (EdF) **[Aubujeault, 2002]**, Virginia Tech **[Yu et al., 2002]**, ABB **[Bengtsson et al., 1997]** etc. utilise such an approach, among which, the piezo-electric acoustic emission sensors of ABB could be considered as the typical case.

3.5.2   ABB Acoustic Detection System

The ABB acoustic detection system included three piezo-electric acoustic emission sensors with the main sensitivity in the range of 50~150kHz, all mounted within one frame to forms a three-transducer detector (TTD). Figure 3.7 shows the upper and lower sides of the system. With a transducer-source distance of 15cm, the instrument gave an angular resolution of about $1°$ under ideal conditions i.e. direct line of sight. Such a system may be regarded as an acoustic manifestation of a primitive tristimulus spatially deployed chromatic sensor.

Upper side   Lower side
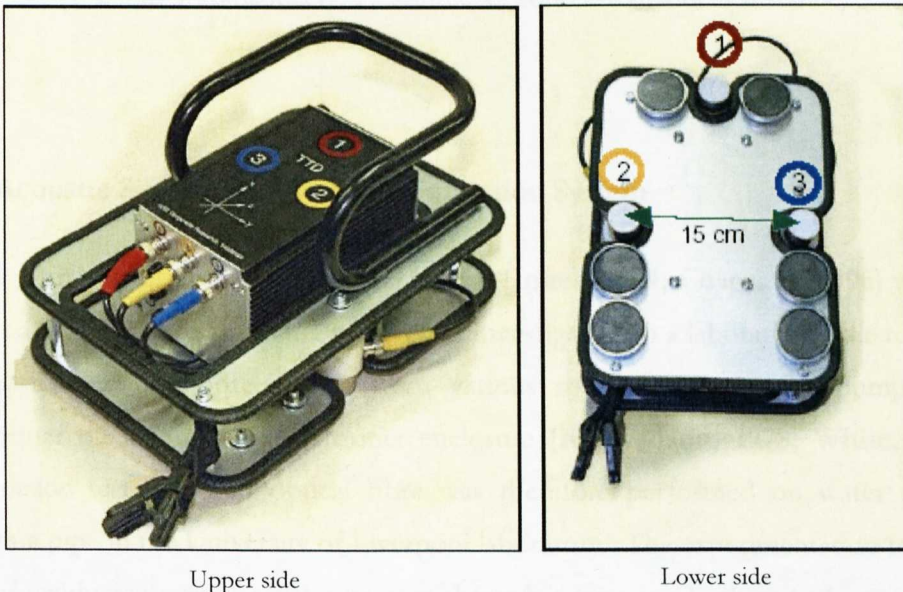
Figure 3.7 ABB three transducer detector system
[Bengtsson et al., 2001] (1, 2 and 3 refer to the three transducers)

3.5.3   ABB PD Source Localisation Method

Figure 3.8 illustrates how the TTD system localises the position of an acoustic source. The numbered rings (1, 2 and 3) indicate the three transducers; and Ps denotes the acoustic source position.
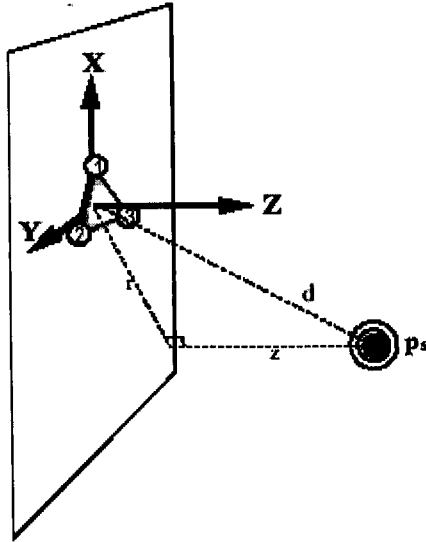
Figure 3.8 Localisation scheme for the ABB TTD system
[Bengtsson et al., 2001]
(1, 2 and 3: transducers; P_s: source; d: source-transducer distance)

3.6   Acoustic Signals Composition Simulation System

Although an optical fibre based sensing system **[Jones, 1994; Cosgrave, 1996]** was not deployed during site tests, such a system was investigated on a laboratory scale to check for possible acoustic interference from various sources such as the pumping of transformer oil within the transformer enclosure **[Richardson, 1978; White, 1994]**. An acoustic test using an optical fibre was therefore performed on water passing through a pipe in the University of Liverpool laboratory. The experimentation took the form of producing irregular water passage through a pipe as a background signal; while a signal generator produced periodic pulses via a loudspeaker coupled rigidly to the pipe to simulate the PD sparks producing pulses. The fundamental problem being

addressed was that of exploring how pulsatile and quasi-continuous waveforms might be separated in terms of signal processing. The diagram in Figure 3.9 shows the acoustic tests system.
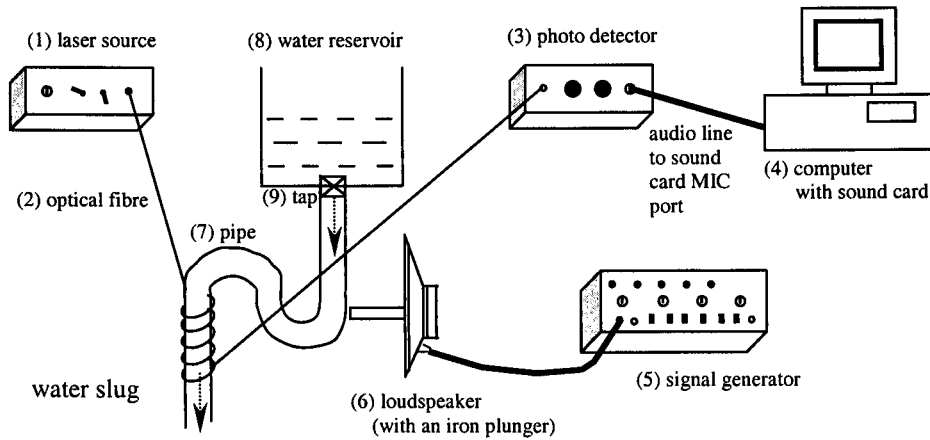
Figure 3.9 Acoustic test on a water pipe with superimposed periodic pulses

After the water reservoir (8) was filled with water, the signal generator (5) was used to produce a periodic square signal and the plunger on the loudspeaker (6) communicated the acoustic pulses to the water pipe (7) periodically. The computer with sound card (4) commenced recording when the water was released from the reservoir. A laser (1) energised optical fibre (2) was used as a homodyne interferometer **[Hale et al., 1993; Jones et al., 1994]** for detecting the acoustic signals from the pipe, the acoustic coupling being achieved by coiling the fibre around the pipe. A photo detector (3) connected to the output of the fibre was used to convert the optical signal to an electrical signal. The Signal was recorded by being linked to the microphone port on the computer sound card (4). The Following are the system specifications.

1) The laser source was a semiconductor laser with a peak power of 25mw, wavelength 828nm operated in a DC mode.

2) The optical fibre was a 10m long, 400um diameter, PVC jacketed multimode glass fibre, connected to both the laser source and detector via ST connectors.

3) The photo detector was a photodiode connected to the fibre output via an axial controlled spatial filter for both gain adjustment and providing suitable spatial resolution for the output interference pattern from the optical fibre.

4) The computer with sound card was a Pentium III 500MHz PC, the recording software being Cool Edit 2000 **[Adobe Audition, 2003]**.

5) The signal generator was a type ISO-TECH IGC2231 instrument capable of providing a square wave output with frequency and voltage adjustable.

6) The loudspeaker was a 10cm-radius-cone loudspeaker with an iron plunger attached.

7) The pipe included two U bends to enhance acoustic effects due to the water flow.

Table 3.4 lists the specification of the signal files recorded. These signals were then processed and analysed by applying chromatic methodologies thereafter.

Table 3.4 File specification in acoustic simulation

Item	Specification
File type	Wave file (Windows PCM, *.wav)
Sample rate	44100Hz, 8kHz
Channel	Mono-channel
Resolution	32-bit

3.7 Summary

This chapter has provided a brief explanation of partial discharges, and their effects in producing physical, chemical and electrical changes. These lead to four main groups of methods for monitoring PD activity in HV transformers namely DGA, temperature, electrical/RF emissions and acoustic emissions changes. The manifestation of these methods utilised in the present investigations by various organisations are classified, compared and discussed. An acoustic system, laboratory based using optical fibre sensing for exploring the interactivity between pulsatile and periodic signals has also been described.

Chapter 4

Results from Site Tests

4.1 Introduction

This chapter presents some typical results obtained with the four main data-sampling and signal-capturing methods (DGA, temperature, electrical/RF emissions and acoustic emissions analyses) introduced in Chapter 3, during tests undertaken at various NGT sites. The results may be divided into two categories, which are: -

- Results from in-service transformers, which include long-term (e.g. 20 years) DGA results from NGT and First Hydro, and half-month oil temperature results from NGT.

- Results from tests at two NGT sites (Neilston and Northfleet) to compare and cross correlate the performance of several diagnosis methods (DGA, electrical/RF and acoustic) and involving 16 project participants (Table 4.1).

The two site tests were performed on transformers designated as Neilston SGT4 and Northfleet SGT3A during 25~27 June 2001 and 13~28 May 2002 respectively. The diagnosis methods utilised during these tests by each participant are summarised in Table 4.1.

Results for DGA, temperature, electrical/RF emissions and acoustic emissions are presented in this sequence, including results from both in-service and site-test transformers.

Table 4.1 List of participants in NGT transformer PD site tests

Participant	Site test 1 (Neilston)	Site test 2 (Northfleet)
ABB	Acoustic	
Alstom		Acoustic
University of Bath	RF (Antennas)	RF (Antennas)
Cutler Hammer		RF (CT)
EdF		Acoustic
Glasgow Caledonian University	ELEC (Bushing test tapping)	ELEC (Bushing test tapping)
IPEC	Acoustic	Acoustic
KEMA	RF, Acoustic	RF, Acoustic
NGT		RF
Serveron	DGA	
Siemens		RF, Acoustic
University of Southampton		RF (CT)
Strathclyde University	RF	
UMIST	ELEC (CT)	ELEC (CT)
Virginia Tech		Acoustic
University of Liverpool	Data analysis	Data analysis

4.2 DGA Results

NGT and First Hydro provided DGA data from a total of 50 tanks, which are summarised in Table 4.2.

Table 4.2 Summary of DGA examined transformer tanks

Count	Transformers
36 NGT Transformers/tanks	Boln1, Boln2, Boln3, Bush2, Bush3, Bush4, Cant1, Cant2, Cape2A, Cape1A, Cape3A Cape5A, Cape5B, Cape6A, Cape6B, Elst1A, Elst1B, Elst2, Elst3A, Elst3B, Elst4, Elst5A Hamh1, Hamh2, Hamh3, Hamh5, Hamh6, Hamh7 Walx1A, Walx2A, Walx2B Wylf1, Wylf2, Wylf4, Neilston4, Northfleet3A
14 First Hydro Transformers/tanks	Ffes1, Ffes2 GMT1 Main Tank ~ GMT6 Main Tank GMT1 Selector Tank ~ GMT6 Selector Tank

The transformers were of various ages ranging from several years to several decades, with oil DGA data records varying from one year to more than twenty years. Most of the oil dissolved gas data was sampled and identified on a monthly basis. A suitable format, spreadsheet was used to arrange the sample records, each of which contains more than 10 gas components. Figure 4.1 shows an extract from the spreadsheet containing the newly organised data records for all 10 gases. Each single row represents one sample record with the first column indicating the sample date and the second to the eleventh column the concentration of each gas component. The unit of concentration is part-per-million (ppm).

	A	B	C	D	E	F	G	H	I	J	K	L	M	N	O
1															
2															
3	SAMPDATE	CO2	CO	CH4	C2H6	C2H4	C2H2	H2	O2	N2	H2O				
4	28-Aug-80	2490	410	10	5	5	1	63	7497	69828	19				
5	11-May-81	2560	50	9	5	4	1	13	7497	69828	14				
6	05-Jul-81	1690	50	6	3	3	1	21	7497	69828	16				
7	06-Aug-81	2305	494	9	4	3	1	51	7497	69828	16				
8	16-Nov-81	2477	50	10	5	4	1	28	7497	69828	11				
9	16-Sep-82	2272	50	8	4	4	1	24	7497	69828	15				
10	05-Aug-83	2651	50	9	4	4	1	52	7497	69828	22				
11	27-Apr-86	1992	50	7	4	3	1	2	7497	69828	21				
12	18-Nov-86	2720	50	20	5	4	1	31	7497	69828	14				
13	12-Aug-87	3048	50	10	5	4	1	28	7497	69828	6				
14	12-Aug-88	3285	50	11	5	3	1	40	7497	69828	12				
15	24-Aug-89	1888	50	7	4	2	1	38	7497	69828	5				
16	22-Aug-91	3582	486	9	5	3	1	33	7497	69828	13				
17	24-Aug-92	2889	516	23	11	9	0.2	39	7497	69828	32				
18	03-Jan-95	3199	546	10	6	5	0.2	28	10607	66964	12				
19	22-Feb-95	3213	471	12	7	5	0.2	30	21476	63091	13				
20	30-Sep-96	4754	814	23	6	8	0.2	34	20049	68446	14				
21	24-Jun-97	3298	563	9	5	3	0.2	24	19322	59596	18				
22	26-Jun-97	3502	621	10	5	4	0.4	34	16406	61933	22				
23	07-Jul-98	2985	597	9	5	3	0.2	29	17125	68686	16				
24	22-Sep-98	2950	564	9	4	3	0.2	29	19871	61516	26				
25	29-Apr-99	2489	397	7	3	2	0.2	19	20140	58747	15				
26	29-Jun-99	1460	312	9	4	3	0.2	33	3784	44833	23				
27															
28															
29															
30															
31															

WYLF1mtb / WYLF2mtb / WYLF4mtb /

Figure 4.1 DGA data in spreadsheet
(Concentration in ppm)

The data is usually presented in one or more orthogonal plots as different coloured curves corresponding to different gas components **[Waters, 2001]**. Such a presentation format is used to show the DGA data of some transformers under typical conditions as examples in the following subsections.

4.2.1   NGT In-service Transformers

Figure 4.2 shows the time-varying plot of the oil-dissolved gases concentration raw data for an NGT in-service transformer tank, WYLF1mtb, a 220MVA, 400/132kV unit,

manufactured in 1967 and installed in 1968, with samples taken over 19 years (August 1980 ~ June 1999). Due to CO_2 and CO having greater concentrations than the other gases, they are shown separately in Figure 4.2(a), while the remaining gases are shown in Figure 4.2(b). The DGA data indicate that the concentration of CO_2 is dominant throughout the monitoring period, the concentration of CO increases to about 500ppm after 1989, all hydrocarbon gases concentrations are below 25ppm and there is almost no C_2H_2 detected throughout the whole period.
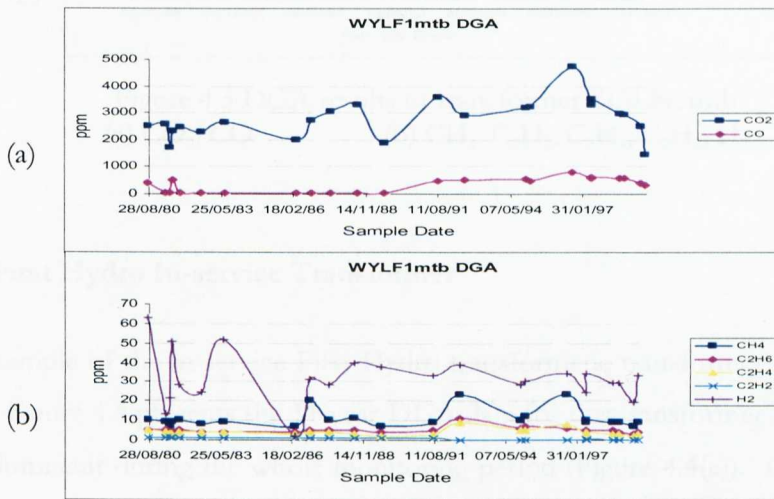
Figure 4.2 DGA results of transformer WYLF1mtb
(a) CO_2, CO   (b) CH_4, C_2H_6, C_2H_4, C_2H_2, H_2

Figure 4.3 shows the concentration data of the oil-dissolved gases from another NGT in-service transformer tank, which is designated BOLN3mtb. This is a 240MVA, 400/132kV transformer installed in 1968 with DGA sample records available from September 1985 until November 1998. These results show that all the gases have an increasing concentration trend, although not at a significant level. In addition there are at least three obvious concentration reductions exhibited by all gases; these are for samples taken around May 1990, October 1995 and July 1998 (probably because of degassing).
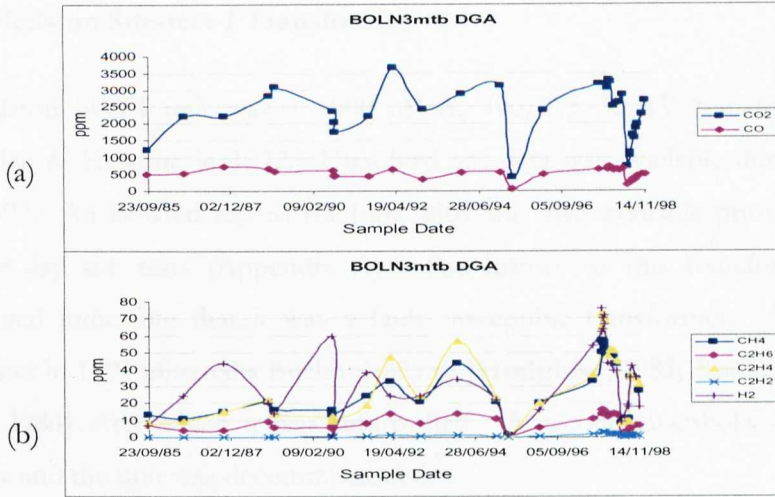
Figure 4.3 DGA results of transformer BOLN3mtb
(a) CO_2, CO   (b) CH_4, C_2H_6, C_2H_4, C_2H_2, H_2

4.2.2   First Hydro In-service Transformer

As an example of the in-service First Hydro transformers, transformer FFES SGT1 is chosen. Figure 4.4 presents the 11-year DGA data for this transformer and shows that CO_2 is dominant during the whole monitoring period (Figure 4.4(a)). Compared with the hydrocarbon gases, H_2 also has a noticeable level of concentration (Figure 4.4(b)). There are at least two high concentration peaks in the CO_2 and H_2 records around the year 1992 and 1999.
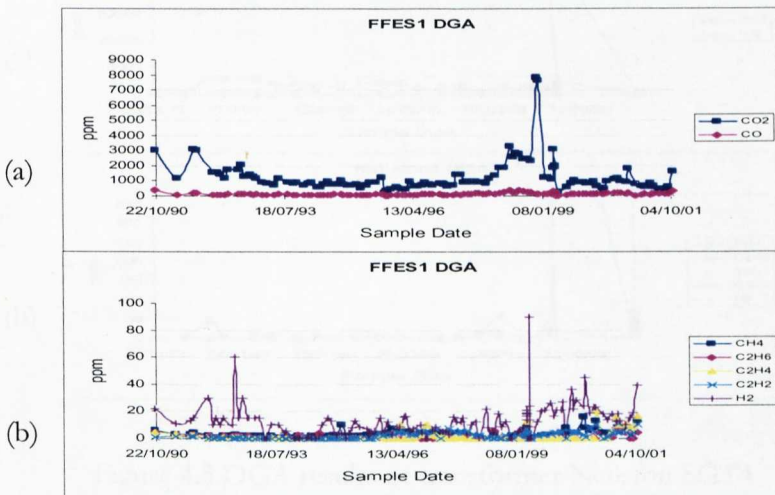
Figure 4.4 DGA results of transformer FFES SGT1
(a) CO_2, CO   (b) CH_4, C_2H_6, C_2H_4, C_2H_2, H_2

4.2.3   Neilston Site-test-1 Transformer

The Neilston SGT4 unit was a 1000 MVA, 400/275/33 kV transformer built by
Hackbridge & Hewittic in 1972. Dissolved gas data was available during the period
1977~1997. An isolated record for June 2001 was also available prior to one of the
present 8-day site tests (Appendix A). The history of this transformer was well
documented indicating that it was a fault susceptible transformer. A fault on the
transformer in 1997 initiated a Buchholz alarm **[Hodgkiss, 1981; Rushton et al., 1981;
Davies, 1984]** after which it was refurbished. A second Buchholz alarm occurred
thereafter and the unit was decommissioned.

The 24-year (November 1977 ~ June 2001) oil-dissolved gases concentration raw data
for the site-test transformer Neilston SGT4 are shown in Figure 4.5. Prior to year 1997
the concentrations of all gases vary within the normal range for in-service transformers
consistent with the results of Sections 4.2.1 and 4.2.2. However during 1997, the
concentrations of CO, CH_4, C_2H_2 and H_2 increased by at least an order of magnitude
above normal values suggesting the occurrence of some significant events and
consistent with the Buchholz alarm sounding.
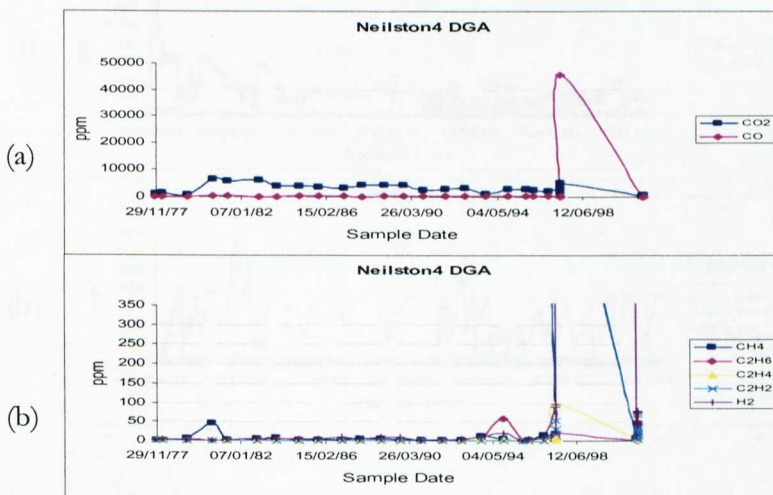
Figure 4.5 DGA results of transformer Neilston SGT4
(a) CO_2, CO   (b) CH_4, C_2H_6, C_2H_4, C_2H_2, H_2

4.2.4   Northfleet Site-test-2 Transformer

The Northfleet SGT3A transformer was a Parsons Peebles 500MVA, 400/275/33kV unit manufactured in 1965. Firstly, T4296 was installed in 1966 and failed in 1973; secondly, T4305 was installed in 1973 and failed in 1987; third, T4281 was installed in 1987 and failed in 1993 – a case with such poor records is unusual. After several installations and failure, the transformer was moved to Northfleet about ten years ago, with T4175, which was installed in 1993 until the present. Since excessive gasses have been produced, there is the possibility that the unit has partial discharge problems.

Figure 4.6 shows the DGA results over the available 9-year period for the Northfleet transformer. For this entire period, CO_2 and H_2 have relatively high and variable concentrations while all other gases have extremely low concentrations. The concentration of H_2 is considerably higher than normal throughout the whole monitored period. This might be relative to the type of transformer, which requires such oil environment.
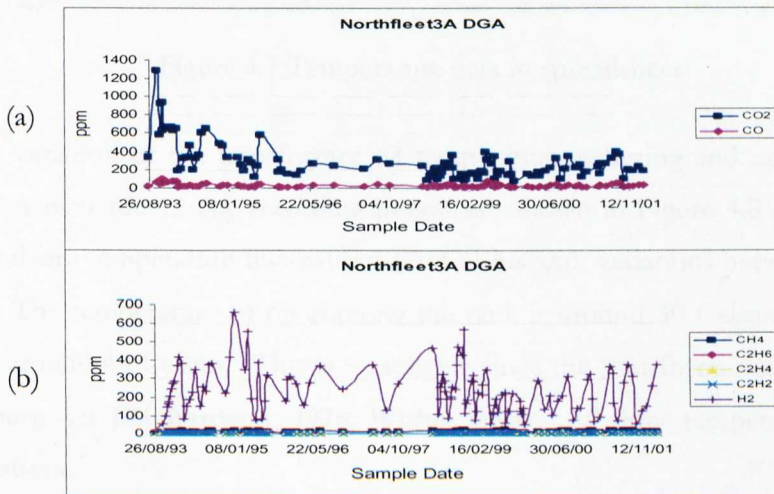
Figure 4.6 DGA results of transformer Northfleet SGT3A
(a) CO_2, CO (b) CH_4, C_2H_6, C_2H_4, C_2H_2, H_2

4.3　Temperature Results

Temperature data were provided by NGT covering a period of 12 days (from 7th 14:20 to 19th 15:05 of July 1999), with sampling every 5 minutes. These consisted of tank and oil temperatures and transformer load data from a particular transformer supplied as a spreadsheet. There were 3466 records (samples) in the spreadsheet, which contained 14 fields (column headings), as shown in Figure 4.7.

	A Date	B Time	C	D Ambient	E Bot. Tan	F Top Tanl	G Top Tanl	H Vibratior	I PD 1	J Oil in	K Oil out	L Load (sc	M Hydran	N PD	O	P	Q Load (MV)	R Oil in °C	S Oil out °C
1	Date	Time		Ambient	Bot. Tan	Top Tanl	Top Tanl	Vibratior	PD 1	Oil in	Oil out	Load (sc	Hydran	PD			Load (MV)	Oil in °C	Oil out °C
2																			
3	07/07/1999	14:20:00		25.8	35.1	52.3	37.6	1.65	3.99	11.185	12.29	1.237	4.71	0			6.8	471.297	42.86875	52.5375
4	07/07/1999	14:25:00		25.6	35	52.7	37.4	1.715	3.99	11.155	12.075	1.24	4.705	0			6.778	472.44	42.60625	50.65625
5	07/07/1999	14:30:00		26.1	34.8	52.8	36.7	1.71	3.995	11.065	11.89	1.23	4.705	0			6.758	468.63	41.81875	49.0375
6	07/07/1999	14:35:00		26	34.7	52.4	36.3	1.695	4	10.965	11.725	1.225	4.71	0			6.747	466.725	40.94375	47.59375
7	07/07/1999	14:40:00		25.8	34.5	51.8	35.9	1.705	3.99	10.87	11.59	1.232	4.705	0			6.77	469.392	40.1125	46.4125
8	07/07/1999	14:45:00		25.6	34.2	51.3	35.5	1.67	3.995	10.785	11.47	1.242	4.705	UNDER			6.765	473.202	39.36875	45.3625
9	07/07/1999	14:50:00		25.5	33.9	51	35.1	1.71	3.99	10.71	11.36	1.242	4.705	0			6.765	473.202	38.7125	44.4
10	07/07/1999	14:55:00		25.6	33.7	50.6	34.8	1.7	3.995	10.645	11.27	1.245	4.71	UNDER			6.795	474.345	38.14375	43.6125
11	07/07/1999	15:00:00		24.9	33.5	50.2	34.6	1.705	3.985	10.585	11.195	1.253	4.705	0			6.77	477.393	37.61875	42.95625
12	07/07/1999	15:05:00		24.9	33.4	49.9	34.3	1.715	3.995	10.53	11.115	1.258	4.705	0			6.787	479.298	37.1375	42.25625
13	07/07/1999	15:10:00		24.5	33.2	49.5	33.9	1.695	3.99	10.485	11.055	1.258	4.71	0			6.773	479.298	36.74375	41.73125
14	07/07/1999	15:15:00		25.1	33	49.2	33.7	1.7	3.99	10.44	11	1.263	4.705	0			6.8	481.203	36.35	41.25
15	07/07/1999	15:20:00		25	32.8	49.1	33.5	1.71	3.99	10.4	10.945	1.273	4.7	0			6.798	485.013	36	40.76875
16	07/07/1999	15:25:00		25.2	32.7	48.9	33.3	1.775	3.995	10.365	10.895	1.273	4.705	0			6.805	485.013	35.69375	40.33125
17	07/07/1999	15:30:00		25.8	32.6	48.8	33.1	1.765	3.99	10.34	10.855	1.28	4.7	0			6.782	487.68	35.475	39.98125
18	07/07/1999	15:35:00		26.2	32.5	48.8	33	1.7	3.995	10.32	10.82	1.278	4.705	0			6.802	486.918	35.3	39.675
19	07/07/1999	15:40:00		26.5	32.4	48.6	32.9	1.71	3.995	10.29	10.79	1.275	4.705	0			6.79	485.775	35.08125	39.4125
20	07/07/1999	15:45:00		26.3	32.4	48.5	32.8	1.685	4	10.28	10.76	1.283	4.705	0			6.782	488.823	34.95	39.15
21	07/07/1999	15:50:00		25.7	32.3	48.4	32.7	1.705	3.995	10.26	10.74	1.285	4.705	0			6.787	489.585	34.775	38.975
22	07/07/1999	15:55:00		25.3	32.3	48.4	32.5	1.71	3.99	10.245	10.715	1.29	4.7	0			6.795	491.49	34.64375	38.75625
23	07/07/1999	16:00:00		24.9	32.1	48.2	32.4	1.68	3.995	10.23	10.695	1.283	4.7	0			6.815	488.823	34.5125	38.58125
24	07/07/1999	16:05:00		25.3	32	48.1	32.3	1.715	3.985	10.215	10.675	1.28	4.695	0			6.832	487.68	34.38125	38.40625
25	07/07/1999	16:10:00		25.7	32	48	32.3	1.695	3.99	10.2	10.66	1.28	4.7	0			6.827	487.68	34.25	38.275
26	07/07/1999	16:15:00		26.3	31.9	48	32.1	1.75	3.995	10.185	10.64	1.28	4.7	0			6.838	487.68	34.11875	38.1
27	07/07/1999	16:20:00		26.4	31.8	47.8	32	1.66	3.995	10.175	10.625	1.285	4.705	UNDER			6.858	489.585	34.03125	37.96875
28	07/07/1999	16:25:00		26.6	31.9	47.7	32	1.72	3.995	10.165	10.605	1.28	4.705	0			6.847	487.68	33.94375	37.79375
29	07/07/1999	16:30:00		26.6	31.8	47.6	32	1.66	3.99	10.155	10.595	1.275	4.7	0			6.827	485.775	33.85625	37.70625
30	07/07/1999	16:35:00		27.1	31.8	47.3	31.9	1.695	3.995	10.14	10.58	1.28	4.705	0			6.832	487.68	33.725	37.575
31	07/07/1999	16:40:00		27.2	31.7	47.3	31.9	1.685	3.995	10.135	10.57	1.28	4.705	0			6.807	487.68	33.68125	37.4875
32	07/07/1999	16:45:00		27	31.6	47.3	31.8	1.72	3.99	10.125	10.555	1.273	4.705	0			6.785	485.013	33.59375	37.35625
33	07/07/1999	16:50:00		25.8	31.5	47.3	31.7	1.71	3.985	10.12	10.55	1.273	4.7	0			6.782	485.013	33.55	37.3125

19_6_99 /

Figure 4.7 Temperature data in spreadsheet

The time variation of the transformer oil temperatures entering and exiting from the transformer over the 12-day recording period are shown in Figure 4.8 along with the diurnal ambient temperature fluctuations (20 Celsius with variations between 10 and 30 Celsius). The temperature of oil entering the tank is around 30 Celsius while that of exiting is around 45 Celsius. This is reasonable since the transformer oil functions for cooling purposes **[Richardson, 1978; White, 1994]**. All three temperatures follow a diurnal pattern.

Figure 4.9 shows the time variation for the 12-day period of the temperatures of three tanks – top tank1, top tank2 and bottom tank. The top tank1 has a temperature variation in the range of 50 to 35 Celsius rather higher than the other two tanks, which show changes of 30 to 25 Celsius. As for the ambient and oil temperature results of Figure 4.8, these three tanks temperatures also exhibit a diurnal variation.

Oil Temperatures Time Variations
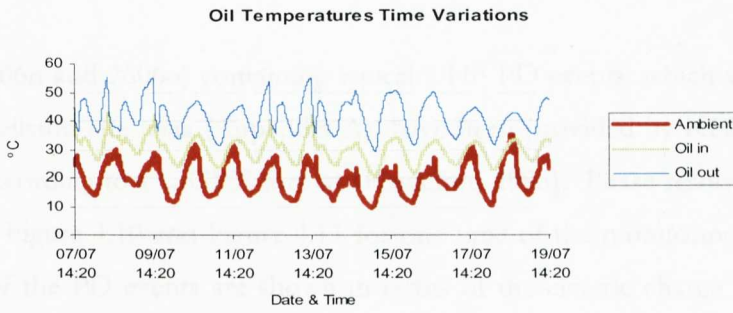
Figure 4.8 Oil temperature data in time-Celsius plot
(Time variation of temperatures for oil entering and exiting the transformer along with
the ambient temperature)

Tank Temperatures Time Variations
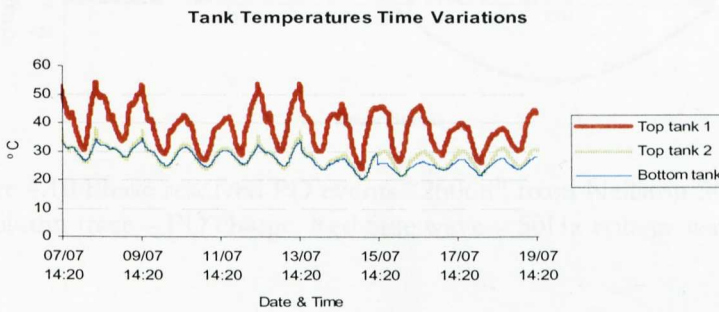
Figure 4.9 Tank temperature data in time-Celsius plot
(Time variation of temperatures for top tanks 1 & 2 and bottom tank)

4.4   Electrical/RF Emissions Results

Electrical and radio frequency results were mainly obtained from two site tests
(Neilston and Northfleet). For the first site test (Neilston) the only reliable electrical
and RF results were those obtained by KEMA. For the second site test (Northfleet)
reliable results were obtained by four academic institutions (Glasgow Caledonian
University, UMIST, University of Southampton and University of Bath) with signals
from sensors of 6 organisations (sensor shared for cross-correlation purpose, Section
3.4.1), the previous 4 providers plus KEMA and Siemens (Table 4.1).

4.4.1   Neilston Site-test-1 Transformer

Two files (2606n and 2606o) containing typical UHF PD events, which were recorded during the Neilston site tests (Appendix A), have been provided by KEMA. The file structure is according to a CIGRE format **[Huecker, 1998]**. Phase resolved PD events are shown in Figure 4.10 and Figure 4.11 for one time of the monitoring period. The magnitudes of the PD events are shown in terms of the electric charge involved pico Coulomb (pC). The 50Hz voltage sine wave is also shown in these two figures.

Phase Resolved PD Events (File 2606n)
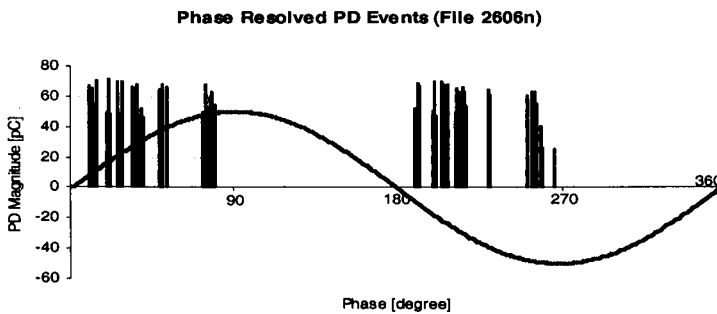
Figure 4.10 Phase resolved PD events "2606n" from Neilston SGT4
(Black column trace – PD charge, Red Sine wave – 50Hz voltage waveform)

Phase Resolved PD Events (File 2606o)
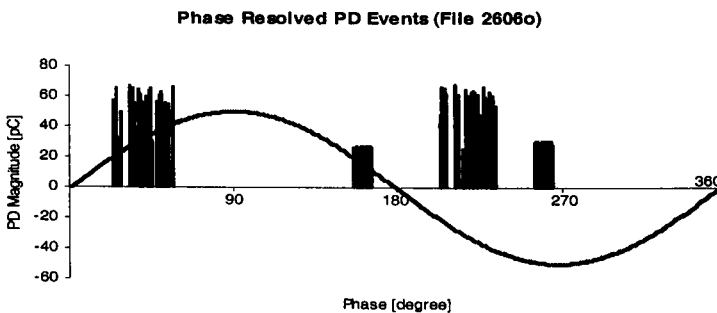
Figure 4.11 Phase resolved PD events "2606o" from Neilston SGT4
(Black column trace – PD charge, Red Sine wave – 50Hz voltage waveform)

As a conventional way to present the PD events, a 3D distribution, either phase-cycle-amplitude **[Judd et al., 2001]** or phase-amplitude-count **[Pearson et al., 1995]**, is usually used. Figure 4.12 shows an example of the latter. It indicates that the largest number of PD events occur with a charge magnitude of 45~50pC (light green).
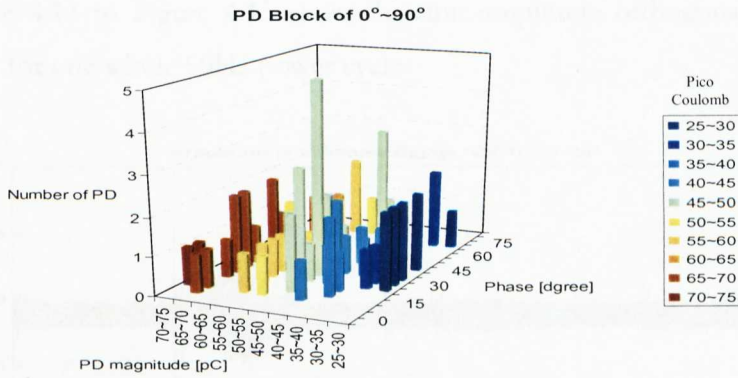
Figure 4.12 PD events 3D plot of "2606n" from Neilston SGT4
(Ref. Figure 4.10)

4.4.2 Northfleet Site-test-2 Transformer

The signals provided by Glasgow Caledonian University, UMIST, University of Southampton and University of Bath are all time-varying signals. Table 4.3 lists some of the properties of the signals received from each participant.

Table 4.3 Properties of available electrical/RF signals

Participant	Signal sample rate	Signal duration
Glasgow Caledonian	10MHz	20ms
UMIST	a) 10MHz, b) 250MHz, c) 500MHz	a) 20ms, b) 20us, c) 10us
Southampton	a) 250MHz, b) 500MHz	a) 20ms, b) 20ms
Bath	2.5 GHz	0.2ms

4.4.2.1 Signals from Glasgow Caledonian University

Three typical signals (namely "C2-10-34-24", "C3-10-34-31" and "C4-10-34-35") recorded during the Northfleet site tests were supplied by Glasgow Caledonian University. The files are in ASCII format. They contain one column of signal amplitude with the last but one and the last number indicating the time of the first sample and the time per sample (i.e. inverse sample rate) respectively. Hence, from the file information, all the three files have the same sample rate 10MHz and number of sample points 200,000 i.e. cover only one cycle of 50Hz-AC power - time duration

20ms. Figure 4.13 to Figure 4.15 show the time-amplitude orthogonal plot of the above signals for one whole 50Hz power cycle.
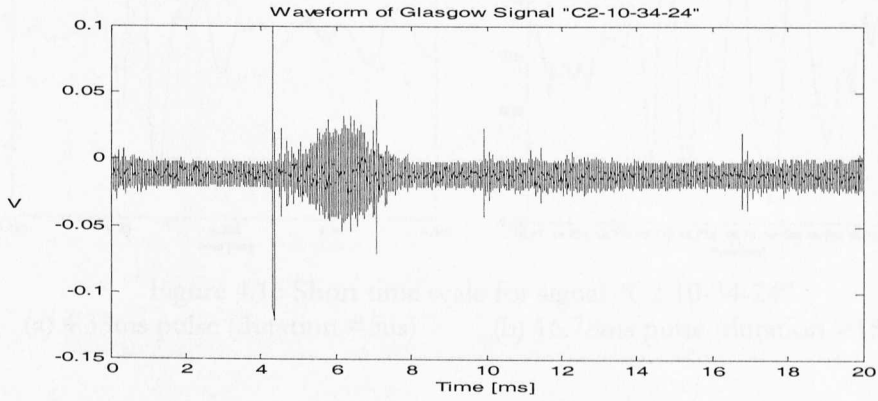
Figure 4.13 Glasgow RF signal "C2-10-34-24" from Northfleet SGT3A
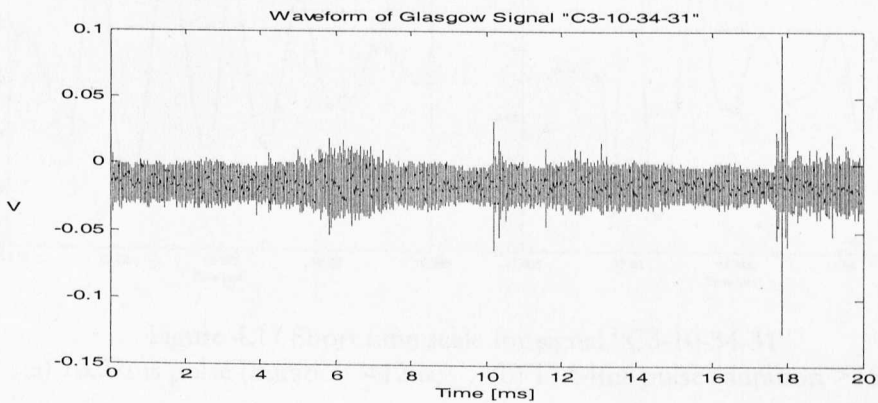
Figure 4.14 Glasgow RF signal "C3-10-34-31" from Northfleet SGT3A
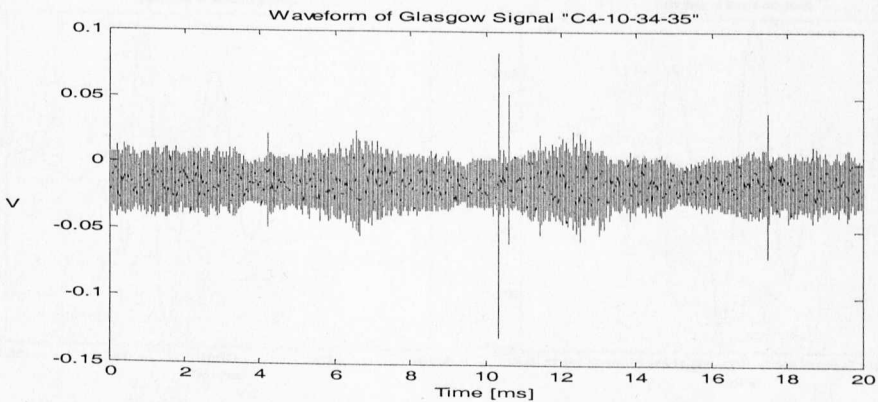
Figure 4.15 Glasgow RF signal "C4-10-34-35" from Northfleet SGT3A
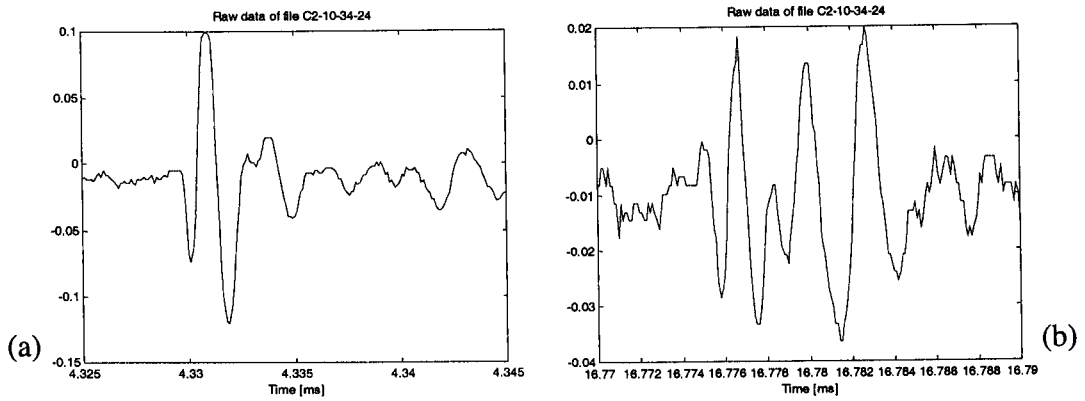
Figure 4.16 Short time scale for signal "C2-10-34-24"
(a) 4.33ms pulse (duration ≈5us)   (b) 16.78ms pulse (duration >15us)
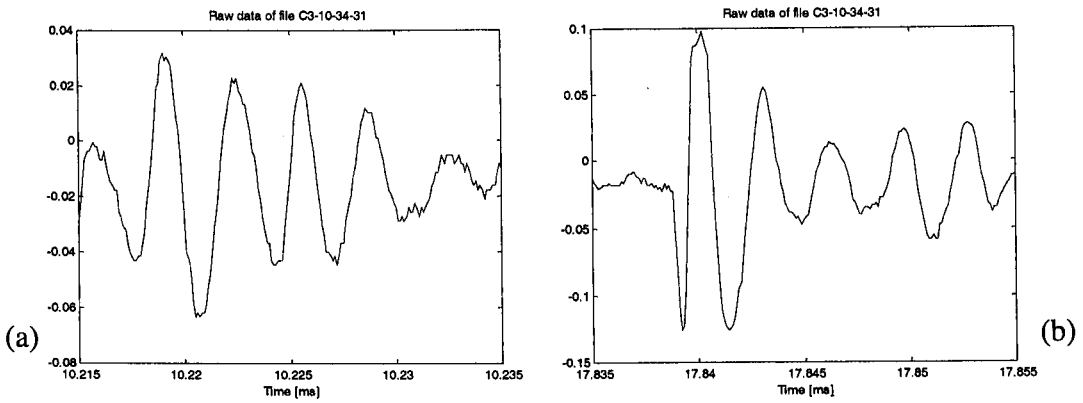
Figure 4.17 Short time scale for signal "C3-10-34-31"
(a) 10.22ms pulse (duration ≈12us)   (b) 17.84ms pulse (duration >15us)
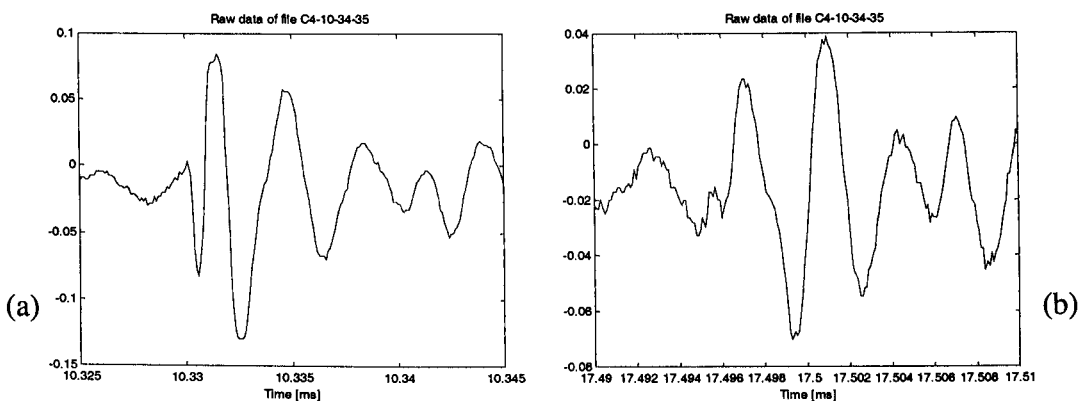
Figure 4.18 Short time scale for signal "C4-10-34-35"
(a) 10.33ms pulse (duration >15us)   (b) 17.5ms pulse (duration >15us)

Details of the pulses and waveforms can be extracted by scanning the signal over a shorter time scale (e.g. 20us). Examples of such signals are shown in Figure 4.16 to Figure 4.18 for each of the larger time scale results of Figure 4.13 to Figure 4.15. For example Figure 4.16 corresponds to Figure 4.13 showing the time expansion of an event at 4.33ms in Figure 4.16(a) and another event at 16.78ms in Figure 4.16(b).

From the focused short time scale waveforms, a judgement can be made that most are broadly similar but differ in detail.

4.4.2.2   Signals from UMIST (Siemens & KEMA signals included)

Seven typical sets of RF signals recorded during the Northfleet site tests were provided by UMIST. In addition to Channel 1, which is gone the synchronous signal, each set contains three channels of PD signals, with UMIST signals on both Channel 2 and Channel 3 and Siemens/KEMA signal on Channel 4. Table 4.4 summarises this information. The files are in ASCII format, contain a header indicating values of "trigger time", "time of first sample", "time per sample" and "number of samples" etc., followed by a column of amplitude data. Some sets of signals have a sample rate of 10MHz, others 250MHz. Figure 4.19 shows one set of signals of the former in time-amplitude orthogonal plots. A number of possible discharge events in the form of distinct pulses are apparent on each trace (a) (b) and (c) of Figure 4.19.

Table 4.4 Information for UMIST signals

Date	Count	Channel 1	Channel 2	Channel 3	Channel 4
25 May 02 *files* 15-26-51 (20ms) 15-27-36 (20ms) 15-31-08 (20ms) 15-33-26 (20us) 15-39-58 (20ms)	5	Synchronise	Phase **C** 400kV bushing	Phase **B** 400kV bushing	Phase C 275kV winding Siemens probe tank bottom
27 May 02 *file* 17-10-05 (10us)	1	Synchronise	Phase **B** 400kV bushing	Phase **C** 400kV bushing	Phase C 275kV winding KEMA probe tank bottom
27 May 02 *file* 17-22-09 (10us)	1	Synchronise	Phase **B** 275kV bushing	Phase **C** 275kV bushing	Phase C 275kV winding KEMA probe tank bottom
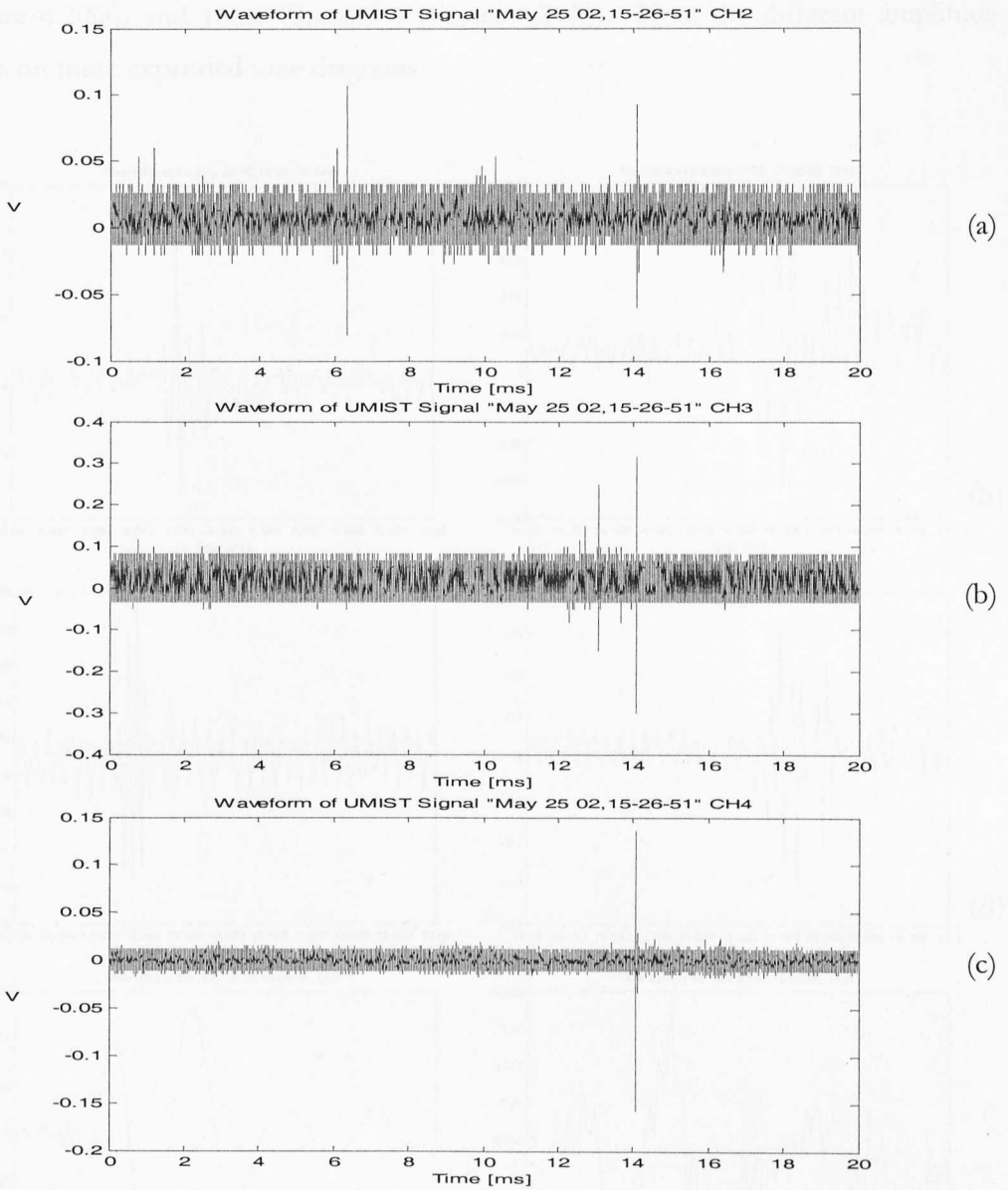
Figure 4.19 UMIST RF signal "May 25 02, 15-26-51" from Northfleet SGT3A
(Sample rate 10MHz) (a) Channel 2, (b) Channel 3, (c) Channel 4

Figure 4.20 shows some pulses from the above signals on an expanded time scale. It should be noted that the high amplitude pulse at approximately 14ms is apparent on all three channels. This pulse is shown on an expanded time scale (10us total) for each of the three channels on Figure 4.20(b), (d) and (e). The other pulses which have been time expanded are at approximately 6ms Channel 2 (Figure 4.20(a)), 13ms Channel 3

(Figure 4.20(c)) and 16ms Channel 4 (Figure 4.20(f)). Note the different amplitude scales on these expanded time diagrams.
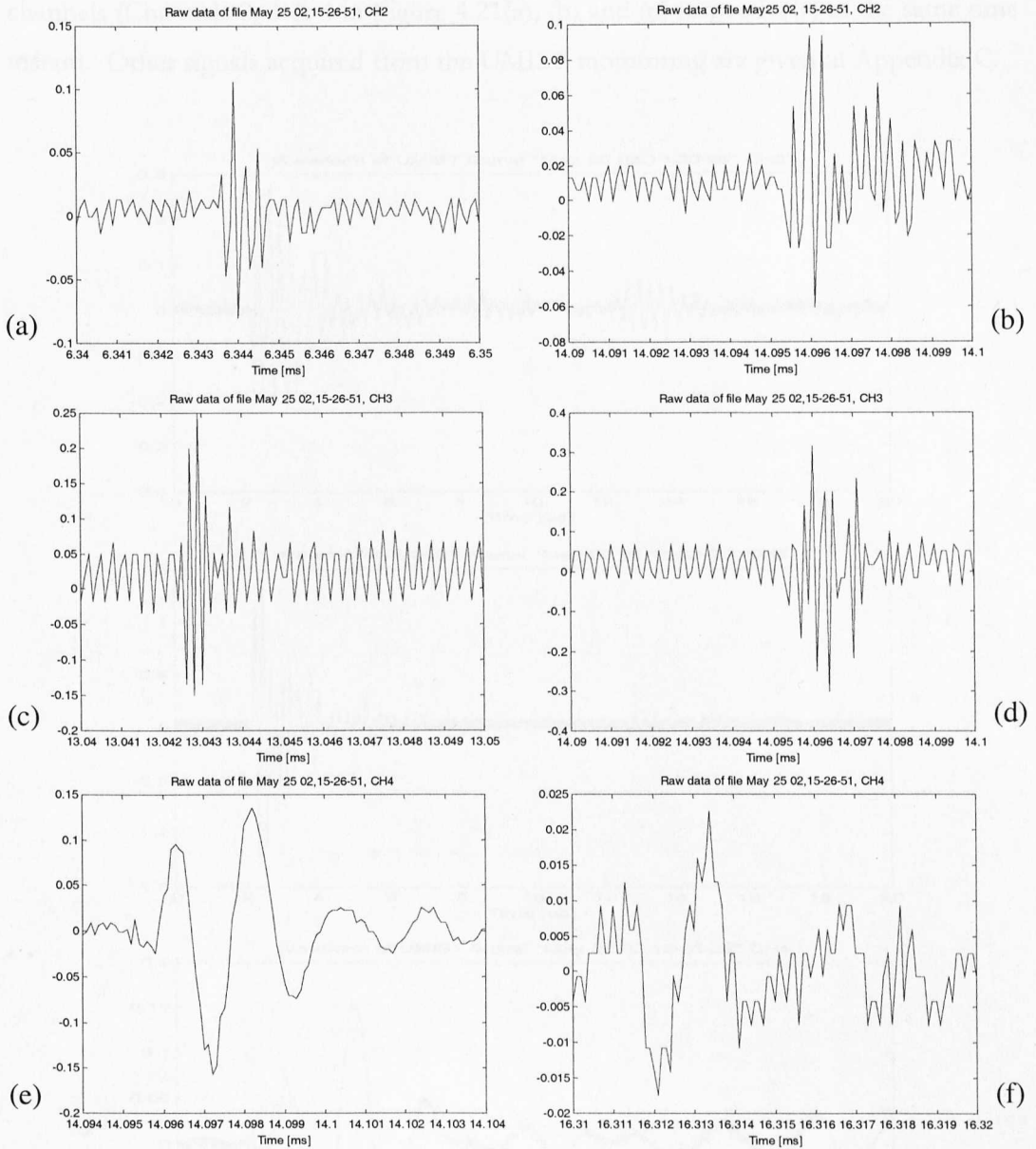
Figure 4.20 Short time scale for signal "May 25 02, 15-26-51"
(Total time duration 10us) (a) Ch2, 6.343ms pulse; (b) Ch2, 14.095ms pulse;
(c) Ch3, 13.042ms pulse; (d) Ch3, 14.095ms pulse;
(e) Ch4, 14.095ms pulse; (f) Ch4, 16.315ms pulse.

Figure 4.21 shows another set of signals with 250MHz sample rate in time-amplitude orthogonal plots. Notice that the total time duration of these signals is 20 microseconds. The signals are of pulses received on each of the three recording channels (Channels 2, 3 & 4 in Figure 4.21(a), (b) and (c) respectively) at the same time instant. Other signals acquired from the UMIST monitoring are given in Appendix C.
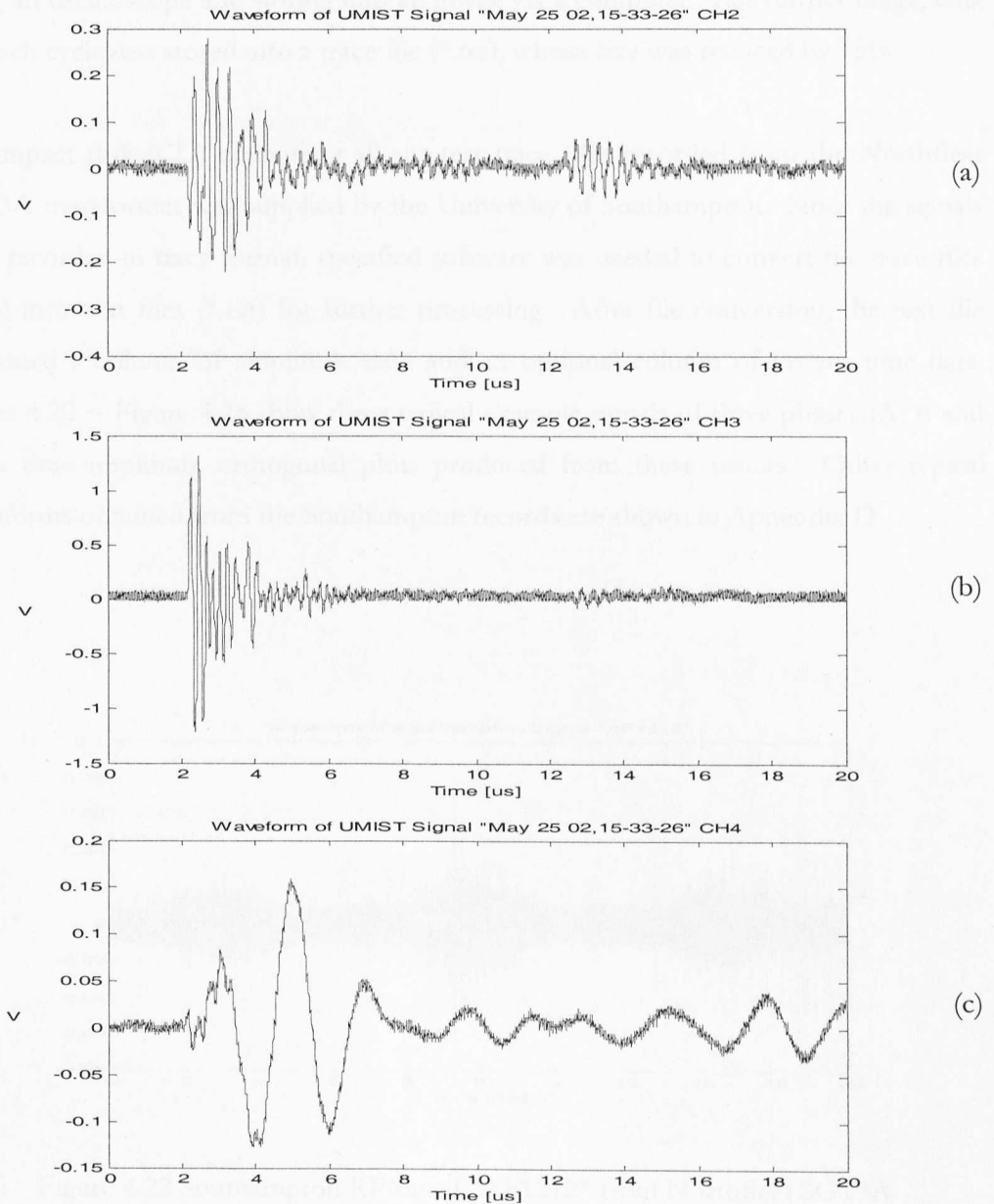
Figure 4.21 UMIST RF signal "May 25 02,15-33-26" from Northfleet SGT3A
(Sample rate 250MHz, total time duration 20us)
(a) Channel 2, (b) Channel 3, (c) Channel 4

4.4.2.3   Signals from Southampton University

Due to the high sample rate (250MHz or 500MHz) used by the University of Southampton to record the RF signals for every single cycle (20ms), there were 5M to 10M sample points per cycle, which required 80 to 160 Mega bytes for storage in an ASCII-format file. For convenience, the signal for each cycle was plotted online by using an oscilloscope and storing into an image via a computer. For further usage, data for each cycle was stored into a trace file (*.trc), whose size was reduced by 75%.

A compact disk (CD) containing all site-test trace files recorded from the Northfleet SGT3A transformer was supplied by the University of Southampton. Since the signals were recorded in trace format, specified software was needed to convert the trace files (*.trc) into text files (*.txt) for further processing. After file conversion, the text file contained a column of amplitude data and an optional column of instant time data. Figure 4.22 ~ Figure 4.24 show three typical example signals of three phases (A, B and C) in time-amplitude orthogonal plots produced from these results. Other typical waveforms obtained from the Southampton records are shown in Appendix D.
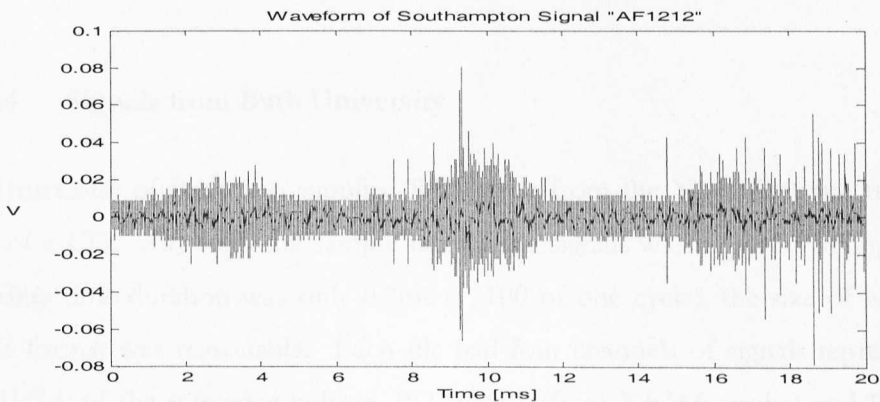
Figure 4.22 Southampton RF signal "AF1212" from Northfleet SGT3A

Waveform of Southampton Signal "BF1310"
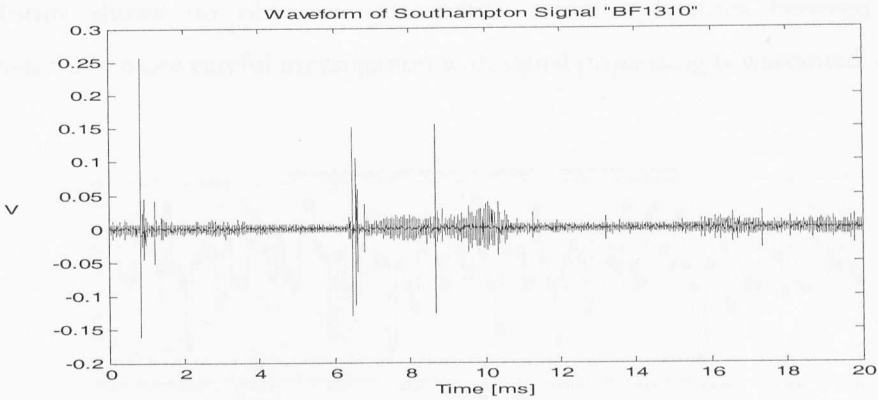
Figure 4.23 Southampton RF signal "BF1310" from Northfleet SGT3A

Waveform of Southampton Signal "CF1207"
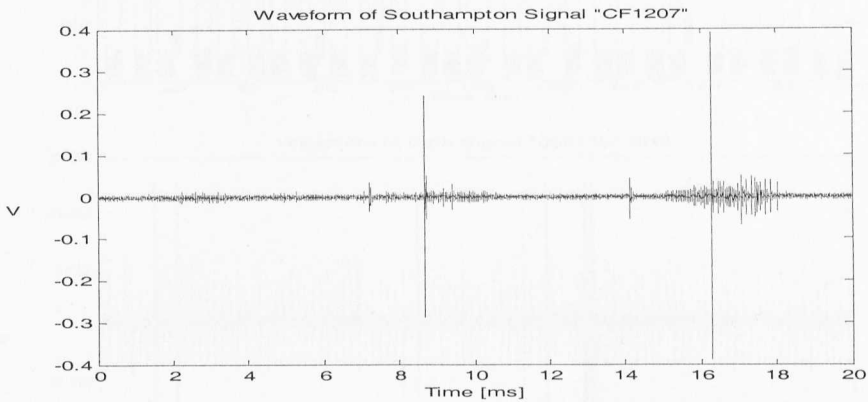
Figure 4.24 Southampton RF signal "CF1207" from Northfleet SGT3A

4.4.2.4   Signals from Bath University

The University of Bath also supplied RF signals from the Northfleet site tests in the form of a CD. Although the sample rate of the signals was high (2.5GHz), since the recording time duration was only 0.2ms (1/100 of one cycle), the size of each file in ASCII format was reasonable. Each file had four channels of signals representing V and dV/dt of the reference voltage, PD signal1 (from KEMA probe) and PD signal2 (from Bath Yagi antenna) in sequence.

Figure 4.25 and Figure 4.26 show two examples of such four-channel signals. These results allow a cross correlation between the voltage, KEMA transformer localised and Bath remotely sensed signals to be explored. An initial superficial examination of the

waveforms shows no obviously discernible common features between the four channels but a more careful investigation with signal processing is warranted.

(a)

(b)

(c)

(d)
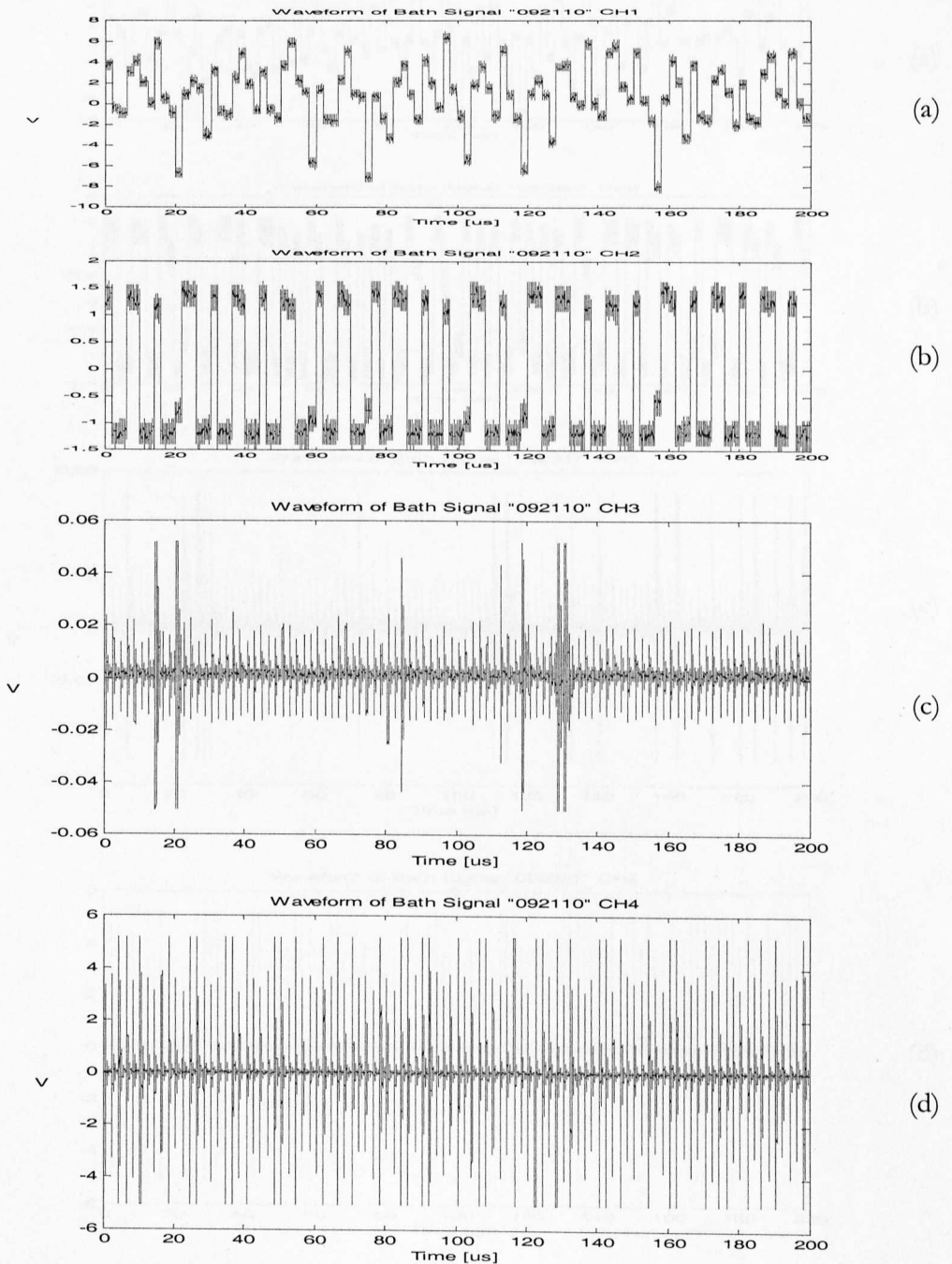
Figure 4.25 Bath RF signal "092110" from Northfleet SGT3A
(a) V of reference voltage, (b) dV/dt of reference voltage
(c) KEMA probe signal, (d) Bath Yagi antenna signal
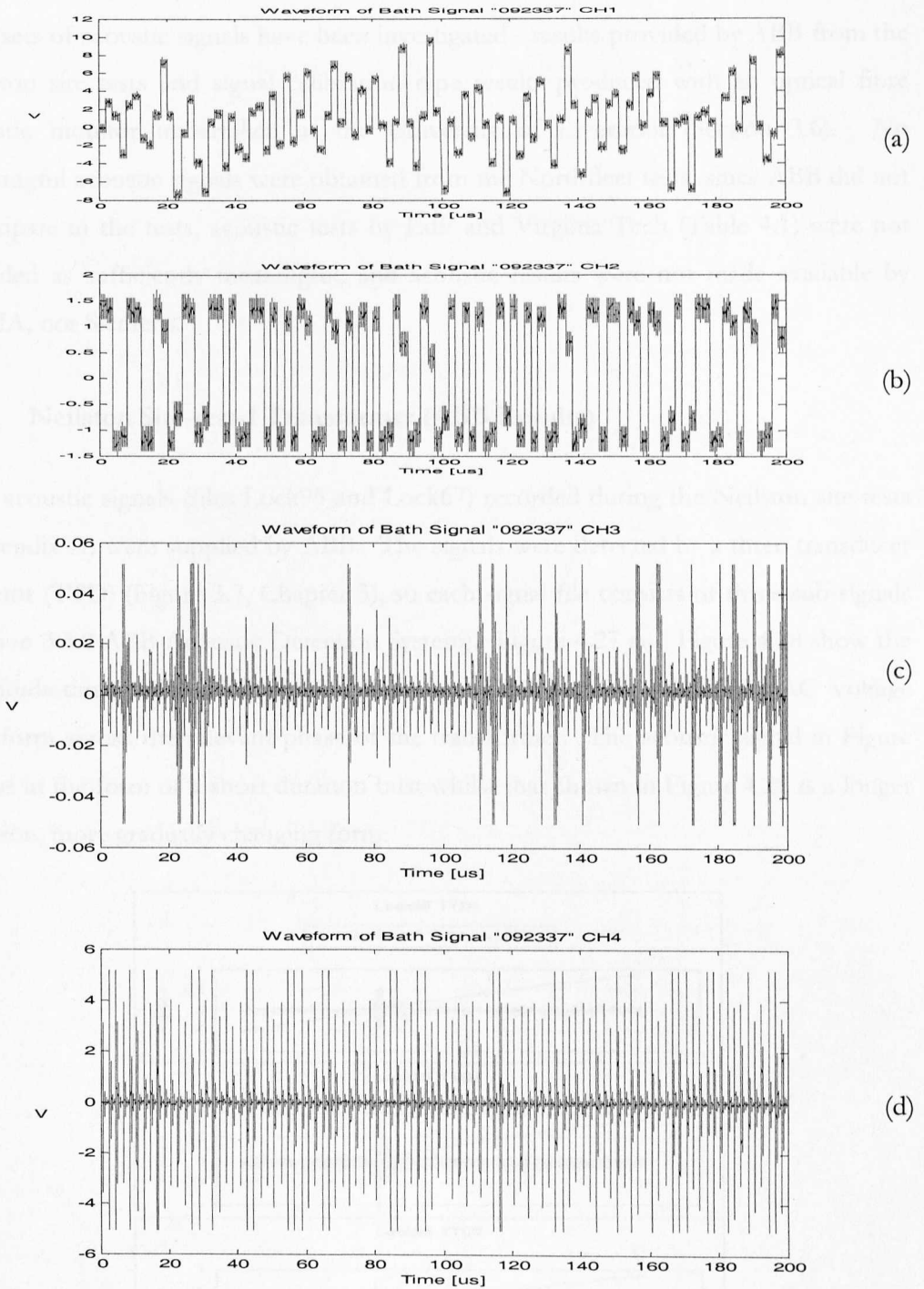
Figure 4.26 Bath RF signal "092337" from Northfleet SGT3A
(a) V of reference voltage, (b) dV/dt of reference voltage
(c) KEMA probe signal, (d) Bath Yagi antenna signal

4.5 Acoustic Emissions Results

Two sets of acoustic signals have been investigated - results provided by ABB from the Neilston site tests and signal calibration type results produced with an optical fibre acoustic monitor undertaken at the University of Liverpool (Section 3.6). No meaningful acoustic signals were obtained from the Northfleet tests, since ABB did not participate in the tests, acoustic tests by EdF and Virginia Tech (Table 4.1) were not regarded as sufficiently meaningful, and acoustic results were not made available by KEMA, nor Siemens.

4.5.1 Neilston Site-test-1 Transformer (ABB Results)

Two acoustic signals (files Lock95 and Lock67) recorded during the Neilston site tests (Appendix A) were supplied by ABB. The signals were detected by a three-transducer detector (TTD) (Figure 3.7, Chapter 3), so each signal file consists of three sub-signals (Section 3.5.2 ABB Acoustic Detection System). Figure 4.27 and Figure 4.28 show the amplitude-time orthogonal plot of the two signals along with 50Hz AC voltage waveform across the relevant phase of the transformer. The acoustic signal in Figure 4.27 is in the form of a short duration bust whilst that shown in Figure 4.28 is a longer duration, more gradually changing form.
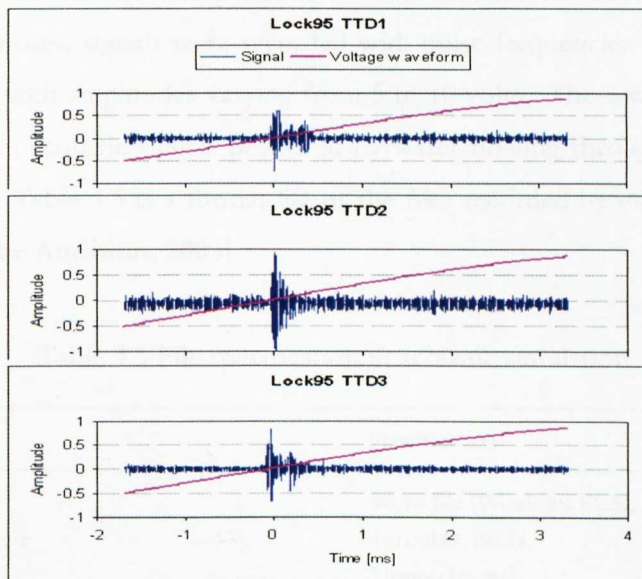
Figure 4.27 ABB acoustic signal "Lock95" from Neilston SGT4
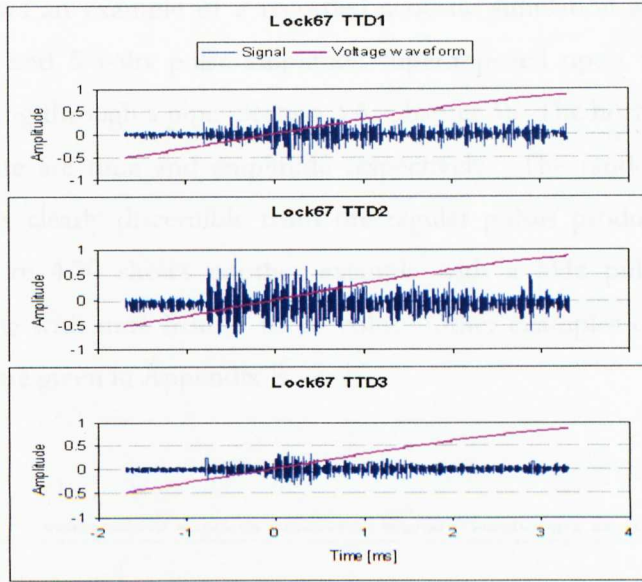
Figure 4.28 ABB acoustic signal "Lock67" from Neilston SGT4

4.5.2   Acoustic Simulation

Laboratory tests with an optical fibre acoustic probe were undertaken at the University of Liverpool laboratories to explore the interactivity of pulsatile and periodic acoustic signals in order to aid the interpretation of the transformer acoustic signals. For comparison purposes, signals were recorded with pulse frequencies set at 1, 5 and 10 Hz respectively, with amplitudes varying from 5 to 10 volts. These were superimposed upon the random acoustic signals produced by water flowing through a pipe (Section 3.6, Chapter 3). Table 4.5 is a format list of the files recorded by using software Cool Edit 2000 **[Adobe Audition, 2003]**.

Table 4.5 File specification in acoustic simulation

Item	Specification
File type	Wave file (Windows PCM, *.wav)
Sample rate	44100Hz, 8kHz
Channel	Mono-channel
Resolution	32-bit

Figure 4.29 shows an example of a recorded acoustic simulation signal, with a 1Hz pulse frequency and 5 volts pulse amplitude superimposed upon an acoustic signal from water flowing through a pipe (Section 3.6, Chapter 3). The horizontal and vertical axes of the figure are time and amplitude respectively. The random water induced acoustic signal is clearly discernible from the regular pulses produced by the signal generator. Figure 4.30 shows another example with a 5Hz pulse frequency and amplitude varying with time from 5 to 10 volts. Other examples of such calibration acoustic signals are given in Appendix E.
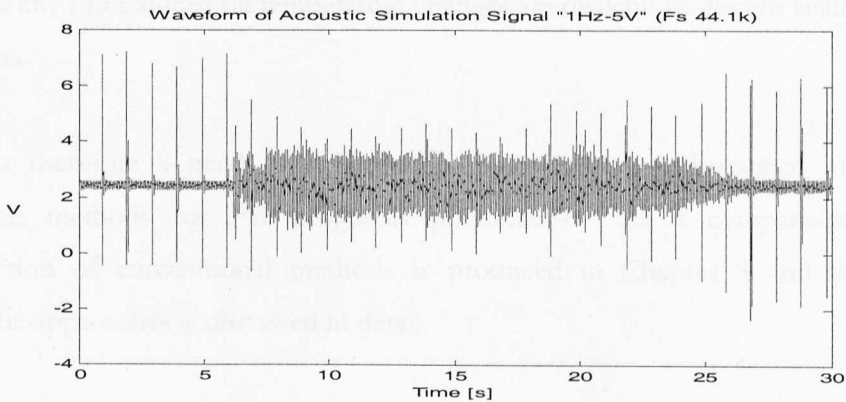
Figure 4.29 Acoustic simulation signal "1Hz-5V"
(Pulse: 1Hz, 5V)
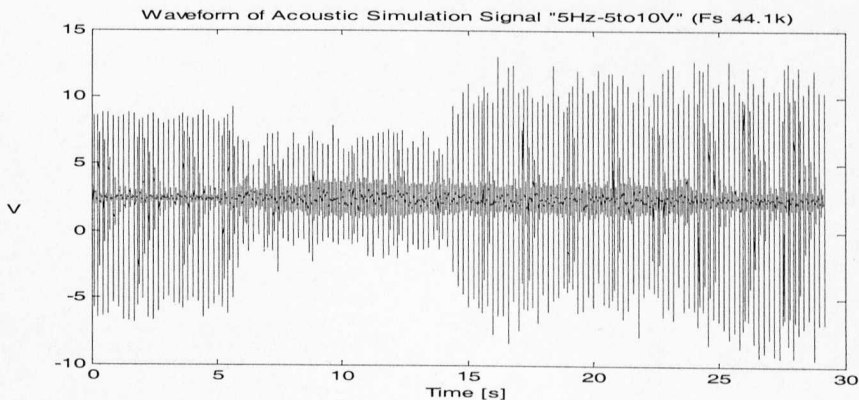
Figure 4.30 Acoustic simulation signal "5Hz-5to10V"
(Pulse: 5Hz, 5~10V)

4.6 Summary

Some typical raw data/signals for DGA, temperature, electrical/RF emissions and acoustic emissions obtained from four different sources have been presented. The DGA data was in the form of measurements from a number of transformers including NGT in-service transformers, First Hydro in-service transformers and site-test transformers. Superficial inspection of this gas concentration data does not yield any obvious trends, which could be useful for prognosis purposes. Similarly the electrical/RF and acoustic signals obtained from site tests are inspected, it is difficult to distinguish PD initiated pulses and impossible to characterise or classify the PD pulses. Likewise any PD induced oil temperature changes are difficult to discern against diurnal variations.

There is therefore a need to explore the use of more sophisticated information extraction methods for PD prognosis possibilities. As a comparison, a brief introduction of conventional methods is produced in Chapter 5 and the use of chromatic approaches is discussed in detail.

<div align="right">

Chapter 5

</div>

Analysis of Results

5.1   Introduction

This chapter is concerned with analysing the complex series of test data presented in Chapter 4. Traditionally, the DGA data is usually presented in one or more orthogonal plots as different shaped/coloured curves corresponding to different gas components (Chapter 4) **[Waters, 2001]**. As mentioned, such a superficial inspection is difficult to extract information for PD prognosis. Later development of IEC/IEEE code for DGA is based on ratios of different pairs of gases **[ANSI, 1992]**. And new techniques such as fuzzy logic, neural networks etc. attempts have been made to improve DGA according to the above code in recent years **[Cao et al., 1993; Su et al., 2000; Guardado et al., 2001; Yang et al., 2001; Ahmad et al., 2002]**. However, the complicated relationship between the code and fault condition, and the uncertain completeness of ratios enumeration result in suspect outcomes. Furthermore, the untraceable process in the "black box" of the new techniques emphasizes the uncertainty of those attempts.

In the aspect of characterisation of electrical/RF PD signals, the development of various methodologies is still undergoing in many research institutions **[Hampton et al., 1988; Bargigia et al., 1992; Pearson et al., 1995; Kemp, 1995; Hamilton et al.,**

1997; Rutgers et al., 1997; Judd et al., 2000; Russwurm, 2000; Ma et al., 2002a; Ma et al., 2002b]. And acoustic diagnostic method is mainly for locating the PD source [Ogihara, 1964; Lundgaard, 1992a; Lundgaard, 1992b; Bozzo et al. 1995; Eleftherion, 1995; Bengtsson et al., 1997] rather than PD characterisation.

Thus, it is being addressed using the chromatic processing techniques described in Chapter 2. The chromatic techniques, which are derived from colour science with sophisticated theory, has advantages of simple algorithm and traceable processing. It also has been practically applied on monitoring of HV circuit breaker, combined heat power plant and environmental condition [Jones et al., 2000; Brazier et al., 2001]. For this research project, the manner in which the chromatic processing needs to be applied to each of the different types of signals (DGA, temperature, electrical/RF emissions and acoustic emissions) is first described in Section 5.2. Thereafter the approach is deployed for interpreting the various signals in the order which they have been presented in Chapter 4 i.e. DGA, temperature, electrical/RF emissions and acoustic emissions.

5.2 Chromatic Processing Applied to Various Signals

5.2.1 Resume of Methodology

As detailed in Section 2.3, with the application of tristimulus processing the signal domain is divided into 3 sectors. These three domains yield three outputs (R, G and B) which are treated algorithmically to yield signal identifying parameters based on dominating domain value (H), nominal signal strength (L) and effective signal bandwidth/spread (S). The results are usefully presented on a chromatic map (H-S and H-L polar plots) as already described in Chapter 2 Section 2.3.

5.2.2 DGA Data Processing

The chromatic methodology deployed with tristimulus filter (R, G and B), which was described in Section 2.3.2 has been applied to the DGA data sets presented in Section 4.2. For this purpose, the three main transformer degradation conditions (Table 3.1) –

cellulose decomposition, oil overheated and electrical discharge activity are assigned each to the three non-orthogonal chromatic processor domains R, G and B as shown in Figure 5.1. The corresponding H-S and H-L polar plots are shown in Figure 5.2. Thus sector $0 \sim 90°$ encompasses the dominance of H_2, C_2H_2, C_2H_4 (electrical stress sector), $90° \sim 180°$ the dominance of C_2H_4, C_2H_6, CH_4 (oil heated sector), $180° \sim 270°$ the dominance of CH_4, CO, CO_2 (cellulose decomposing sector). The S value indicates the spread of gases produced ($S=1$ corresponding to a single gas) whilst the L value indicates the extent of gassing produced. A hue angle of $180°$ suggests that CH_4 may dominate if $L \rightarrow 1$.
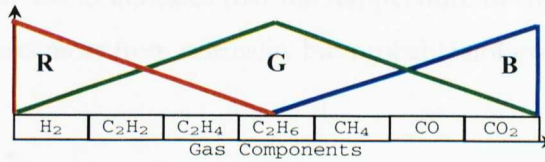
Figure 5.1 Configuration of tristimulus filter in DGA
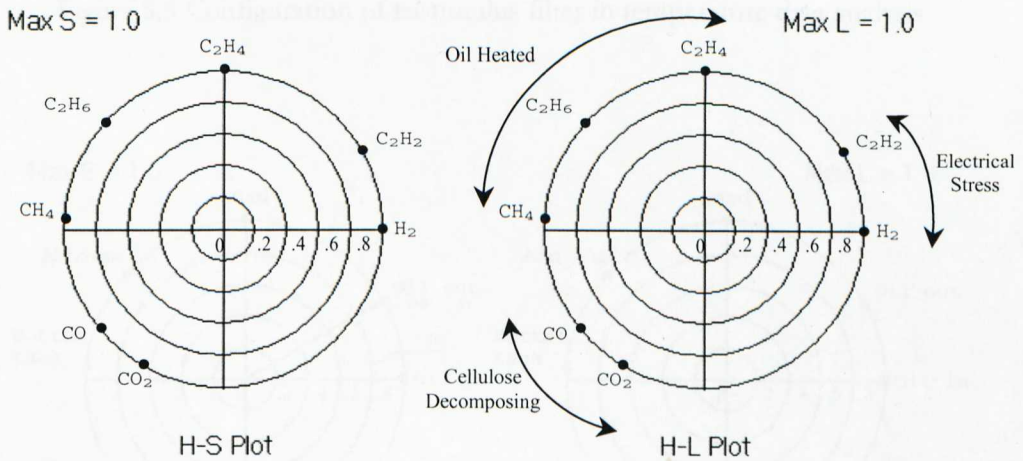
Figure 5.2 Dominant gas species represented by hue angle

For practical deployment the need is to identify firstly whether there is significant gas produced (i.e. L greater than a threshold) and then the extent to which the gas is of a single or mixed components (i.e. S greater than a predetermined threshold).

5.2.3   Temperature Signatures Processing

The chromatic processing of discrete data described in Section 2.3.2 has been deployed with tristimulus filters (R, G and B) to the temperature results presented in Section 4.3. For this purpose, the various factors listed in Table 3.2 (Chapter 3) have been clustered into R (oil in, oil out, load), G (ambient temperature plus all other factors) and B (bottom tank, top tank2, top tank1) as shown in Figure 5.3. The corresponding hue angle, factor calibration is given in Figure 5.4. Thus a hue angle of 180° with $S \rightarrow 1$ means that the bottom tank temperature shows the greatest departure from normality, whilst the condition $S \approx 0$ indicates that the whole system is operating near normal. A hue angle of 30° with $S \approx 0.5$ indicates that the temperature of the oil circulated out of the transformer departs most from normality but probably not excessively so.
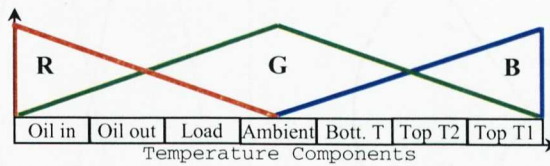
Figure 5.3 Configuration of tristimulus filter in temperature data analysis
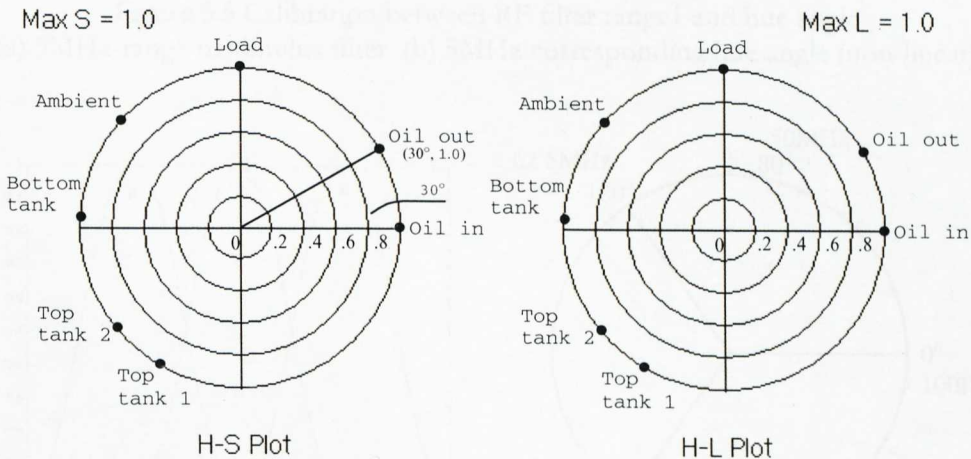
Figure 5.4 Dominant temperature factors represented by hue angle

5.2.4   Eletrical/RF Signal Processing

For the purpose of PD pulse detection and identification, the chromatic methodology deployed with tristimulus filters (R, G and B) for continuous signal processing, which was described in Section 2.3.1, has been applied to the electrical and RF signals presented in Section 4.4. In this case the parameter axis is radio frequency and three Gaussian processors are deployed non-orthogonally to cover the entire frequency range monitored (Figure 5.5(a) 100Hz~5MHz, Figure 5.6(a) 100Hz~125MHz, Figure 5.7(a) 100Hz~1.25GHz, the lower end covered from 100Hz is to avoid the interference with the power frequency, which is about 50Hz).

(a)   (b)
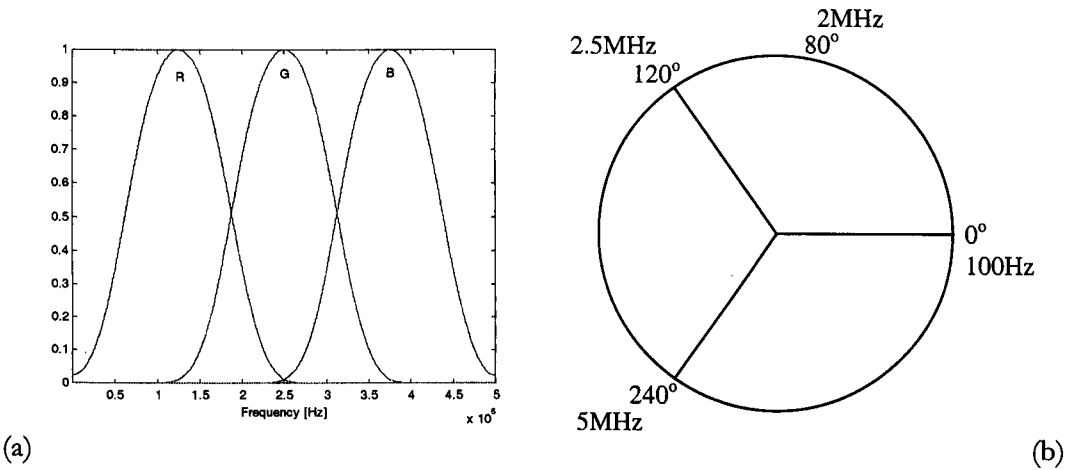
Figure 5.5 Calibration between RF filter range1 and hue angle
(a) 5MHz-range tristimulus filter (b) 5MHz corresponding hue angle (non-linear)

(a)   (b)
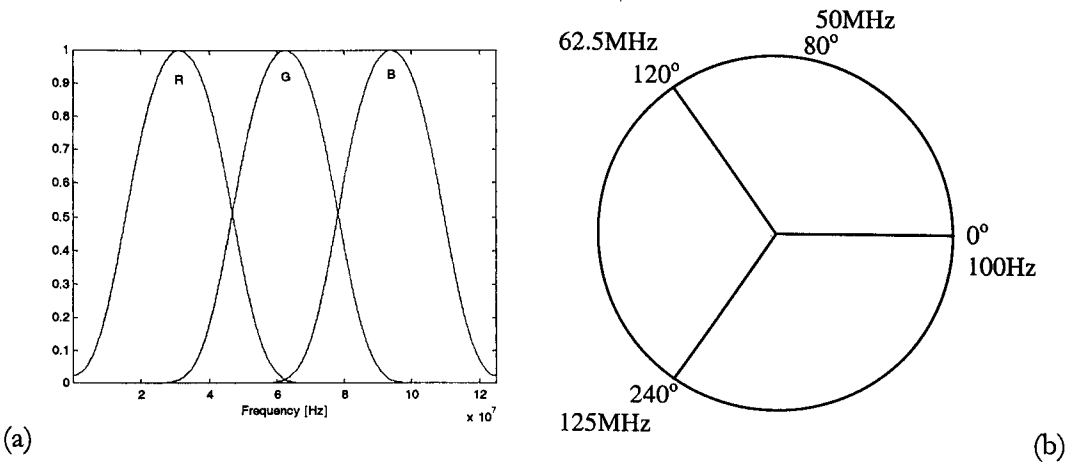
Figure 5.6 Calibration between RF filter range2 and hue angle
(a) 125MHz-range tristimulus filter (b) 125MHz corresponding hue angle (non-linear)
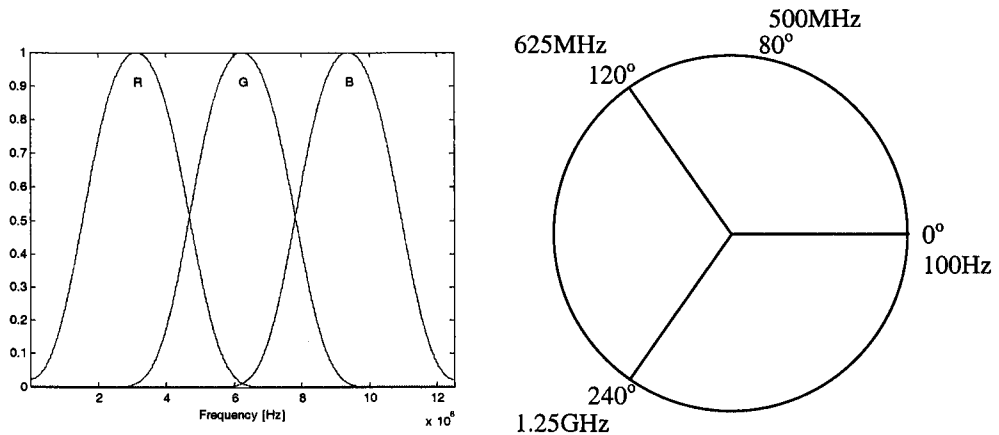
(a)   (b)

Figure 5.7 Calibration between RF filter range3 and hue angle
(a) 1.25GHz-range tristimulus filter (b) 1.25GHz corresponding hue angle (non-linear)

The corresponding *H* polar diagrams are shown in Figure 5.5(b), Figure 5.6(b) and Figure 5.7(b) respectively, from which the non-linear relationships between hue angle and dominant frequency can be extracted. The variations of *H*, *L* and *S* (dominating frequency, effective signal strength and nominal signal bandwidth) with time can then be produced to characterise the time variation of the signals.

5.2.5   PD Pulse Processing

The chromatic methodology deployed with tristimulus filters (R, G and B) for discrete data processing, which was described in Section 2.3.2, may be applied for processing the PD pulse/event data. The data consists of a number of PD occurrences according to the magnitude of the electric charge in pico Coulomb (pC) during each quarter phase of the 50Hz AC waveform (i.e. $0°\sim90°$, $90°\sim180°$ etc.). Figure 5.8 shows the manner in which filters were applied to the discharges data which is presented in tabular form whereby individual discharges are classified according to the charge magnitude (pC) and waveform sector $(x°)$.   H-S and H-L polar plots may then be produced for characterisation and classification purposes as shown in Figure 5.9. These show the calibration of hue angle in terms of charge (pC) i.e. $0°\sim90°$ corresponding to $25\sim35$pC, $90°\sim180°$ corresponding to $40\sim55$pC, $180°\sim270°$ corresponding to $60\sim75$pC.

	25pC~	30pC~	35pC~	40pC~	45pC~	50pC~	55pC~	60pC~	65pC~	70pC~	◄── Magnitude
0 ~ 90°	9	4	5	7	18	6	7	1	12	2	
90~180°	0	0	0	0	0	0	0	0	0	0	no. of PD
180~270°	11	12	2	13	11	8	5	8	9	1	
270~360°	0	0	0	0	0	0	0	0	0	0	
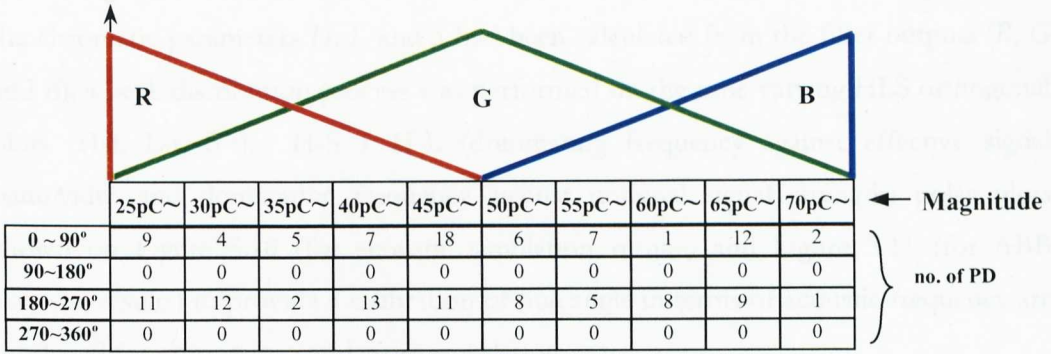
Figure 5.8 Tristimulus filter applied to PD events statistical data
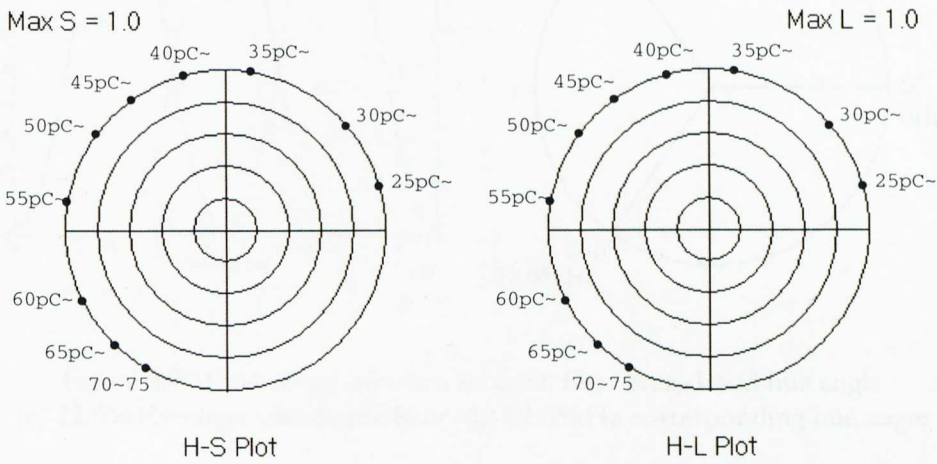
Figure 5.9 Chromatic map for PD events characterisation

Thus a hue angle of approximately 90° and $S \approx 1$ implies a dominating charge magnitude of 35pC with very little other charge activity. If additional $L \rightarrow 1$ the implication is that the 35pC discharges are well above normal. Conversely $S \rightarrow 0$ indicates a normal distribution of discharge activity being relatively insignificant if $L \approx 0$ but considerable if $L \rightarrow 1$.

5.2.6 Acoustic Signal Processing

The continuous signal processing technique described in Section 2.3.1 and already deployed for RF signals processing (Section 5.2.4) may also be used for acoustic signal

processing. However, since the acoustic signals were noisier than the RF signals, after the chromatic parameters *H*, *L* and *S* had been calculated from the filter outputs (*R*, *G* and *B*), a peak distribution process was performed on the time varying HLS orthogonal plots (H-t, L-t, S-t). H-S / H-L (dominating frequency against effective signal bandwidth and dominating frequency against nominal signal strength) polar plots shown on Figure 5.10 (for acoustic simulation results) and Figure 5.11 (for ABB acoustic results) to provide a calibration of hue angle in terms of acoustic frequency are produced for comparison and cross correlation.
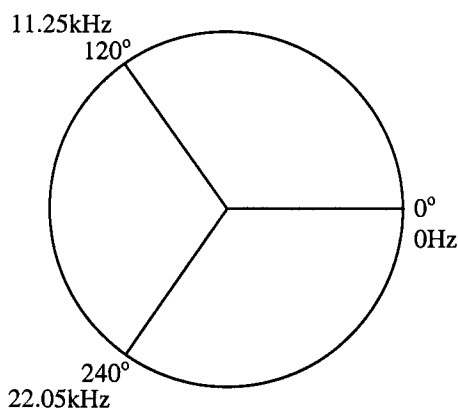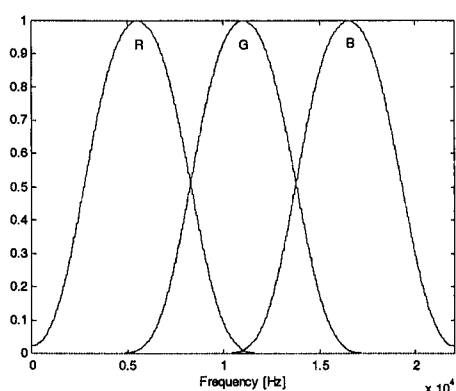
(a)   (b)

Figure 5.10 Calibration between acoustic filter range1 and hue angle
(a) 22.05kHz-range tristimulus filter (b) 22.05kHz corresponding hue angle
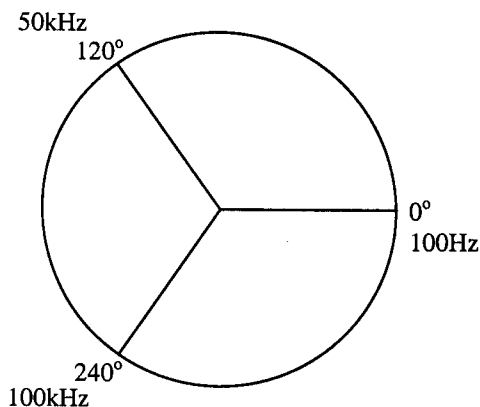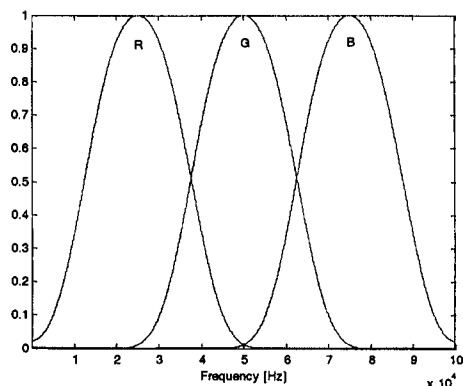
(a)   (b)

Figure 5.11 Calibration between acoustic filter range2 and hue angle
(a) 100kHz-range tristimulus filter (b) 100kHz corresponding hue angle

5.3   Chromatically Processed DGA Results

The techniques described in Section 5.2.2 are applied for chromatically processing the DGA results of NGT in-service transformers, First Hydro in-service transformers, site-test-1 transformer Neilston SGT4 and site-test-2 transformer Northfleet SGT3A.

5.3.1   NGT In-service Transformers

Chromatic results for transformer WYLF1mtb, which has operated for more than thirty years, are shown in Figure 5.12. Note that the maximum of the saturation is 1.0 with one circle in the H-S plot being 0.2. However, for better focusing on the data points, the maximum scale of the lightness map is set to 0.5 with one circle in the H-L plot representing 0.1. The entire set of data (28/08/1980 ~ 29/06/1999) has been included in the diagram, which so illustrates the degree of information compression, which is achievable with the approach.

The triangle in the H-S plot indicates the initial condition i.e. the first sampled record (28/08/1980) of the seven dissolved gases for the transformer, and the circle indicates the end point (29/06/1999). The curve passing through the points represents the time progression between start and end.

To interpret the chromatic results, it is advisable to proceed in the following order:

1) The L magnitude needs to be observed to determine the level of gas production.

2) The H value needs to be considered to determine which gas dominates.

3) The S value needs to be considered to determine the spread of gas types emitted.

It is clear for transformer WYLF1mtb that the L level is low (<0.1) indicating only low levels of gases production. Of these CH_4 is dominant throughout the sampled duration. This implies that the oil was probably being overheated above 150 °C, but there seems to be no serious partial discharges or arcing (i.e. no high level of H_2 and C_2H_2, Table 3.1). The implication is of a relatively safe status.
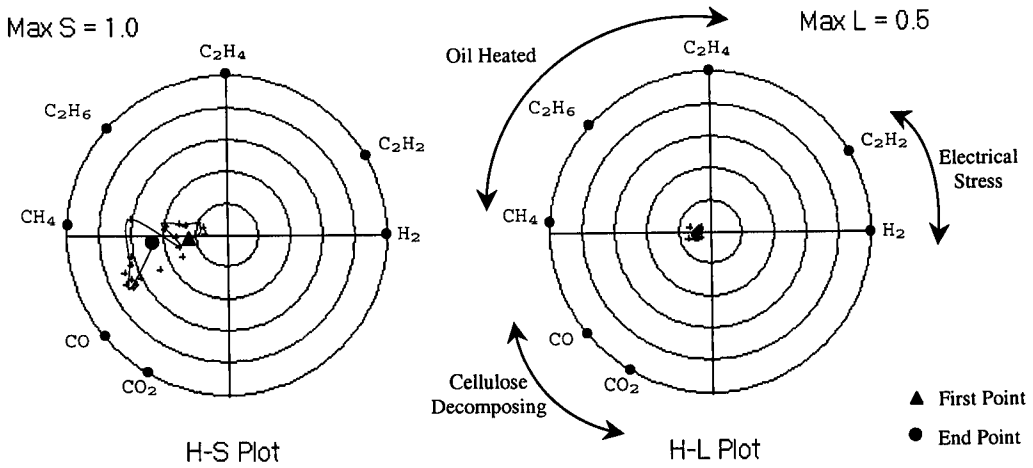
Figure 5.12 DGA chromatic map of transformer WYLF1mtb
(Sampled 28/08/1980 ~ 29/06/1999) ($S=0$~1, $L=0$~0.5)

Figure 5.13 shows the processed results for transformer BOLN3mtb. The H-L plot shows that although the L value remains low (<0.27), there is a clear change to the electrical stress area (C_2H_2) beyond about the year 1990. The H-S plot shows that the electrical stress component C_2H_2 dominates with a maximum-recorded value of $S\approx0.8$ and a subsequent reduction of S to about 0.3. Thus although there has been a decrease in L, nonetheless C_2H_2 (indicating electrical stress) remains dominant. This suggests that there is a need to maintain a watching brief on this transformer.
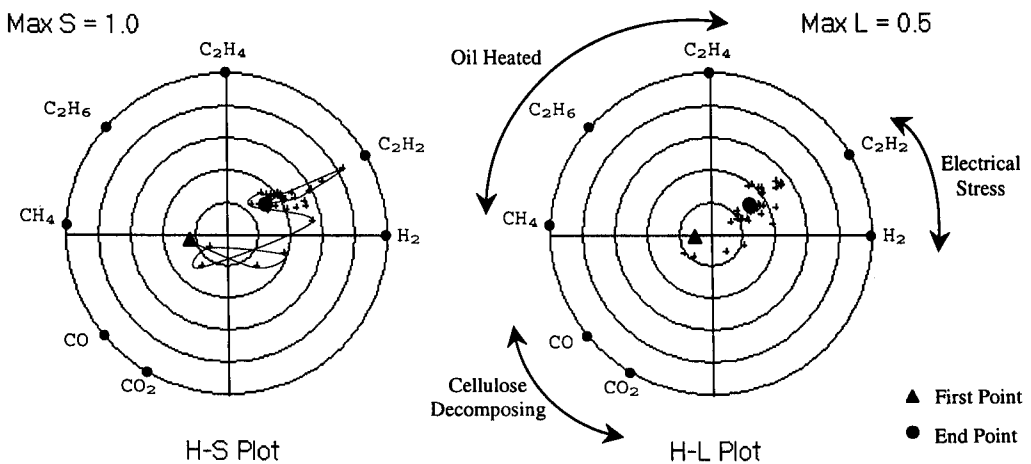
Figure 5.13 DGA chromatic map of transformer BOLN3mtb
(Sampled 23/09/1985 ~ 30/11/1998) ($S=0$~1, $L=0$~0.5)

5.3.2   First Hydro In-service Transformer

Figure 5.14 shows chromatically processed results for a First Hydro transformer plotted in the same manner as the NGT results in Section 5.3.1. The time at which a sample was taken is colour-coded – dark blue 1990 through yellow 1997 to brown 2001. Thus the first point is indicated by a dark blue triangle, the end point by a brown circle. During the life of the transformer there were outages and the oil was reconditioned. The occurrence of these events is designated by a coloured hollow circle and the last record prior to that is designated by a coloured hollow triangle. For example, the oil reconditioning on 08/09/95 is designated by a hollow light blue circle and the last record before that event by a hollow light blue triangle. The yellow open circle and triangle correspond to a similar process on 09/09/97.
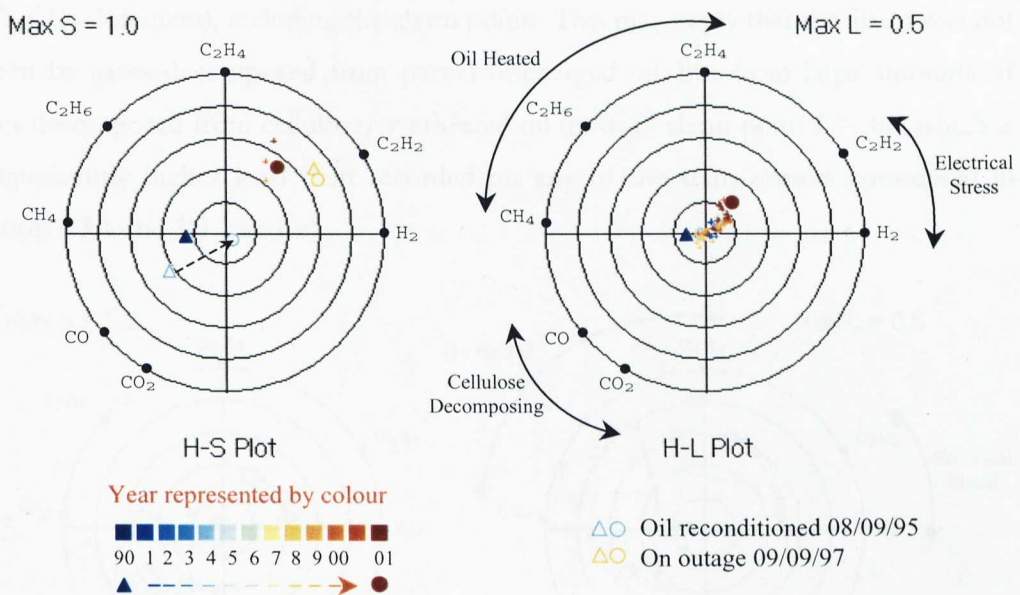
Figure 5.14 DGA chromatic map of transformer FFES SGT1
(Sampled 22/10/1990 ~ 28/10/2001) ($S=0\sim1$, $L=0\sim0.5$)

The H-L plot shows that although the L value remains about 0.1, there is a clear change to the electrical stress area (H_2-C_2H_2) beyond about the year 2000. This suggests that there is a need to maintain a watching brief on this transformer. The H-S plot shows that for the significant concentration results ($L \geq 0.1$) the electrical stress component C_2H_2 dominates with a value of $S \approx 0.6$. The oil recondition in 1995 did reset the

condition to the origin. Thereafter the points changed to the electrical stress area step by step. The 1997 oil "outage" does not seem to have had a pronounced rehabilitation effect. However all the points before/at the oil recondition and outage have a lightness less than 0.1.

5.3.3 Neilston Site-test-1 Transformer

Figure 5.15 shows the chromatic map (H-S and H-L polar plots) for transformer Neilston SGT4, which according to site experience (Section 4.2.3) is an example of an imminently faulty unit (triangle – initial condition, circle – end point, square points – samples just after a Buchholz alarm). From both the H-S and H-L plots all points sampled until an alarm occurred in 1997 are located in the cellulose decomposition area (CO, CO_2 dominant), including the alarm point. This may imply that the alarm was not driven by gases decomposed from partial discharged oil, but from large amounts of gases decomposed from cellulose/overheated oil (note 1st alarm point $L = 0.4$ which is a significantly higher level than recorded on any of the transformers considered in Section 5.3.1 and 5.3.2 above).
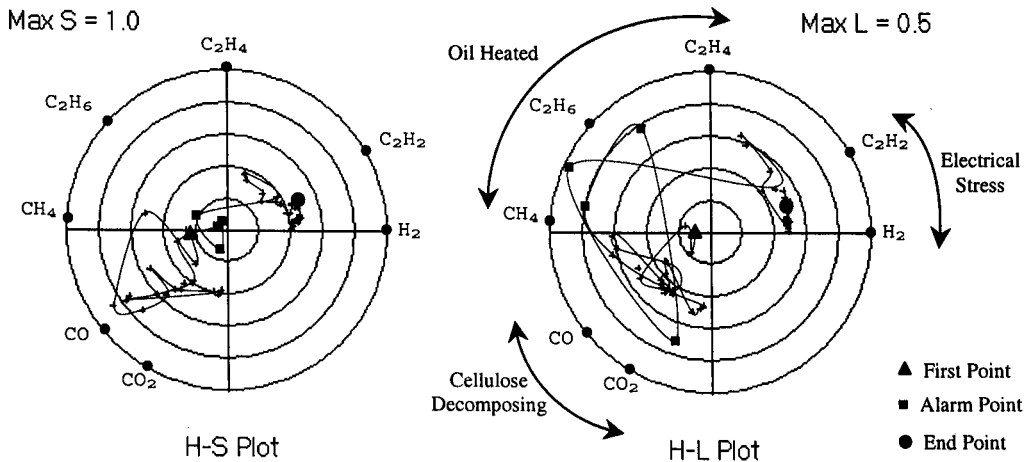
Figure 5.15 DGA chromatic map of transformer Neilston SGT4
(Sampled 29/11/1977 ~ 28/06/2001) (S=0~1, L=0~0.5)

However, the later alarm points represent a change in the deteriorating progression with movement into the C_2H_2 and H_2 sector. The low S value (≤ 0.2) indicates that

there is probably a spread of gases with almost equal amounts of CO, CO_2 and C_2H_2, H_2; the large L values (0.35~0.5) indicates copious gas production. After the alarm, the C_2H_2 and H_2 gases become dominant ($S \approx 0.4$) but with other gases also present; an L value of about 0.25~0.3 represents a level of concern particularly when located in the C_2H_2, H_2 sector which is indicative of excessive discharge activity. The vigorous excursion of the locus of the dominant points is also indicative of the relative volatility in the gases being produced both in nature and quantity. This suggests that the transformer condition was deteriorating further after the alarm; partial discharges appear to have occurred frequently especially during the site tests with this transformer.

5.3.4 Northfleet Site-test-2 Transformer

Figure 5.16 shows the chromatically processed DGA results for the transformer Northfleet SGT3A, which was being tested during 18th~23rd May 2002. Due to no dissolved gases results being available from these latter tests, only historical data points have been analysed up to 18/02/2002. The results are colour coded according to the date of acquisition, with the colour code being given below the diagram.
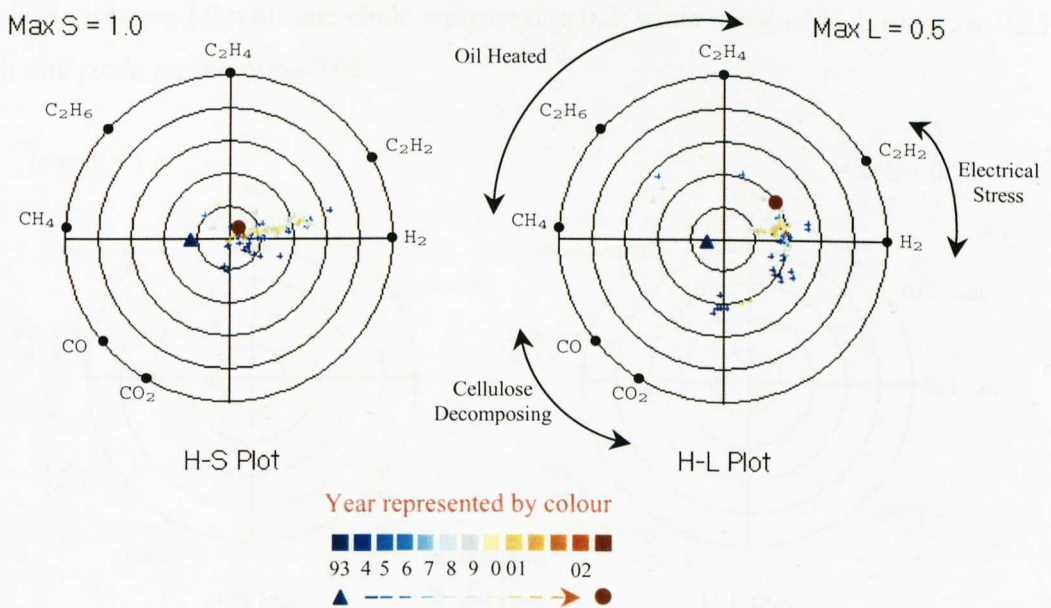
Figure 5.16 DGA chromatic map of transformer Northfleet SGT3A
(Sampled 26/08/1993 ~ 18/02/2002) (S=0~1, L=0~0.5)

The chromatic map of Northfleet SGT3A show a similar layout to that of BOLN3mtb in Figure 5.13. On the H-L plot, the L value remains about 0.2~0.3, and most of the results lie in the electrical stress area (H_2). The examination of the H-S plot shows that the electrical stress components (C_2H_2-H_2) dominate with a maximum value of $S \approx 0.65$ and a subsequent reduction of S to about 0.1. Thus although there has been a decrease in S, nonetheless C_2H_2-H_2 dominant with considerable level. This also suggests a need to maintain a watching on this transformer.

5.4   Chromatically Processed Temperature Results

The temperature data presented in Section 4.3 (Chapter 4) for the transformer tank and oil have been chromatically processed using the methods described in Section 5.2.3 "Temperature Signatures Processing". The deployment of the various parameters monitored within clusters associated with each chromatic processor is as already described in Figure 5.3 (Section 5.2.3). The components of these clusters are also indicated on the hue axis of the resulting H-S, H-L polar plots. Various combinations of parameters have been explored and these are shown in Figure 5.17, Figure 5.18 and Figure 5.19 for the temperature results included in the spread sheet of Figure 4.7 and covering a time period of 7th~19th July 1999. On these figures the maximum scales of the H-S plots are 1.0 with one circle representing 0.2, while those of H-L plots are 0.25 with one circle representing 0.05.
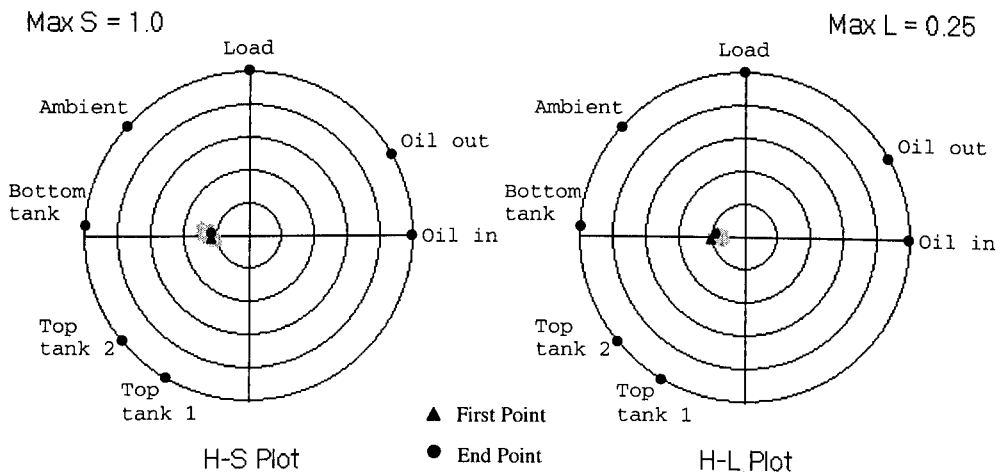
Figure 5.17 Temperature data analysis in arrangement 1
(oil in, oil out, load/ load, ambient, bottom tank/ bottom tank, top tank2, top tank1)
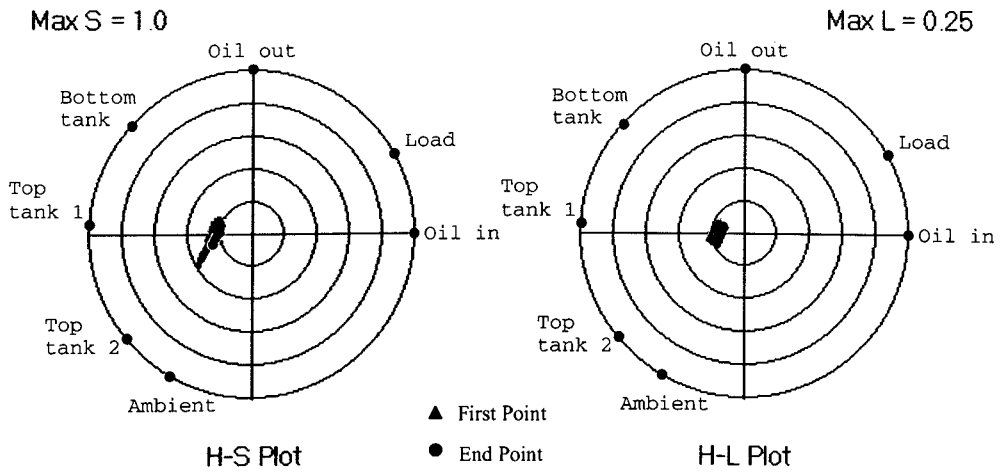
Figure 5.18 Temperature data analysis in arrangement 2
(oil in, load, oil out/ oil out, bottom tank, top tank1/ top tank1, top tank2, ambient)
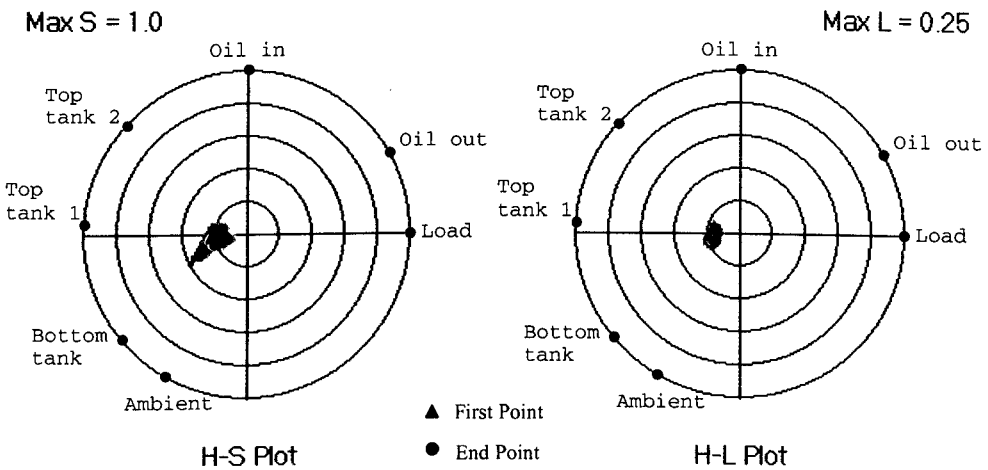
Figure 5.19 Temperature data analysis in arrangement 3
(load, oil out, oil in/ oil in, top tank2, top tank1/ top tank1, bottom tank, ambient)

The data points in Figure 5.17 vary within a small area around the initial point ($L{\approx}0.05$, $S{\approx}0.2$) with the first and end points aligning closely. This indicates a normal operation situation based on the seven factors. It is consistent by the similar results obtained by rearranging the clusters as shown in Figure 5.18 and Figure 5.19. No predominant component exists. The hue value varies around 180 degree, saturation oscillates without exceeding circle of 0.4 and lightness values are almost within the 0.05 circle.

Table 5.1 shows the extent of the excursions in *H*, *L* and *S*. The consistency between the values regardless of the clustering selected is self-evident.

Table 5.1 HLS value distributions in temperature analysis

| | Hue value | | Lightness value | | Saturation value | |
	Minimum	Maximum	Minimum	Maximum	Minimum	Maximum
Arrangement 1	168	198	0.0254	0.0503	0.177	0.305
Arrangement 2	156	212	0.0260	0.0511	0.174	0.376
Arrangement 3	159	212	0.0257	0.0514	0.083	0.383

5.5   Chromatically Processed Electrical/RF Results

Given the wide diversity of electrical and RF measurements produced by the various test participants (Table 4.1 KEMA, Glasgow Caledonian, UMIST, Southampton, Bath), a number of different deployments of the chromatic methodology have been used as indicated in Section 5.2. Thus the chromatic methodology for discrete data analysis (Section 2.3.2) has been used for PD pulse/event characterisation and classification (Section 5.2.5) of the Neilston transformer results. On the other hand, the techniques detailed in Section 2.3.1 "Continuous Signal Processing" and Section 5.2.4 "Eletrical/RF Signal Processing" have been used for processing the time-varying electrical/RF PD signals provided by Glasgow Caledonian, UMIST, Southampton and Bath for the Northfleet transformer.

5.5.1   Neilston Site-test-1 Transformer

The PD events presented in Figure 4.10 and Figure 4.11 (Chapter 4) can be recast for convenience on a polar plot with the azimuthal angle representing the phase during a single 50Hz period and the radius representing a normalized PD charge magnitude. Each PD event can therefore be conveniently mapped on such a polar diagram. The results of Figure 4.10 and Figure 4.11 are presented on such polar diagram in Figure 5.20 and Figure 5.21 respectively.
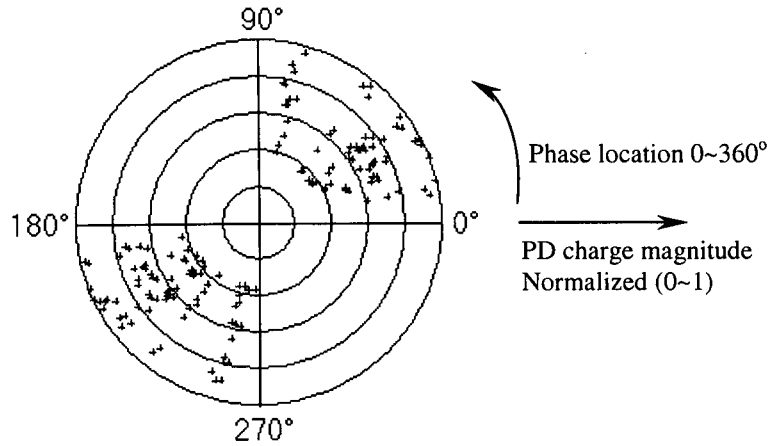
Figure 5.20 Phase resolved PD events polar plot of Neilston "2606n"
(Ref. Figure 4.10 and Appendix A)
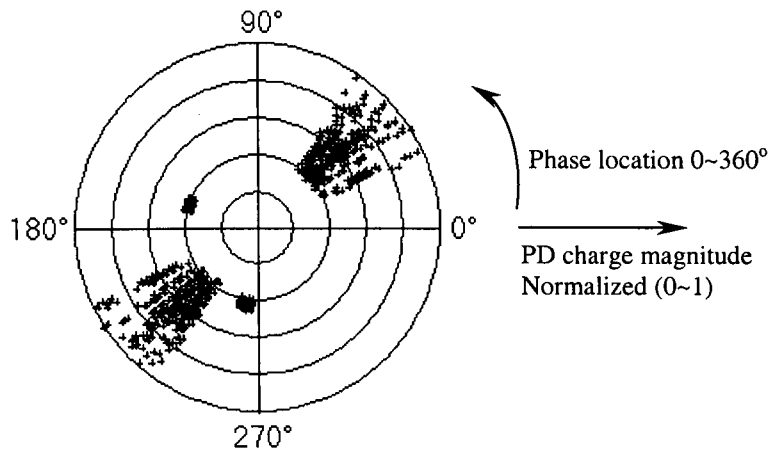
Figure 5.21 Phase resolved PD events polar plot of Neilston "2606o"
(Ref. Figure 4.11 and Appendix A)

These results show that the Figure 5.21 events have a more concentrated phase location, being restricted to two major bands (approx. $30°\sim60°$, $210°\sim240°$ i.e. similar phases on both +ve and -ve going voltages) and two side bands ($H\approx150°$, $L=0.4$; $H\approx260°$, $L=0.4$). In the case of the Figure 5.20 results, the experimental points are more scattered on the H-L plot ($H=10°\sim80°$, $190°\sim260°$) but the phase location on both +ve and -ve going voltage are again similar.

The chromatic approach, which was detailed in Section 5.2.5 "PD Pulse Processing" may be deployed onto PD event data classified according to the magnitude of charge (Figure 5.8) during each quarter phase of the AC waveform, to produce a higher level of data compression (Figure 5.9).

Figure 5.22 shows examples of the extracted results obtained from the raw data of Figure 4.10. The 1st quadrant results are represented by a red triangle, the 2nd quadrant by green square, the 3rd blue pentagon etc. The hue angle gives the PD magnitude, lightness indicates the total number of PD and saturation represents the spread across the charge (PD) categories. For this case, there are no signals for the 2nd and 4th quadrants, so their corresponding points are located at the origin.
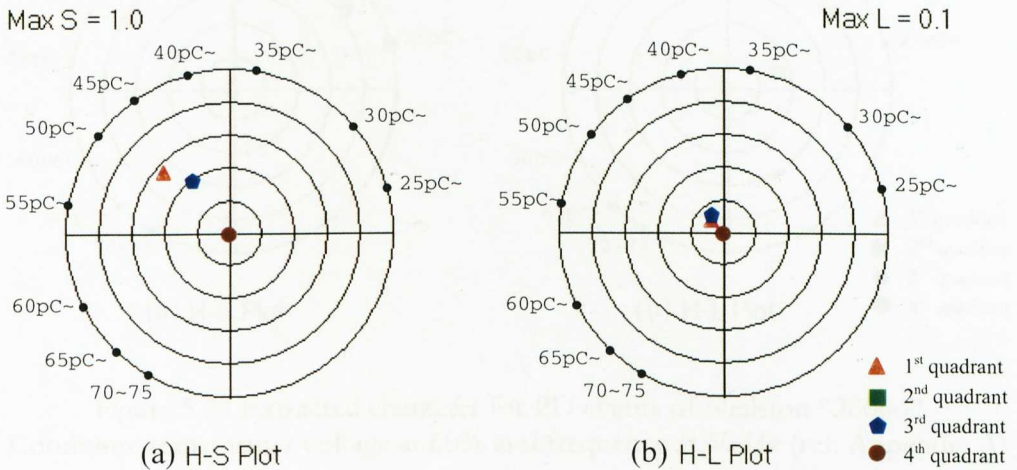
Figure 5.22 Extracted character for PD events of Neilston "2606n"
Condition: transformer voltage at 60% and frequency at 50 Hz (ref. Appendix A)

Comparing the 1st and 3rd quadrants, Figure 5.20 shows that their charge distributions are similar. Figure 5.22(a) shows that charge in the range of 50~55pC is dominant in the 1st quadrant whilst in the 3rd quadrant the dominant charge is 5pC less but with a slightly greater number (larger L, Figure 5.22(b)) and broader spread (smaller S, Figure 5.22(a)). This illustrates how the chromatic technique can quantify the PD events in terms of H, L and S values conveniently whilst retaining the most important signal features.

Figure 5.23 shows the chromatic results extracted from the raw data of Figure 4.11. Since there is no signal for the 4th quadrant, its point is located at the origin. Again the distributions (Figure 5.21) for the 1st and 3rd quadrants are similar to each other except for the second small block in the 3rd quadrant. There is now a cluster of events also in the 2nd quadrant. PD magnitudes of 30~35pC are dominant in both 1st and 3rd quadrants; these have a similar number of PD (L, Figure 5.23(b)) and spread extent (S, Figure 5.23(a)). The 2nd quadrant PDs have a smaller dominant charge (25~30pC), less spread (S, Figure 5.23(a)) and are smaller number (L, Figure 5.23(b)).
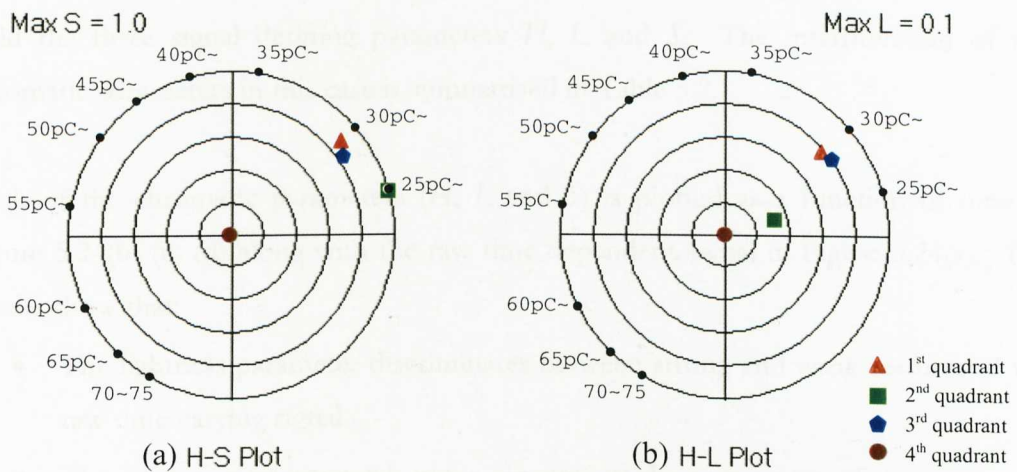
Figure 5.23 Extracted character for PD events of Neilston "2606o"
Condition: transformer voltage at 60% and frequency at 50 Hz (ref. Appendix A)

Comparing the results of Figure 5.22 and Figure 5.23, it may be concluded that:

- Test 2606o has lower levels of dominating discharges than 2606n.

- There is significantly less spread (S) for 2606o (>0.85) than for 2606n (0.4~0.55).

- There are significantly more discharges for 2606o ($L=0.03~0.08$) than for 2606n ($L \approx 0.01$).

Note that test 2606n was performed approximately 5 minutes before 2606o (Appendix A) i.e. it suggests that discharge activity was increasing with time.

5.5.2   Northfleet Site-test-2 Transformer

5.5.2.1   Signals from Glasgow Caledonian University

Figure 5.24 shows the chromatically processed results of signal "C2-10-34-24" (Glasgow Caledonian), which has been shown in raw time varying form previously in Figure 4.13. Figure 5.24(a) is the raw time-varying signal. This has been processed by passing the signal through three broadband non-orthogonal filters (R, G and B) (Figure 5.5(a)) with a window averaging width of 64 bits (6.4us duration). The outputs from the three R, G and B filters are then mathematically processed (Equation (2.6)~(2.8)) to yield the three signal defining parameters H, L and S. The interpretation of the chromatic parameters in this case is summarised in Table 5.2.

Each of the chromatic parameters (H, L and S) is plotted as a function of time in Figure 5.24(b) (c) (d) along with the raw time dependent signal in Figure 5.24(a). The results show that:

- The lightness parameter discriminates between strong and weak features of the raw time varying signal.

- The saturation parameter is more sensitive to the occurrence of some types of pulses compared to others.

- The hue parameter provides a third and finer level of discrimination.

The broad pulse (5~7ms, Figure 5.24(a)) is identifiable via changes in all the chromatic parameters H, L and S. With $S \rightarrow 0$ (Figure 5.24(d)), it is implied that the pulse is highly polychromatic, containing frequencies in the range $H=100°~340°$ (several kHz to 5MHz). The sharp pulse at 4ms preceding the broad pulse (Figure 5.24(a)) is only reflected by changes in L and S (Figure 5.24(c) and (d)), and not H (Figure 5.24(b)). Other narrow pulses apparent on the raw signal (Figure 5.24(a)) are characterised by only changes in S and not H or L (e.g. at 10ms and 17ms). Thus a number of signal events within the 20 ms record window produce different responses on the three chromatic parameters H, L and S.
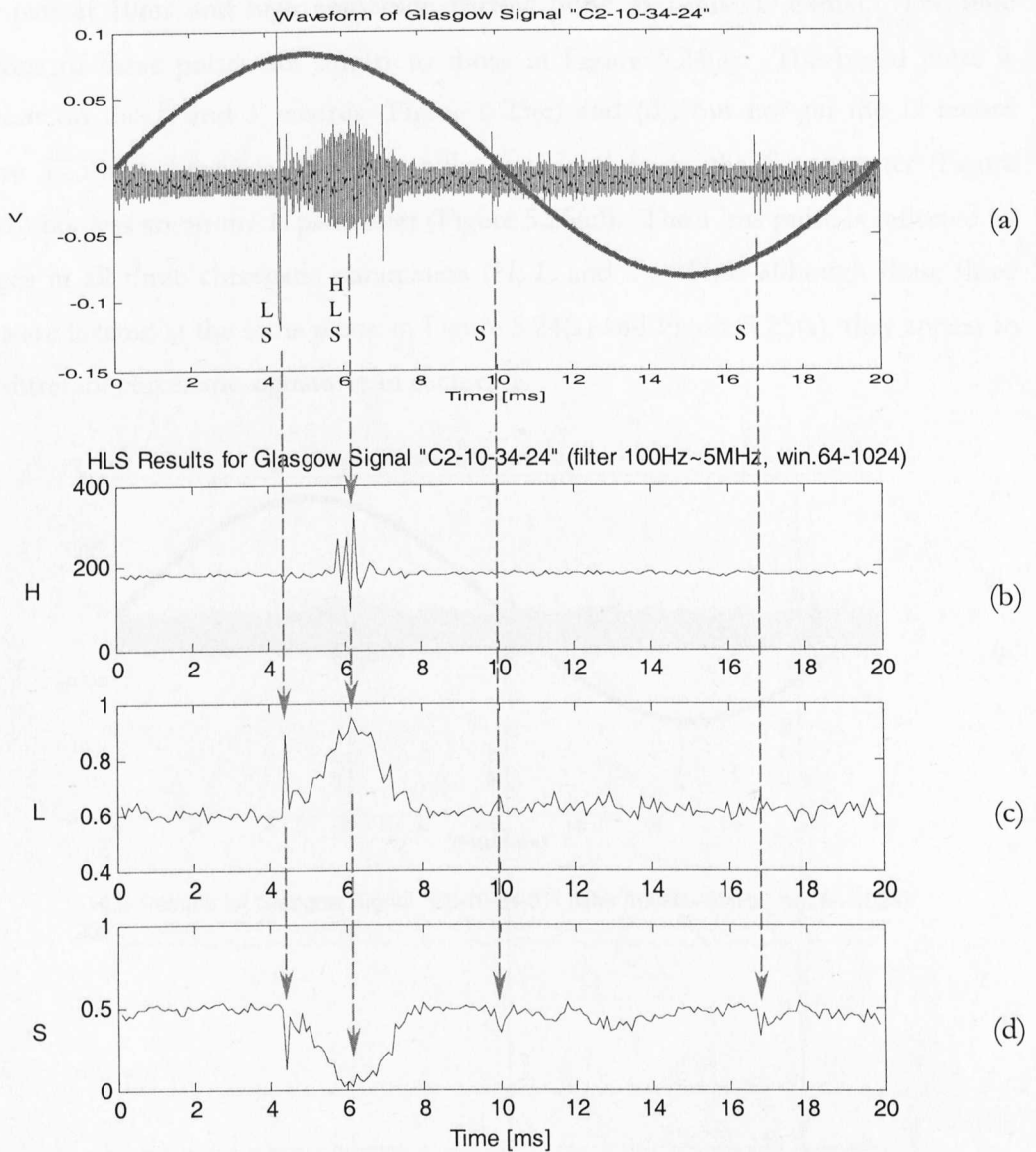
Figure 5.24 HLS results for Glasgow RF signal "C2-10-34-24"
(Ref. Figure 4.13) (a) Raw time-varying signal, (b) Hue, (c) Lightness, (d) Saturation

Table 5.2 HLS representations in RF signal processing

Symbol	Full name	Meaning	Corresponding range
H	Hue	Dominating frequency	$0\sim240° \rightarrow 100Hz\sim5MHz$
L	Lightness	Nominal signal strength	$0\sim1 \rightarrow 0\sim\pm1$
S	Saturation	Effective signal bandwidth	$0\sim1 \rightarrow 5MHz\sim0Hz$

Figure 5.25 shows the chromatically processed results of signal "C3-10-34-31". There are three major pulse regions apparent – a low amplitude broad pulse at 5~7ms, a short

pulse pair at 10ms and high amplitude narrow pulse at 17ms (17.84ms). The time locations of these pulses are similar to those in Figure 5.24(a). The broad pulse is apparent on the L and S records (Figure 5.25(c) and (d)) but not on the H record (Figure 5.25(b)). Likewise the 10ms pulse pair is clear on the S parameter (Figure 5.25(d)) but less so on the L parameter (Figure 5.25(c)). The 17ms pulse is reflected by changes in all three chromatic parameters (H, L and S). Thus although these three pulses are located at the same phase in Figure 5.24(a) and Figure 5.25(a), they appear to have different chromatic signatures in each case.
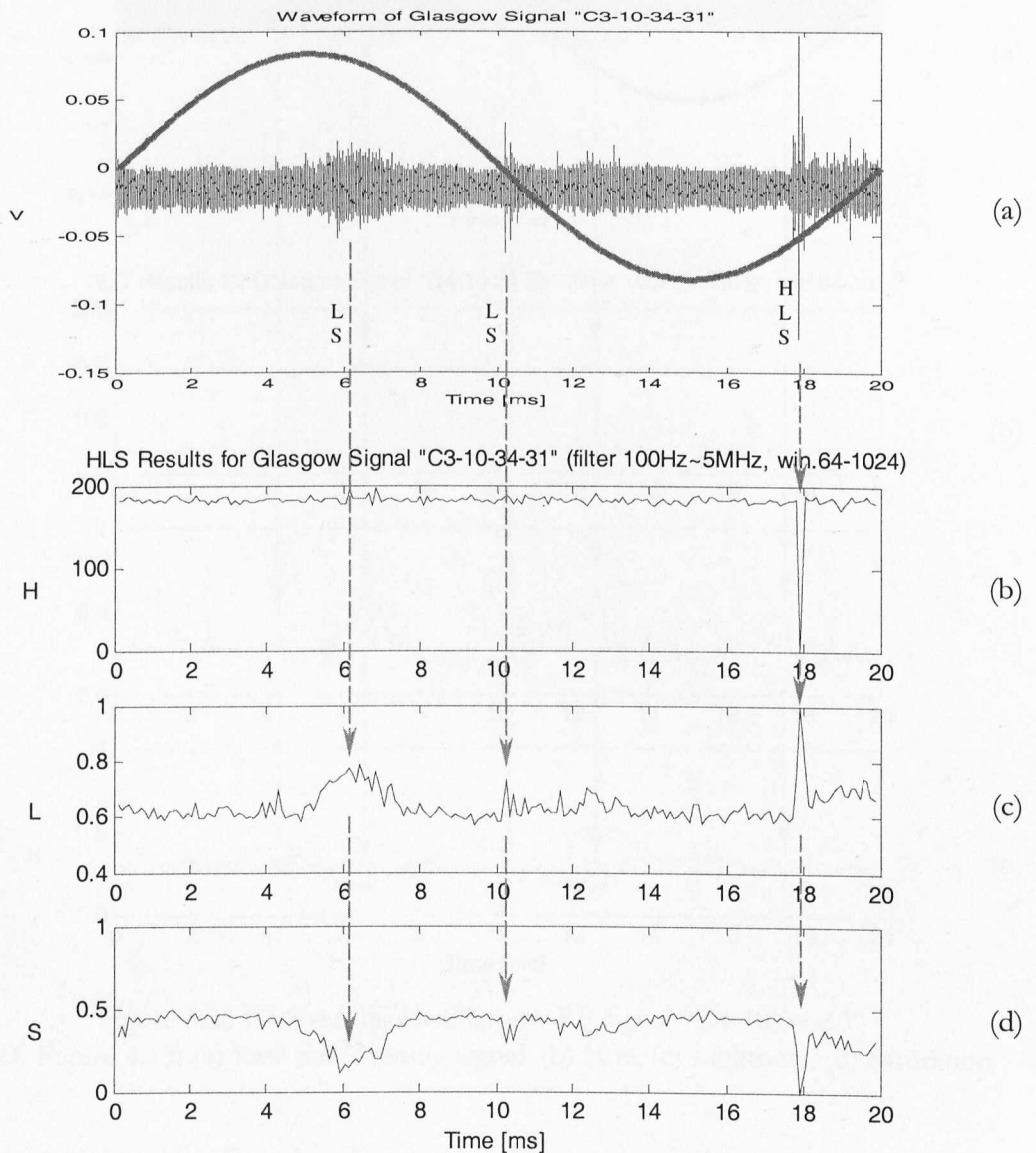
Figure 5.25 HLS results for Glasgow RF signal "C3-10-34-31"
(Ref. Figure 4.14) (a) Raw time-varying signal, (b) Hue, (c) Lightness, (d) Saturation

Figure 5.26 shows the processed results of signal "C4-10-34-35" (Figure 4.15). Broad, relatively low amplitude pulses occur at 5~7ms, 11~14ms, 16~17ms. Notable narrow pulses occur at 4ms, 10ms and 17ms. The narrow pulses at 4ms and 17ms are apparent on S (Figure 5.26(d)), less so on L (Figure 5.26(c)) and not on H (Figure 5.26(b)). The narrow pulse at 10ms affects all three chromatic parameters H, L and S.
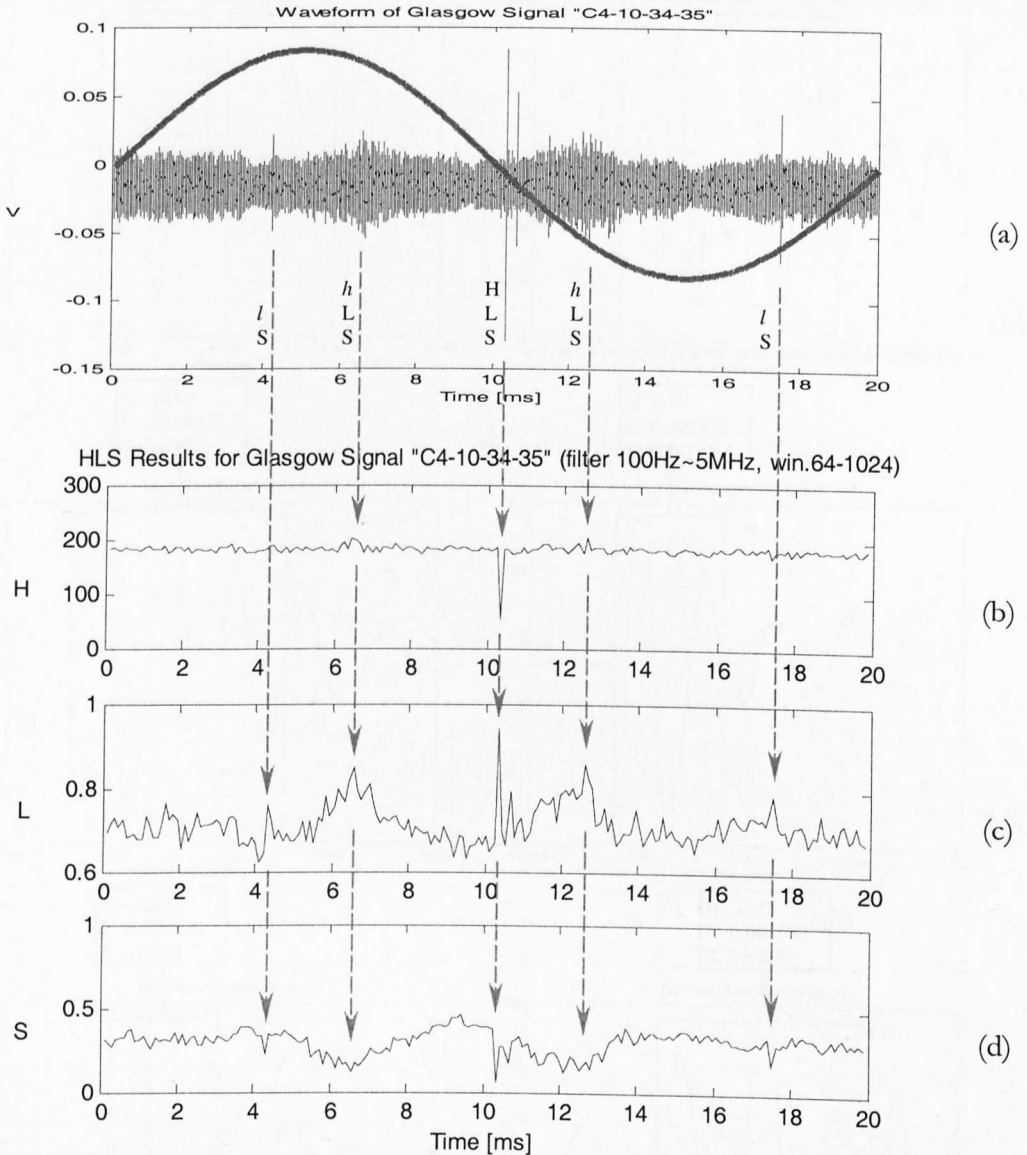
Figure 5.26 HLS results for Glasgow RF signal "C4-10-34-35"
(Ref. Figure 4.15) (a) Raw time-varying signal, (b) Hue, (c) Lightness, (d) Saturation

The detailed nature of the pulses identified in Figure 5.24, Figure 5.25 and Figure 5.26 may be investigated by time expanding the pulse signals. This has been done for the

4ms and 17ms pulses of Figure 5.24, the 10ms and 17ms pulses of Figure 5.25 and the 10ms and 17ms pulses of Figure 5.26. These expanded time scale pulses are shown in Figure 5.27(a) to (f).
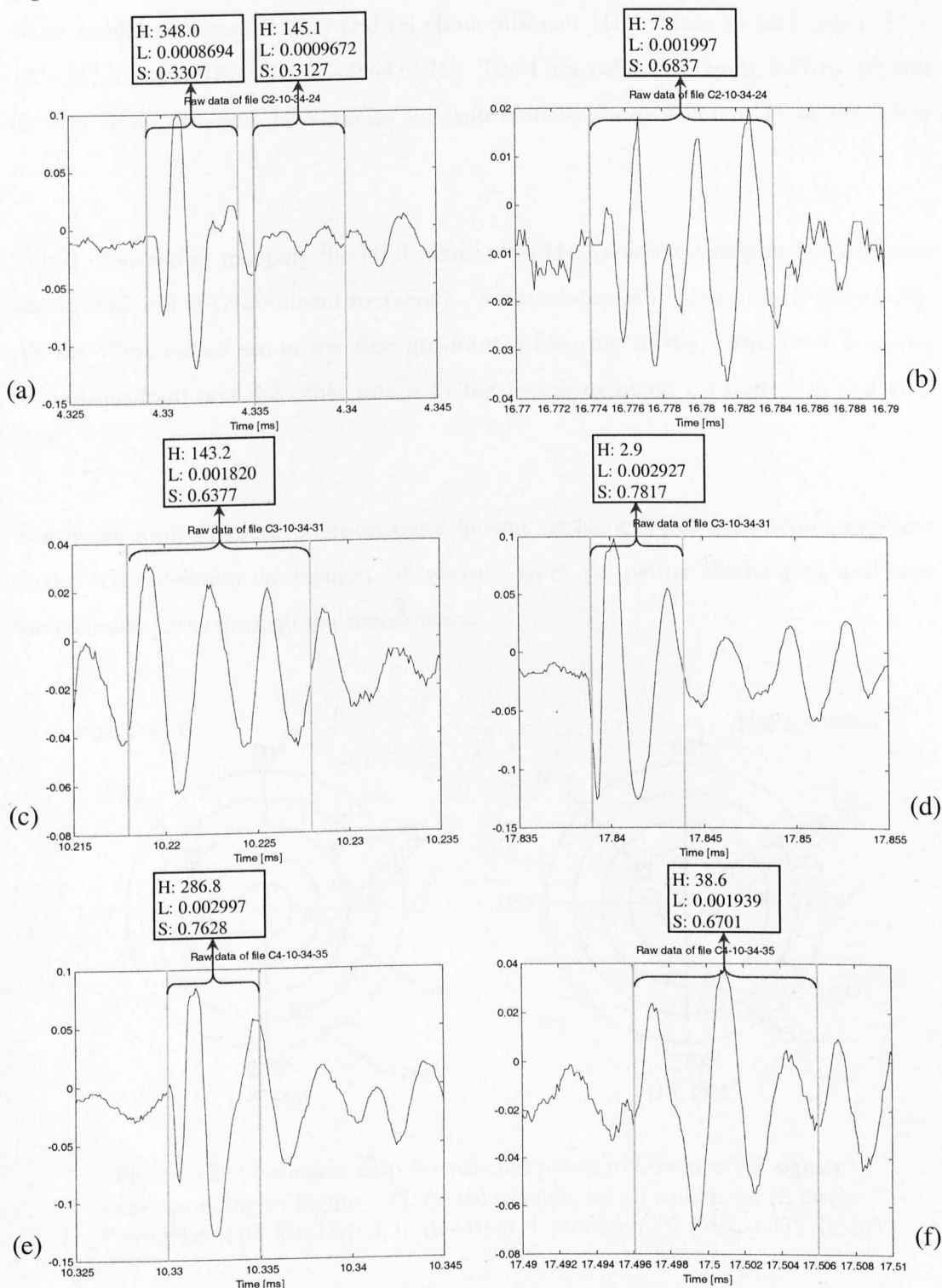
Figure 5.27 HLS results for selected pulses in Glasgow RF signals
(Ref. Figure 4.16 ~ 4.18) C2: (a) and (b), C3: (c) and (d), C4: (e) and (f)

Short time scale HLS values may then be calculated for these pulses from the waveforms in Figure 5.27. It is interesting to compare the nature and HLS values of pulses at corresponding times on Figure 5.24, Figure 5.25 and Figure 5.26. Thus the 10ms results of Figure 5.27(c) and (e) show different HLS values to each other ($H -$ 143/287, $L -$ 0.0018/0.003, $S -$ 0.64/0.76). The 17ms results of Figure 5.27(b), (d) and (f) also show different HLS values but substantially more different from the 10ms results.

This is clearer after mapping the HLS values onto H-S (dominant frequency – effective bandwidth) and H-L (dominant frequency – nominal strength) polar plots (Figure 5.28). All the 17ms pulses are in the first quadrant, while one of the 10ms pulse is in the second quadrant and the other one is in the fourth quadrant on both H-S and H-L plots.

The implication of these point-on-wave (power frequency) pulse signatures warrants further consideration in relation of various types of partial discharging and also transmission paths through the transformer.
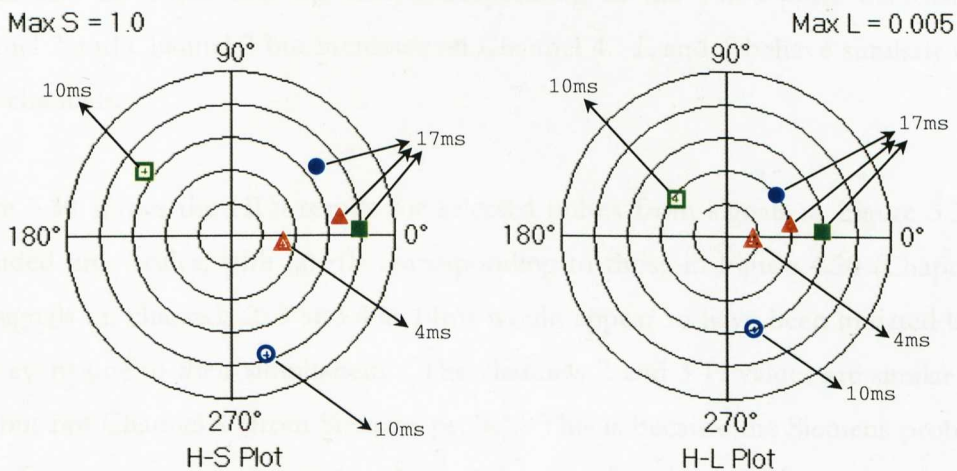
Figure 5.28 Chromatic map for selected pulses in Glasgow RF signals
Corresponding to Figure 5.27: (a) (b) triangle, (c) (d) square, (e) (f) circle
H: 0° (100Hz), 240° (5MHz); S: 0 (Δ5MHz), 1 (Δ0Hz); L: 0 (0V), 0.005 (0.5mV)

5.5.2.2   Signals from UMIST (Siemens & KEMA signals included)

The methodology (Figure 5.5) used for chromatically processing Glasgow Caledonian results has also been applied to the UMIST results with 10MHz sample rate. Figure 5.29 shows the processed results of signal "May 25 02, 15-26-51" already presented in Figure 4.19. Figure 5.29(a), (b) and (c) show the time varying raw signals of Channel 2, 3 and 4 respectively. Figure 5.29(d), (e) and (f) show the time variation of the chromatic parameters for the records of Figure 5.29(a), (b) and (c), each containing H, L and S variations. The subscripts H_n, L_n, S_n designate the relevant Channel n, i.e. H_2, L_2, S_2 relate to Channel 2 (Figure 5.29(a)).

Figure 5.29(a) (Channel 2) shows sharp pulses at 1, 1.5, 6, 10 and 14ms, Figure 5.29(b) (Channel 3) 13, 14ms and Figure 5.29(c) (Channel 4) a single 14ms pulse. On Channel 2, the 6ms pulse is discernible on H_2, L_2, S_2, the 10ms pulse on L_2, S_2 and the 14ms pulse is particularly apparent on H_2, L_2 and S_2. On Channel 3, the 14ms pulse is highly distinguishable on H_3, L_3, S_3; this pulse on Channel 4 is also clearly visible on H_4, L_4 and S_4. It is noteworthy that despite its greater amplitude the Channel 2 6ms pulse chromatic signatures are less pronounced than those for Channel 2 14ms one. It should also be noted that the hue corresponding to the 14ms pulse decreases on Channel 2 and Channel 3 but increases on Channel 4. L and S behave similarly on all three channels.

Figure 5.30 shows the HLS results for selected pulses from signals in Figure 5.29 on expanded time scales, with (a)~(f) corresponding to those in Figure 4.20 (Chapter 4). The signals on channels 2, 3 and 4 at 14ms would appear to have been initiated by the same event due to their simultaneity. The channels 2 and 3 H values are similar (204, 216) but not Channel 4 (from Siemens probe). This is because the Siemens probe is a lower frequency resonant system. Notice that the L value of Channel 3 (0.018) is substantially greater than channels 2 (0.006) and 4 (0.0085). This might relate to the source position.
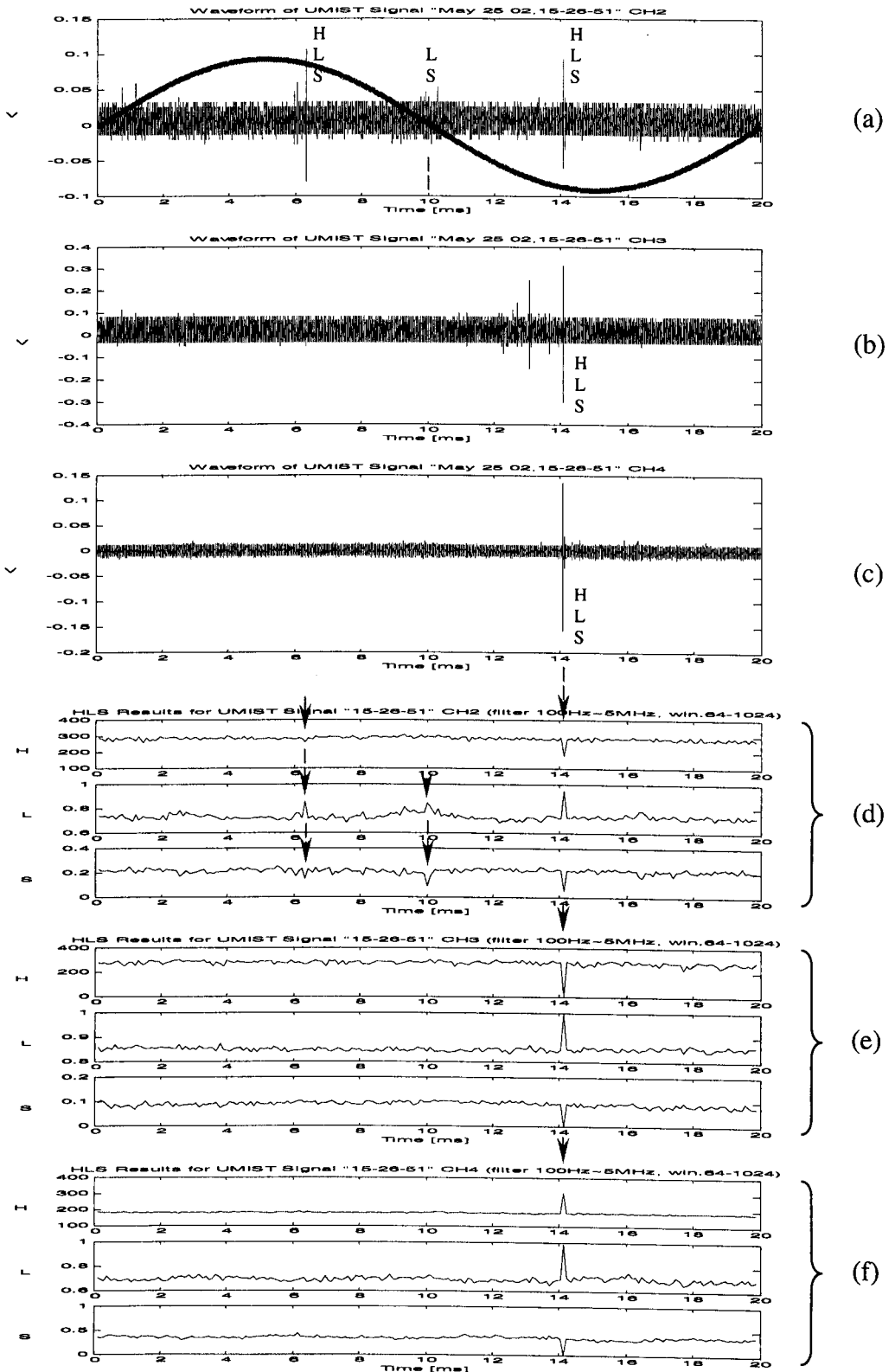
Figure 5.29 HLS results for UMIST RF signal "May 25 02, 15-26-51"
(Ref. Figure 4.19) (a), (b) & (c) Raw time-varying signal for channels 2, 3 & 4
(d), (e) & (f) HLS results for channels 2, 3 & 4

H: 223.7
L: 0.004145
S: 0.4888

H: 204.1
L: 0.006332
S: 0.4520

H: 224.7
L: 0.01548
S: 0.7878

H: 215.9
L: 0.01839
S: 0.7496

H: 348.6
L: 0.008549
S: 0.8350

H: 340.0
L: 0.005395
S: 0.7682

H: 293.2
L: 0.001821
S: 0.3463

H: 284.9
L: 0.001719
S: 0.3557
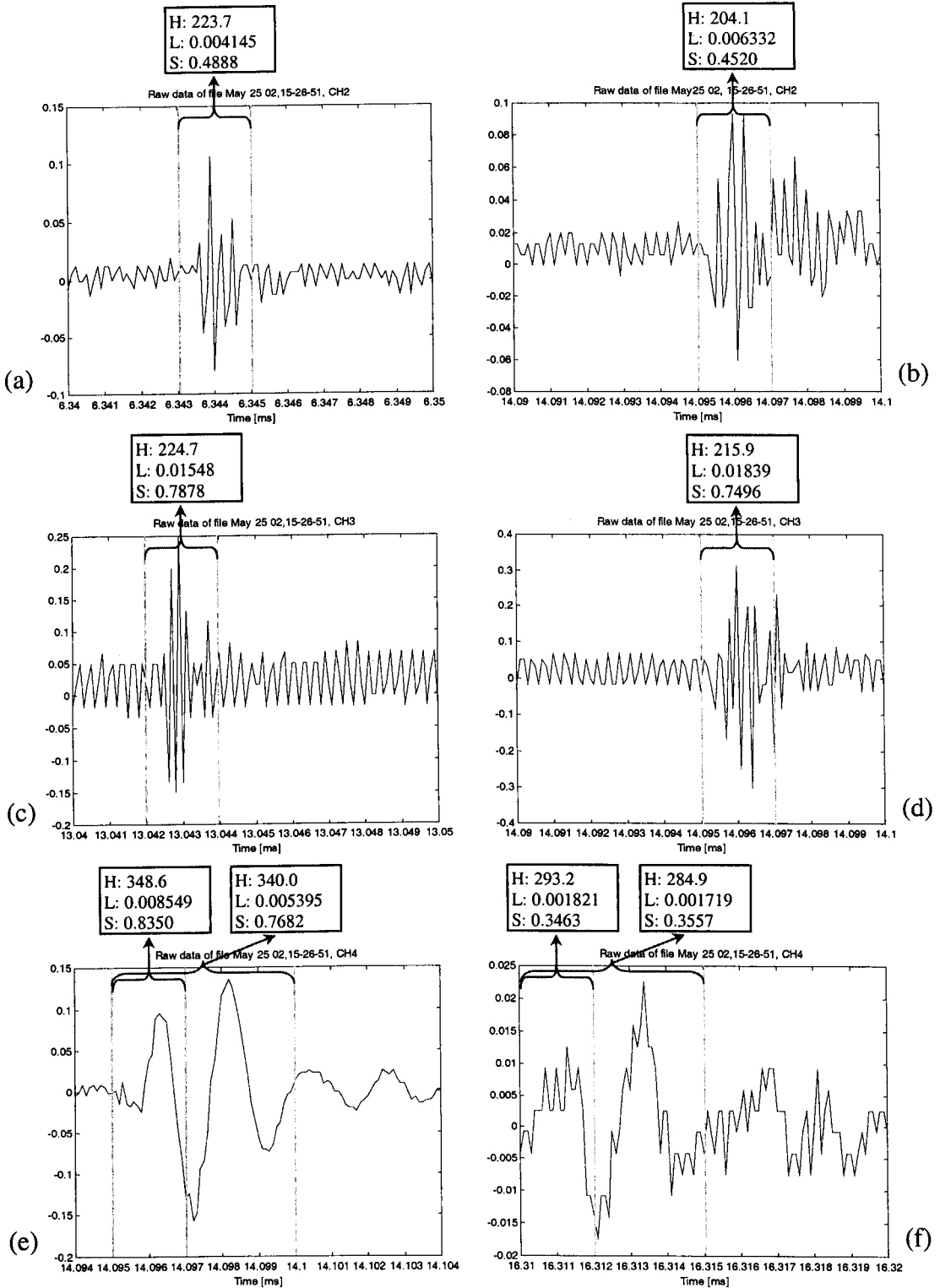
Figure 5.30 HLS results for selected pulses in UMIST RF signals
(Ref. Figure 4.20) (a) CH2, 6.343ms pulse   (b) CH2, 14.095ms pulse
(c) CH3, 13.042ms pulse   (d) CH3, 14.095ms pulse
(e) CH4, 14.095ms pulse   (f) CH4, 16.315ms pulse

The HLS values shown in Figure 5.30 are also mapped onto H-S and H-L polar plots (Figure 5.31) for better presentation and direct information. The chromatic map indicates that pulses on channels 2 (red triangles) and 3 (green squares) are similar but different from those on Channel 4 (blue circles). This is also true for the pulses at 14ms in all three channels, although they are probably stimulated by the same PD event. The difference is due to the different behaviour of the UMIST and Siemens probes (the latter is a lower frequency resonant system (Figure 5.30)). And the L radius difference of green squares from others is related to different pulse source positions.
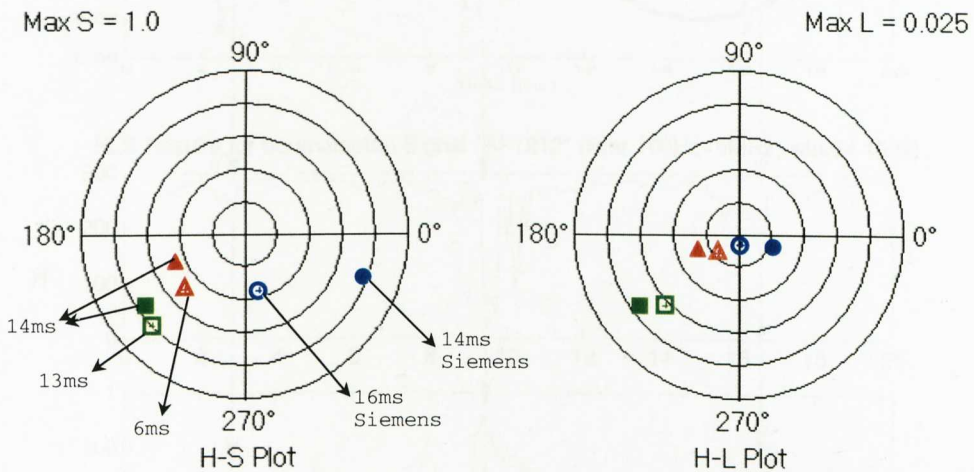
Figure 5.31 Chromatic map for selected pulses in UMIST RF signals
Corresponding to Figure 5.30: (a) (b) triangle, (c) (d) square, (e) (f) circle
H: 0° (100Hz), 240° (5MHz); S: 0 (Δ5MHz), 1 (Δ0Hz); L: 0 (0V), 0.005 (0.5mV)

5.5.2.3   Signals from Southampton University

The tristimulus filters shown in Figure 5.5 have been deployed to the signals from University of Southampton (reduced sample rate 10MHz). Figure 5.32 shows the processed results of Southampton signal "AF1212". Figure 5.32(a) is the time-varying raw signals, which was shown in Figure 4.22, while Figure 5.32(b), (c) and (d) are hue, lightness and saturation results respectively produced according to the scheme described in Section 5.2.4. There are three broad pulses at 2~4ms, 8~12ms and 16~20ms, all of which produce responses on the three chromatic parameters H, L and S. With $S\rightarrow0$, containing frequencies in the range of $H=50°\sim300°$, the pulse at

8~12ms is more polychromatic than the other two pulses, which have $S \approx 0.2$ and H varying between 200° and 300°.
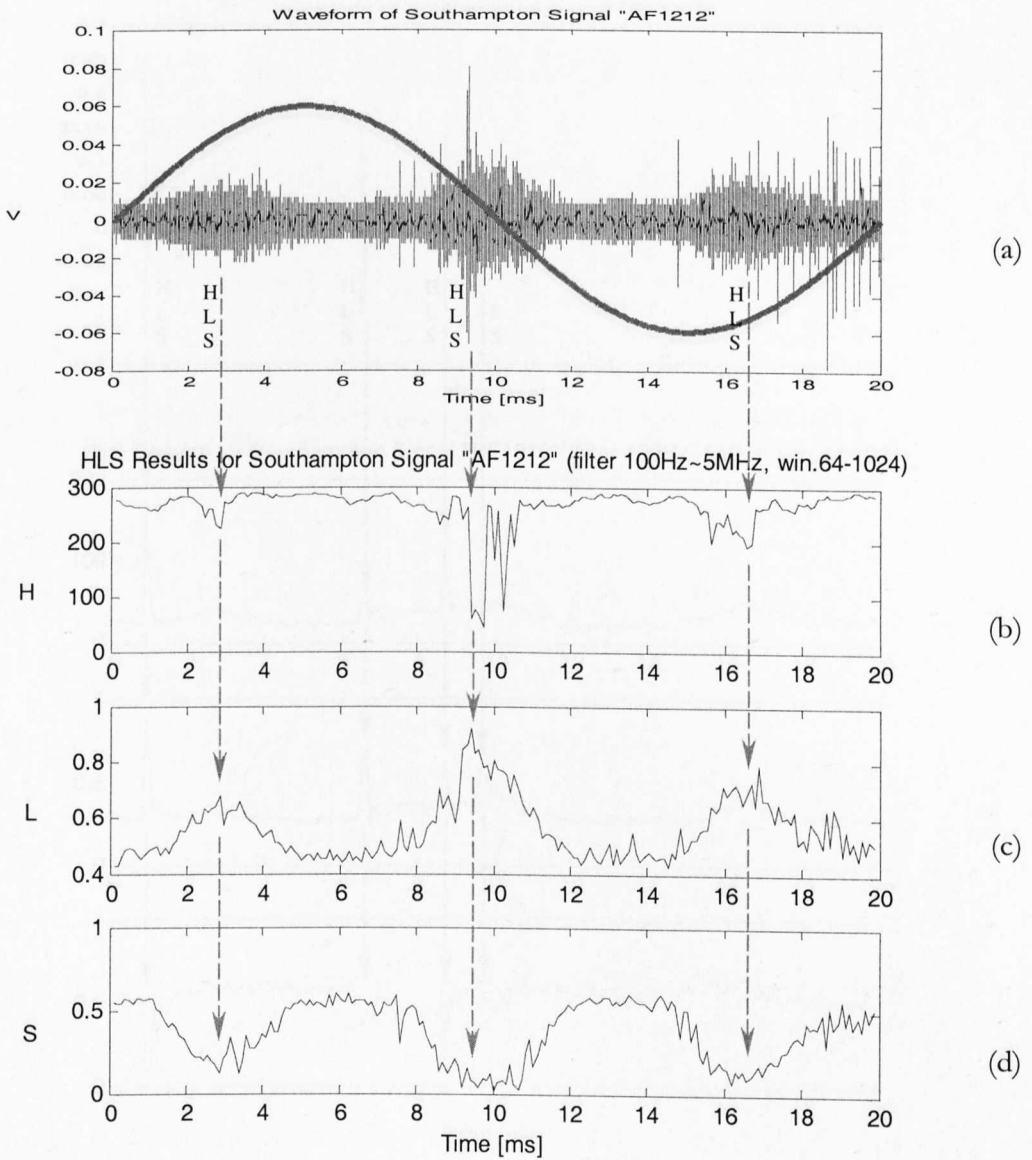

Figure 5.32 HLS results for Southampton RF signal "AF1212"
(Ref. Figure 4.22) (a) Raw time-varying signal, (b) Hue, (c) Lightness, (d) Saturation

Figure 5.33 shows similar chromatic results of the transformer phase B based upon the signal "BF1310" of Figure 4.23. Figure 5.33(a) is the time-varying raw signals (already shown in Figure 4.23). Figure 5.33(a) shows that there are one broad pulse at 10ms and three sharp pulses at 1ms, 7ms and 9ms. The broad pulse is discernible on L and S,

whilst the three sharps are all discernible on the HLS graphs of Figure 5.33(b) (c) (d). The following features are notewartty:
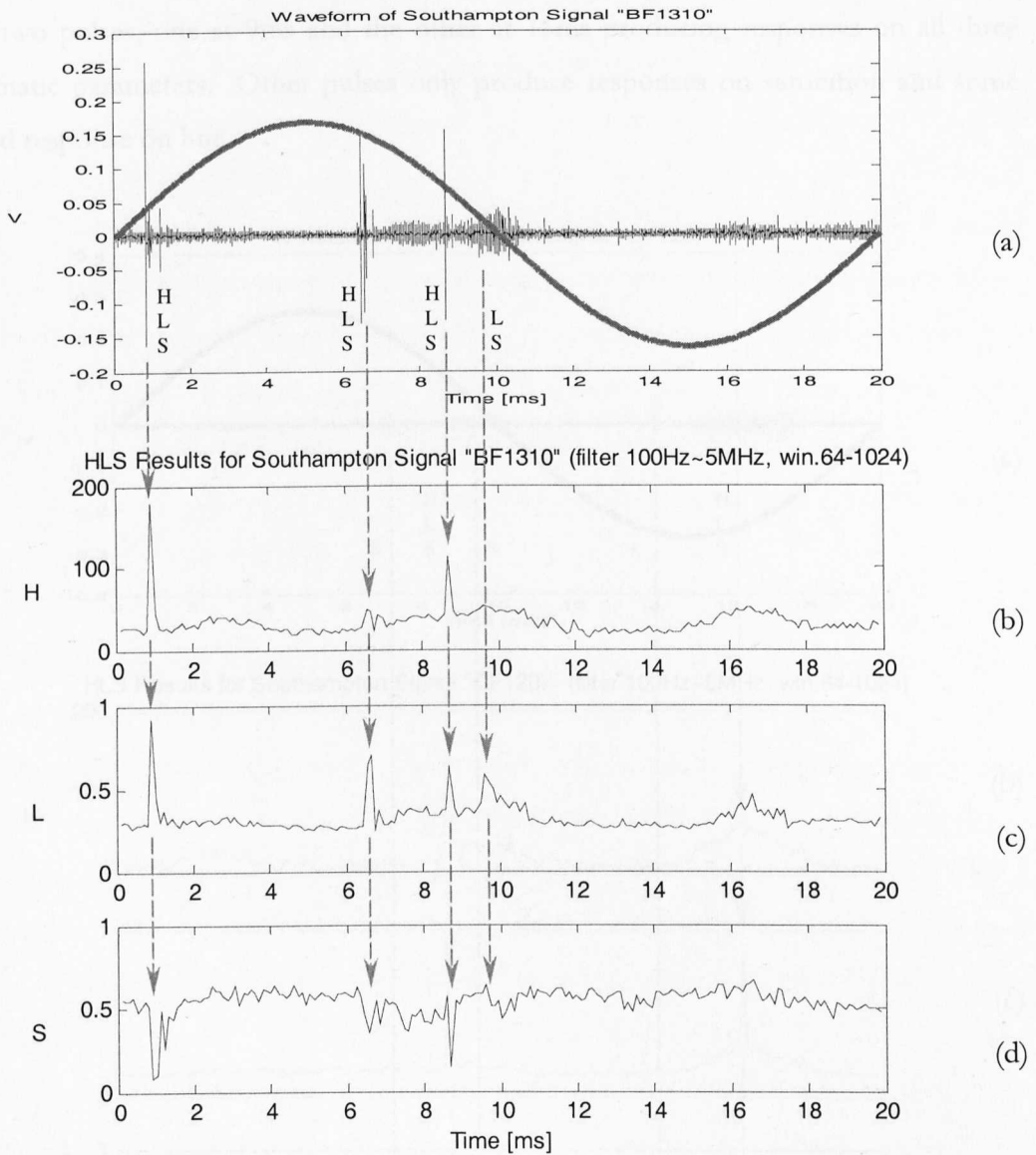

Figure 5.33 HLS results for Southampton RF signal "BF1310"
(Ref. Figure 4.23) (a) Raw time-varying signal, (b) Hue, (c) Lightness, (d) Saturation

- The pulse at 1ms has the highest lightness value and the most frequency components (lowest S) compared with the other two pulses

- Although the pulse at 7ms has a higher lighteness value than the one at 9ms, it contains fewer frequency components.

Figure 5.34 shows the chromatic results of the transformer phase C based upon the signal "CF1207" of Figure 4.24. Figure 5.34(a) is the time-varying raw signals (already shown in Figure 4.24). From the HLS result in Figure 5.34(b), (c) and (d), there are only two pulses, one at 9ms and the other at 16ms producing responses on all three chromatic parameters. Other pulses only produce responses on saturation and some muted response on hue.
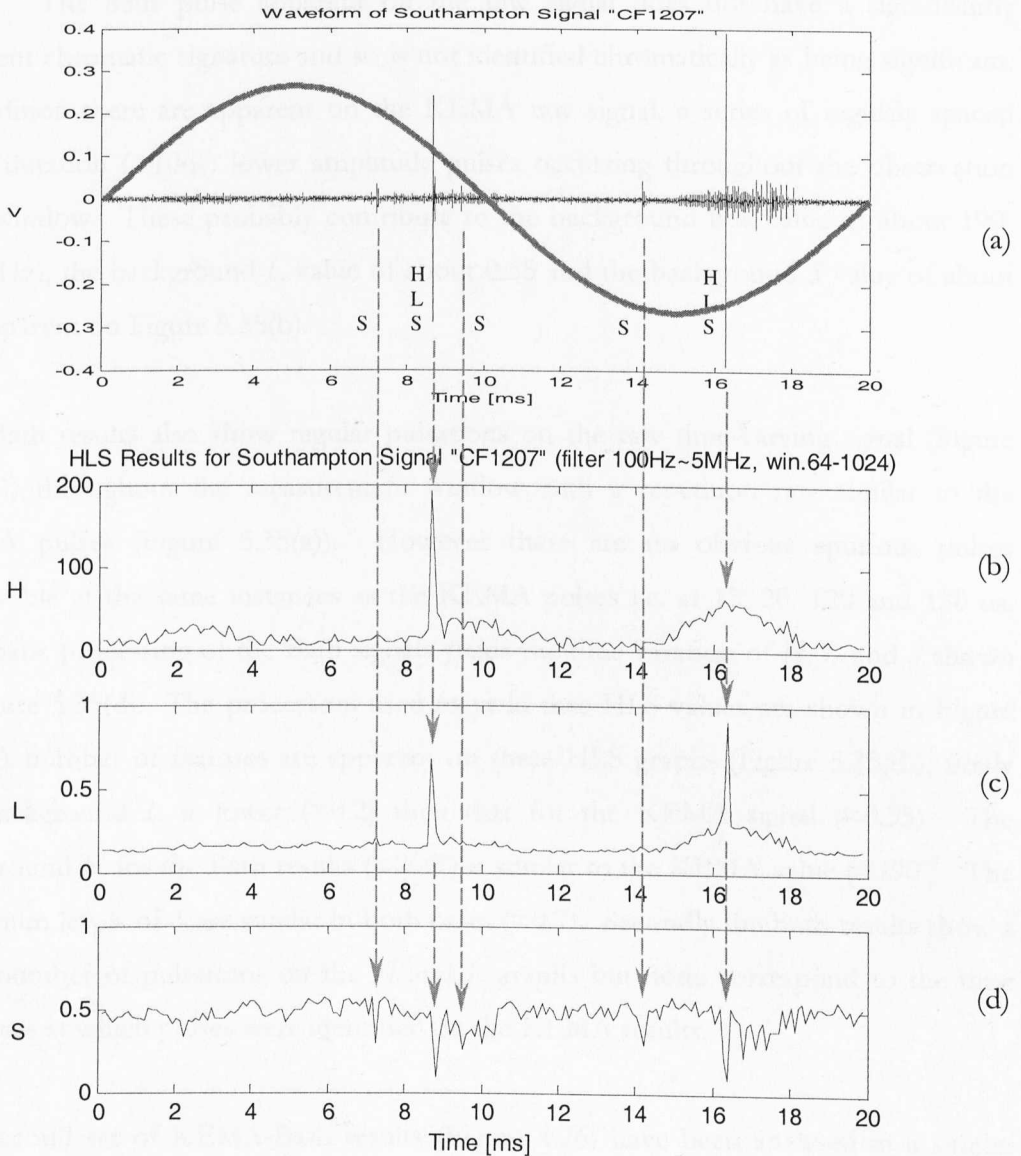
Figure 5.34 HLS results for Southampton RF signal "CF1207"
(Ref. Figure 4.24) (a) Raw time-varying signal, (b) Hue, (c) Lightness, (d) Saturation

5.5.2.4   Signals from Bath University

The tristimulus filters shown in Figure 5.7 have been applied to the signals from University of Bath. Figure 5.35 shows the chromatically processed results of Bath signal "092110" together with raw PD signals (channels 3&4), which were shown in Figure 4.25, for cross-checking purposes. The HLS results of the Channel 3 signal (from KEMA probe) indicate four significant pulses at around 15us, 20us, 120us and 130us. The 85us pulse apparent on the raw signal does not have a significantly different chromatic signature and so is not identified chromatically as being significant. In addition there are apparent on the KEMA raw signal, a series of regulaly spaced short duration ($\approx$10ns) lower amplitude pulses occurring throughout the observation time window. These probably contribute to the background hue value of about 190° ($\approx$1GHz), the background L value of about 0.55 and the background S value of about 0.7 apparent on Figure 5.35(b).

The Bath results also show regular pulsations on the raw time-varying signal (Figure 5.35(c)) throughout the measurement window with a repetition rate similar to the KEMA pulses (Figure 5.35(a)). However there are no obvious spurious pulses observable at the same instances as the KEMA pulses i.e. at 15, 20, 120 and 130 us. chromatic processing of the Bath signals yields the time varation of H, L and S shown in Figure 5.35(d). The processors used to yield thse HLS values are shown in Figure 5.7. A number of features are apparent on these HLS graphs (Figure 5.35(d)), firstly the background L is lower ($\approx$0.2) than that for the KEMA signal ($\approx$0.55). The background H for the Bath results ($\approx$200°) is similar to the KEMA value ($\approx$190°). The maximum levels of S are similar in both cases ($\approx$0.7). Secondly the Bath results show a large number of pulsations on the H and L graphs but none correspond to the time instances at which pulses were identified on the KEMA results.

The second set of KEMA-Bath results (Figure 4.26) have been analysed in a similar manner and the results are shown in Figure 5.36(a) (b) for the KEMA signals and (c) (d) for the Bath signals. The trends identified in Figure 5.35 are also apparent in Figure 5.36.
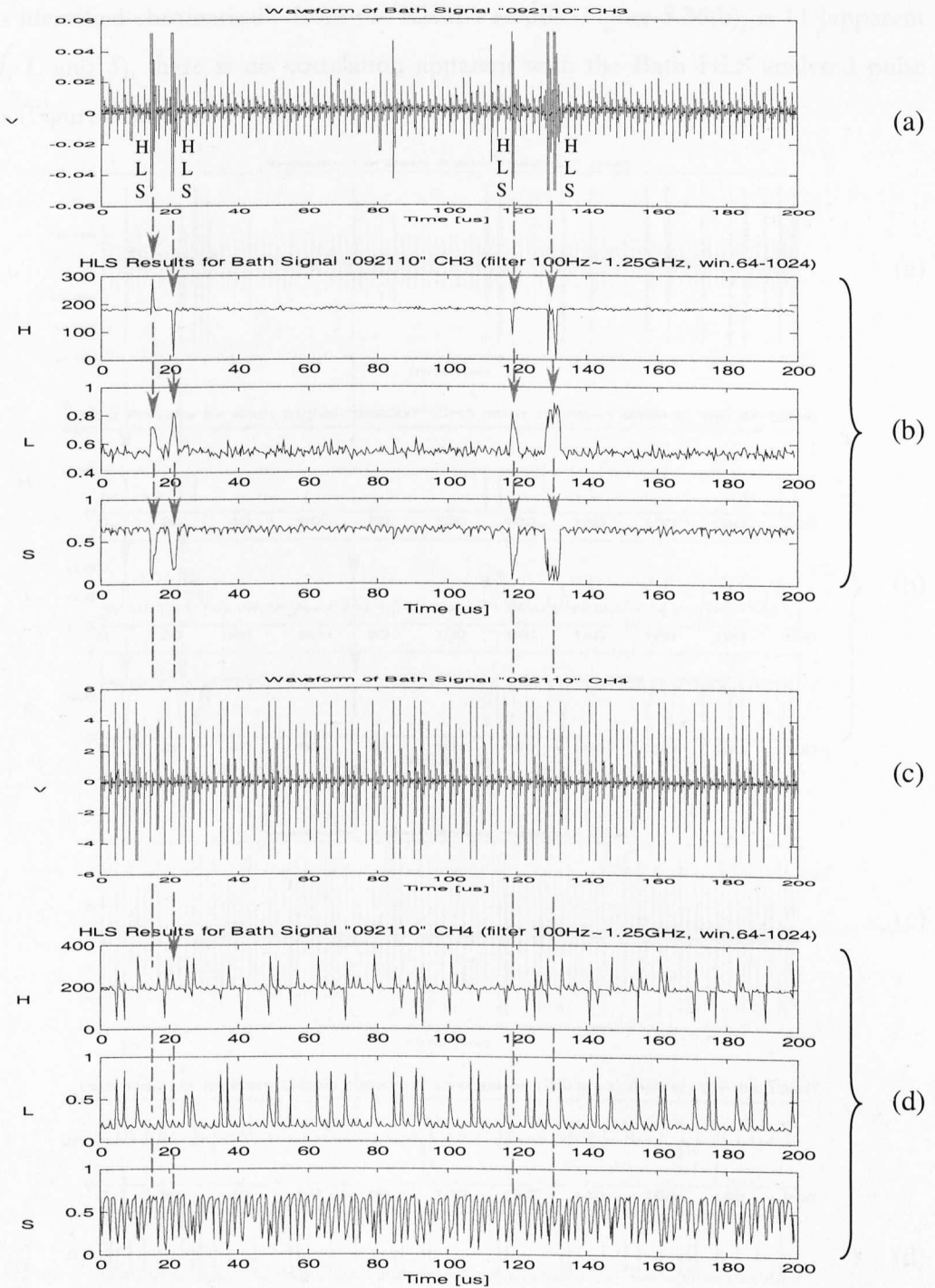
Figure 5.35 HLS results for Bath RF signal "092110"
(a) Channel 3 (KEMA probe) raw signal (b) Channel 3 HLS results
(c) Channel 4 (Bath Yagi antenna) raw signal (d) Channel 4 HLS resutls

Thus the Bath background L level (≈ 0.2) is less than the KEMA background (≈ 0.55) whilst the background H levels are similar ($H \approx 190° \sim 200°$). Although the number of

pulses identified chromatically from the KEMA resutls (Figure 5.36(b)) is 11 (apparent on *H*, *L* and *S*), there is no correlation apparent with the Bath HLS analysed pulse values (Figure 5.36(d)).
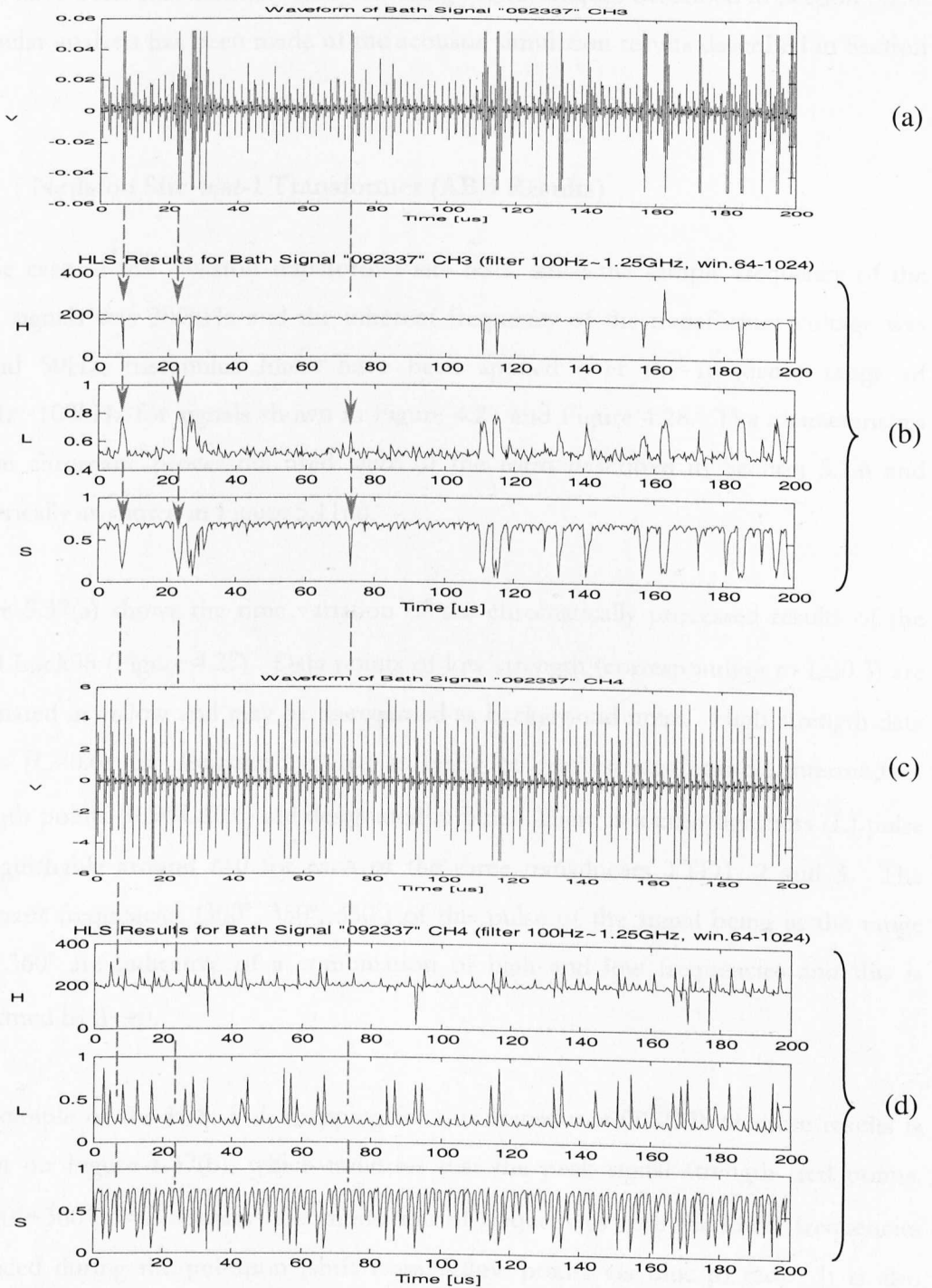
Figure 5.36 HLS results for Bath RF signal "092337"
(a) Channel 3 (KEMA probe) raw signal (b) Channel 3 HLS results
(c) Channel 4 (Bath Yagi antenna) raw signal (d) Channel 4 HLS resutls

5.6   Chromatically Processed Acoustic Results

The acoustic signals supplied by ABB from the Neilston transformer tests (Section 4.5.1) have been chromatically analysed using the techniques described in Section 5.2.6. A similar analysis has been made of the acoustic simulation results described in Section 4.5.2.

5.6.1   Neilston Site-test-1 Transformer (ABB Results)

In the case of the Neilston transformer site tests, since the sample frequency of the TTD signals was 200kHz and the inherent frequency of the transformer voltage was around 50Hz, tristimulus filters have been applied over the frequency range of 100Hz~100kHz for signals shown in Figure 4.27 and Figure 4.28. The characteristics of the chromatic processors used were of the form described in Section 5.2.6 and numerically as shown in Figure 5.11(a).

Figure 5.37(a) shows the time variation of the chromatically processed results of the signal Lock95 (Figure 4.27). Data points of low strength (corresponding to $L \leq 0.3$) are designated in yellow and may be disregarded as background noise. High strength data points ($L > 0.6$) are designated in red as being of greatest significance; intermediate strength points ($0.3 < L \leq 0.6$) are designated in blue. There is a clear lightness (L) pulse distinguishable around $t=0$ for each of the three transducers TTD1, 2 and 3. The dominant frequencies (300°, 350°, 350°) of this pulse of the signal being in the range 240°~360° are indicative of a combination of high and low frequencies and this is confirmed by $S \rightarrow 0$.

An example of the H-S, H-L mapping for one transducer (TTD3) of these results is shown on Figure 5.37(b), which indicates that the peak signal strength (red points, $H \approx 280° \sim 360°$, $S \approx 0$) contains a combination of frequencies with the lower frequencies produced during the pulsation (shift from yellow points via blue to red). It is also interesting to note from the aspect of using the acoustic signals for fault location by triangulation that the earliest signal onset is by transducer TTD3 and the latest by TTD2 which however records the loudest signal.
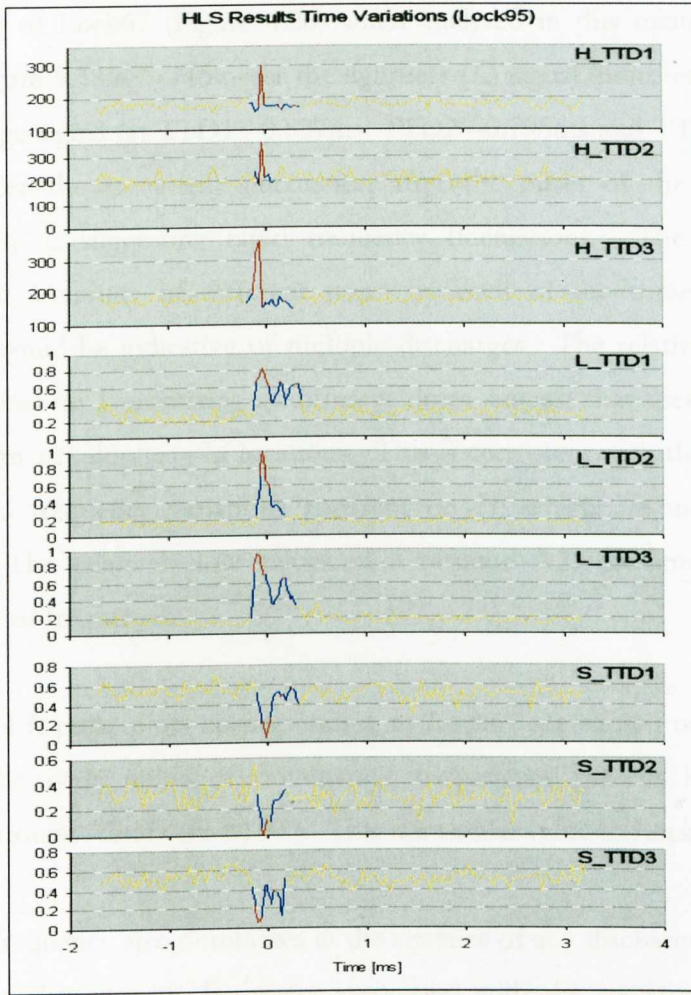
(a)
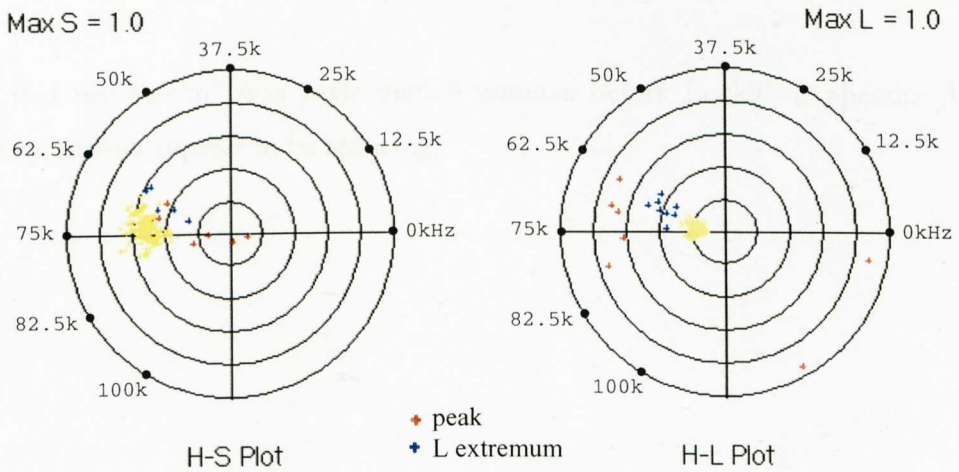
(b)

Figure 5.37 HLS results for ABB acoustic signal "Lock95"
(Ref. Figure 4.27) (a) HLS values time variations for each of the three transducers
(b) H-S, H-L polar plots for TTD3

The results of Lock67 (Figure 4.28) when analysed in this manner are considerably noisier (Figure 5.38(a)). However the lightness (L) signal indicates clearly the onset of the discharge signal (at TTD1 –0.827ms, TTD2 –0.795ms and TTD3 –0.827ms). The H parameter shows violent fluctuation after the onset of the discharge signal as indicated by L suggesting rapid frequency fluctuations. The loudest signals are recorded at a variety of different times by each of the three transducers. This behaviour could be indicative of multiple discharges. The relative magnitudes of the signal features on L occurring at different times suggest that these various discharges may be from a multiplicity of locations. This is consistent with the more complex and pronounced frequency variations apparent on H, which are independent of signal intensity. The relatively low values of S (around 0.2) confirm the existence of a multiplicity of frequencies.

The H-S, H-L polar plots corresponding to Lock67 are shown on Figure 5.38(b) and illustrate the wide range of dominating frequencies present but with a possible clustering around 75kHz (H =180°). This is a similar value to Lock95 (Figure 5.37(b)).

Since this frequency also dominates in the absence of any discharging, it is possible that it reflects a characteristic frequency associated with the transformer itself (note the implication is not of a resonant frequency since S ≤0.6 for both signals implying a moderate level of polychromaticity)

Note that test Lock67 was performed 8 minutes before Lock95 (Appendix A) i.e. discharge activity appears to be reducing.
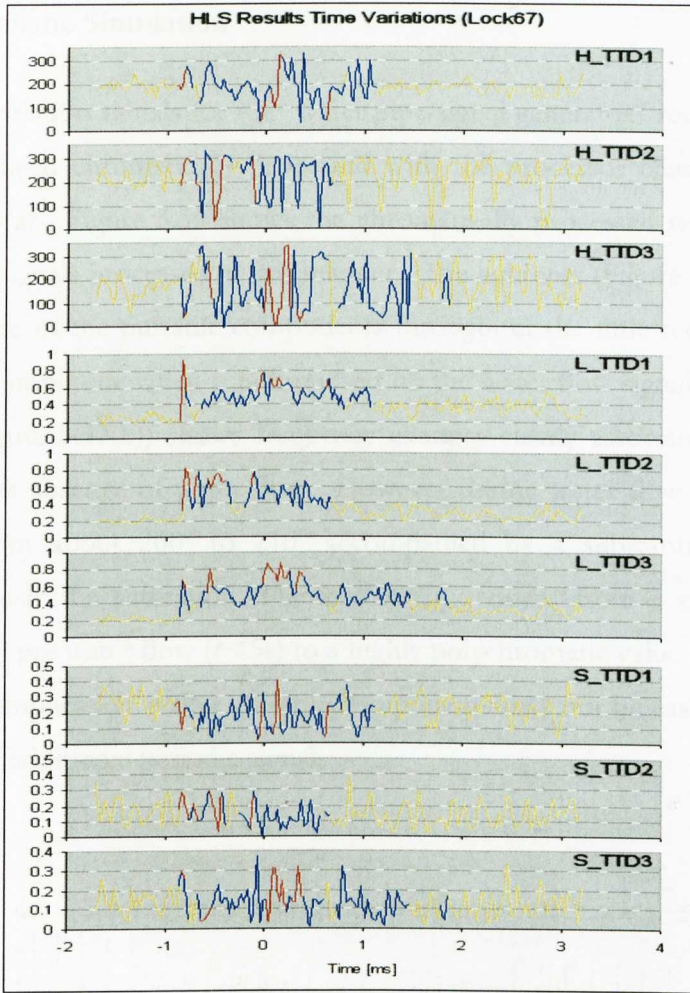
(a)
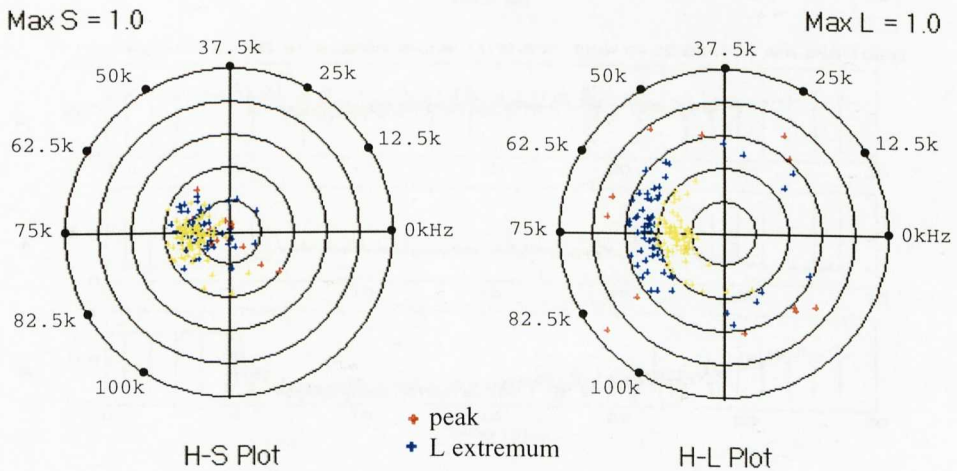
(b)

Figure 5.38 HLS results for ABB acoustic signal "Lock67"
(Ref. Figure 4.28) (a) HLS values time variations for each of the three transducers
(b) H-S, H-L polar plots for TTD1

5.6.2 Acoustic Simulation

The time variation signals for the "water pipe-signal generator" results shown in Figure 4.29 have been chromatically processed with the processor characteristics shown in Figure 5.10(a). Figure 5.39 shows the chromatically processed results of the acoustic simulation signals processed in this manner. The lightness (Figure 5.39(c)) signal shows the existence of the pulsatile components throughout the time recording period albeit of reduced amplitude when superimposed on the water flow signal. The time variation of hue (Figure 5.39(b)) shows frequency changes clearly associated with the acoustic pulses in the absence of water flow. However during water flow the background hue reduces from about $260°$ to $210°$ accompanied by a substantial fluctuation level. Simultaneously the saturation (Figure 5.39(d)) reduces from a near monochromatic value (≈ 0.8) pre water flow ($t < 5s$) to a highly polychromatic value (≈ 0.15) during water flow. The implication is that pulsatile components may not be easily identifiable in the presence of additional periodic signals.
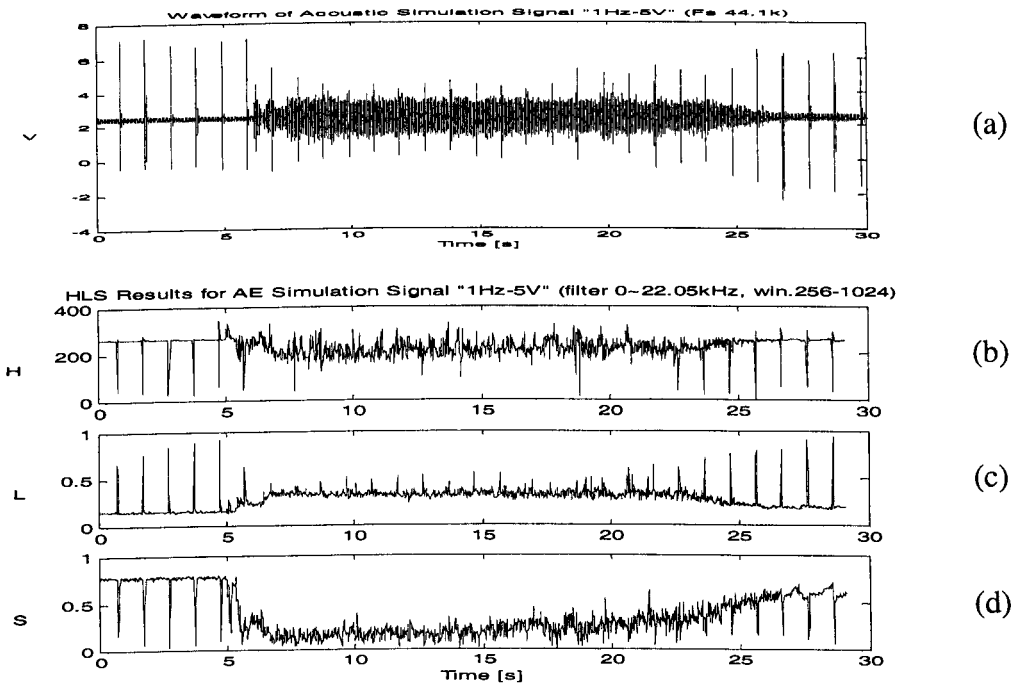

Figure 5.39 HLS results for acoustic simulation signal "1Hz-5V"
(Ref. Figure 4.29) (a) Raw time-varying signal, (b) Hue, (c) Lightness, (d) Saturation
Pulse: 1Hz, 5V

This also gives the reason for why all the tristimulus filters (Figure 5.5 ~ Figure 5.7, Figure 5.10 ~ Figure 5.11) applied to electrical/RF and acoustic signals covered the frequency range from 100Hz, avoiding the 50Hz AC voltage waveform.

A further test was performed whereby the amplitude of the pulsatile component was increased during the water flow period by a factor of 2 (Figure 4.30). The resulting lightness time-variation result is shown in Figure 5.40(b). This result shows clearly the increased magnitude of the lightness of the pulsatile component during the water flow period. It indicates that acoustic pulsatile signals may be detectable when superimposed periodic signals exist provided the lightness of the pulsatile component is approximately an order of magnitude greater than that of the periodic signal (i.e. $L \approx 0.8$ compared with 0.1 Figure 5.40(b)).
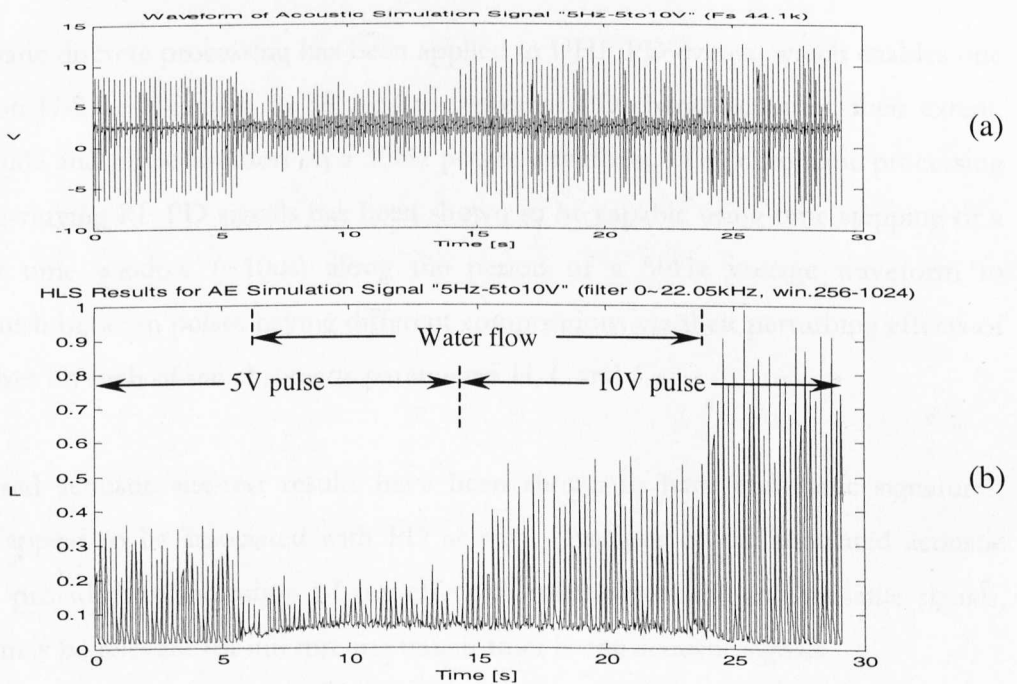
Figure 5.40 Lightness result for acoustic simulation signal "5Hz-5to10V"
(Ref. Figure 4.30) (a) Raw time-varying signal, (b) Lightness
Pulse: 5Hz, 5~10V

5.7   Summary

This chapter has described the chromatic analysis of the experimental results in Chapter 4 from four different sets of experimental data, which are DGA, temperature, electrical/RF emissions and acoustic emissions.

The DGA chromatic results enable the working conditions of a transformer to be classified, faulty transformers to be distinguished from others and imminent faults on in-service transformers to be identified.

Chromatic processing of transformer temperature data has been used to explore the representation of significant PD induced temperature trends against a background of diurnal variations in ambient temperature and transformer loading. A number of different schemes for clustering the relevant parameters have been investigated all of which are well behaved under normal transformer operating conditions.

Chromatic discrete processing has been applied to UHF PD events, which enables one point on H-S or H-L map to be used to represent PD charge activities, their extent, magnitude and phase location on a 50Hz power waveform. The chromatic processing of time-varying RF PD signals has been shown to be capable using time stepping of a narrow time window (~10us) along the period of a 50Hz voltage waveform to distinguish between pulses having different compositions via their perturbing effects of the pulses on each of the chromatic parameters H, L and S.

Processed acoustic site-test results have been shown to have chromatic signatures, which appear to be associated with PD activity. Analysis of the simulated acoustic signals provided an indication of the effect of mixing periodic and pulsatile signals, which may be relevant for interpreting transformer borne acoustic signals

The chromatic results obtained from the individual parameter investigations described in this chapter will be further processed and discerned when integrated to combine the information extracted from each parameter results in Chapter 6.

Chapter 6

Discussion of Results

6.1 Introduction

With the results analysed in Chapter 5, this chapter discusses broader interpretations of these results. This discussion is undertaken within the context that the DGA and temperature results are primarily used for the purpose of identifying a transformer, which may be approaching a faulty condition. The RF and acoustic results are used to confirm the existence of electrical discharging and possibly identify the location of such discharging within the transformer.

This chapter therefore addresses first the possibility of using chromatically deduced parameters from the DGA measurements for indicating the probability that a faulty condition may be evolving. This is followed by an attempt to classify RF signals to indicate the occurrence of partial discharges as apposed to other discharge activities such as external corona. Finally a chromatically based method for combining signals from three acoustic transducers used for triangulation is explored in an attempt to classify such signals.

6.2　DGA

6.2.1　Normalization Schemes

In order to have meaningful and comparable DGA results for all transformer tanks, a normalization process is needed. After considering the advantages and disadvantages of different normalization schemes and comparing the meaning of the results processed by these different schemes, the chromatic DGA results (Chapter 5) were normalized using a ten-time-of-first-record (TTFR) normalization method. The outcome of this is discussed.

6.2.1.1　General Normalization

The general normalization method is to choose the maximum of each gas component over a long period as the base for normalization. However this is not attractive because of the following disadvantages:

- For online monitoring the maximum is not known a priori

- The method misuses the chromatic space

- The highest values for various gases may occur at different times during the period (e.g. 20 years).

6.2.1.2　Database Normalization

The database normalization method is to choose a calculated value of each gas component from a number of transformer tanks as the normalization standard or criterion.

In one respect, the calculated value may be the maximum (or average) of each individual maximum. For example, if the maximum (or average) value of all inspected tanks' maximum CO_2 records is chosen as the normalization criterion for CO_2, then the maximum (or average) value of all inspected tanks' maximum H_2 records would be chosen as the normalization criterion for H_2, similarly for other gases. This approach does not overcome all the disadvantages of the general normalization method (Section 6.2.1.1).

In another respect, the calculated value may be the maximum (or average) of each individual first record. For example, if the maximum (or average) value of all inspected tanks' first CO_2 records is chosen as the normalization criterion for CO_2, then the maximum (or average) value of all inspected tanks' first H_2 records would be chosen as the normalization criterion for H_2, etc. The distributions in Figure 6.1 show a similar trend distribution. Furthermore, regarding the average, the ppm level for a specified percentage (e.g. 50% or 80%) of transformers can also be chosen as the criterion. For example in the case of 80%, the level of 2000ppm would be chosen as the CO_2 criterion, 300ppm as the CO criterion, 20ppm as the CH_4 criterion, and so on.

If this is the case, the first two problems stated in the general normalization method might be solved, but the third remains.

A major problem with this database normalization method is that it is non-specific in the sense that the calculated criteria may not be a meaningful value for a specified transformer. This is because different manufacturers produce transformers with different oil compositions, and each manufacturer may produce different types of transformers. In addition, different transformers have various oil dissolved gas percentages initially.

Note that the unit of these gas concentration data is "part per million" (ppm), it is a unit of proportion and it only has meaning when comparing gas components within their source collectivity i.e. the individual transformer tank itself. For instance, 500ppm H_2 from transformer tank A does not have the same meaning as 500ppm H_2 in transformer tank B. Furthermore there is no guarantee that the mass of either of these two 500ppm H_2 is larger than that of 400ppm H_2 in transformer tank C; on the contrary, they may be larger than that of 800ppm H_2 in transformer tank D. But for tank A, 500ppm H_2 in the first record and 700ppm H_2 in the second record which is sampled sometime later, at least indicate the proportion of H_2 in this tank A has increased in a quantifiably meaningful manner.

(a)

(b)

(c)

(d)

(e)

(f)

(g)
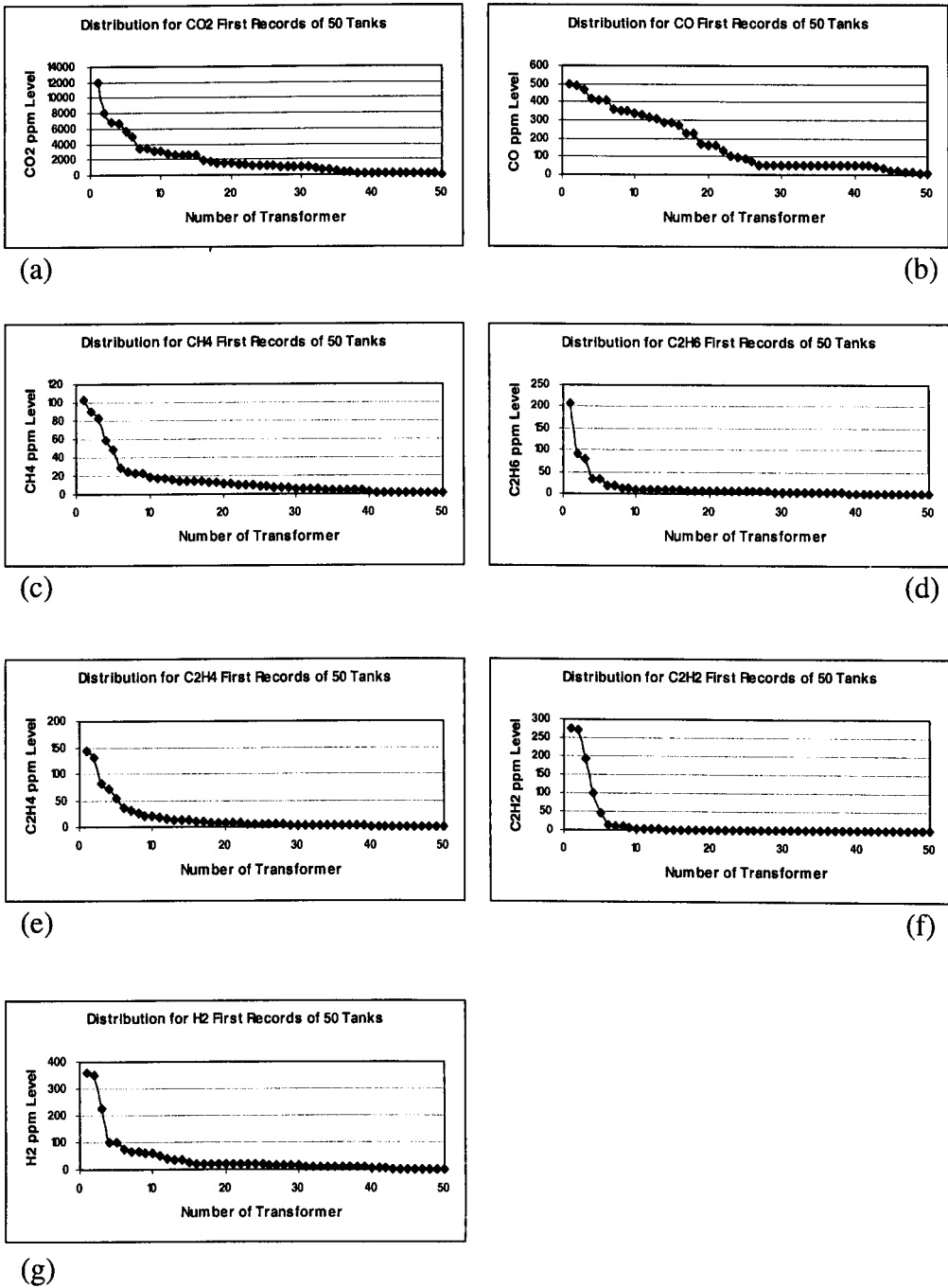
Figure 6.1 Distribution for gases first records of 50 tanks
(a)~(g) are corresponding to CO_2, CO, CH_4, C_2H_6, C_2H_4, C_2H_2, H_2 respectively

6.2.1.3 TTFR Normalization

Since both the general and the database normalization methods have so many disadvantages, other schemes should be applied for better effect. A new normalization method is therefore proposed. It is based on the first assumed value multiplied by ten of each gas component in the individual transformer tank i.e. ten times of first record (TTFR) normalization.

Normalized value at time t,

$$x(t)_N = \frac{x(t)}{10x(1)} \qquad\qquad (6.1)$$

where

$x(1)$ is the assumed initial value; $x(t)$ is the value at time t.

Figure 6.2 gives a schematic explanation for this TTFR normalization method. It has the following advantages.

- The initial value of H-S is identifiable, but has low weighting

- Subsequent initial values restricted to circle $S \leq S_1$

- Highlights excesses about initial value giving scale up to $x(t) = 10x(1)$ i.e. order of magnitude

(a)

(b)
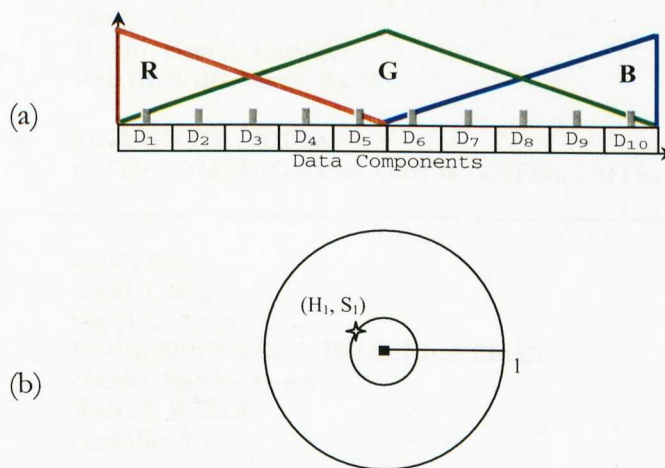
Figure 6.2 TTFR normalization schematics
(a) Original data field: starting point $x(t_1) = x(1)$; $x(t_1)_N = 0.1$
(b) HLS field starting point (H_1, S_1): H_1 and S_1 are specified values depending on the number of data components $D_\#$

Thus normalization based on records of the transformer itself is more reasonable than the other two methods mentioned above. Although applying this normalization to different transformers may appear as using different criteria, but it does in fact provide a convenient means for comparing different transformers. TTFR normalization based on the first record of the transformer itself can be regarded as an attractive comparison method.

6.2.2 Three Status of Transformer Conditions

DGA results from a total of 50 tanks have been analysed chromatically by using the TTFR normalization method described above. From the chromatic map (H-S and H-L polar plots), some typical examples of which were shown in Chapter 5, they may be classified into three categories corresponding to "safe", "changing" and "fault imminent" status (Table 6.1).

Table 6.1 Classification of DGA chromatically examined transformer tanks

Status	Count	Transformers
Safe	NGT 17	Boln1, Bush2, Bush3, Bush4, Cape2A, Cape5A, Cape5B, Cape6A, Cape6B, Elst2, Hamh1, Hamh5, Hamh6, Walx1A, Wylf1, Wylf2, Wylf4,
	First Hydro 10	Ffes2, GMT1s, GMT2m, GMT3m, GMT3s, GMT4m, GMT4s, GMT5m, GMT5s, GMT6m
Changing	NGT 18	Boln2, Boln3, Cant1, Cant2, Cape1A, Cape3A, Elst1A, Elst1B, Elst3A, Elst3B, Elst4, Elst5A, Hamh2, Hamh3, Hamh7, Walx2A, Walx2B, Northfleet3A
	First Hydro 4	Ffes1, GMT1m, GMT2s, GMT6s (warning)
Faulty	1	Neilston4

Results for transformers corresponding to the "safe" status have similar chromatic map to WYLF1mtb, which is shown in Figure 5.12 (Chapter 5). The chromatic map of this category has the following characteristics.

- Most of the points on the H-L plot are within the 0.1 circle and no point exceeds the 0.2 circle; <u>and</u>

- Most of the points on the H-S plot are within the Cellulose Decomposing area (CO_2-CO) or Oil Heated area (CH_4-C_2H_6-C_2H_4) and no point exceeds the 0.4 circle in the Electrical Stress area (C_2H_2-H_2).

Results for transformers corresponding to the "changing" status have similar chromatic maps to BOLN3mtb, FFES SGT1 or Northfleet SGT3A, which are shown in Figure 5.13, Figure 5.14 and Figure 5.16 respectively. The chromatic map of this category has the following characteristics.

- Some of the points on the H-L plot exceeds the 0.2 circle; <u>or</u>

- Some of the points on the H-S plot exceed the 0.4 circle within the Electrical Stress area (C_2H_2-H_2).

The chromatic map of the Neilston SGT4 transformer, Figure 5.15, demonstrates the "fault imminent" status. Comparing these results with those of the in-service transformers, there is an implication that a unit may be tending to failure if the lightness value exceeds 0.4, based on this seven-key-gas analysis. If the H value were in the range of C_2H_2/H_2 in addiction to $L > 0.4$ then the risk of failure would seem to be enhanced. One possible precursor to this is the indication from the H-S plot for predominance of CO followed by CO_2 before moving towards C_2H_2. On both H-S and H-L plots the trend to C_2H_2/H_2 during recent tests is noticeable. Therefore the characteristic of this category can be summarised here.

- Some of the points on the H-L plot exceeds the 0.4 circle; <u>and</u>

- Some of the points on the H-S plot exceed the 0.4 circle within the Electrical Stress area (C_2H_2-H_2).

6.2.3   Probability of Transformer Failure

A further aspect to which the chromatic analysis may be applied is for exploring the probability of failure with respect to critical values of the parameters H, L and S. To explore this possibility, use is made of the DGA results. It is first assumed that the probability of failure may be governed by a pseudo Gaussian probability **[Kenney, 1940; Papoulis et al., 2002]**.

$$P(x) = P_0 \exp[-\frac{1}{2}(\frac{x - x_m}{\sigma})^2]$$

(6.2)

where

σ, standard deviation; x_m, mean; P_0 may be 1.

From the chromatic mapping it is known that

- If there is copious gas production, then P is high i.e. $P(L)$.

- If there is a predominance towards C_2H_2, H_2, then P is high. Rearranging the chromatic map so that $H_{high} \rightarrow C_2H_2$, H_2; $H_{low} \rightarrow CO$, CO_2; Then $P(H)$.

- If one gaseous species of the high risk ones dominates, then P is high i.e. $P(S)$.

This arises because the dominating determinant is the quantity of gas produced (i.e. L large). If that gas is predominantly C_2H_2, H_2 (i.e. H arranged to be high) the probability of failure is even greater. Finally if there is a spread in the gases produced (i.e. S large) the failure probability may be somewhat increased. Thus the hierarchical order of HLS in determining the probability of failure is $L \geq H \geq S$. Then it might be postulated that

$$P(L, H, S) = l \cdot P_L + h \cdot P_H + s \cdot P_S$$
$$= P_0 \{l \cdot \exp[-\frac{1}{2}(\frac{L - L_m}{\sigma_L})^2] + h \cdot \exp[-\frac{1}{2}(\frac{H - H_m}{\sigma_H})^2] + s \cdot \exp[-\frac{1}{2}(\frac{S - S_m}{\sigma_S})^2]\}$$

(6.3)

where

l, h, s are scaling factors with $l > h > s$ and $l + h + s = 1$

$L_m = 1$, $S_m = 1$, $H_m = 240°$.

In order to deploy this formulation in practice, values are needed for l, h, s and σ_L, σ_H, σ_S. Inspection of the results presented in Section 6.2.2 for 50 transformer tanks leads to the suggestion that $l = 0.5$, $h = 0.3$, $s = 0.2$ and at the point of probability-half-height, $L_{p/2} = 0.2$, $H_{p/2} = 120$ and $S_{p/2} = 0.4$. This leads to the probability distribution curves shown in Figure 6.3. Thus "half-height-bandwidth" of L (Figure 6.3) is 2-0.2-0.2 = 1.6 ($\approx 2.4\ \sigma_L$), i.e. $\sigma_L \approx 0.67$, similarly, $\sigma_H \approx 100$ and $\sigma_S \approx 0.5$.
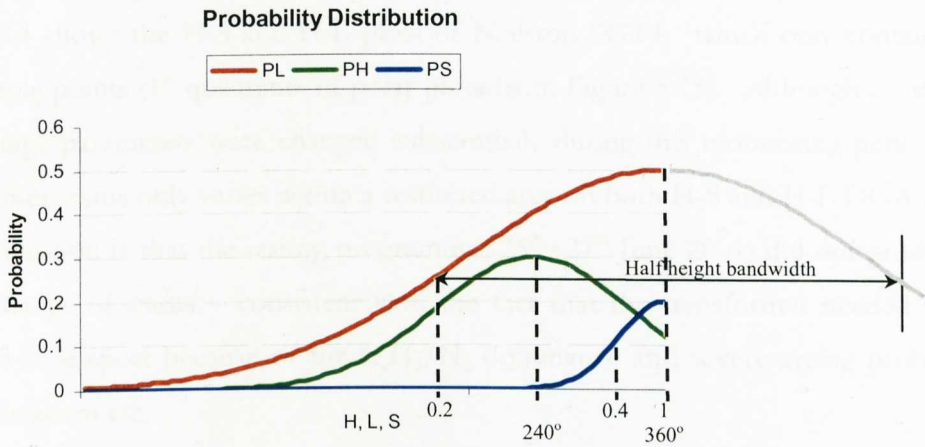
Figure 6.3 Probability of failure as a function of the components P_L, P_H, P_S (Equation (6.2))

As a result of this approach the 50 transformer tanks with DGA results, which have been classified on Table 6.1, can be justified in a quantifiable manner:

- Safe status

  The last record of "WYLF1mtb" chromatic results (Page 157[+], Slide 7):

  $$L = 0.034,\ H = 128,\ S = 0.207$$

  $$P = P_L + P_H + P_S = 0.17 + 0.16 + 0.06 = 0.39$$

- Changing status

  The last record of "FFES SGT1" chromatic results (Page 157[+], Slide 9):

  $$L = 0.161,\ H = 208,\ S = 0.785$$

  $$P = P_L + P_H + P_S = 0.23 + 0.28 + 0.18 = 0.69$$

- Faulty status

  The last record of "NeilstonSGT4" chromatic results (Page 157[+], Slide 8):

  $$L = 0.314,\ H = 223,\ S = 0.700$$

  $$P = P_L + P_H + P_S = 0.29 + 0.30 + 0.17 = 0.76$$

6.2.4   DGA Short-time Variations

Conventional practice is to undertake DGA analysis periodically usually over extended time periods (months/years). However it is useful to inspect DGA trends in the presence of fault conditions over short durations (hours). Some Neilston transformer results enable some quasi-continuous monitoring of DGA to be explored.

Figure 6.4 shows the H-S and H-L plots of Neilston SGT4, which only contain site test sample points (1st quadrants of polar plots from Figure 5.15). Although excitation and voltage parameters were changed substantially during this monitoring period, the transformer status only varies within a restircted area on both H-S and H-L DGA plots. The implication is that the testing programme (25th~27th June 2001) did not produce a major change of status – consistent with the fact that the transformer needed to be regarded as suspect because of the C_2H_2/H_2 dominance and severe arcing problems, Buchholz alarm etc.
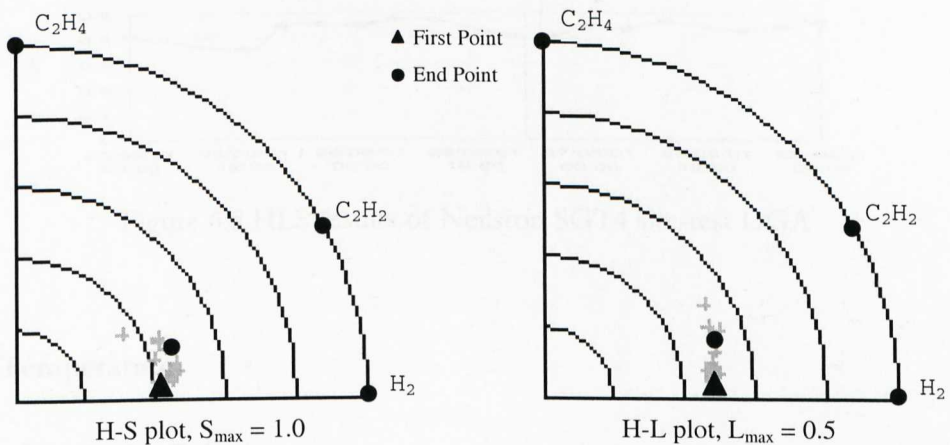
Figure 6.4 Neilston SGT4 site-test DGA (00:00 25/06/01 ~ 00:00 28/06/01)
($S=0$~1, $L=0$~0.5) (Part of Figure 5.15)

To examine these results in more detail, the HLS values have been plotted as a function of time during the tests from 0:00 25/06/2001 to 0:00 28/06/2001. The results are given on Figure 6.5. These show that the L values remain relatively constant (≈ 0.25). The S results show a small tendency for the S value to marginally increase (0.4~0.48, one gas becaming rather more dominant). The H results show a trend for H to increase a little (from 5° to 15°) implying a trend for C_2H_2 to dominate over H_2. The

rate of change of H with time may give an approximate indication of the time response of dissolved gases to fault occurrence.

Also shown on Figure 6.5 are the time instances at which some acoustic and RF signals were captured (ref. Appendix A and Chapter 4). This data for RF and three acoustic sources during this short time interval indicate that there was radio frequency and acoustic pulses produced, probably indicating partial breakdowns inception.
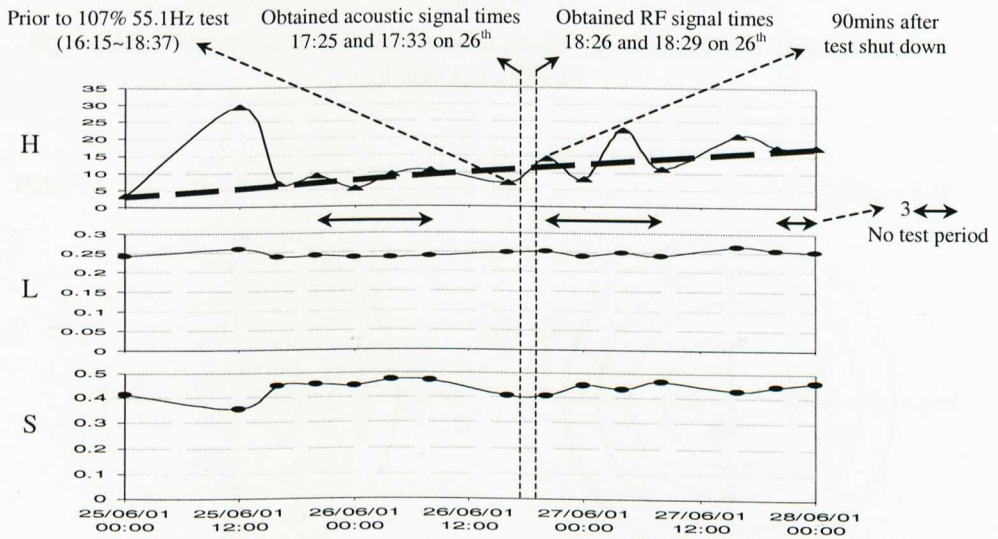
Figure 6.5 HLS results of Neilston SGT4 site-test DGA

6.3   Temperature

6.3.1   Sensitivity Calculation

With the processing experience from DGA, the temperature data, which also contains discrete sample records, were processed using a similar method applied for DGA with TTFR normalization as well. In order to examine the sensitivity of the applied tristimulus approach, the only temperature data, which has less variation than the DGA data, is chosen to inspect the HLS chromatic map calculated based on different normalization values. Figure 6.6 to Figure 6.8 show some interesting results in the form of H-S and H-L polar plots with results normalized with three different reference values.
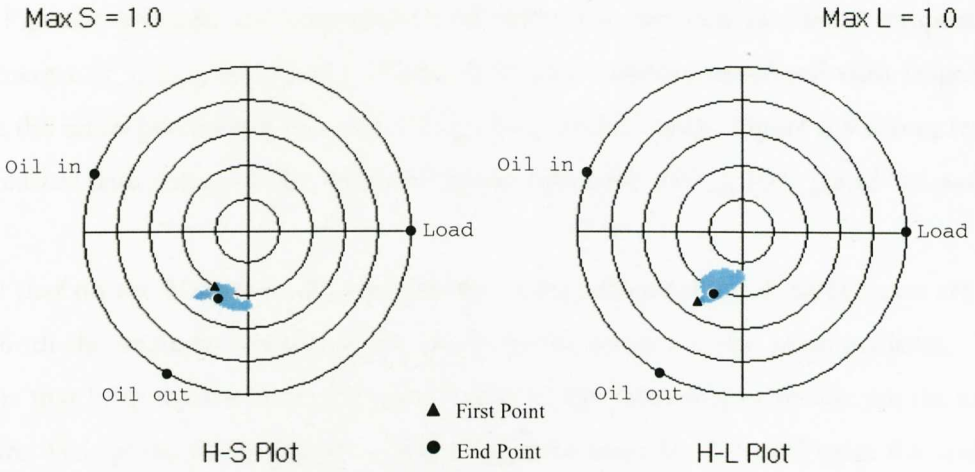
Figure 6.6 Temperature normalization based on one time of first records
(S=0~1, L=0~1)
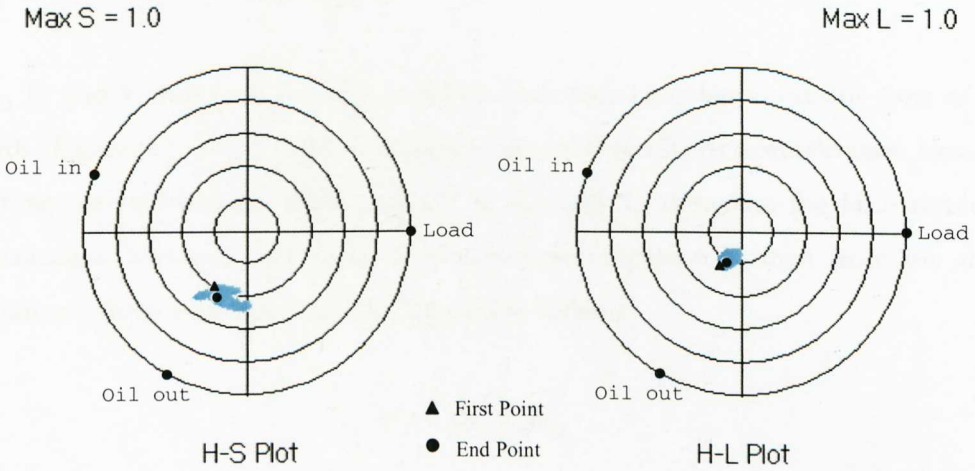
Figure 6.7 Temperature normalization based on two times of first records
(S=0~1, L=0~1)
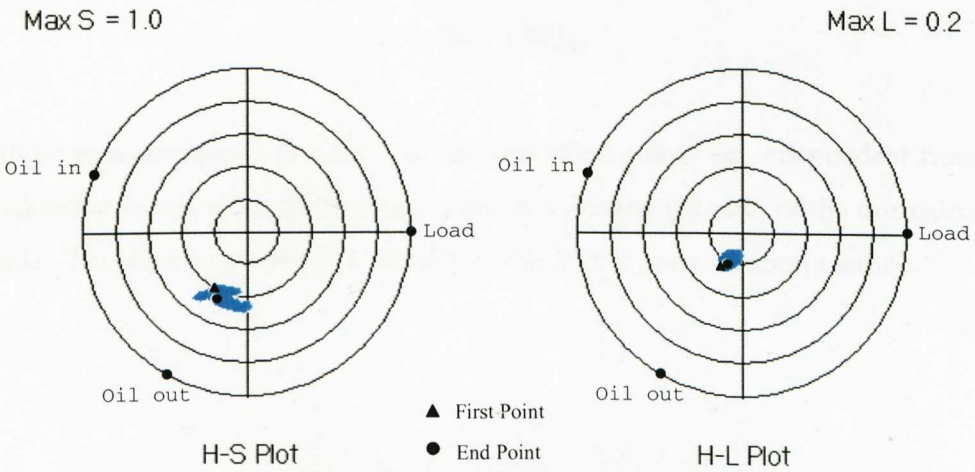
Figure 6.8 Temperature normalization based on ten times of first records
(S=0~1, L=0~0.2)

The Figure 6.6 results are normalized with respect to the first measured temperature parameters (T_{in0}, T_{out0} and $Load_0$). Figure 6.7 shows results normalized with respect to twice the initial parameters values (i.e. $2T_{in0}$, $2T_{out0}$ and $2Load_0$). Figure 6.8 shows results normalized with respect to ten times the initial values (i.e. $10T_{in0}$, $10T_{out0}$ and $10Load_0$).

Note that on the H-S plots, the maximums of the saturation in all three cases are 1.0, and both the angle and radius of the result points remain at the same position. This means that both the hue and saturation values of the three sets of results are the same. For the H-L plots, the maximums of the lightness scale are 1.0 on Figure 6.6 and 6.4 but 0.2 on Figure 6.8 for clarity. Considering the locations of the result points, the hue angles for all three cases are unchanged, but the radii vary according to the multiple number used in the normalization.

If H_1, L_1 and S_1 designate the HLS results of normalization based on one time of first records (Figure 6.6); H_2, L_2 and S_2 designate the HLS results of normalization based on two times of first records (Figure 6.7); H_{10}, L_{10} and S_{10} designate the HLS results of normalization based on ten times of first records (Figure 6.8); then from the above illustrations, three equations may be deduced as follows.

$$H_1 = H_2 = H_{10}$$

$$S_1 = S_2 = S_{10}$$

$$L_1 = 2L_2 = 10L_{10}$$

The three equations prove that the hue and saturation values are independent from the normalization values while the lightness value is reflecting the ratio of the normalization multiple. This also supports the feasibility of the TTFR normalization method.

6.4   Electrical/RF

6.4.1   Normalization Scheme

Unlike DGA or temperature data, RF signals provide instant information, since each set of the RF signals recorded lasts no more than one power cycle (20ms) but contains at least 200,000 sample points. The normalization difficulties experienced with the DGA results are therefore removed. Also there is only a single result value for the RF technique at one time instant compared with 7 DGA gas components. Thus, in the chromatic processing of RF signals, a tristimulus filter is not directly applied on the raw data in the time domain but in the frequency domain.

From the frequency spectrum, some of the RF signals contain high frequency components with extremely high density as shown in Figure 6.9 – the logarithm scale in Figure 6.9 (b) enhances the details of the low frequency components. If the R, G and B filters have equivalent gains over the whole frequency spectrum of such a signal, then the output of the low frequency end, which might contain useful PD information, will be neglected since the output of the high frequency end (B filter) is several hundreds or thousands times larger than that of the low frequency end (R filter). This should be avoided. Hence, for RF signal chromatic processing, a pseudo normalization processing is applied on the outputs of R, G and B filters.

(a)   (b)
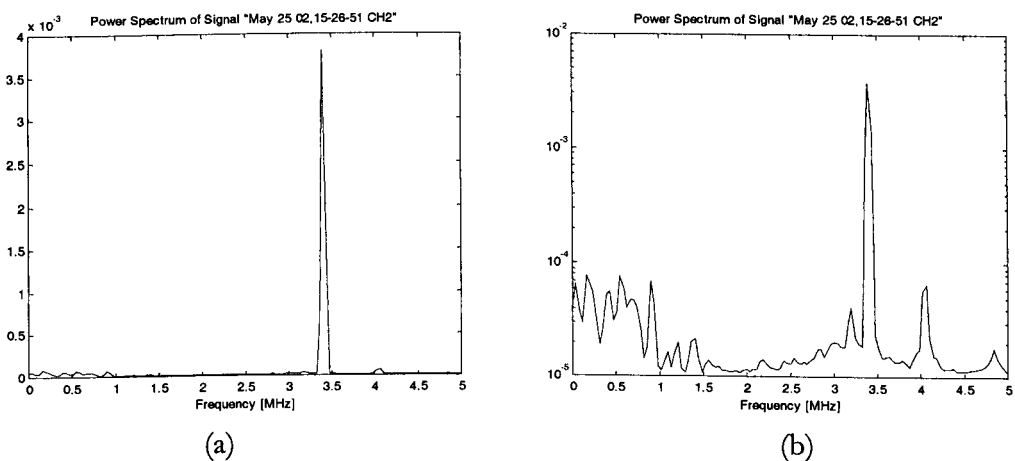
Figure 6.9 Power spectrum of UMIST RF signal "May 25 02, 15-26-51"
(a) Linear scale for signal CH2 (b) Logarithm scale for signal CH2

The pseudo normalization is by simply adjusting the RGB outputs onto a comparable level by applying R/R_{max}, G/G_{max} or B/B_{max} individually (R_{max}, G_{max} and B_{max} are the maximums of the outputs R, G and B sequences respectively). This means that the useful low frequency components are enhanced with the high frequency component still available but attenuated. Unlike setting a threshold or changing the frequency range of the filters, the extreme high frequency range is not simply cut off, which might have some other information.

6.4.2 General Signal Observations

There are at least five types of short duration ($\leq$ 10us) pulsed waveforms observed on Figure 5.27 and Figure 5.30. These are

- Pulsed waveform with the same frequency as the background but with increased amplitude

- Pulsed waveform with an additional frequency component superimposed on the background signal and increased amplitude

- Pulsed waveforms on different channels with different frequencies (probes related (Figure 5.30))

- Pulsed waveforms having different time duration

- Pulsed waveforms having different envelope shapes

These different pulse forms are all concerned with the interactivity of at least two signal waveforms one of which may be regarded as "background". There is also evidence of two forms of interactivity between the simultaneously occurring waveforms, which are

- Additional superposition which leads to interference

- Multiplication which is modulation in nature

The latter often occurs under pulsatile conditions.

Analysis of these waveforms to extract a deeper level of information will need to respect all these different manifestations, distinguish between them and relate to different physical effects. The chromatic processing has the capability of providing such signal discrimination leading to the need to relate various signal features to particular physical phenomena.

Chromatic processing of the RF signals has been shown to be capable of yielding the following information:

- By time stepping a narrow time window (~10us) along the period of a 50Hz voltage waveform it is possible to distinguish between pulses having different composition via the perturbing effects of the pulses on each of the chromatic parameters H, L and S. This means that not only should it be possible to identify the point-on-wave of a pulse but also to identify its nature and so provide a map of point-on-wave occurrence of different pulse types.

- Once the pulses have been located they may be chromatically probed on shorter time scales (~10us) in order to provide more detailed signal discrimination in terms of the HLS chromatic parameters. The implication is that it may be possible for the HLS numerical classification to provide a means for identifying pulses from different sources (air corona, partial discharge inside the tank but outside the windings and PD inside the windings).

- Analysis of pulses on various phases of the transformer also has the potential of identifying the offending phase and distinguishing it from pick up on the other phases

6.4.3   Electrical/RF Signal PD Pulses Classification

Attempts can be made to chromatically classify the various pulse forms detected by the different radio frequency techniques and measurements made on the Northfleet transformer by six organizations (Glasgow Caledonian, UMIST, Siemens, KEMA, Southampton and Bath) described in Chapter 5 and Section 6.4.1, 6.4.2 of this present chapter. For this purpose various results provided by the above organizations have been chromatically analysed as already described and are summarized in Table 6.2.

This lists the various RF tests results provided by the investigations and indicates as a function of point on 50Hz wave (0~20ms) the occurrence or non-occurrence of RF pulses. Each detected pulse is then shown according to changes, which occurred from the background signal in terms of each of the chromatic parameters H, L and S. Thus,

-*H* indicates that the hue value decreased; +*L* indicates that the lightness value increased etc.

Table 6.2 List of criteria for PD RF signal processing

Sample \ t [ms]	1	2	3	4	5	6	7	8	9	10	11	12	13	14	15	16	17	18	19	20
G-C2				f		a				g							g			
G-C3						f				f							c			
G-C4				f		a				c	a						f			
U-1526-2						c				f				c						
U-1526-3														c						
U-1526-4s														a						
U-1527-2		c				f														
U-1527-3		c																		
U-1527-4s		c																		
U-1531-2			e														f			
U-1531-3			c														f			
U-1531-4s			c														f			
U-1539-2			d					g					c							
U-1539-3			c										g							
U-1539-4s			c										f							
U-1533-A																				
U-1710-A																				
U-1722-A																				
S-AF1212			c							c						c				
S-AF1335	c																			
S-BF1218	b							c		c					c	c				
S-BF1310	a						a		a	f										
S-CF1207							g		a	g				g		a				
S-CF1226	c							c		c			c		c		c			
B-0921-3k	a	c										c	c							
B-0921-4																				
B-0923-3k	c	c	c			f					c	c	2f	c	c	a	2f	c	f	2c
B-0923-4																				

Symbol	a	b	c	d	e	f	g
Pattern	+*H*+*L*-*S*	-*H*+*L*+*S*	-*H*+*L*-*S*	-*H*+*L*	+*L*+*S*	+*L*-*S*	-*S*
Count	11	1	40	1	1	18	7

Notes for signal sample names:
G: Glasgow, e.g. Glasgow C2-10-34-24 (G-C2), Figure 5.24
U: UMIST, e.g. UMIST May2502 15-26-51CH2 (U-1526-2), CH4 Siemens (U-1526-4s), Figure 5.29
S: Southampton, e.g. Southampton AF1212 (S-AF1212), Figure 5.32
B: Bath, e.g. Bath 092110 CH4 (B-0921-4), Bath 092110 CH3 KEMA (B-0921-3k), Figure 5.35

There are seven categories of chromatic signal changes observed which are -*S*, +*L*±*S*, -*H*+*L*, +*H*+*L*-*S* and –*H*+*L*±*S*. Table 6.2 shows that the most predominant signal type occurring during the rising part of the voltage waveform on a positive half cycle (1~4ms) is the "-*H*+*L*-*S*" type. Since this would appear to be the expected period

when partial discharges might be expected to occur **[Kemp, 2001; Kemp et al., 2002]**, the "*-H+L-S*" type signal may be the signature which distinguishes such discharges from others (e.g. air corona).

In order to explore the occurrence of this signal pattern relative to others, the number of such signals compared with others during each time interval of a full cycle is shown on Figure 6.10. From these results the predominance of "*-H+L-S*" during the rising voltage parts of the cycle (both positive and negative going) is clearly demonstrated. Furthermore the ratio of this to other signature types is somewhat greater during a positive going voltage half cycle. It is also interesting to note that this PD signature is identifiable on all the different sources of signals producing signatures.
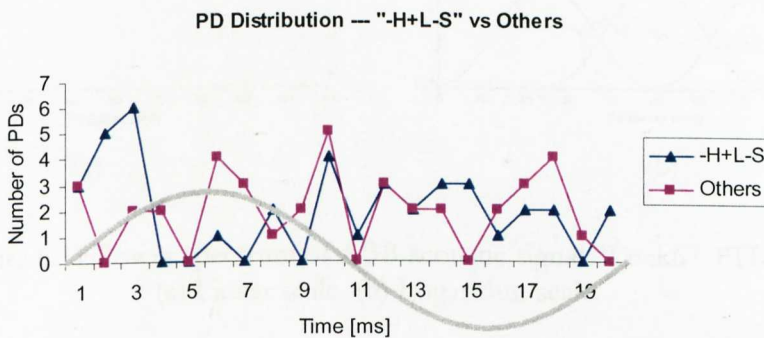
Figure 6.10 PD Electrical/RF chromatic-signature pattern statistics

6.5   Acoustic

6.5.1   Different Frequency Range Inspections

The time varying acoustic signals have been presented in Chapter 4 on Figure 4.27 and Figure 4.28, the chromatic processes on Figure 5.11 and the relevant HLS results on Figure 5.37 and Figure 5.38. The power spectra of these latter two signals are shown on Figure 6.12 and Figure 6.11. Both the linear and logarithmic plots (Figure 6.11 (a) (b) and Figure 6.12 (a) (b)) show that most of the power density is within the frequency range 0~10kHz (possibly 20kHz) and the inherent frequency of the transformer voltage

was about 50Hz, so that the two acoustic signals Lock67 and Lock95 were first

inspected in the frequency range 100Hz~10kHz (avoiding 50Hz interference –

experience from acoustic simulation Section 5.6.2). However, results of the form given

on Figure 6.11 and Figure 6.12 allow *HLS* values to be extracted by applying chromatic

processors to other various frequency ranges (e.g. 90k~100kHz and 100Hz~100kHz).

(a)   (b)
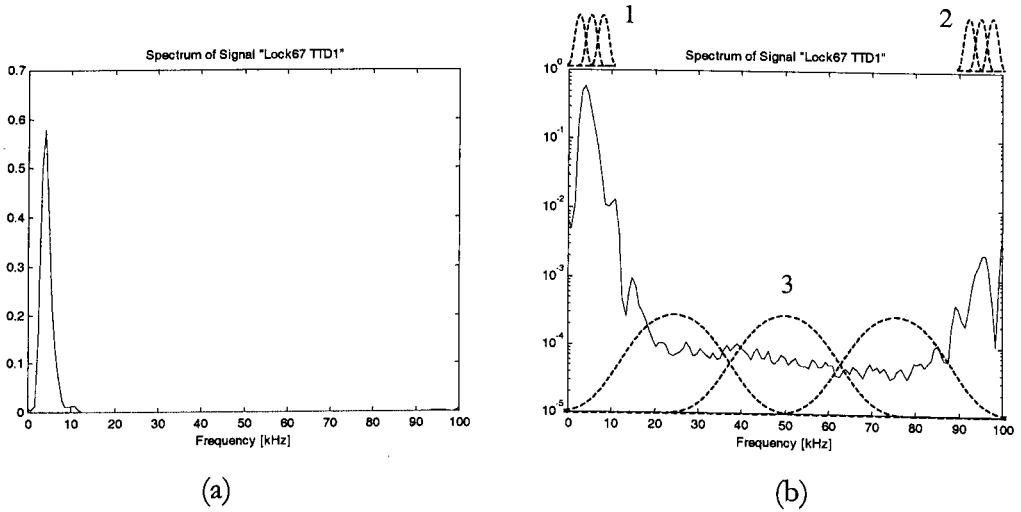
Figure 6.11 Power spectrum of ABB acoustic signal "Lock67 TTD1"
(a) Linear scale (b) Logarithm scale

(a)   (b)
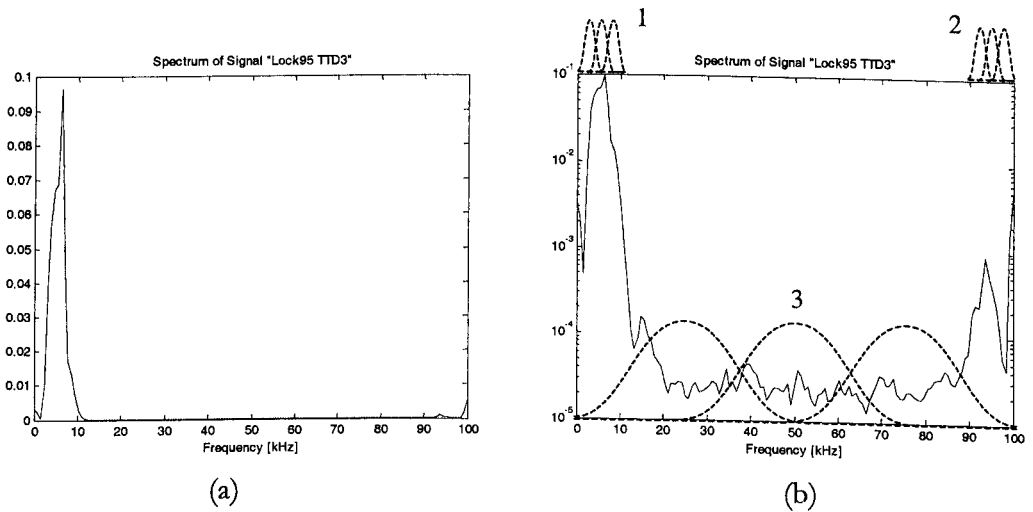
Figure 6.12 Power spectrum of ABB acoustic signal "Lock95 TTD3"
(a) Linear scale (b) Logarithm scale

The logarithmic plots in Figure 6.11(b) and Figure 6.12(b) also suggest that in order to increase the weight of the lower amplitude components it would be profitable to weight accordingly inputs into the chromatic processors.

6.5.1.1   Logarithmic and Exponential Processing

The possibility of pre-processing the acoustic signals logarithmically or exponentially has been investigated to exaggerate the partial discharge effects with respect to noise and standard 50Hz signal. Such weighting has been applied to the measured time varying signals of Figure 4.27 and Figure 4.28 and also to the outputs of the chromatic processors of Figure 5.11 i.e. *R*, *G* and *B*. Two different weightings have been evaluated viz. $\log_{10}(x)$, 10^x. These two functions are shown on Figure 6.13.

These investigations show that the time varying signals (Figure 4.27 and Figure 4.28) have most values in the range 0~0.2 and some negative values leading to unhelpful logarithmic function (Figure 6.13). The use of the function 10^x with these time varying signals leads to only small changes in 10^x of $10^0 = 1$, $10^{0.2} \approx 1.58$ which is not helpful in suppressing noise.
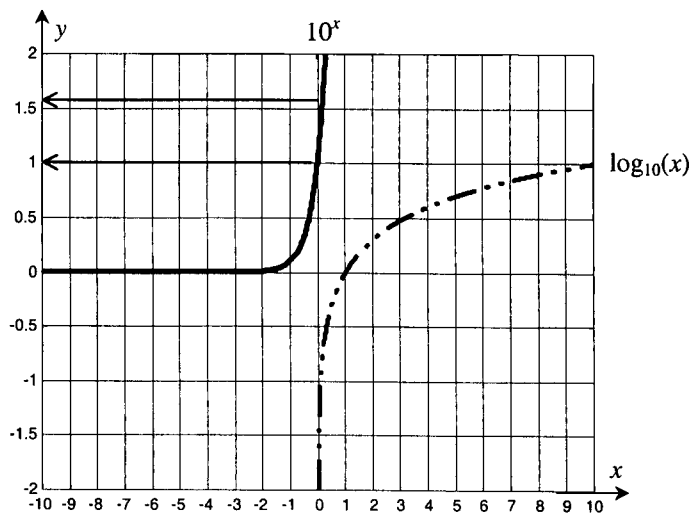
Figure 6.13 Logarithm and exponent functions

The R, G and B values derived from the time varying signals have been analysed similarly i.e.:

$$10^x \qquad [x = R, \ G \ or \ B]$$

$$\log_{10}(x) \qquad [x = R, \ G \ or \ B]$$

The results of these investigations may be summarized as follows:

1) The methods of applying 10^x $[x = R, \ G \ or \ B]$ and $\log_{10}(x)$ $[x = R, \ G \ or \ B]$ can suppress noise with good performance for most of the frequency ranges, especially the 10^x weighting. This is because the RGB values of the background in the two signals were in the range 0~0.2 and those of the signals were within the range 0.5~1, i.e. from Figure 6.13, $10^{0.2} \approx 1.58$, $10^1 = 10$; $\log_{10}(0.2) \approx -0.7$, $\log_{10}(1) = 0$. In both cases the differences are expanded by the exponential or logarithmic processing, especially the exponent function.

2) For most of the frequency ranges analysed, the hue and saturation variations are clarified after applying exponential or logarithmic processing of the RGB values, whilst the lightness is a good indicator all the time (Figure 6.14).

3) Results for the frequency range 100Hz~100kHz are not greatly affected by whether logarithm or exponent processing is utilized (Figure 6.15(a) and (b)).

The most obvious features of the results presented on Figure 5.37 and Figure 5.38 are that Lock67 has an exceptionally longer duration and sharper but relatively weaker front than Lock95. This suggests that the discharges may be of two different types. More detailed inspection of the H-S, H-L polar plots of Figure 5.37 and Figure 5.38 show that the most dominating frequencies are $\approx$70kHz for both Lock67 and Lock95.
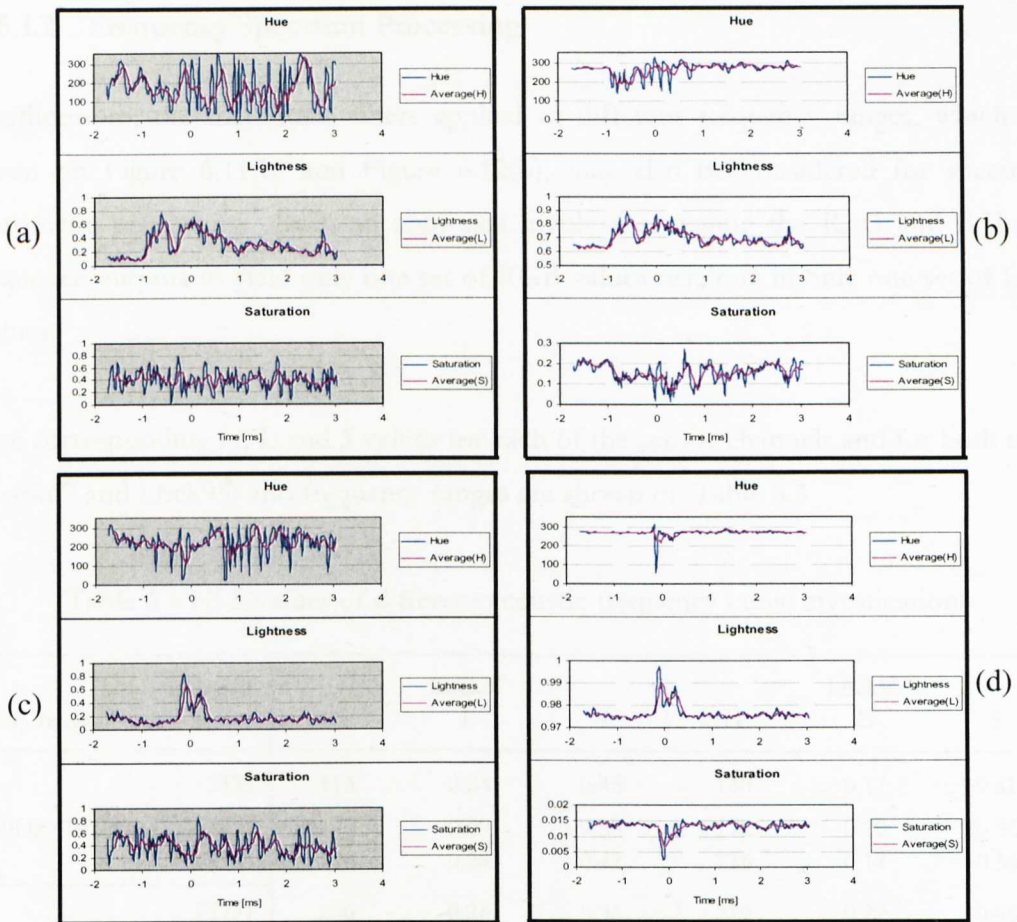
Figure 6.14 Acoustic Ex1 HLS results with exponential/logarithmic processing
Lock67 TTD2 (100Hz~10kHz) exponential processing (a) without, (b) with
Lock95 TTD1 (90k~100kHz) exponential processing (c) without, (d) with
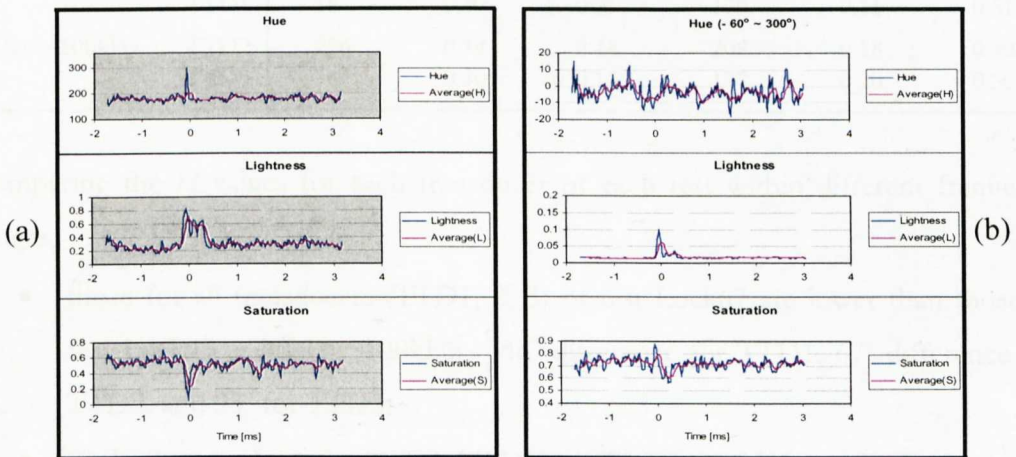
Figure 6.15 Acoustic Ex2 HLS results with exponential/logarithmic processing
Lock95 TTD1 (100Hz~100kHz) exponential processing (a) without, (b) with

6.5.1.2   Frequency Spectrum Processing

Furthermore, the tristimulus filters applied to different frequency ranges, which are given on Figure 6.11(b) and Figure 6.12(b), may also be considered for spectrum chromatic processing. Such an approach involves averaging the *R*, *G* and *B* three-sequence outputs to yield only one set of RGB values resulting in only one set of HLS values.

The corresponding *H*, *L* and *S* values for each of the sensor channels and for both tests (Lock67 and Lock95) and frequency ranges are shown on Table 6.3.

Table 6.3 HLS values of different acoustic frequency range investigations

Freq. range	Signal	Lock67			Lock95		
		H	L	S	H	L	S
	TTD1	116	0.24	0.45	140	0.17	0.41
100Hz~10kHz	TTD2	170	0.29	0.39	172	0.20	0.56
	TTD3	178	0.24	0.42	136	0.14	0.56
	TTD1	206	0.28	0.36	229	0.29	0.56
100Hz~20kHz	TTD2	260	0.35	0.44	220	0.22	0.55
	TTD3	202	0.31	0.33	230	0.25	0.67
	TTD1	177	0.27	0.42	223	0.17	0.39
90kHz~100kHz	TTD2	180	0.31	0.33	247	0.20	0.60
	TTD3	141	0.28	0.35	234	0.17	0.64
	TTD1	187	0.40	0.21	179	0.31	0.51
100Hz~100kHz	TTD2	226	0.34	0.14	208	0.18	0.30
	TTD3	167	0.40	0.13	177	0.20	0.50

Comparing the *H* values for each transducer of each test within different frequency ranges,

- those for all transducers (TTD1, 2, 3) of test Lock67 are lower than those of test Lock95 at 90kHz~100kHz – 46° difference for TTD1, 67° difference for TTD2, and 93° for TTD3;

- for both tests those for TTD1, TTD2 and TTD3 at 100Hz~100kHz show only a small difference – 8°~18° and neither test has greater value than the other for all TTDs;

- those within other frequency ranges of both tests have a moderate difference $2°\sim42°$, but neither test has greater values than the other for all TTDs.

Comparing the L values for each transducer of each test within different frequency ranges, almost all the L values for all TTDs of Lock67 are greater than those of Lock95 (differences mostly about 0.1 varying from 0.07 to 0.2), except the one for TTD1 at 100Hz~20kHz (difference -0.01).

Comparing the S values for each transducer of each test within different frequency ranges, almost all S values for all TTDs of Lock67 are smaller than those of Lock95 (differences mostly about -0.2 varying from -0.11 to -0.37), except the one for TTD1 at 100Hz~10kHz (difference 0.04) and the other one for TTD1 at range 90kHz~100kHz (difference 0.03).

Thus, to summarise, the test Lock67 contains more frequency components (smaller S, polychromatic) and higher spectrum density (larger L) than Lock95 at all ranges. The two tests are fully discriminated within the frequency range 90kHz~100kHz. These facts indicate that Lock67 involves more activities (possibly different PDs or noise) than Lock95 and the possible PD pulses captured in Lock95 are mainly within the frequency range 90kHz~100kHz.

6.5.2   Time Domain Processing

Since acoustic time scales are significantly longer than those for ultra-high radio frequencies and the acoustic signals were noisier than the RF signals, it is not possible to discriminate individual discharge events so clearly with the acoustic technique, as with the UHF technique when a substantial multiplicity of discharge events occurs. A different chromatic processing approach needs to be utilised. Thus a time-domain chromatic process was performed on the time-varying acoustic signals as well. Figure 6.16 shows the scheme of how the tristimulus filters were applied to a time-varying acoustic signal.

Acoustic Signal Time-domain Chromatic Processing
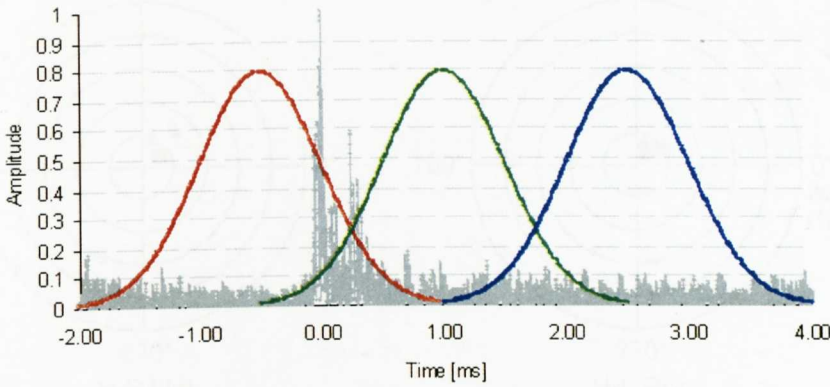
Figure 6.16 Acoustic signal time-domain chromatic processing

For the two sets of TTD time-varying signals, Lock67 and Lock95, the time-domain chromatically processed results are shown in Figure 6.17 and Figure 6.18 respectively. The interpretation for HLS parameters is as follows: -

- The hue angle indicates a dominant time instant (phase location according to one power waveform cycle) at which the signal occurs.

- The lightness value indicates the nominal signal strength – the higher the value, the stronger the strength.

- The saturation value indicates the effective pulses duration – the higher the value, the shorter the duration.
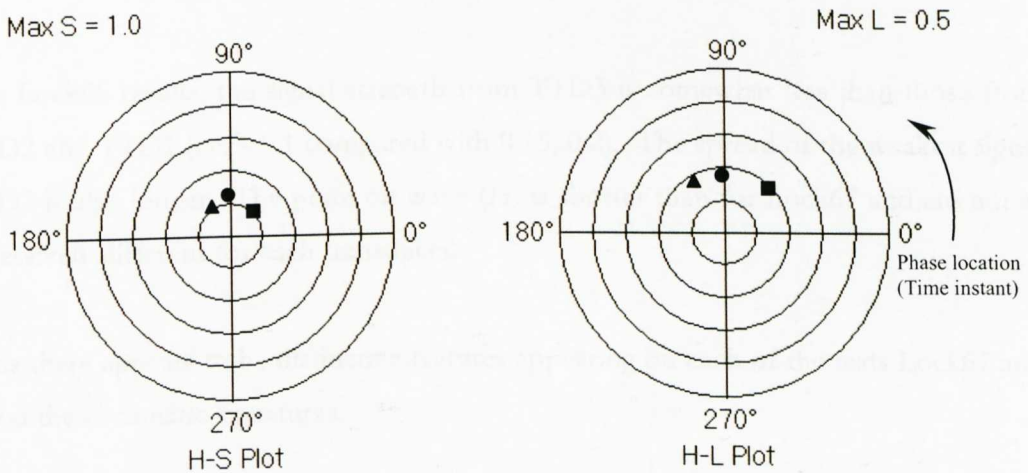
Figure 6.17 Time-domain chromatically processed results for signal "Lock67"
TTD1: triangle, TTD2: square, TTD3: circle
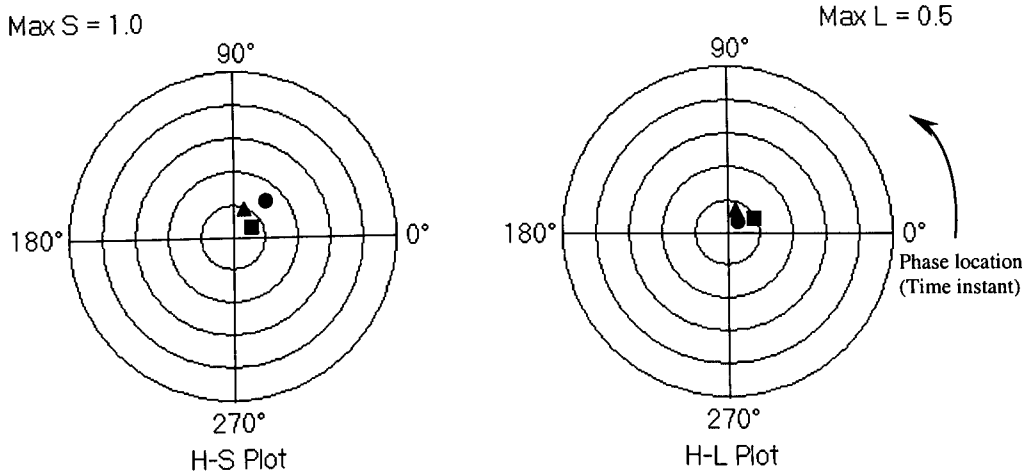
Figure 6.18 Time-domain chromatically processed results for signal "Lock95"
TTD1: triangle, TTD2: square, TTD3: circle

Thus the results shown in Figure 6.17 and Figure 6.18 yield the following implications.

For Lock67 the signals from each of the three transducers have similar strengths (H-L plot $L \approx 0.4$) and spreads (H-S plot $S \approx 0.2$). Thus the main differences are in the dominant phase with phase increasing in the order TTD2, TTD3 and TTD1 all occurring during the first half cycle of voltage. The implication is that the signals to each transducer are approximately equally attenuated, but have different dominant points on wave, suggesting that the propagation paths are differently affected.

The Lock95 results, the signal strength from TTD3 is somewhat less than those from TTD2 and TTD1 (i.e. ≈ 0.1 compared with 0.15, 0.2). The spread of the weakest signal TTD3 is also longer. The point on wave (H) is shorter than for Lock67 and are not as excessively different for each transducer.

Thus there appears to be distinctive features appearing on each of the tests Lock67 and 95 on the chromatic signatures.

6.5.3 Combinatorial Chromaticity Theory

Combinatorial chromaticity is concerned with the problem of combining three separate sets (e.g. TTD1, TTD2 and TTD3) of chromatic parameters (H, L, S) to produce heavier compression with control of discrimination being retained as well as traceability. The approach to a fusion of chromatic signals via second generation chromatic processing is illustrated in Figure 6.19.

The first step is to map the HLS values for each of the TTD1, TTD2 and TTD3 results, as demonstrated in Section 6.5.2. The resultant three chromatic maps are shown individually as step 1 on Figure 6.19.

The second step shows the equivalent Gaussian distribution for the TTD1, TTD2 and TTD3 results. H defines the weighted central time of the signal, L the signal strength and S the nominal time spread of the signal. This follows from the general definition of the Gaussian distribution (density function) **[Papoulis et al., 2002]**:

$$f(x) = \frac{1}{\sqrt{2\pi\sigma^2}} \exp[-\frac{1}{2}(\frac{x-\mu}{\sigma})^2]$$

(6.4)

where

σ, standard deviation; μ, mean

Assuming the horizontal parameter axis is normalized to 1, for a particular hue angle H of a 360° circle, its central position on the axis, μ, would be:

$$\frac{\mu}{1} = \frac{H}{360}$$

(6.5)

Considering a monochromatic ($S = 1$) signal, which only contains a single frequency component, its half height bandwidth is equal to 0, i.e. $\sigma = 0$; conversely, an extreme polychromatic ($S = 0$) signal contains frequency components covering the whole bandwidth, i.e. $\sigma \rightarrow \infty$. Hence,

$$\sigma = \frac{1-S}{S}$$

(6.6)
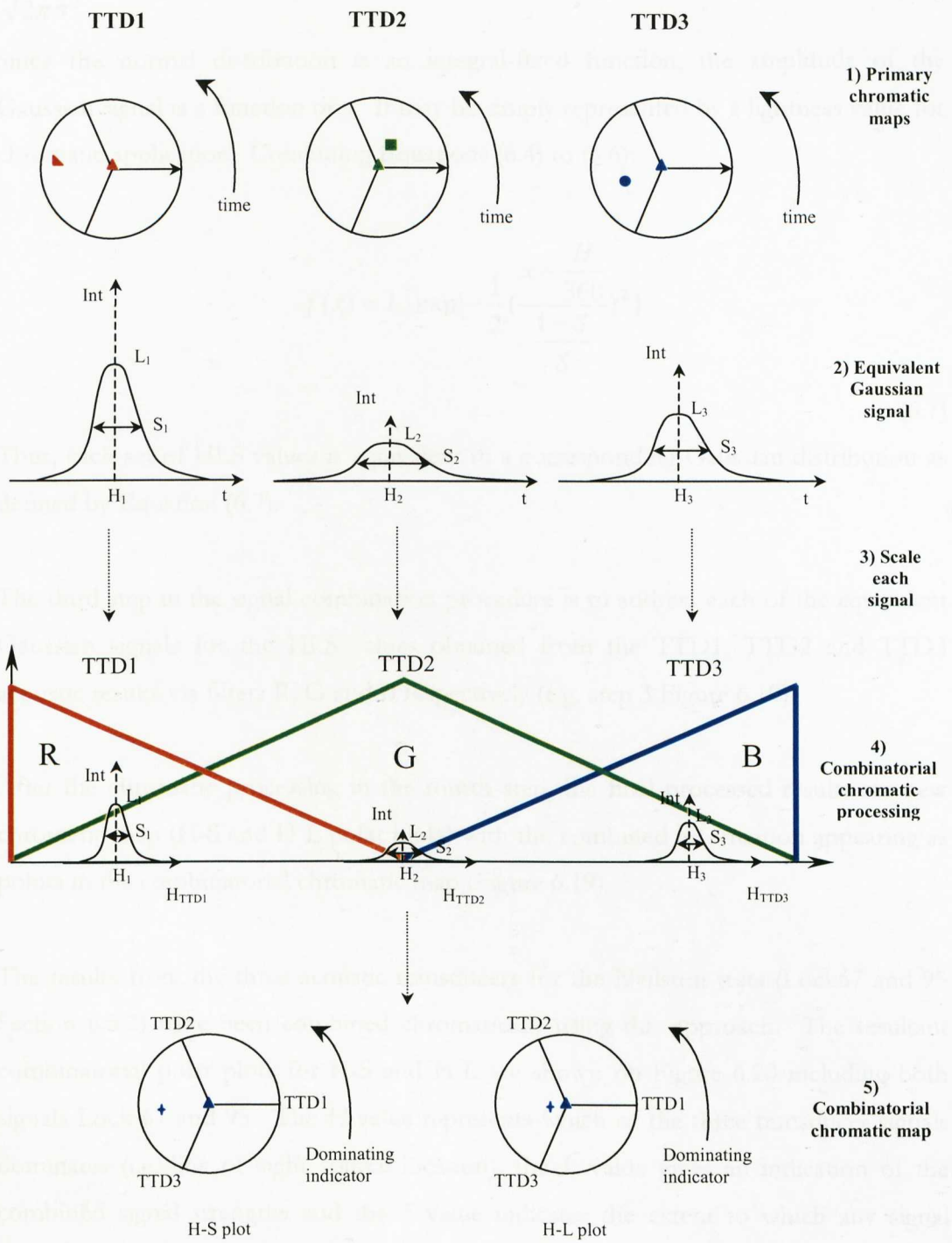
Figure 6.19 Combinatorial chromaticity schematics
(For the trio of acoustic transducers TDD1, 2 and 3)

$\dfrac{1}{\sqrt{2\pi\sigma^2}}$ in Equation 6.1 may be considered the amplitude of the Gaussian signal. Since the normal distribution is an integral-fixed function, the amplitude of the Gaussian signal is a function of σ. It may be simply represented by a lightness value for chromatic application. Combining Equations (6.4) to (6.6):

$$f(x) = L \cdot \exp[-\frac{1}{2}(\frac{x - \dfrac{H}{360}}{\dfrac{1 - S}{S}})^2]$$

(6.7)

Thus, each set of HLS values is equivalent to a corresponding Gaussian distribution as defined by Equation (6.7).

The third step in the signal combination procedure is to address each of the equivalent Gaussian signals for the HLS values obtained from the TTD1, TTD2 and TTD3 acoustic results via filters R, G and B respectively (e.g. step 3 Figure 6.19).

After the chromatic processing in the fourth step, the final processed results are new chromatic map (H-S and H-L polar plots) with the combined information appearing as points in the combinatorial chromatic map (Figure 6.19).

The results from the three acoustic transducers for the Neilston tests (Lock67 and 95 Section 6.5.2) have been combined chromatically using this approach. The resultant combinatorial polar plots for H-S and H-L are shown on Figure 6.20 including both signals Lock 67 and 95. The H value represents which of the three transducer signals dominates (i.e. line of sight source location), the L value gives an indication of the combined signal strengths and the S value indicates the extent to which any signal transducer is dominant.

Max S = 1.0   Max L = 0.5

H-S Plot   H-L Plot
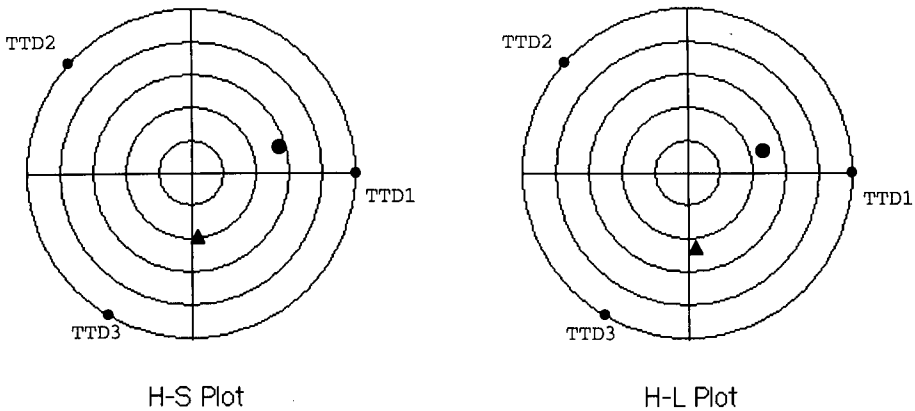
Figure 6.20 Combinatorial chromatic results of ABB acoustic signals
Lock67: triangle, Lock95: circle

The results in Figure 6.20 show that signals of TTD1 and TTD3 are dominating in test Lock67 and mainly TTD1 signal is dominating in Lock95. Both tests have the same combined signal strengths.

6.6 Summary

This chapter has deployed some discussions on the individual parameter investigations (DGA, temperature monitoring, electrical/RF emissions and acoustic emissions analyses) respectively.

The investigations in DGA have classified the transformer working conditions into three statuses (safe, changing and faulty). A calculation of the probability of transformer failure has been introduced, yielding a quantifiable manner to justify the DGA results. It also has been suggested to pay more attention to short-time DGA variations. In aspect to the temperature monitoring discussion the outcomes of chromatic map sensitivity has been investigated. A numerical PD classification has been established based on the various pulses chromatically detected from the RF PD

signal. The discussion in acoustic signal processing has involved different frequency range inspection with either exponential/logarithmic processing or frequency spectrum processing; both have provided chromatic signatures in different manner. The time-domain chromatic processing used in acoustic signal investigations has yielded an application of combinatorial chromaticity. The combination analyses have suggested a constructive means to further compress information.

All these outcomes and summaries in previous chapters lead to the conclusions detailed in the final chapter followed.

Chapter 7

Conclusions and Further Work

Since all the sections in previous chapters of this thesis are presented in the sequence DGA, temperature, electrical/RF and acoustic, the conclusions drawn and detailed in this chapter also follow the same order, likewise the discussion of further work.

7.1 Conclusions

7.1.1 DGA

Chromatic DGA signatures have been established using results from 50 transformer tanks (36 from NGT, 14 from First Hydro) colleted over a period of 27 years. These results are capable of yielding trend patterns, which appear to be associated with indications of a transformer leading to increased risk of failure. Three categories of transformer working conditions (safe, alert and faulty) have been established based on such chromatic DGA signatures.

A transformer failure probability theory has been introduced. By implementing a calculation of the probability of transformer failure, the DGA results can be justified in a quantifiable manner. Consequently the project has made good progress towards the objective of achieving an early identification of incipient transformer failures due to partial discharges.

Clearly the gathering of dissolved gas analyses for a large number of transformer units could provide a valuable statistical approach. The software package produced during this project is being provided to NGT for their use to analyse their continued growth in transformer DGA database.

The discrete data chromatic processing with innovative normalization scheme produced and implemented in DGA investigations has been made contribution to the chromatic theory further development.

7.1.2 Temperature

Chromatic processing of transformer temperature data has been used to explore the representation of temperature trends, possibly significant PD induced, against a background of diurnal variations in ambient temperature and transformer loading. A number of different schemes for clustering the relevant parameters have been investigated. These have shown that the transformer was well behaved under normal transformer operating conditions.

The sensitivity of chromatic map has been investigated for the temperature analysis of one transformer using different chromatic parameters normalization schemes. The results prove that of the three chromatic parameters, both H and S are independent of the normalization method. It was only the signal strength L, which varied with the normalization base, consistent with expectation.

7.1.3 Electrical/RF

Chromatic electrical/RF PD signatures have been derived from a number of test results provided by KEMA obtained during one set of site tests and by Glasgow Caledonian University, UMIST (including results via Siemens and KEMA probes), University of Southampton and University of Bath obtained during a second set of site tests.

A new informative representation method of PD events on a polar plot has been developed for better understanding of PD events distribution related to the transformer power waveform.

Chromatic discrete processing applied to UHF PD events, enables one point on a H-S or H-L map to be used to represent PD activity, its extent, magnitude and phase location on a 50Hz power waveform. Such a simplified and informative diagram helps engineers to grasp the vital information.

The chromatically detected and identified PD pulses in the time-varying electrical/RF signals indicate the possibility that the HLS numerical classification might provide a means for identifying pulses from different sources (air corona, PD inside the tank but outside the windings and PD inside the windings).

Various noise reduction attempts implemented in the continuous signal chromatic processing have been provided valuable research experience for the chromatic applications in other areas.

7.1.4 Acoustic

Acoustic chromatic signatures have been derived from a more limited number of results provided by ABB obtained during the first set of site tests described in this thesis.

Different PD characteristics can be identified chromatically based on acoustic signals processed in the frequency domain, in terms of dominating frequency component, level of discharge and frequency of occurrence.

The time-domain chromatic integration for the acoustic signal from each of the 3 acoustic transducers resulting in 3 points on either H-S or H-L plot, enables the arrival time-delay of the 3 signals to be quantified. This could improve the 3D triangular calculation for PD source localisation, which for example is performed by ABB (Section 3.5).

Due to the three-in-one specialties of the acoustic signals, the chromatic combination for signals from three transducers has provided a constructive means to further compress the acoustic information. Also it has explored the extent of the chromatic methodology.

7.2 Further Work

7.2.1 DGA

For the DGA, results of Section 6.2.2 the three states of transformer condition (safe, alert and faulty) are classified according to the layout of points on a chromatic map (H-S and H-L polar plots), and takes account the time factor. However the probability calculation detailed in Section 6.2.3 only considered the final set of LHS values, which neglects the history of the transformer. An improvement to this approach, which takes account of the transformer history, may be considered as follows.

The formulae presented in Section 6.2.3, which only took the final values into account, may be considered as a "Static Analysis":

$$P = P_1(L_f, H_f, S_f) = l \cdot P_L(L_f) + h \cdot P_H(H_f) + s \cdot P_S(S_f) \tag{7.1}$$

where

L_f, H_f, S_f are final values of L, H, S.

Consequently an analysis taking all historical sets of LHS values into account may be regarded as a "Dynamic Analysis". This leads to the formulation:

$$P_D = l \cdot [P_{\nabla L}(L_L) + P_{\nabla L}(H_L) + P_{\nabla L}(S_L)] +$$
$$h \cdot [P_{\nabla H}(L_H) + P_{\nabla H}(H_H) + P_{\nabla H}(S_H)] +$$
$$s \cdot [P_{\nabla S}(L_S) + P_{\nabla S}(H_S) + P_{\nabla S}(S_S)]$$

$$= [l \cdot P_{\nabla L}(L_L) + h \cdot P_{\nabla H}(L_H) + s \cdot P_{\nabla S}(L_S)] +$$
$$[l \cdot P_{\nabla L}(H_L) + h \cdot P_{\nabla H}(H_H) + s \cdot P_{\nabla S}(H_S)] +$$
$$[l \cdot P_{\nabla L}(S_L) + h \cdot P_{\nabla H}(S_H) + s \cdot P_{\nabla S}(S_S)]$$

$$= P_1(L_L, L_H, L_S) + P_1(H_L, H_H, H_S) + P_1(S_L, S_H, S_S)$$

$$\text{or} = \sum \left\{ \gamma \sum [P_{\nabla \Gamma}(\Psi_\Gamma)] \right\}$$

(7.2)

where

$$\gamma = l, h, s; \quad \Gamma = L, H, S; \quad \Psi_\Gamma = L_\Gamma, H_\Gamma, S_\Gamma$$

Figure 7.1 shows the schematics of such a DGA dynamic chromatic processing scheme yielding second-generation LHS values. Thus there are 9 chromatic parameters needed to characterise any specified transformer throughout its life based on DGA data.
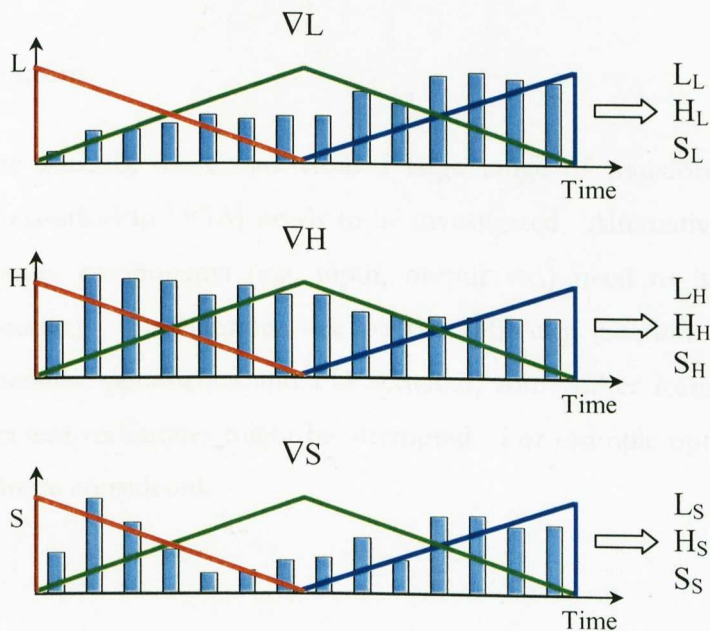
Figure 7.1 DGA dynamic chromatic processing

As detailed in Section 5.2.2, the first-generation of L, H and S parameters provide information of the extent of gassing produced, the dominating gas and the spread of gases produced. Hence the meaning of the second-generation parameters may be considered as follows (subscripts indicate the first-generation parameters):

L_L, Total gas produced historically;

H_L, Dominant time with the largest amount of gas produced;

S_L, Time spread of gas produced;

L_H, Total amount of "dominant species" produced;

H_H, Effective time of "dominant species" occurrence during overall tests;

S_H, Time distribution of relative amounts of "dominant species" during overall tests;

L_S, Time integrated "spread of gases" during overall tests;

H_S, Effective time at which "spread of gases" production is focussed during tests;

S_S, Time distribution of "spread of gases" during overall tests.

Research into the relationship between the above parameters and a formulation for probability of failure calculation using the 9 parameters is now being undertaken within The Centre for Intelligent Monitoring Systems (CIMS).

7.2.2 Temperature

For temperature analysis, more data from a large range of transformers (e.g. with different status classified in DGA) needs to be investigated. Alternative arrangements of the temperature components (e.g. input, output etc.) need to be explored for chromatic processing. Furthermore due to the difficulty (Section 1.2) of linking condition temperature parameters and PD activities, some other forms of heat/light related measurement techniques might be attempted. For example optical fibre based techniques might be considered.

7.2.3   Electrical/RF

With regard to electrical/RF emissions, the cross-correlation of results obtained by different university research groups requires further analysis. For example, what type of PD classified in the Glasgow Caledonian University results corresponds to the one having a chromatic character "$+H+L-S$"; how do these correspond to identifiers produced by UMIST, University of Southampton, University of Bath and others?

7.2.4   Acoustic

In the case of acoustic emissions, some innovative chromatic space-modelling methodology might be created for locating the exact PD position within a transformer.

End of Chapters

Publications

1. IEE Seminar, 2001

TRACKING TRENDS IN THE CHEMICAL COMPOSITION OF SYSTEMS USING CHROMATIC MAPPING

J. Zhang[1], X. Du[1], W. D. Yuan[1], A. Deakin[1], J. W. Spencer[1], G. R. Jones[1], J. R. Gibson[1], W. B. Hall[2], A. McGrail[3], H. Tonge[4]

Introduction.

Chromatic processing was first used on complex optical spectra and with particular application in the field of optical fibre based sensors [1]. The technique was later used for monitoring changes in complex acoustic signals [2] and for monitoring the operation of industrial plant [3]. The technique is capable of tracking changes in both optical and acoustic spectra. The application of the chromatic methodology has been extended to provide a means of tracking trends in the chemical composition of three different systems.

The first system is a high voltage oil filled transformer where unwanted discharge activity may lead to the formation of a range of decomposition products. The second is a waste reduction facility which involves the production of methane. Whilst, the third examines the recombination of SF6 gas which is used as an electrical arc quenching medium for fault current interruption on electrical distribution and transmission systems. The chemical composition for the first application is obtained from residual gas analysis and for the second and third applications from mass spectrometers.

The chromatic methodology provides a rapid means of characterising data so that it can be displayed on a chromatic information map. Data is characterised on this information map by three chromatic parameters. These parameters are used to track changes in the chemical composition and provide qualitative assessment of the relative concentration of the components in that composition.

The applicability and flexibility of the chromatic processing technique as a means for tracking trends is demonstrated through these three applications. The results show that for all these cases the chromatic algorithms permits the tracking of trends in the chemical composition and direct interpretation of these chromatic parameters enabling rapid assessment of the status of the system without being overwhelmed by the incumbent data.

Chromatic Methodology.

Chromatic processing involves the cross correlation of a signal with three non-orthogonal filters [1]. The method was originally used for tracking changes in optical spectra but the technique has been applied to a number of other different signal types, e.g. acoustic [2]. However, the optical terminology remains. In general terms three non-orthogonal filters cover the range of signal that is chosen to be of interest. The shape and the degree of non-orthogonality of the selected filters increase the sensitivity of the detection system to changes in the signal [3].

Applying the chromatic method to data derived from either a residual gas analysis or from a mass spectrometer requires modification of the detail of the filter characteristics and also to the order of the data. Rather than using Guassian filters as previously [1], triangular filters are used. The

chemical species under each of the filters may be grouped according their relevance to the systems (e.g. Hydro-carbons, oxy-carbons) rather than increasing wavelength as for optical signals [1]. Figure 1 shows one set of triangular filters overlaid on a generalised set of chemical components.
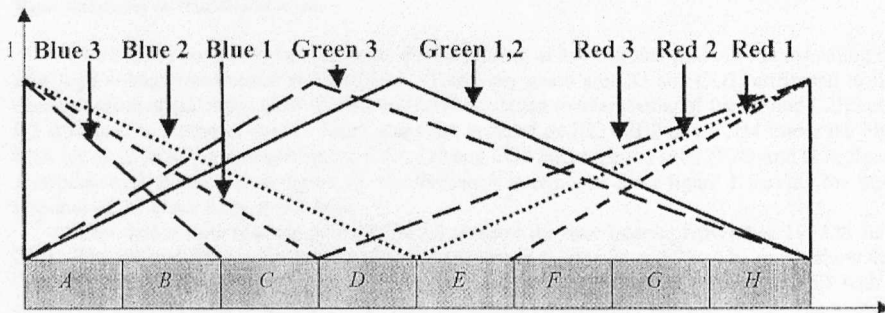
Figure 1. Generalised view of filter characteristics and chemical species.
(A - H are chemical components)

The products of the concentration of each chemical species and the values of the filter at each species are summed over the range of each filter profile. This gives rise to three outputs, known as R, G and B. These are transformed into chromatic parameters using the following algorithms.

$r = R - \min(RGB)$ $g = G - \min(RGB)$ $b = B - \min(RGB)$

If $r = 0$ then Hue $= 120° - 120° [g/(g + b)]$ Saturation $= \dfrac{\max(RGB) - \min(RGB)}{\max(RGB) + \min(RGB)}$

If $g = 0$ then Hue $= 360° - 120° [b/(b + r)]$

If $b = 0$ then Hue $= 240° - 120° [r/(r + g)]$ Lightness $= [\max(RGB) + \min(RGB)]/2$

The three chromatic parameters are known as Hue (H), Lightness (L) and Saturation (S). Hue is represented as an angle (0 to 360), and lightness and saturation from 0 to 1. They are usually represented on two polar plots showing HS and HL. The composition of the gas may be deduced from the chromatic values and changes in the gas composition may also be deduced from changes in the HLS values. For example, a Hue value between 0 and 120 implies that the product of the red filter value and the components covered by this filter are small compared to the others. The difference between the filter with maximum output and minimum output is indicated by the value of saturation. A saturation of 0 implies that the outputs for all filters are the same and a value of 1 implies a large difference between the minimum and maximum filter outputs. If the Hue value is close to 0 then the implication is that the output from the blue filter is small compared to that from the green filter. A Hue value closer to 120 implies that the output from the blue filter is greater than the green. The lightness value provides an indication of the overall concentration.

Rather than providing absolute values for concentration the chromatic approach provides a means for tracking changes in the relative concentration of species and which may be related to the operational status of the system. The three examples below demonstrate the power of the chromatic technique in dealing with this type of chemical data.

Chromatic processing of Residual Gas Analysis and Mass Spectrometric Data.

Prior to the processing, the chemical species need to be ordered according to the nature of the information to be extracted so that any changes in the grouped species can be related to particular

physical events. This front-end requirement requires some care but it drives the end user to evaluate the process to be monitored from the aspect of identifying possibly predominant species.

Residual gases in transformer oil.

As a first example of the technique, the monitoring of key residual gases in the insulating oil of a high voltage transformer is considered. These key gases are CO and CO2, attributed to the decomposition of cellulose, CH4, C2H6 and C2H4 attributed to overheating of the oil and C2H2 and H2 attributed to electrical stress. These gases are grouped as H2, C2H2 and C2H4 under the blue filter (A, B, C in figure 1 respectively), CH4, CO and CO2 under the red filter (F, G and H in figure 1 respectively), C2H6 (D in figure 1). Component E is removed from figure 1 leaving the peak response of the green filter over C2H6.

Test data for the residual gases in the oil spanned the time interval November 1977 to June 2001. The HS and HL plots over this period are shown in figures 2a and 2b. The result show that from the date of commissioning up to May 2001 the average saturation value was 0.52 with a significant increase initially to 0.87. Over time the saturation gradually reduced to 0.2. The average Hue angle during this initial period was 225 and the average lightness value was 0.2. The hue value reflected the dominance of CO2 and CO. Changes in the Hue and lightness values were smaller than for saturation. In the second period from May 2001 to the end of June there was a significant change in all three chromatic values. This change coincided with an alarm being raised in the substation over the transformer's condition. The Hue value changed from the 180 - 270 sector to the 0 - 90 sector oscillating between 0 and 80 with an average value of 15. The saturation value was between 0.2 and 0.3 and the lightness value steady at 0.25. The new hue value represented a significant change in the chemical composition which was now dominated by H2, C2H2 and C2H4.

In the period leading up to May 2001 the results imply that there may have been adverse heating of the paper insulator around the transformer windings for a significant period of time producing CO and CO2, both products of cellulose decomposition. The trend in the saturation towards the end of this first period is towards zero. This either implies that the CO, CO2 components are decreasing or that the C2H4, C2H2 and H2 components are increasing. The latter case is the more probable as the lightness value increases during this period implying an increase in the total amount of residual gases. The decrease in the hue is coincident with a warning alarm being sounded in the substation. Both the alarm and the chromatic tracking method detected a significant increase in H2, C2H2 and C2H4, residual gases produced during electrical stress arising from partial discharges and arcing.

The onset of decomposition of the cellulose insulator on the transformer windings which leads to excessive electrical stress is one of the possible failure modes for a transformer. The chromatic method tracked the events leading up to the potential hazardous conditions of partial discharges and arcing.

Methanogenesis in a waste reduction system.

The second example of the technique deals with the monitoring of the composition of gases produced in an experimental industrial waste reduction system through the decomposition of organic waste. In the process methane is produced which is used in a combine heat and power unit. The conditions within the system must be suitable for methanogenesis to take place. This is achieved by temperature control and maintaining a suitable pH of the material. The waste is placed in one of five concrete cells and the gases produced in each cell are continuously monitored with a mass spectrometer and the data being stored on a computer for later processing with a chromatic technique. The chemical species chosen to be of interest are N2, O2, Ar, H2O, CO2, H2, CH4 and CH3. The blue filter has been extended to cover CH3, CH4, H2 and CO2, (A, B, C and D, blue filter

2 in figure 1). The red filter covers H2O, Ar, O2 and N2 (E, F, G and H, red filter 2 in figure 1). The green filter covers all species with a peak value as shown in figure 1 (green 1,2).

Figure 3a and 3b show the HS and HL changes over a period of 11 days from when the cell was filled with waste. Initially after filling, the H and S values show that the dominant gaseous component in the gas flow from the cell is N2 but with a low flow rate as shown by the lightness value. However, progressively over a period of five days the hue value tracks towards the 180 - 270 sector. With this hue value and with saturation close to 1, the dominant component in the out flow of gas from the cell is methane and that the flow of gas has increased significantly as shown by the increase in lightness. The progressive transition from N2 to methane indicates that methanogenesis has been initiated and that conditions in the cell, e.g. temperature, pH are suitable for this to occur. Eventually, as more of the organic material decomposes the saturation value reduces to near zero accompanied by a decrease in the lightness value, implying that there is not only methane in the out flow but also one or more of the other gases.

The fluctuations in L and S during methane production are due to the cell being opened for periodic inspection and therefore the gas samples are momentarily contaminated with air.

Also shown on figure 3a is the expected track HS given ideal conditions. Although there are detailed differences the experimental data confirms the expected trend.

It is clear that the HLS values can readily track changes in these waste reductions cells without the need to store large amounts of data.

Residual Gas Components in SF6 after Current Interruption.

The third example of the technique concerns the monitoring of residual fragments of SF6 gas produced by electrical arcing in high voltage circuit breakers. Ideally, there should be no decomposition in the SF6 gas. However, due to the severity of electric arcing the SF6 dissociates and some fragments will recombine with copper vapour produced from the arc electrodes and water vapour from the chamber walls. One of the by-products formed is the chemically aggressive HF. To monitor changes in the composition of SF6 the components F, S, SF, SF2, SF3, SF4 and SF5 have been selected from the mass spectra data and processed using chromatic algorithms. Chemical species C in figure 1 is deleted in order to accommodate the 7 chemical components. The blue filter covers F and S (A, B filter blue profile 3 in figure 1), the red filter covers SF, SF2, SF3, SF4 and SF5 (D, E, F, G, H and filter profile red 3). The green filter covers all masses with a peak value between B and D (C being omitted) as shown by profile green 3 in figure 1.

Figure 4a and 4b show the HS and HL changes from new clean gas for a test of three 30kA peak current half sinusoidal arc discharges and when the gas is left in the arcing chamber for a period of 28 hours after discharges activity had ceased. A molecular filter was also placed inside the test chamber to absorb moisture and any HF produced. The results show that there are three distinct events occurring during the test. The first is related to the dissociation of the SF6 gas by the arc discharge. The HS and HL points for the three separate discharges are almost coincident and displaced from the original clean gas point. The displacement is marked as a decrease in the Hue angle and lightness and a slight increase in saturation. The second is related to the initial recovery of the gas. The trend after the initial 4 hours is for a further reduction in Hue angle and lightness and an increase in saturation. The third shows a trend which tracks towards the initial starting point. The implications of these results are that during arcing the higher order SFx components increase in concentration relative to the other chemical species but there does not appear to be a substantial accumulative build up for the three arcing events. Four hours after arcing there is a further increase in SFx components. The trend is reversed after 23 and 28 hours showing a relative decrease in SFx components compared to S and F, demonstrating the effectiveness of the molecular filter.

Conclusion.

The three cases reported above clearly demonstrate the uses of the chromatic technique for tracking trends in the composition of chemical species. Changes in the chromatic values are attributed to physical changes within the system. The relative concentration of the grouped chemical species relative to each other can be monitored and used to provide valuable feedback on the operational status of the system. The importance of arranging the chemical data into a predefined order allows the user to control the nature of the information extracted. This ordering is a major advantage in the technique and permits traceability within the processing technique. Furthermore, the sensitivity to variations in one or more of the chemical components can be readily adjusted either by changing its position within a group or by changing the shape of the filter.

References.
[1].   Jones G. R,., Jones R. E. and Jones R. "Multimode Optical Fibre Sensors" Chpt. 1 in "Optical Fibre Sensor Technology". (Advanced Applications - Bragg Gratings and Distributed Sensors). Ed. Grattan and Megitt, pp 1- 77, 2000. ISBN 0-7923-7946-2.
[2].   Russell P.C., Cosgrave J., Tomtsis A., Vourdas A., Sterigoulos L. and Jones G. R. "Extraction of information from acoustic signals using Gabor transform type devices". Meas. Sci. Technol. Pp1282 - 1290, Vol 9, 1998.
[3].   Russell P.C., Craven A., Deakin A., Cooke R., Furlong S., Spencer J.W. and Jones G. R. "Intelligent monitoring of industrial plasmas". Sensors and their applications. Ed. White & Augousti). IOP Publishing, pp 245 - 250, 1999. ISBN 0-7503-0662-9.
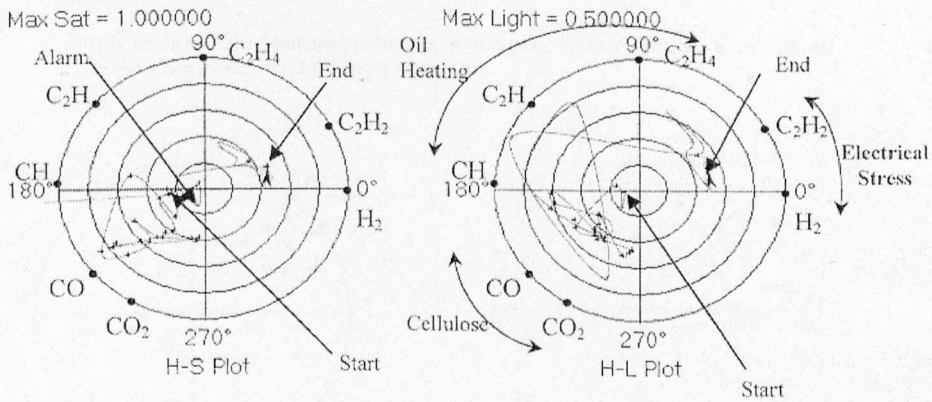
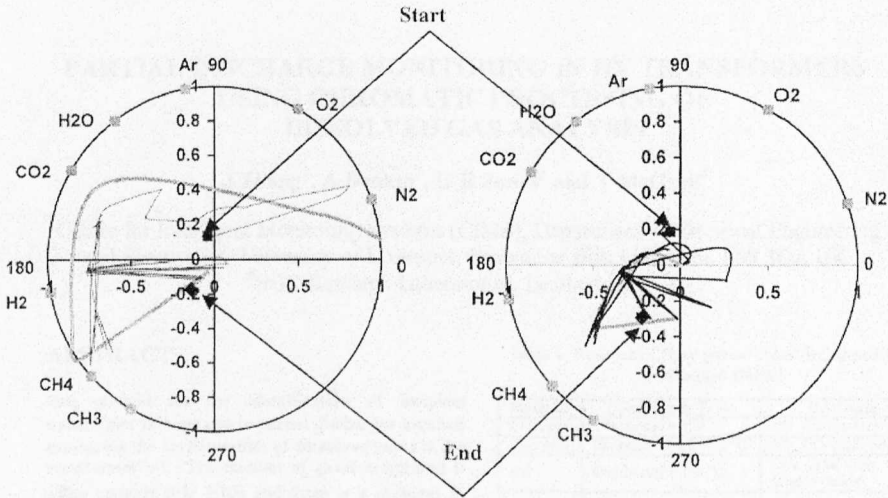Figures 2a and 2b. HS and HL values for residual gas analysis from transformer oil.

Figure 3a and 3b. Methane production from organic waste reduction. Experimental trend - black line; Expected trend - grey line.
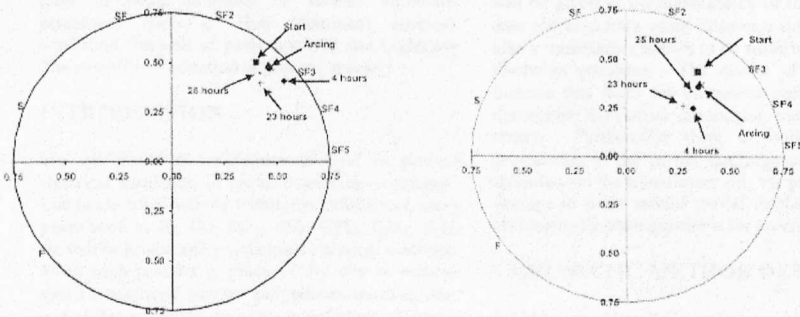

Figure 4a and 4b. SF6 gas monitoring after interruption fault currents.

2. The XIV International Conference GD2002

PARTIAL DISCHARGE MONITORING IN HV TRANSFORMERS USING CHROMATIC PROCESSING OF DISSOLVED GAS ANALYSIS

J Zhang[1], A Deakin[1], G R Jones[1] and T McGrail[2]

[1]Centre for Intelligent Monitoring Systems (CIMS), Department of Electrical Engineering and Electronics, University of Liverpool, Brownlow Hill, Liverpool, L69 3GJ, UK
[2]NGC Research Laboratories, Leatherhead, UK

ABSTRACT

One method for the identification of incipient transformer failures due to partial discharges involves measuring the concentration of dissolved gases in the transformer oil. The number of gases monitored is often considerable (≥ 10) and there is a problem in tracking time varying patterns of the concentration of these gases to yield meaningful prognostic information. This contribution describes the use of chromatic processing techniques in the gas identification domain for yielding conveniently assimilable information in the form of chromatic maps for prognostic purposes. Such maps take the form of polar diagrams of various chromatic parameters such as Hue (dominant species), Saturation (breadth of gases percent) and Lightness (the overall concentration of gaseous species).

INTRODUCTION

The oil inside a transformer is used to provide electrical insulation to prevent sparking occurring. Due to electrical activity within the transformer, many gases such as H_2, CO, CO_2, CH_4, C_2H_2, C_2H_4, C_2H_6 etc will be produced by associated chemical reactions. Since each product is produced by one or several specific reactions, various gas statuses are associated with different conditions of the transformer. Analysis of hydrocarbon gases dissolved in the transformer oil is an especially important part of such condition monitoring [1]. Table 1 summarises the key gases produced by various decomposition mechanisms found in the transformer during service [2].

Table 1 indicates that, if cellulose is overheated to around 150 Celsius, carbon monoxide (CO) and carbon dioxide (CO_2) will be produced. Oil at such a temperature will produce methane (CH_4), ethane (C_2H_6) and ethylene (C_2H_4). With a temperature greater than 1000 Celsius, the transformer oil will decompose into hydrogen (H_2) and acetylene (C_2H_2); at 1000 Celsius cellulose will still produce carbon monoxide and carbon dioxide, but extra products produced would change the output from water to carbon/tar.

Table 1. Sources of "key gases" from decomposition of cellulose and oil

Material	Condition & Temp	Key Gases
Cellulose	Overheated > 150 °C	CO CO_2 (water)
Cellulose	Excessive heat >1000 °C	CO CO_2 (carbon/tar)
Oil	Overheated > 150 °C	CH_4 C_2H_6 C_2H_4 (organic acids)
Oil	Electrical Stress (Partial Discharges and Arcing to 1000 °C)	H_2 C_2H_2 (waxes & water)

In this paper, the chromatic technique [3] using tristimulus deployment is applied to the dissolved gas analysis (DGA) of the above key gas data. Examples will be given of the applicability of the approach to data obtained from some in service transformers and also a transformer known to be suffering from partial discharge problems. The results of the approach indicate that there are chromatic signatures, which distinguish the partial discharging transformer from others. Furthermore there is evidence that the progression of the partial discharge effect from the influence on the transformer oil, via paper insulation damage to more serious partial discharging may be chromatically distinguishable for prognostic purposes.

CHROMATIC METHOD DETAILS

In order to describe complex signals in a simple perspicuous two-dimensional space, the chromatic methodology [3] may be deployed with three processors to analyse the gases dissolved in the transformer oil.
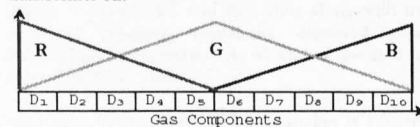

Figure 1. Configuration of tristimulus filters

Figure 1 shows a particular configuration of the three processors/filters, which might be used and which are denoted by R, G and B. It shows how these three non-orthogonal processors may be applied to an array of data ($D_1 \sim D_{10}$). The output of each processor

constitutes the integrated product of the data and the gradient of the processor response.

For signal processing applications, the HLS (hue, lightness and saturation) system provides a particularly useful bridge between colour concepts and spectral signal forms [3]. For the three processors outputs R, G and B we have:

$$i_1 = R - \min(RGB); \quad if \quad i_1 = 0, \quad H = 240 - 120(\frac{i_2}{i_2 + i_3})$$

$$i_2 = G - \min(RGB); \quad if \quad i_2 = 0, \quad H = 360 - 120(\frac{i_3}{i_3 + i_1})$$

$$i_3 = B - \min(RGB); \quad if \quad i_3 = 0, \quad H = 120 - 120(\frac{i_1}{i_1 + i_2})$$

$$L = \frac{\max(RGB) + \min(RGB)}{2}$$

$$S = \begin{cases} \dfrac{\max(RGB) - \min(RGB)}{\max(RGB) + \min(RGB)} & if \quad L < 0.5 \\[2mm] \dfrac{\max(RGB) - \min(RGB)}{2 - \max(RGB) - \min(RGB)} & otherwise \end{cases}$$

In this case the two-dimensional chromatic map is formed from the cylindrical coordinates $0 = (\theta = H) < 360°$, $0 = (r = S) = 1$ and the chromatic boundary encompassing all signals now remains fixed as a circle of unity radius. So the two-dimensional mapping allows complex signals to be represented as a single point in a polar plot. As a result the relationship between two signals is easily visualised [3].

Based on the data arrangement shown in Figure 1, the relationship between the dominant products and hue angles is shown in Figure 2. The hue angle of a dominant product is calculated as follow. By setting all the data values of the products to be zero except for D_1, applying the chromatic processing described above, the calculated hue angle of D_1 is 15° with a saturation value equalling 1. Similarly the hue angles of all the other single dominant products can be calculated in this manner. Their juxtaposition is shown on the polar plot (Figure 2).
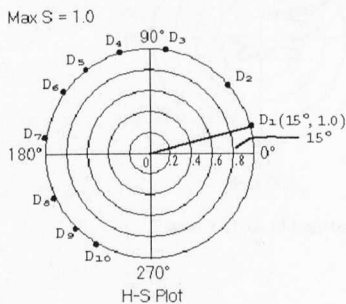
Max S = 1.0

Figure 2. Hue angle represents dominant product

The dominating gas species is indicated by the H value, i.e. the polar coordinate D_θ on the H-S plot, the value of S indicates the extent to which the dominant component dominates. For the parameters of hue and lightness, an H-L polar plot can also be sketched similar to the H-S plot. The H-L plot indicates, via the L value, the extent of gassing – the higher the gassing the larger L and the larger the radius at which the experimental point is registered.

For example, a point with polar coordinates H, L, S (i.e. θ, r) having values 15°, 1, 1 indicates that there is only a single component (S=1) which is D_1 (H=15°) and that it has a relatively high concentration (L=1). Consequently, coordinates (15°, 0.1, 0.1) indicates that D_1 marginally dominates a low concentration (L=0.1) mixture of several components (S=0.1).

In order to focus on results for significant concentrations in some cases, the points on the H-S plot, which have L values less than 0.1, will be omitted (since these points are close to the origin on the H-L plot i.e. contain less gassing strength than others do).

SCOPE OF TEST DATA

The results, which follow, include some results of two in-service transformers designated as A and B, also a transformer, C, known to be suffering from partial discharge problems.

Details of the transformer A are that it is a 220 MVA, 400/132 kV unit, manufactured in 1967 and installed in 1968, with samples taken from 1980 until 1999. Samples of transformer B, a 240 MVA, 400/132 kV unit installed in 1966, were taken from 1985 until 1998. The unit C was a 1000 MVA, 400/275/33 kV transformer built in 1972. Dissolved gases data has been available during the period 1977-1997. An isolated record for June 2001 was also available prior to an 8-day site test. The history of this transformer was well documented indicating that it was a fault susceptible transformer. A fault on the transformer in 1997 initiated a Buchholz alarm after which it was refurbished. A second Buchholz alarm occurred thereafter and the unit was decommissioned.

CHROMATIC RESULTS

Figure 3 shows H-S and H-L plots along with the dominant products, containing dissolved gases information of transformer A, which has operated for more than thirty years.

Note that the maximum of the saturation is 1.0 with one circle in the H-S plot being 0.2. However, for better focusing on the data points, the maximum scale of the lightness is set to 0.5 with one circle in the H-L plot representing 0.1.
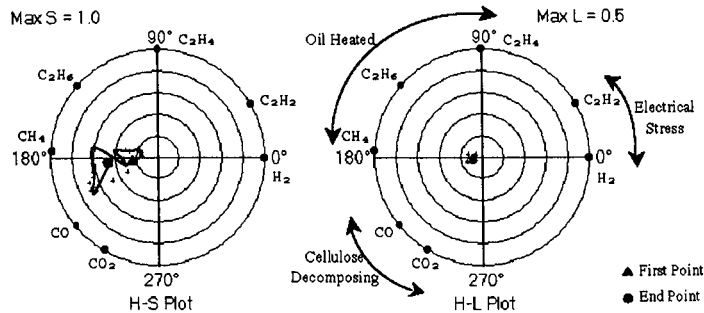
Figure 3. DGA of transformer A (sampled 28/08/1980 ~ 29/06/1999)
(S=0~1, L=0~0.5)

The triangle in the H-S plot indicates the initial condition i.e. the first sampled record of the seven dissolved gases in the corresponding transformer, and the circle indicates the end point. The curve along the points represents the time tracking between start and end.

It is clear that for transformer A, CH_4 is dominant among the key gases throughout the sampled duration. This implies that the oil was overheated above 150 °C, but there seems to be no serious partial discharges or arcing (i.e. no high level of H_2 and C_2H_2 listed in Table 1). Note that the lightness level is low and all points are within 0.1 circle, near to the initial point, indicating a reliably safe status.

Figure 4 shows another example, the results for transformer B. The H-L plot shows that although the L value remains low (<0.27), there is a clear change to the electrical stress area (C_2H_2) beyond about the year 1990. The H-S plot shows that the electrical

stress component C_2H_2 dominates with a maximum-recorded value of S≈0.8 and a subsequent reduction of S to about 0.3. Thus although there has been a decrease in L, nonetheless C_2H_2 (indicating electrical stress) remains dominant. This suggests that there is a need to maintain a watching brief on this transformer.

Figure 5 shows the H-S, H-L chromatic maps for transformer C (triangle – initial condition, circle – end point, square points – samples just after the Buchholz alarm). From both the H-S and H-L plots all points sampled until an alarm occurred in 1997 are located in the cellulose decomposition area (CO, CO_2 dominant), including the alarm point. This may imply that the alarm was not driven by gases decomposed from partial discharged oil, but from large amounts of gases decomposed from cellulose/overheated oil (note 1st alarm point L = 0.4 which is a significantly higher level than recorded on any of the transformers A or B).

Figure 4. DGA of transformer B (sampled 23/09/1985 ~ 30/11/1998)
(S=0~1, L=0~0.5)

Figure 5. DGA of transformer C (sampled 29/11/1977 ~ 28/06/2001)
(S=0~1, L=0~0.5)

However, the later alarm points represent a change in the deteriorating progression with C_2H_2 and H_2 becoming influential with 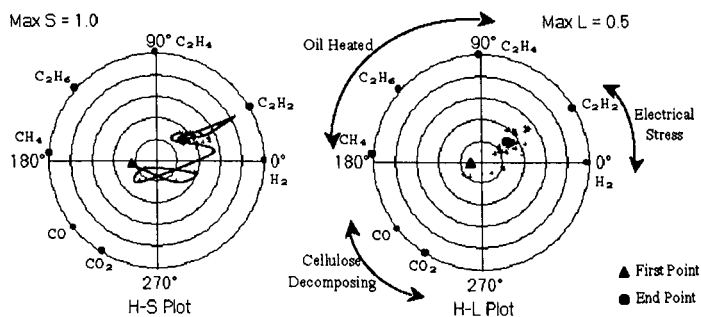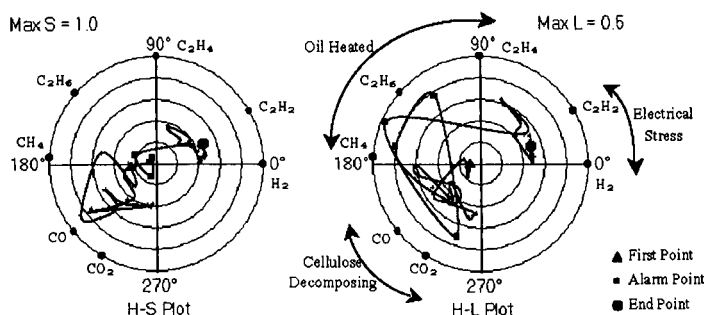CO and CO_2 indicating oil overheating. The low S value (≤ 0.2) indicates almost equal amounts of CO, CO_2 and C_2H_2, H_2; the large L values (0.35~0.5) indicates copious gas production. After the alarm, C_2H_2, H_2 gases become dominant (S≈0.4) but with other gases also present; an L value of about 0.25~0.3 represents a level of concern particularly when located in the C_2H_2, H_2 sector. The vigorous excursion of the locus of the dominant points is also indicative of a relative volatility in the gases being produced both in nature and quantity. This suggests that the transformer condition was deteriorating further after the alarm; partial discharges appear to have occurred frequently especially during site tests with this transformer.

Comparing these results with those of the in-service transformers A and B, there is an implication that a unit may be tending to failure if the lightness value exceeds 0.4, based on this seven-key-gas analysis. If the H value were in the range of C_2H_2/H_2 in addiction to L>0.4 then the risk of failure would seem to be enhanced. One possible precursor to this is the indication from the H-S plot for a predominance of CO followed by CO_2 before moving towards C_2H_2. On both H-S and H-L plots the trend to C_2H_2/H_2 during recent tests is noticeable.

CONCLUSIONS

The chromatic analysis of the dissolved gases is capable of yielding trend patterns, which appear to be associated with indications of a transformer leading to increased risk of failure. Clearly a gathering of dissolved gas analysis for a large number of transformer units could provide a valuable statistical

approach. Such results are currently being acquired and evaluated.

ACKNOWLEDGEMENT

REFERENCES

[1] H M Ryan, "High Voltage Engineering and Testing" , Peregrinus, Stevenage, ISBN 0863412939, 1994.

[2] G R Cardwell, "Oil Testing and Dissolved Gas Analysis for Identifying Faults in Power Transformers" ,Elektron (Johannesburg), vol. 6, no. 2, pp. 12-17, Feb 1989.

[3] G R Jones, P C Russell, A Vourdas, J Cosgrave, L Stergioulas and R Haber, "The Gabor Transform Basis of Chromatic Monitoring" , Measurement Science & Technology, vol. 11, no. 5, pp. 489-498, May 2000.

[4] M K Domun, "Assessing Parameters for Condition Monitoring of HV Transformers by Accelerated Ageing Experiments", 6th INSUCON 1990 BEAMA International Electrical Insulation Conference, BEAMA, pp. 131-136, London, UK, May 1990.

[5] "Mineral oil-impregnated electrical equipment in service - Guide to the interpretation of dissolved and free gases analysis" , British Standard Institution, BS EN 60599:1999, April 1999

3. NGT Oil R&D Seminar, 2003

Presentation on *NGT Oil R&D Seminar*, 4th September 2003, Kenilworth, UK.

Discrete Chromatic Processing of DGA Results for HV Transformer Oil

J. Zhang[1] and G. R. Jones[1]

Outline
- DGA Introduction
- Chromatic method
- Three typical results
- Failure probability
- Conclusion

[1]CIMS, University of Liverpool
Sponsor: NGT

University of Liverpool

1

DGA introduction

- Transformer oil dissolved gas consists of more than 10 species
- Key gases: H_2, CO, CO_2, CH_4, C_2H_2, C_2H_4, C_2H_6

Material	Condition & Temp	Key Gases
Cellulose	Overheated > 150 ℃	CO CO_2 (water)
Cellulose	Excessive heat >1000 ℃	CO CO_2 (carbon/tar)
Oil	Overheated > 150 ℃	CH_4 C_2H_6 C_2H_4 (organic acids)
Oil	Electrical Stress (Partial Discharges and Arcing to 1000 ℃)	H_2 C_2H_2 (waxes & water)

University of Liverpool

2

Distribution for gases first records of 50 tanks
(a)-(g) are corresponding to CO_2, CO, CH_4, C_2H_6, C_2H_4, C_2H_6, H_2 respectively

3

Dissolved gases raw data

University of Liverpool

4

Configuration of tristimulus filters

| R | G | B |
| D_1 | D_2 | D_3 | D_4 | D_5 | D_6 | D_7 |

Gas Components (e.g. D_1 = CO_2, D_2 = CO etc.)

R, G, B = Chromatic Processors
→ H - Dominant gas
S - Spread of gases
L - Integrated level of gases

University of Liverpool

5

The two basic chromatic map components H-S and H-L

University of Liverpool

6

Slide 7

DGA chromatic map of transformer A (status safe)
(19 years, 28/08/1980 ~ 29/06/1999, courtesy NGT)

- Most of the points on the H-L plot are within the 0.1 circle and no point exceeds the 0.2 circle; and
- Most of the points on the H-S plot are within the Cellulose Decomposing area (CO_2-CO) or Oil Heated area (CH_4-C_2H_6-C_2H_4) and no point exceeds the 0.4 circle in the Electrical Stress area (C_2H_2-H_2).

University of Liverpool

Slide 8

DGA chromatic map of transformer C (status faulty)
(24 years, 29/11/1977 ~ 28/06/2001, courtesy NGT)

- Some of the points on the H-L plot exceeds the 0.4 circle; and
- Some of the points on the H-S plot exceed the 0.4 circle within the Electrical Stress area (C_2H_2-H_2).

University of Liverpool

Slide 9

DGA chromatic map of transformer B (status changing)
(11 years, 22/10/1990 ~ 28/10/2001, courtesy First Hydro)

- Some of the points on the H-L plot exceeds the 0.2 circle; or
- Some of the points on the H-S plot exceed the 0.4 circle within the Electrical Stress area (C_2H_2-H_2).

University of Liverpool

Slide 10

Classification of DGA-examined 50 transformer tanks
(courtesy NGT, First Hydro)

Status	Count		Transformer tanks
safe	NGT 17		Boln1, Bush2, Bush3, Bush4, Cape2A, Cape5A, Cape5B, Cape6A, Cape6B, Elst2, Hamb1, Hamb5, Hamb6, Wals1A, Wylf1, Wylf2, Wylf4.
	First Hydro 10		Ffes2, GMT1s, GMT2m, GMT3m, GMT3s, GMT4m, GMT4s, GMT5m, GMT5s, GMT6m.
changing	NGT 18		Boln2, Boln3, Cant1, Cant2, Cape1A, Cape3A, Elst1A, Elst1B, Elst3A, Elst3B, Elst4, Elst5A, Hamb2, Hamb3, Hamb7, Wals2A, Wals2B, NorthFleet1A
	First Hydro 4		Ffes1, GMT1m, GMT2s, GMT6s (Warning)
faulty	NGT 1		Neilston4

University of Liverpool

Slide 11

Examples of practical DGA results for failure probability

Safe Status:
L=0.034, H=128, S=0.207
Probability=$P_L + P_H + P_S$ = 0.17+0.16+0.06 = 0.39

Changing Status:
L=0.161, H=208, S=0.785
$P = P_L + P_H + P_S$ = 0.23+0.28+0.18 = 0.69

Faulty Status:
L=0.314, H=223, S=0.700
$P = P_L + P_H + P_S$ = 0.29+0.30+0.17 = 0.76

University of Liverpool

Slide 12

Slide 13
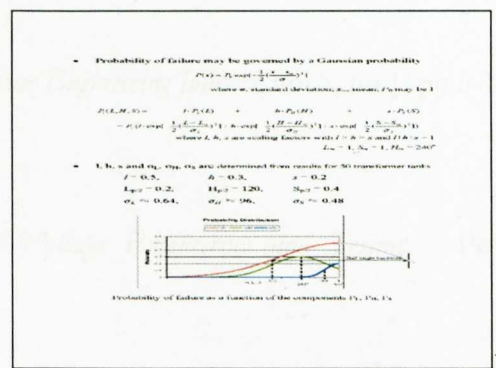
Conclusion

- 50 tanks evaluated
- Chromatic DGA - yielding trend patterns
- Failure probability - quantifiable manner

Acknowledgements: NGT, First Hydro

University of Liverpool

Slide 14

Static and dynamic chromatic probabilities

- Static analysis

$$P = l \cdot P_L(L_f) + h \cdot P_H(H_f) + s \cdot P_S(S_f)$$

where L_f, H_f, S_f are final values of L, H, S.

- Dynamic analysis

$$P_d = l \cdot [P_{VL}(L_L) + P_{VL}(H_L) + P_{VL}(S_L)]$$
$$+ h \cdot [P_{VH}(L_H) + P_{VH}(H_H) + P_{VH}(S_H)]$$
$$+ s \cdot [P_{VS}(L_S) + P_{VS}(H_S) + P_{VS}(S_S)]$$

$$= \sum [\gamma \sum P_{VT}(\Psi_T)]$$

where $\gamma = l, h, s$; $T = L, H, S$, $\Psi = L_T, H_T, S_T$.

University of Liverpool

References

Adobe Audition (2003)
"Cool Edit Pro is now Adobe Audition", *Adobe Official Web Site*, [Online], 6 paragraphs. Available: http://www.cooledit.com/ [2003, October 1] or http://www.adobe.com/special/products/audition/syntrillium.html [2003, October 1].

Ahmad M.B. & bin Yaacob Z. (2002)
"Dissolved gas analysis using expert system", Proceedings of *2002 Student Conference on Research and Development* (SCOReD2002), pp.313-316. IEEE, 16-17 July 2002, Shah Alam, Malaysia.

Allan D.J. (1991)
"Power transformer - the second century", *Power Engineering Journal*, vol.5, no.1, pp.5-14.

Allan D.J. (1994)
"Introduction" in Ryan H.M. (ed.), *High Voltage Engineering and Testing*. Peter Peregrinus, Stevenage, UK.

ANSI (1992)
"IEEE guide for the interpretation of gases generated in oil-immersed transformers", *IEEE Power Engineering Society*, ANSI/IEEE Std C57.104-1991.

Anupriya S. (2001)
Multi-sensor Data Fusion for Aircraft Fuel Systems Using Chromatic Processing. PhD thesis, The University of Liverpool, UK.

Ashton N. & Mellor E.J. (1981)

"Protective transformers" in The Electricity Council (ed.), *Power System Protection 1*, 2nd edition. Peter Peregrinus, Stevenage, UK.

Aubujeault O. (2002) [Personal Communication]
Report on SGT3A Transformer Tests Carried Out at Northfleet West. Unpublished report, EdF, France.

Babnik T. (2001) [Personal Communication]
PD Measurements in Scotland Neilston Substation, June 25-27, 2001. Unpublished report, Department of Electronic and Electrical Engineering, University of Bath, Bath, UK.

Babnik T., Aggarwal R. & Moore P. (2002) [Personal Communication]
Preliminary Report on Diagnostic Tests of SGT3A at Northfleet Substation 22-28 May 2002. Unpublished report, Department of Electronic and Electrical Engineering, University of Bath, Bath, UK.

Bargigia A., Koltunowicz W. & Pigini A. (1992)
"Detection of partial discharge in gas-insulated substation", *IEEE Transactions on Power Delivery*, vol.7, no.3, pp.1239-1249.

Bengtsson T., Kols H. & Jönsson B. (1997)
"Transformer PD diagnosis using acoustic emission technique", Proceedings of *the 10th International Symposium on High Voltage Engineering* (ISH-97), vol.4, pp.115. 25-29 August 1997, Montreal, Canada.

Bengtsson T. & Hedberg J. (2001) [Personal Communication]
Acoustic Detection and Localisation of PD Sources on Transformer SGT4 at Neilston Substation, July 25-27, 2001. Unpublished report, ABB Corporate Research, SE-721 78, Västerås, Sweden.

Birren F. & Cleland T.M. (1969)
A Grammar of Color. Van Nostrand, New York.

Bozzo R. & Guastavino F. (1995)

"PD detection and localization by means of acoustic measurements on hydrogenerator stator bars", *IEEE Transactions on Dielectrics and Electrical Insulation*, vol.2, no.4, pp.660-666.

Bracewell R.N. (1978)

The Fourier Transform and its Applications, 2nd edition. McGraw-Hill, New York.

Brazier K.J., Deakin A.G., Cooke R.D., Russell P.C. & Jones G.R. (2001)

"Colour space mining for industrial monitoring" in Braha D. (ed.), *Data Mining for Design and Manufacturing*. Kluwer Academic Publishers, Netherlands.

BSI (1970)

Specification for Power Transformers. BS 171:1970, British Standards Institution.

BSI (1973)

Specification for Current Transformers. BS 3938:1973, British Standards Institution.

BSI (1999)

Mineral Oil-impregnated Electrical Equipment in Service – Guide to the Interpretation of Dissolved and Free Gases Analysis. BS EN 60599:1999, British Standards Institution.

Cao L.J. & Liang Y.C. (1993)

"Dissolved-gas analysis of transformer oil using neural-network", Proceedings of *World Congress on Neural Networks 1993* (WCNN'93), vol.I, pp.329-332. INNS, 11-15 July 1993, Portland, Oregon, USA.

Cardwell G.R. (1989)

"Oil testing and dissolved gas analysis for identifying faults in power transformers", *Elektron* (Johannesburg, South Africa), vol.6, no.2, pp.12-17.

Champeney D.C. (1973)

Fourier Transforms and their Physical Applications. Academic Press, London.

CIE (1932)

Commission Internationale de l'Eclairage Proceedings, 1931. Cambridge University Press, Cambridge.

Cobine J.D. (1941)

Gaseous Conductors: Theory and Engineering Applications. McGraw-Hill, New York.

Cosgrave J.A. (1996)

Acousto-optic Monitoring of Electric Power Equipment Using Chromatic Signal Processing. PhD thesis, The University of Liverpool, UK.

Culshaw B. & Dakin J. (1997)

Optical Fiber Sensors, V.3 Components and Subsystems. Artech House, Boston.

Cunningham M.J. & Bibby G.L. (1993)

"Measurement and instrumentation" in Jones G.R., Laughton M.A. & Say M.G. (eds.), *Electrical Engineer's Reference Book*, 15th edition. Butterworth-Heinemann, Oxford.

Davies T. (1984)

Protection of Industrial Power Systems. Pergamon, Oxford.

Deng X. (2000)

Chromatic Signature as A Feature Detector and Colour Discriminator in Colour Images. Unpublished MSc thesis, The University of Liverpool, UK.

Domun M.K. (1990)

"Assessing parameters for condition monitoring of HV transformers by accelerated ageing experiments", Proceedings of *the 6th BEAMA International Electrical Insulation Conference*, pp.131-136. BEAMA, 21-24 May 1990, Brighton, UK.

Eleftherion P.M. (1995)

"Partial discharge XXI: acoustic emission-based PD source location in transformers", *IEEE Electrical Insulation Magazine*, vol.11, no.6, p.22-26.

Elgerd O.I. (1977)

Basic Electric Power Engineering. Addison-Wesley, Reading, Massachusetts.

Erinmez I.A. & Morgan C.J. (1994)

"Electric power transmission and distribution system: Part 1" in Ryan H.M. (ed.), *High Voltage Engineering and Testing.* Peter Peregrinus, Stevenage, UK.

Fitzgerald A.E., Kingsley C. & Umans S. (2003)

Electric Machinery, 6th edition. McGraw-Hill, Boston; London.

Flux R.W. (1993)

"Power transformers" in Jones G.R., Laughton M.A. & Say M.G. (eds.), *Electrical Engineer's Reference Book*, 15th edition. Butterworth-Heinemann, Oxford.

Foley J.D., van Dam A., Feiner S.K. & Hughes J.F. (1995)

Computer Graphics: Principles and Practice, 2nd edition in C. Addison-Wesley, Reading, Massachusetts.

Furlong S.A. (1999)

Characterisation of Electromagnetic Emissions from Circuit Breaker Arcs. PhD thesis, The University of Liverpool, UK.

Gabor D. (1946)

"Theory of communication", *Journal of the Institute Electrical Engineers*, vol.93, pp.429-457.

Glass R.M. (1977)

"Dissolved gas analysis of transformer oil", *Transmission & Distribution*, vol.29, no.1, pp.22-24, 26, 28-29.

Golubev A. (2002) [Personal Communication]

Engineering Report to EPRI on Sensors Installation, Calibration and PD Measurements on SGT3A Auto-transformer 400 kV/275 kV, 500 MVA Northfleet Sub, Gravesend, UK.

Unpublished report, Predictive Diagnostics Division, Cutler-Hammer, 5421 Feltl Road Suite 190, Minnetonka, Minnesota 55343.

Granttan K.T.V. & Meggitt B.T. (1998)
Optical Fiber Sensor Technology, V.3 Applications and Systems. Chapman & Hall, London.

Guardado J.L., Naredo J.L., Moreno P. & Fuerte C.R. (2001)
"A comparative study of neural network efficiency in power transformers diagnosis using dissolved gas analysis", *IEEE Transactions on Power Delivery*, vol.16, no.4, pp.643-647.

Hale P.G. & Jones G.R. (1993)
"Optical fibre technology and application" in Jones G.R., Laughton M.A. & Say M.G. (eds.), *Electrical Engineer's Reference Book*, 15th edition. Butterworth-Heinemann, Oxford.

Hamilton D.J. & Pearson J.S. (1997)
"Classification of partial discharge sources in gas-insulated substations using novel preprocessing strategies", *IEE Proceedings Science, Measurement and Technology*, vol.144, no.1, pp.17-24.

Hampton B.F. & Meats R.J. (1988)
"Diagnostic measurements at UHF in gas insulated substations", *IEE Proceedings Generation, Transmission and Distribution*, vol.135, no.2, pp.137-145.

Han B. (2002) [Personal Communication]
Partial Discharge On-line Testing of Northfleet SGT3A. Unpublished report, High Voltage Laboratory, Department of Electronics and Computer Science, University of Southampton, Highfield, Southampton SO17 1BJ, UK.

Haydon S.C. (1964)
An Introduction to Discharge and Plasma Physics. Dept of University Extension, Armidale.

Hill B., Roger Th. & Vorhagen F.W. (1997)

"Comparative analysis of the quantization of color space on the basis of the CIELAB color-difference formula", *ACM Transactions on Graphics*, vol.16, no.2, pp.109-154.

Hodgkiss J.W. (1981)
"Relays" in The Electricity Council (ed.), *Power System Protection 1*, 2nd edition. Peter Peregrinus, Stevenage, UK.

Huecker T. (convenor) (1998)
"CIGRE data format for GIS partial discharge software applications", *Electra*, no.177, pp.87-93.

Jenkins B.D. (1967)
Introduction to Instrument-Transformers. Newnes, London.

Jennison R.C. (1961)
Fourier Transforms and Convolutions for the Experimentalist. Pergamon, Oxford.

Jones G.R. (1994)
"Optical fibre based monitoring of high voltage power equipment" in Ryan H.M. (ed.), *High Voltage Engineering and Testing.* Peter Peregrinus, Stevenage, UK.

Jones G.R., Russell P. & Khandaker I. (1994)
"Chromatic interferometry for an intelligent plasma processing system", *Measurement Science and Technology*, vol.5, no.6, pp.639-647.

Jones G.R., Russell P.C., Vourdas A., Cosgrave J., Stergioulas L. & Haber R. (2000)
"The Gabor transform basis of chromatic monitoring", *Measurement Science and Technology*, vol.11, no.5, pp.489-498.

Judd D.B. (1933)
"1931 ICI standard observer and coordinate system for colorimetry", *Journal of the Optical Society of America*, vol.23, pp.359-374.

Judd M.D., Farish O., Pearson J.S., Breckenridge T. & Pryor B.M. (2000)
"Power transformer monitoring using UHF sensors: installation and testing", Proceedings of *Conference Record of the 2000 IEEE International Symposium on Electrical Insulation* (ISEI2000), pp.373-376. IEEE, 2-5 April 2000, Piscataway, New Jersey, USA.

Judd M.D. & Cleary G. (2001) [Personal Communication]
Report on Diagnostic Tests of SGT4 at Neilston Substation. Unpublished report, Institute for Energy and Environment, University of Strathclyde, Glasgow, UK.

Kelly J.J. (1980)
"Transformer fault diagnosis by dissolved-gas analysis", *IEEE Transactions on Industry Applications*, vol.16, no.6, pp.777-782.

Kemp I.J. (1995)
"Partial discharge plant monitoring technology - present and future developments", *IEE Proceedings Science, Measurement and Technology*, vol.142, no.1, pp.4-10.

Kemp I.J. (2001) [Personal Communication]
Neilston Transformer Measurements (taken June 2001) Summary of Results. Unpublished report, School of Engineering, Science and Design, Glasgow Caledonian University, Glasgow, UK.

Kemp I.J., Stewart B., Nesbitt A. & Zhou C. (2002) [Personal communication]
Testing of Northfleet SGT3A 400/275kV Transformer Summary Report. Unpublished report, School of Engineering, Science and Design, Glasgow Caledonian University, Glasgow, UK.

Kenney J.F. (1940)
Mathematics of Statistics. Chapman & Hall, London.

Kreuger F.H. (1992)
Industrial High Voltage 4, 5, 6. Delft University Press, Netherlands.

Kufner A. & Kadlec J. (1971)

Fourier Series. English translation edited by Toombs G. A., Iliffe Books, London.

Lapworth J.A. (1994)

"Transformer user requirements, specifications and testing" in Ryan H.M. (ed.), *High Voltage Engineering and Testing.* Peter Peregrinus, Stevenage, UK.

Levkowitz H. & Herman G.T. (1993)

"GLHS: a generalized lightness, hue, and saturation color model", *CVGIP-Graphical Models & Image Processing*, vol.55, no.4, pp.271-285.

Lundgaard L.E. (1992a)

"Partial Discharge - Part XIII: Acoustic Partial Discharge Detection - Fundamental Considerations", *IEEE Electrical Insulation Magazine*, vol.8, no.4, pp.25-31.

Lundgaard L.E. (1992b)

"Partial Discharge - Part XIV: Acoustical Partial Discharge Detection - Practical Application", *IEEE Electrical Insulation Magazine*, vol.8, no.5, pp.34-43.

Ma X., Zhou C. & Kemp I.J. (2002a)

"Automated wavelet selection and thresholding for PD detection", *IEEE Electrical Insulation Magazine*, vol.18, no.2, pp.37-45.

Ma X., Zhou C. & Kemp I.J. (2002b)

"Interpretation of wavelet analysis and its application in partial discharge detection", *IEEE Transactions on Dielectrics and Electrical Insulation*, vol.9, no.3, pp.446-457.

Marshall A.G. & Verdun F.R. (1990)

Fourier Transforms in NMR, Optical, and Mass Spectrometry. Elsevier, Amsterdam.

McPherson G. & Laramore R.D. (1990)

An Introduction to Electrical Machines and Transformers, 2nd edition. Wiley, New York.

Miller R.H. (1970)

Power System Operation. McGraw-Hill, New York.

Moon P.H. & Spencer D.E. (1981)

The Photic Field, MIT Press, Cambridge, Massachusetts.

Moore P.J., Portugues I.E. & Glover I.A. (2002) [Personal Communication]

Northfleet Transformer Tests 22-25 May 2002. Unpublished report, Department of Electronic and Electrical Engineering, University of Bath, Bath, UK.

Munsell A.H. (1946)

A Color Notation, 2nd edition. Munsell Color Company, Baltimore, Boston, Massachusetts.

Naidu M.S. & Kamaraju V. (1995)

High Voltage Engineering, 2nd edition. McGraw-Hill, New York.

Naylor J. (1981)

"Fault calculation" in The Electricity Council (ed.), *Power System Protection 1*, 2nd edition. Peter Peregrinus, Stevenage, UK.

NGT (2000)

"Introduction of transformer partial discharge project", *National Grid Transco PD Website*, [Online], 9 paragraphs. Available: http://www.partialdischarge.co.uk/ intro.htm [2003, October 1].

Ogihara H. (1964)

"Detection and location of coronas in oil immersed transformer with corona detector", *Electrical engineering in Japan*, vol.84, no.9, pp.12-21.

Oommen T.V., Moore H.R. & Luke L.E. (1982)

"Experience with gas-in-oil analysis made during factory tests on large power transformers", *IEEE Transactions on Power Apparatus and Systems*, vol.101, no.5, pp.1048-1052.

Pagan E. (1998)

"Diagnostic techniques track CT aging", *Transmission & Distribution*, vol.50, no.8, pp.48, 50, 52.

Papoulis A. & Pillai S. U. (2002)

Probability, Random Variables, and Stochastic Processes, 4th edition. McGraw-Hill, Boston; London.

Pearmain A.J. & Clegg A.G. (1993)

"Insulators" in Jones G.R., Laughton M.A. & Say M.G. (eds.), *Electrical Engineer's Reference Book*, 15th edition. Butterworth-Heinemann, Oxford.

Pearson J.S., Farish O., Hampton B.F., Judd M.D., Templeton D., Pryor B.W. & Welch I.M. (1995)

"Partial discharge diagnostics for gas insulated substations", *IEEE Transactions on Dielectrics and Electrical Insulation*, vol.2, no.5, pp.893-905.

Raja K. & Luna G. (2002) [Personal Communication]

Northfleet West SGT3A Transformer Partial Discharge Tests. Unpublished report, ALSTOM, Diversa House, 34 Dover Street, London W1S 4NG, UK.

Richardson D.V. (1978)

Rotating Electric Machinery and Transformer Technology. Reston, Reston, Virginia.

Rolls T.B. (1982)

Power Distribution in Industrial Installations. Peter Peregrinus, Stevenage, UK.

Rushton J. & Mewes K.G.M. (1981)

"Protection of generators, transformers, generator-transformer units and transformer feeders" in The Electricity Council (ed.), *Power System Protection 3*, 2nd edition. Peter Peregrinus, Stevenage, UK.

Russell P.C., Cosgrave J., Tomtsis D., Vourdas A., Stergioulas L. & Jones G.R. (1998)
"Extraction of information from acoustic vibration signals using Gabor transform type devices and application to circuit breakers", *Measurement Science and Technology*, vol.9, no.8, pp.1282-1290.

Russwurm D. (2000)
"Partial discharge measurements and diagnostics on power transformers using a multi channel digital PD detector", *HV Testing, Monitoring and Diagnostics Workshop*, 13-14 September 2000, paper no.14, pp.1-5, Alexandria, Virginia.

Rutgers W.R. & Fu Y.H. (1997)
"UHF PD-detection in a power transformer", Proceedings of *the 10th International Symposium on High Voltage Engineering* (ISH-97), vol.4, pp.219-222. 25-29 August 1997, Montreal, Canada.

Rutgers W.R., van den Aardweg P. & Atmadji A.M.S. (2001) [Personal Communication]
Transformer PD: UHF Measurement at Neilston Substation. Unpublished report, KEMA T&D Power, Utrechtseweg 310, 6812 AR Arnhem, Netherlands.

Rutgers W.R. & van den Aardweg P. (2002) [Personal Communication]
UHF PD Measurements on Transformer SGT-3A. Unpublished report, KEMA T&D Power, Utrechtseweg 310, 6812 AR Arnhem, Netherlands.

Schwarz M.W., Cowan W.B. & Beatty J. C. (1987)
"An experimental comparison of RGB, YIQ, LAB, HSV and opponent color models", *ACM Transactions on Graphics*, vol.6, no.2, pp.123-158.

Smith A.R. (1978)

"Color gamut transform pairs", *Computer Graphics*, vol.12, no.3, pp.12-19.

Smith C. (2001) [Personal Communication]

Report on Transformer Tests Carried Out at Neilston. Unpublished report, IPEC Ltd, Williams House, Manchester Science Park, Lloyd St. North, Manchester M15 6SE, UK.

Smith C. (2002) [Personal Communication]

Report on Transformer Tests Carried Out at Northfleet West. Unpublished report, IPEC Ltd, Williams House, Manchester Science Park, Lloyd St. North, Manchester M15 6SE, UK.

Stergioulas L. (1997)

Time-frequency Methods in Optical Signal Processing. PhD thesis, The University of Liverpool, UK.

Stergioulas L.K. & Vourdas A. (1998)

"Robust quantum state engineering using coherent states on a truncated von Neumann lattice", *Journal of Modern Optics*, vol.45, no.6, pp.1155-1161.

Stergioulas L.K., Vourdas A. & Jones G.R. (2000)

"Gabor representation of optical signals using a truncated von Neumann lattice and its practical implementation", *Optical Engineering*, vol.39, no.7, pp.1965-1971.

Su Q., Mi C., Lai L.L. & Austin P. (2000)

"A fuzzy dissolved gas analysis method for the diagnosis of multiple incipient faults in a transformer", *IEEE Transactions on Power Systems*, vol.15, no.2, pp.593-598.

Tolstov G.P. (1976)

Fourier Series. Translated from the Russian by Silverman R. A., Dover, New York.

Tsai S., Chen L. & Liu Y. (2002) [Personal Communication]

Report Part II: Northfleet West SGT3A 500MVA, 400kV/275kV Transformer On-site PD Measurement Signal Processing. Unpublished report, Virginia Tech, Power IT Laboratory, 340 Whittemore Hall, Blacksburg VA 24060, USA.

Tu Y., Wang Z. & Crossley P. (2001) [Personal Communication]
Report on Partial Discharge Activity within 400/275kV Transformer at Neilston Substation, NGC Test Sequence:- June 2001. Unpublished report, UMIST, Manchester M60 1QD, UK.

Tu Y., Wang Z. & Crossley P. (2002) [Personal Communication]
Report on Partial Discharge Activity within the 400/275kV Auto-transformer SGT3A at Northfleet West Substation, National Grid Test:- May 2002. Unpublished report, UMIST, Manchester M60 1QD, UK.

Tyler D.W. (1997)
Electrical Power Technology. Newnes, Oxford.

Unsworth J. & Tallis D. (2002) [Personal Communication]
Evaluation of Siemens Transformer VIGIL™ - Version 2 Installed on A 500 MVA Parsons Auto Transformer at National Grid Northfleet 400 KV Substation as Part of EPRI Test Review 20th - 27th May 2002. Unpublished report, Siemens Ltd, Power Transmission & Distribution Services, 73 Talavera Road, North Ryde, NSW 2113, Australia.

von Neumann J. (1955)
Mathematical Foundations of Quantum Mechanics. Princeton University, Princeton.

Waters T. (2001) [Personal Communication]
NGC Partial Discharge Experiment at Neilston Substation. Unpublished report, Serveron Corporation, 3305 NW Aloclek Drive, Hillsboro.

Weedy B.M. & Cory B.J. (1998)
Electric Power Systems, 4th edition. Wiley, Chichester, UK.

Weiss L.G. (1994)

"Wavelets and wideband correlation processing", *IEEE Signal Processing Magazine*, vol.11, no.1, pp.13-32.

White A. (1994)

"Design of high voltage power transformers" in Ryan H.M. (ed.), *High Voltage Engineering and Testing*. Peter Peregrinus, Stevenage, UK.

Wyszecki G. & Stiles W.S. (1967)

Color Science: Concepts and Methods, Quantitative Data and Formulas. Wiley, New York.

Wyszecki G. & Stiles W.S. (1982)

Color Science: Concepts and Methods, Quantitative Data and Formulae, 2nd edition. Wiley, New York.

Yang H.T., Liao C.C. & Chou J.H. (2001)

"Fuzzy learning vector quantization networks for power transformer condition assessment", *IEEE Transactions on Dielectrics and Electrical Insulation*, vol.8, no.1, pp.143-149.

Yu B., Kim D.W., Cockey W. & Wang A. (2002) [Personal Communication]

Report Part I: Package and Installation of Fiber Optic PD Sensors PD Detection in Northfleet West SGT3A 400KV Transformer. Unpublished report, Virginia Tech, Center for Photonics Technology, 460 Turner St., Suite 303 Blacksburg, VA 24061, USA.

Zhang J., Deakin A., Jones G.R. & McGrail T. (2002)

"Partial discharge monitoring in HV transformers using chromatic processing of dissolved gas analysis", Proceedings of *the XIV International Conference on Gas Discharges and their Applications* (GD2002), vol.2, pp164-167. The University of Liverpool, 1-6 September 2002, Liverpool, UK.

Bibliography

Adobe (2001)

Technical Guides – Color Models, [Online], 10 paragraphs. Available: http://www.adobe.com/support/techguides/color/colormodels/main.html [2003, October 1].

Adobe (2002)

"CIE color standard general information", *Adobe Support Knowledgebase*, [Online], 14 paragraphs. Available: http://www.adobe.com/support/techdocs/30b6.htm [2003, October 1].

Adobe (2003)

"The Lab color mode in Photoshop", *Adobe Support Knowledgebase*, [Online], 14 paragraphs. Available: http://www.adobe.com/support/techdocs/34ea.htm [2003, October 1].

Beyer W.H. (1991)

CRC Standard Mathematical Tables and Formulae, 29th edition. CRC Press, Boca Raton (Fla).

Box G.E.P. & Draper N.R. (1987)

Empirical Model-building and Response Surfaces. Wiley, Chichester.

Box G.E.P. & Hunter J.S. (1957)

"Multi-factor experimental designs for exploring response surfaces", *Annals of Mathematical Statistics*, vol.28, no.1, pp.195-241.

Chen A.P. & Lin C.C. (2001)

"Fuzzy approaches for fault diagnosis of transformers", *Fuzzy Sets and Systems*, vol.118, no.1, pp.139-151.

CVRL (2000)

"CVRL colour & vision database", *Colour & Vision Research Laboratories*, [Online], 8 paragraphs. Available: http://www-cvrl.ucsd.edu/index.htm [2003, October 1].

Devins J.C. (1984)

"The physics of partial discharges in solid dielectrics", *IEEE Transactions on Electrical Insulation*, vol.19, no.5, pp.475-495.

Duval M. & dePablo A. (2001)

"Interpretation of gas-in-oil analysis using new IEC publication 60599 and IEC TC 10 databases", *IEEE Electrical Insulation Magazine*, vol.17, no.2, pp.31-41.

Duval M. (2002)

"A review of faults detectable by gas-in-oil analysis in transformers", *IEEE Electrical Insulation Magazine*, vol.18, no.3, pp.8-17.

Duval M. (2003)

"New techniques for dissolved gas-in-oil analysis", *IEEE Electrical Insulation Magazine*, vol.19, no.2, pp.6-15.

Foley J.D., van Dam A., Feiner S.K., Hughes J.F. & Phillips R.L. (1994)

Introduction to Computer Graphics. Addison-Wesley, Reading, Massachusetts.

Gonzalez R.C. & Woods R.E. (2002)

Digital Image Processing, 2nd edition. Prentice Hall, Upper Saddle River, New Jersey.

Granttan K.T.V. & Meggitt B.T. (1995)

Optical Fiber Sensor Technology. Chapman & Hall, London.

Hendee W.R. & Wells P.N.T. (1993)

The Perception of Visual Information. Springer, New York.

Huang Y.C. (2003a)

"Evolving neural nets for fault diagnosis of power transformers", *IEEE Transactions on Power Delivery*, vol.18, no.3, pp.843-848.

Huang Y.C. (2003b)

"Fault identification of power transformers using genetic-based wavelet networks", *IEE Proceedings Science, Measurement and Technology*, vol.150, no.1, pp.25-29.

Judd D.B. & Wyszecki G. (1975)

Color in Business, Science and Industry, 3rd edition. Wiley, New York.

Kimbark E.W. (1948)

Power System Stability. Wiley, New York.

Knight U.G. (1972)

Power Systems Engineering and Mathematics. Pergamon, Oxford.

Kuwahara W. (1976)

"Partial discharge characteristics in silicone liquids", *IEEE Transactions on Electrical Insulation*, vol.11, no.3, pp.86-91.

Lachman M.F. & Walter W. (1999)

"Experience with on-line diagnostics and life management of high-voltage bushings", Proceedings of *the Sixty-sixth Annual International Conference of Doble Clients.* Doble Engineering Company, April 12-16, 1999, Boston, USA.

Lachman M.F., Walter W. & von Guggenberg P.A. (2000)

"On-line diagnostics of high-voltage bushings and current transformers using the sum current method", *IEEE Transactions on Power Delivery*, vol.15, no.1, pp.155-162.

Levkowitz H. & Herman G.T. (1987)

"GIHS: A generalized color model and its use for the representation of multiparameter medical images" in Viergever M.A. & Todd-Pokropek A.E. (eds.), *Mathematics and Computer Science in Medical Imaging*, pp.389-399. Springer-Verlag, Berlin.

McDermid W., Lachman M.F., Walter W. & von Guggenberg P.A. (2000)

"Discussion of 'On-line diagnostics of high-voltage bushings and current transformers using the sum current method' closure to discussion", *IEEE Transactions on Power Delivery*, vol.15, no.4, p.1356.

Mosinski F. & Piotrowski T. (2003)

"New statistical methods for evaluation of DGA data", *IEEE Transactions on Dielectrics and Electrical Insulation*, vol.10, no.2, pp.260-265.

Quinlan J.R. (1986)

"Induction of decision trees", *Machine Learning*, vol.1, no.1, pp. 81-106.

Russell P.C. (2000) [Personal Communication]

Chromatic Analysis of Transformer Data. Unpublished report, Centre for Intelligent Monitoring Systems (CIMS), Dept. of EEE, University of Liverpool, Liverpool, UK.

Smith T. & Guild J. (1932)

"The C.I.E. colorimetric standards and their use", *Transactions of the Optical Society*, vol.33, no.3, pp.73-134.

Spiegel M.R. (1975)

Schaum's outline Series, Theory and Problems of Probability and Statistics. McGraw-Hill, New York.

Steinhaus H. (1983)

Mathematical Snapshots, 3rd American edition. Oxford University Press, Oxford.

Wang M.H. (2003)

"A novel extension method for transformer fault diagnosis", *IEEE Transactions on Power Delivery*, vol.18, no.1, pp.164-169.

Whittaker E.T. & Robinson G. (1940)

The Calculus of Observations: A Treatise on Numerical Mathematics, 3rd edition.   Blackie, London.

Wood J.W., Sedding H.G., Hogg W.K., Kemp I.J. & Zhu H. (1993)

"Partial discharges in HV machines: initial considerations for a PD specification", *IEE Proceedings Science, Measurement and Technology*, vol.140, no.5, pp.409–416.

Appendices

Appendix A. Neilston Site-test Diary

Table A.1 Neilston SGT4 off-line PD measurements time line of energisation

Time		Note
25/6		
00:00	DGA	1
12:00	DGA	2
14:55	Started gen-sets	
15:02	Increased excitation to max (110%) at 50.3 Hz (no volts on tested transformer)	
	Closed breaker to energise transformer	
15:21	Increased volts to 49% at 55.7 Hz	
15:33	Increased volts to 60%	
15:41	Increased volts to 69%	
15:52	Increased volts to 80%	
15:59	Increased volts to 87%	
16:00	DGA	3
16:14	Reduced volts to 25%	
	Shut-down	
17:42	Started gen-sets and closed breaker	
17:45	Increased volts to 87% at 55.7 Hz	
18:28	Reduced volts to zero and opened breaker	
	Increased excitation up to 110% (no volts on tested transformer)	
	Shut-down	
20:00	DGA	4
26/6		
00:00	DGA	5
04:00	DGA	6
08:00	DGA	7
	Started gen-sets and closed breaker	
10:32	Increased volts to 85%	
10:44	Increased volts to 90%	
10:52	Increased volts to 95%	
11:02	Increased volts to 100%	
11:40	Shut-down (local lightning and rain)	
15:00	Started gen-sets and closed breaker	
15:08	Increased volts to 100%	
15:15	Switched off oil pumps - RCD supplying cabins tripped	
15:17	Re-set RCD	
15:47	Shut-down	
15:50	Switched oil circulation pumps back on	
16:00	DGA	8
16:15	Started gen-sets and closed breaker	

Table A.1 Continued

16:19	Increased volts to 100%	
16:38	Changed frequency to 50 Hz	
17:12	Changed frequency back to 55.1 Hz	
17:17	Increased voltage to 105%	
17:25	Acoustic test (ABB), file "Lock67"	
17:33	Acoustic test (ABB), file "Lock95"	
17:43	Increased voltage to 107%	
17:53	Reduced voltage to 60% and frequency to 50 Hz	
18:26:16	UHF test (KEMA), file "2606n"	
18:29:53	UHF test (KEMA), file "2606o"	
18:37	Shut-down	
20:00	DGA	9

27/6

00:00	DGA	10
04:00	DGA	11
08:00	DGA	12
10:00	Started gen-sets and closed breaker	
10:03	Increased voltage to 100% at 50 Hz	
10:25	Shut-down	
	Started gen-sets and closed breaker	
12:25	Increased voltage to 100% at 50 Hz	
13:01	Reduced voltage to 60 %	
13:17	Shut-down	
14:17	Acoustic test (KEMA), file "2706m"	
	Changed excitation transformer to tap 1 (+5%)	
14:20	Started gen-sets and closed breaker	
14:28	Shut-down	
15:06	Started gen-sets and closed breaker	
15:09	Increased voltage to 100% at 50 Hz	
15:15	Reduced voltage to 60%	
15:21	Increased voltage to 100%	
15:28	Increased voltage to 112% (at 50 Hz)	
15:35	Reduced voltage to 100%	
15:37	Reduced voltage to 0%	
15:45	Increased voltage to 85% at 60 Hz	
15:54	Increased voltage to 90% and then to 95%	
15:55	Increased voltage to 100%	
16:00	DGA	13
16:02	Increased voltage to 110%	
16:10	Increased voltage to 115%	
16:21	Acoustic test (KEMA), file "2706s"	
16:26	Shut-down	
17:26	Started gen-sets and closed breaker	
17:31	Increased voltage to 100% at 60 Hz	
17:47	Increased voltage to 115%	
18:00	Shut-down	
20:00	DGA	14
24:00	DGA	15

Appendix B. DGA Chromatic Maps for Additional Transformers
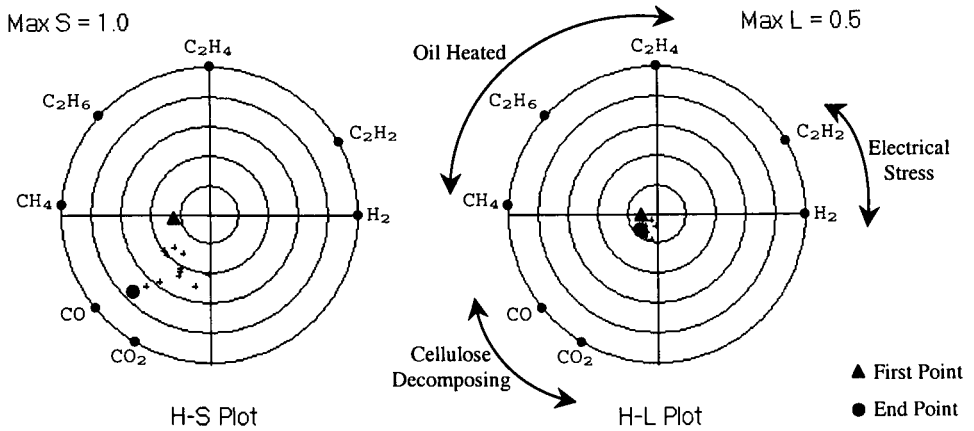
Figure B.1 DGA chromatic map of transformer BOLN1mtb
(Sampled 23/09/1985 ~ 30/03/1999)
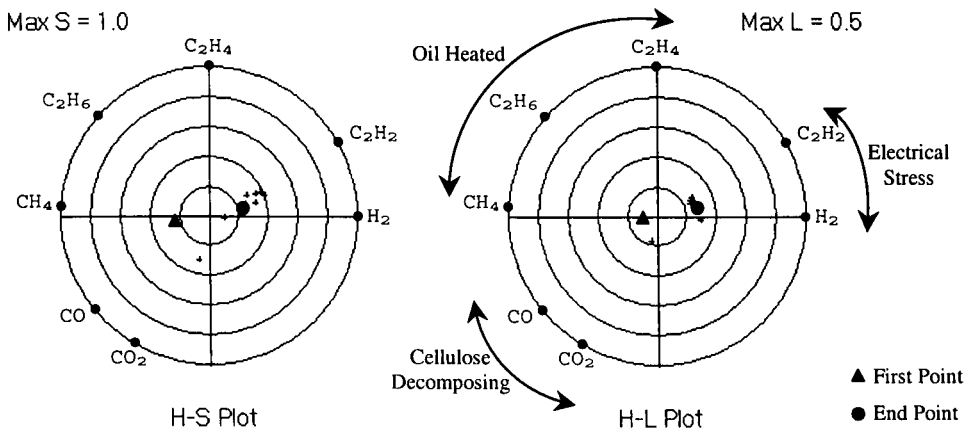
Figure B.2 DGA chromatic map of transformer BOLN2mtb
(Sampled 23/09/1985 ~ 28/10/1998)
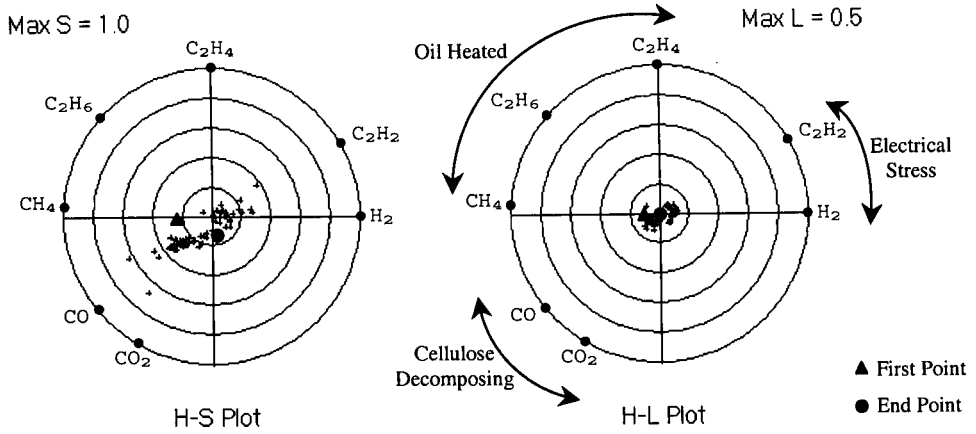
Figure B.3 DGA chromatic map of transformer BUSH2mtb
(Sampled 24/07/1972 ~ 09/11/1999)
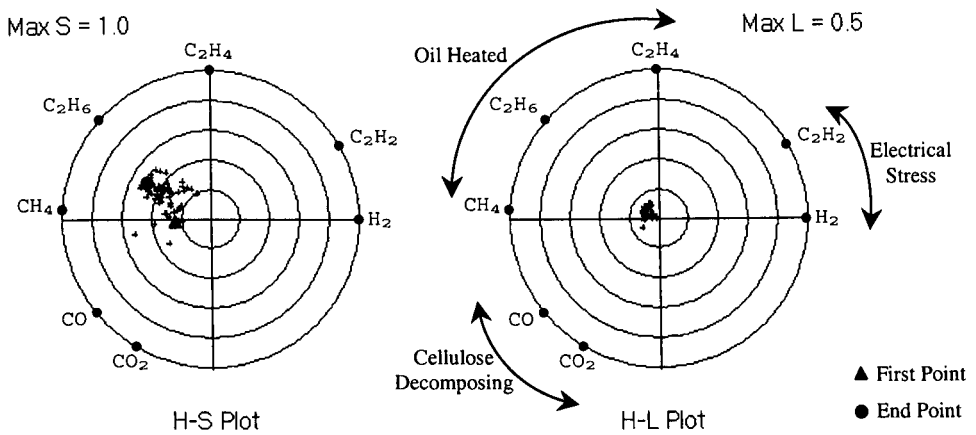
Figure B.4 DGA chromatic map of transformer BUSH3mtb
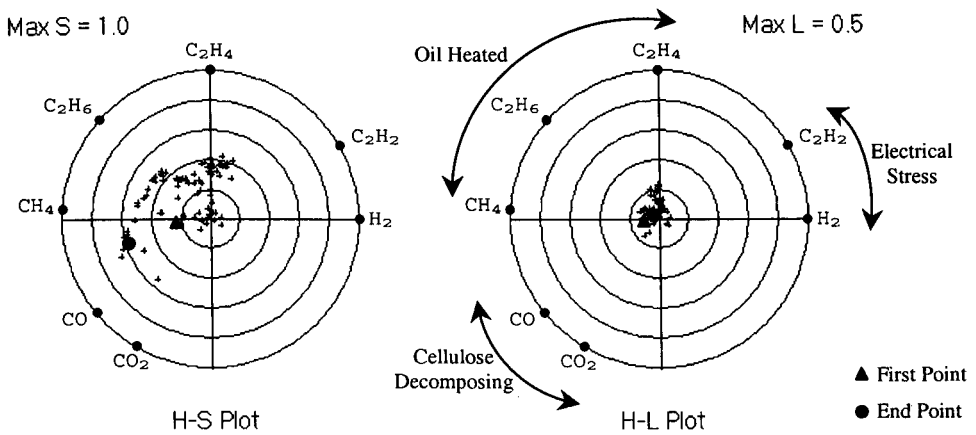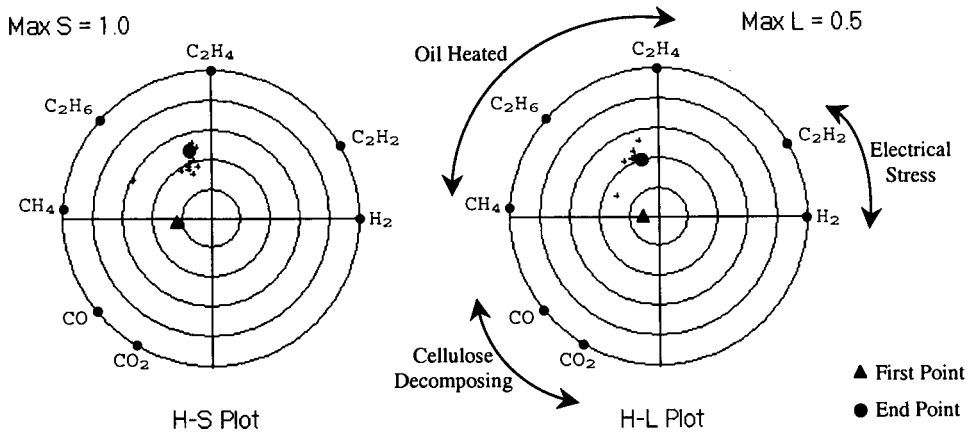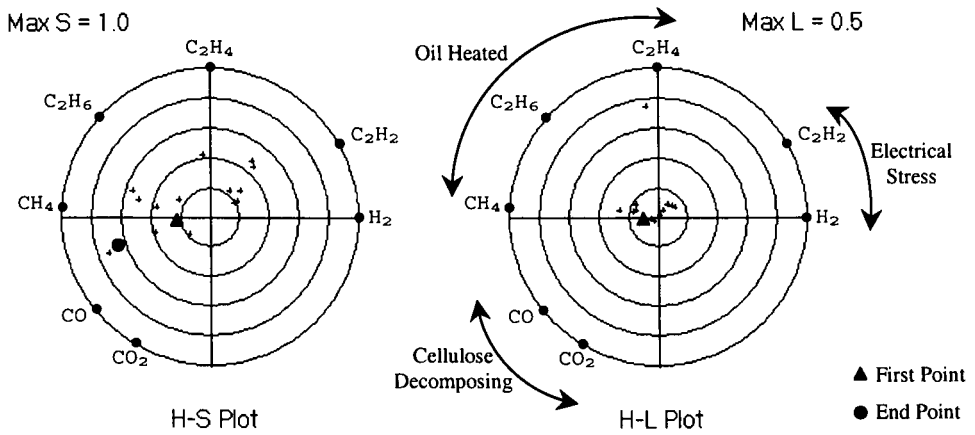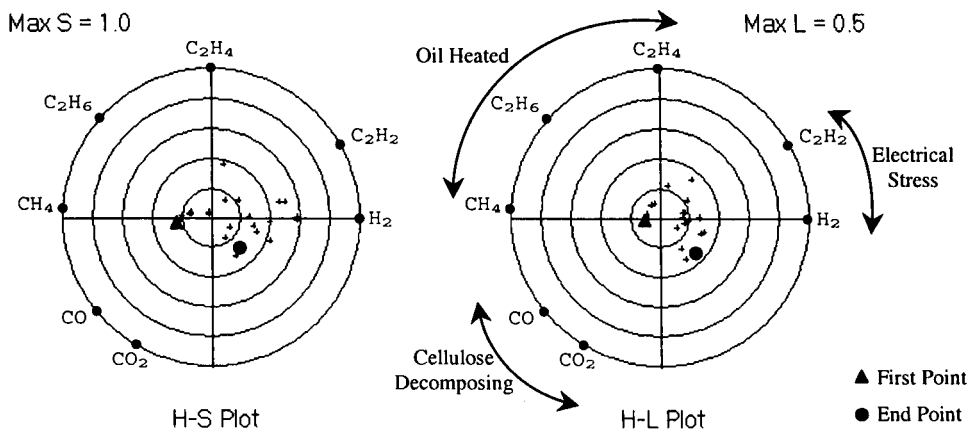(Sampled 24/07/1972 ~ 09/11/1999)

Figure B.5 DGA chromatic map of transformer BUSH4mtb
(Sampled 24/07/1972 ~ 09/11/1999)

Figure B.6 DGA chromatic map of transformer CANT1mtb
(Sampled 18/02/1986 ~ 25/06/1999)

Figure B.7 DGA chromatic map of transformer CANT2mtb
(Sampled 26/05/1994 ~ 25/06/1999)

Figure B.8 DGA chromatic map of transformer CAPE1Amtb
(Sampled 22/01/1985 ~ 05/09/1997)
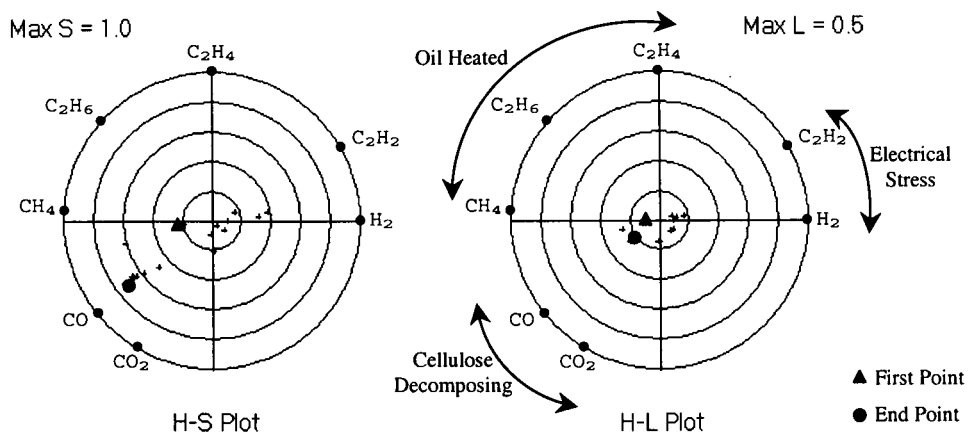
Figure B.9 DGA chromatic map of transformer CAPE2Amtb
(Sampled 13/09/1977 ~ 04/09/1997)
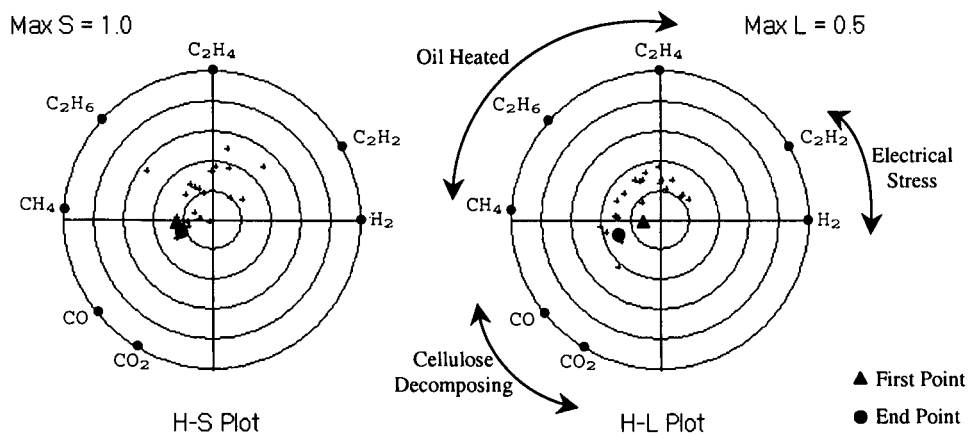
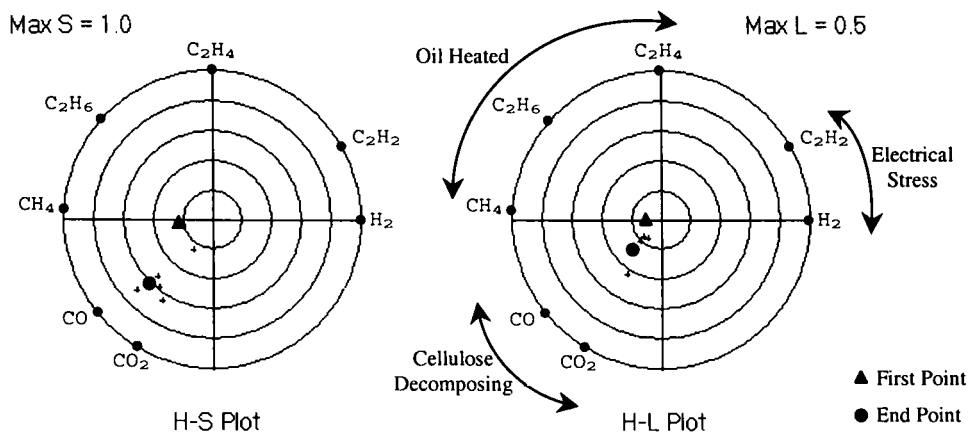Figure B.10 DGA chromatic map of transformer CAPE3Amtb
(Sampled 09/01/1974 ~ 30/07/1999)
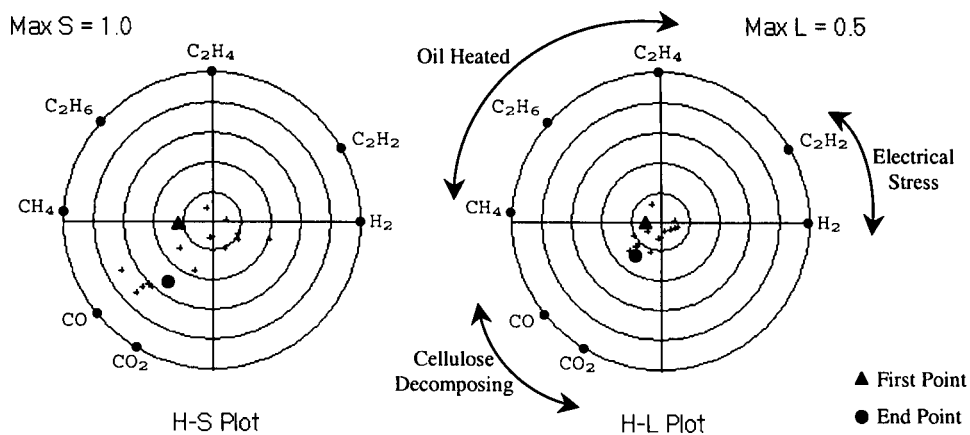
Figure B.11 DGA chromatic map of transformer CAPE5Amtb
(Sampled 15/08/1980 ~ 13/08/1997)
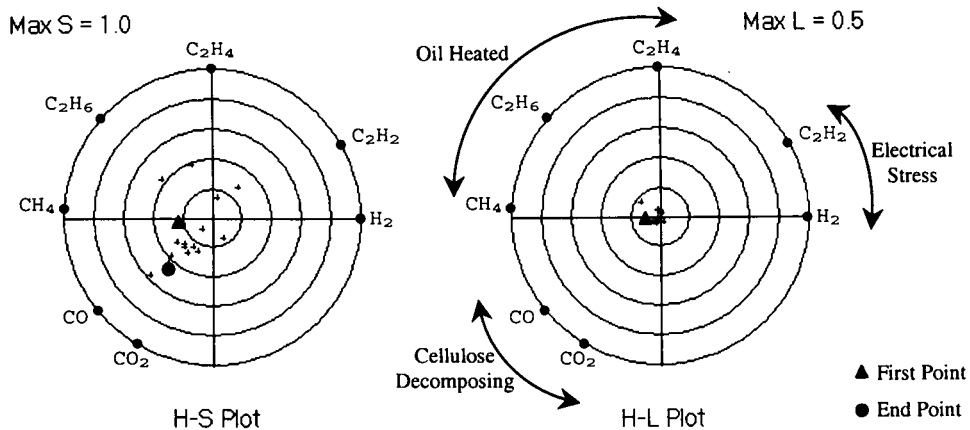
Figure B.12 DGA chromatic map of transformer CAPE5Bmtb
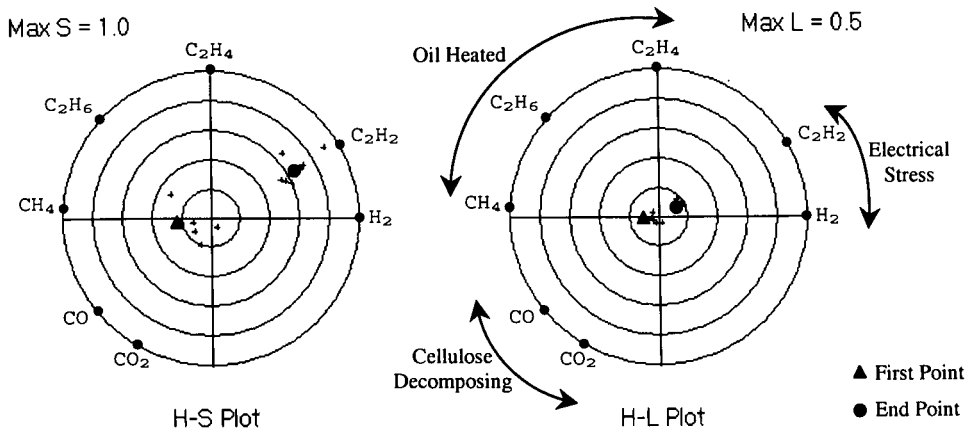(Sampled 09/01/1974 ~ 13/05/1997)
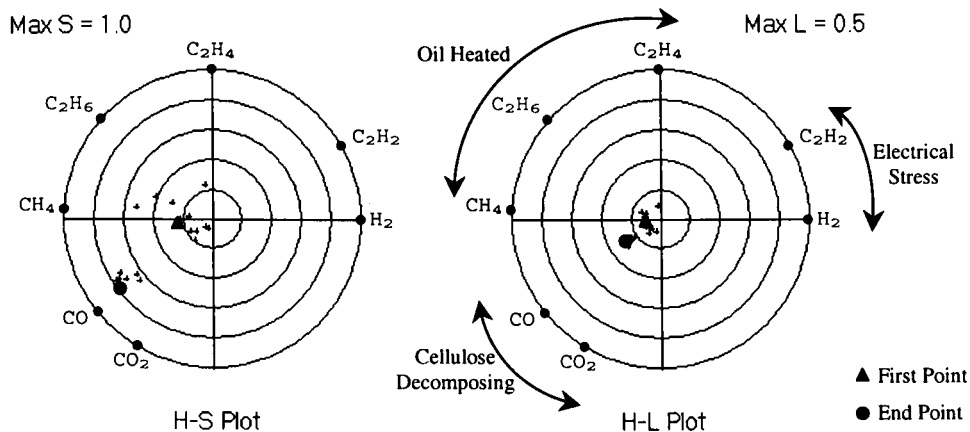
Figure B.13 DGA chromatic map of transformer CAPE6Amtb
(Sampled 03/01/1979 ~ 13/05/1997)

Figure B.14 DGA chromatic map of transformer CAPE6Bmtb
(Sampled 01/05/1997 ~ 18/03/1998)

Figure B.15 DGA chromatic map of transformer ELST1Amtb
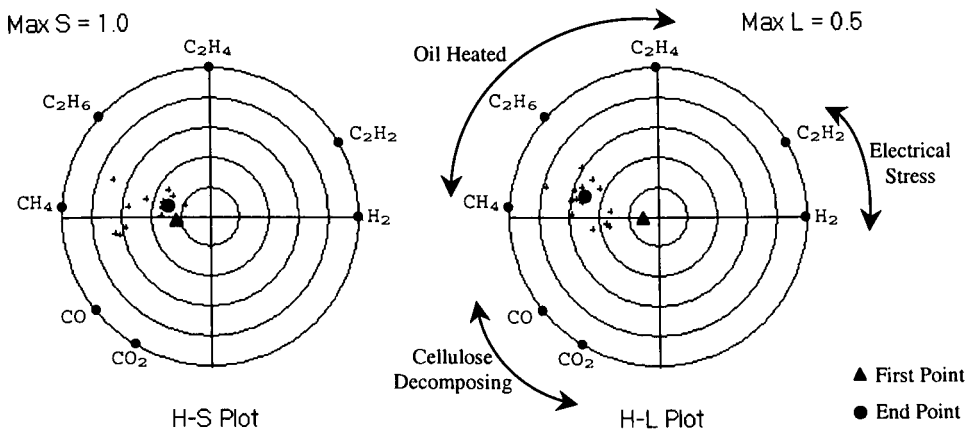(Sampled 29/01/1985 ~ 15/02/1999)

Figure B.16 DGA chromatic map of transformer ELST1Bmtb
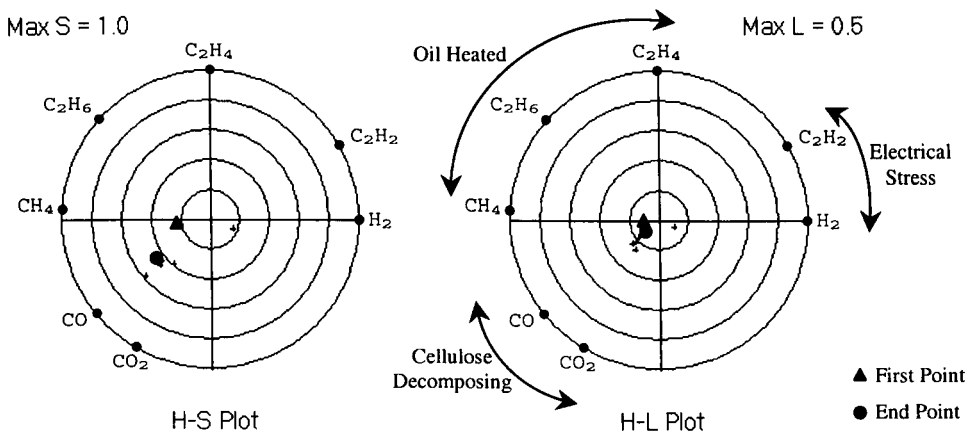(Sampled 29/01/1985 ~ 15/02/1999)

Figure B.17 DGA chromatic map of transformer ELST2mtb
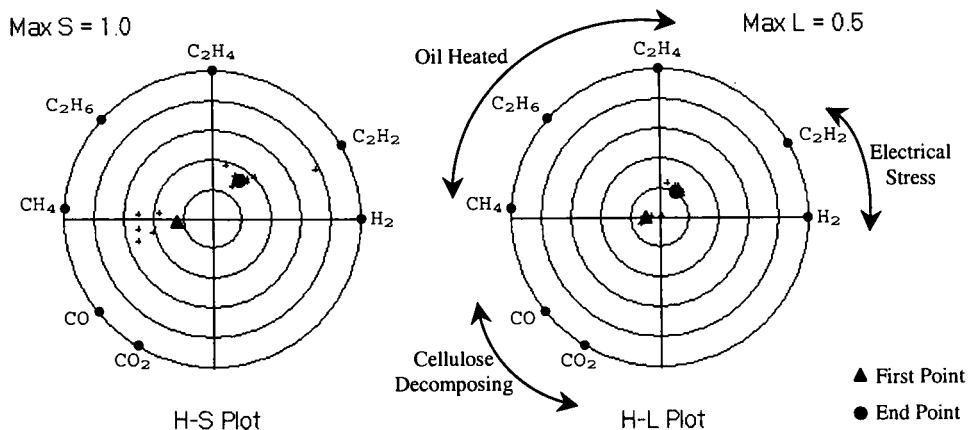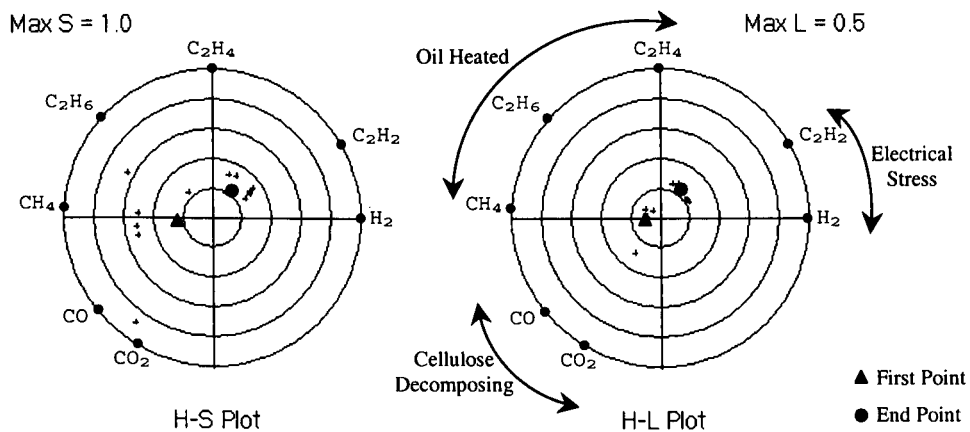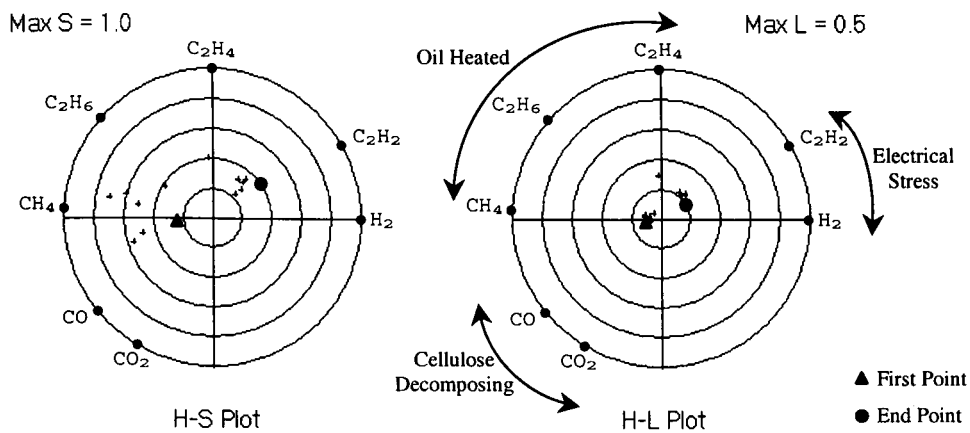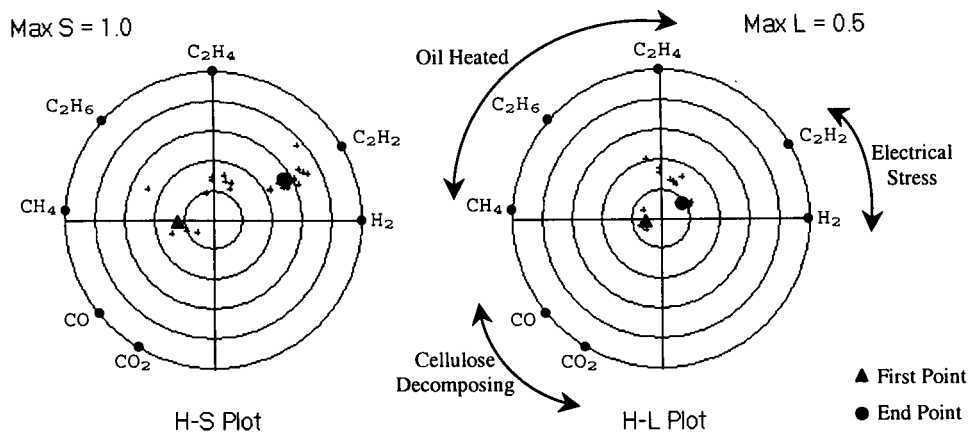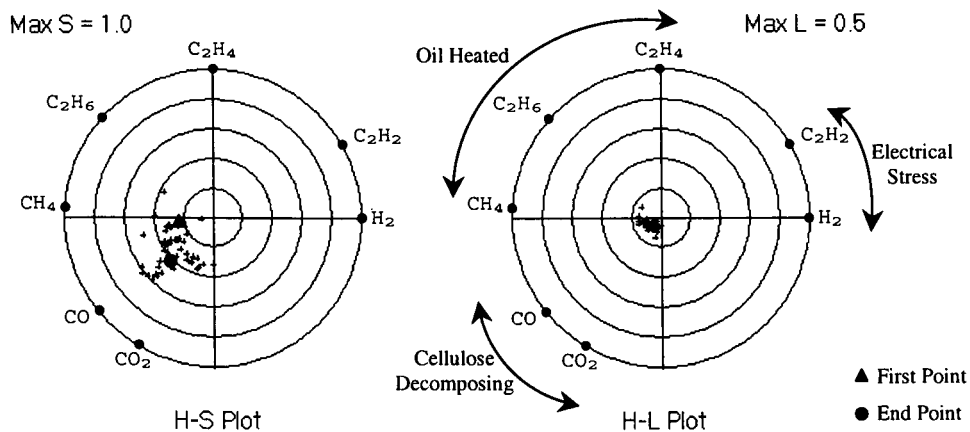(Sampled 01/08/1996 ~ 15/02/1999)

Max S = 1.0   Max L = 0.5

Oil Heated

Electrical
Stress

Cellulose
Decomposing

H-S Plot   H-L Plot

▲ First Point
● End Point

Figure B.18 DGA chromatic map of transformer ELST3Amtb
(Sampled 29/01/1985 ~ 16/02/1999)

Max S = 1.0   Max L = 0.5

Oil Heated

Electrical
Stress

Cellulose
Decomposing

H-S Plot   H-L Plot

▲ First Point
● End Point

Figure B.19 DGA chromatic map of transformer ELST3Bmtb
(Sampled 29/01/1985 ~ 16/02/1999)

Max S = 1.0   Max L = 0.5

Oil Heated

Electrical
Stress

Cellulose
Decomposing

H-S Plot   H-L Plot

▲ First Point
● End Point

Figure B.20 DGA chromatic map of transformer ELST4mtb
(Sampled 29/01/1985 ~ 17/02/1999)

Max S = 1.0   Max L = 0.5

H-S Plot   H-L Plot

▲ First Point
● End Point

**Figure B.21 DGA chromatic map of transformer ELST5Amtb
(Sampled 29/01/1985 ~ 21/07/1999)**

Max S = 1.0   Max L = 0.5

H-S Plot   H-L Plot

▲ First Point
● End Point

**Figure B.22 DGA chromatic map of transformer HAMH1mtb
(Sampled 22/08/1972 ~ 30/11/1998)**

Max S = 1.0   Max L = 0.5

H-S Plot   H-L Plot

▲ First Point
● End Point
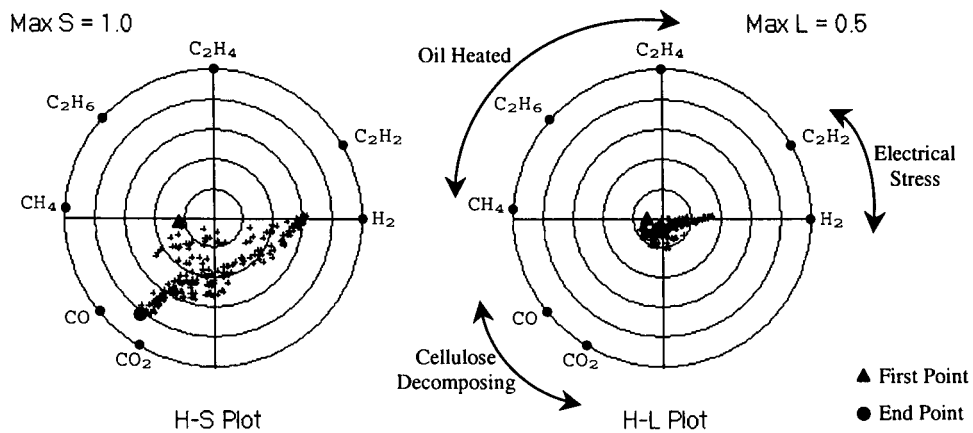
**Figure B.23 DGA chromatic map of transformer HAMH2mtb
(Sampled 22/08/1972 ~ 11/10/1999)**

Max S = 1.0   Max L = 0.5

H-S Plot   H-L Plot
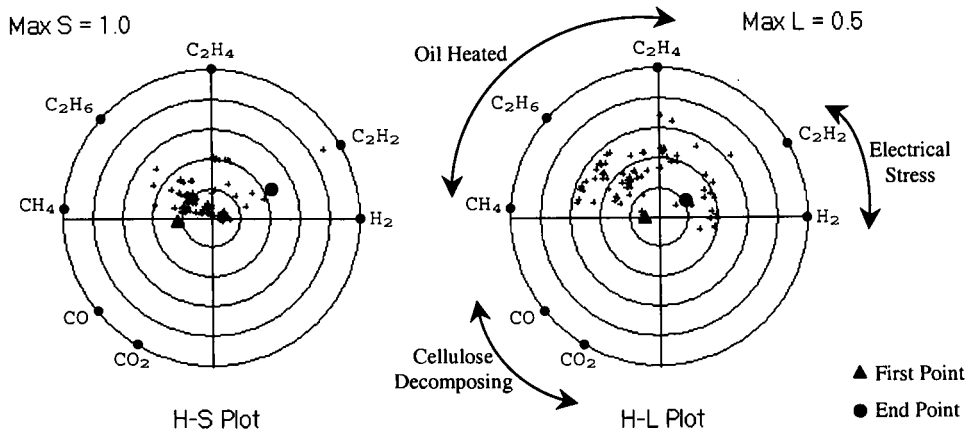
Figure B.24 DGA chromatic map of transformer HAMH3mtb
(Sampled 22/08/1972 ~ 23/11/1998)

Max S = 1.0   Max L = 0.5

H-S Plot   H-L Plot
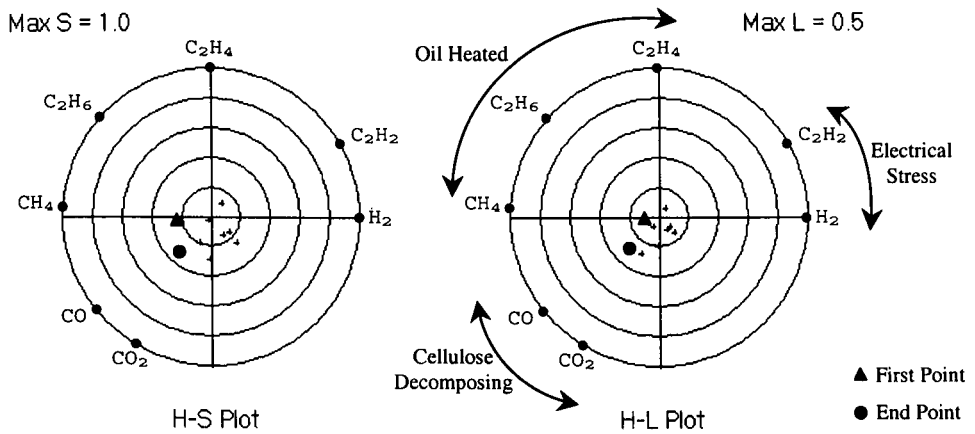
Figure B.25 DGA chromatic map of transformer HAMH5mtb
(Sampled 08/04/1998 ~ 26/05/1999)

Max S = 1.0   Max L = 0.5
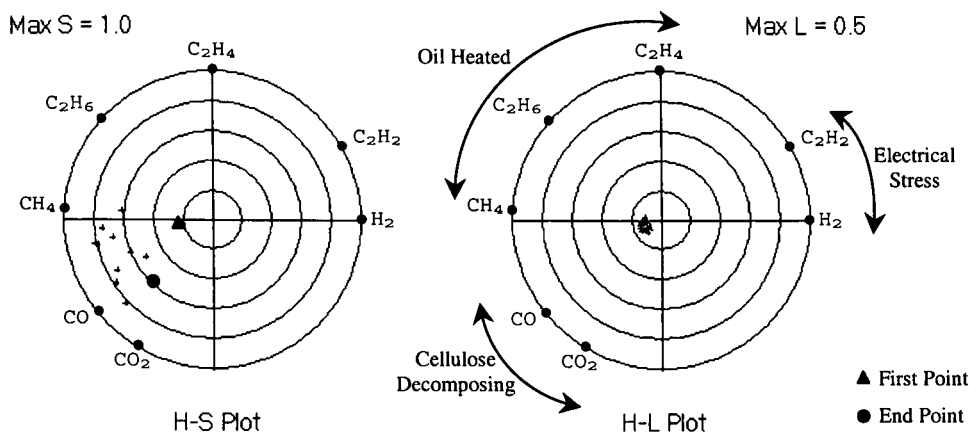

H-S Plot   H-L Plot

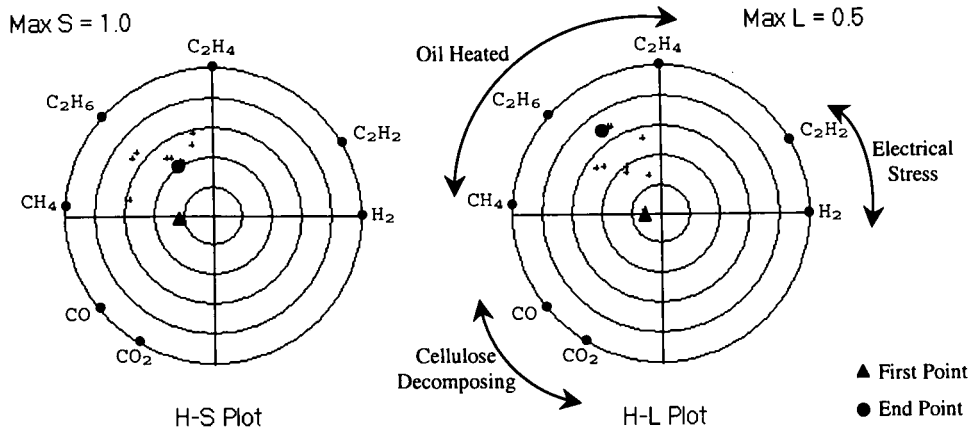Figure B.26 DGA chromatic map of transformer HAMH6mtb
(Sampled 30/12/1992 ~ 23/11/1998)

Figure B.27 DGA chromatic map of transformer HAMH7mtb
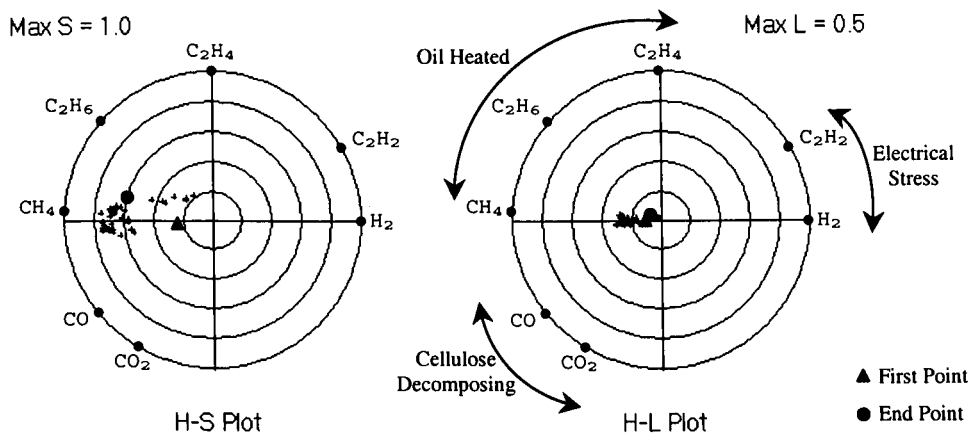(Sampled 24/02/1993 ~ 23/11/1998)

Figure B.28 DGA chromatic map of transformer WALX1Amtb
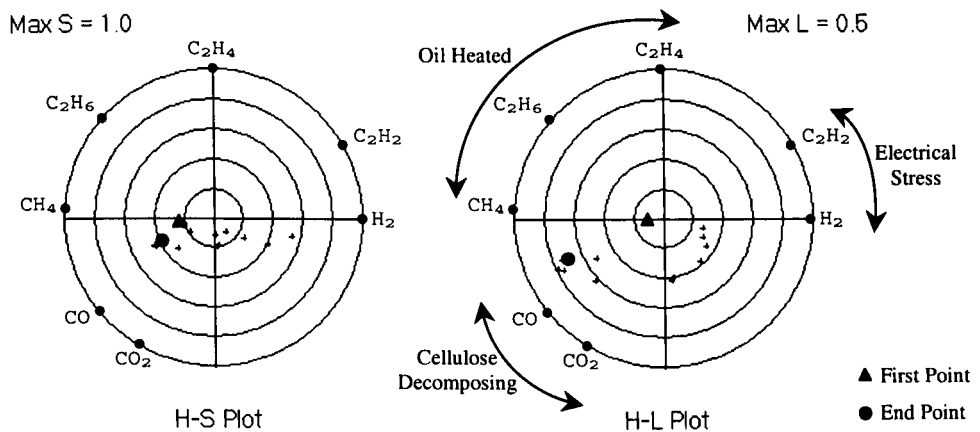(Sampled 27/05/1986 ~ 30/03/1999)

Figure B.29 DGA chromatic map of transformer WALX2Amtb
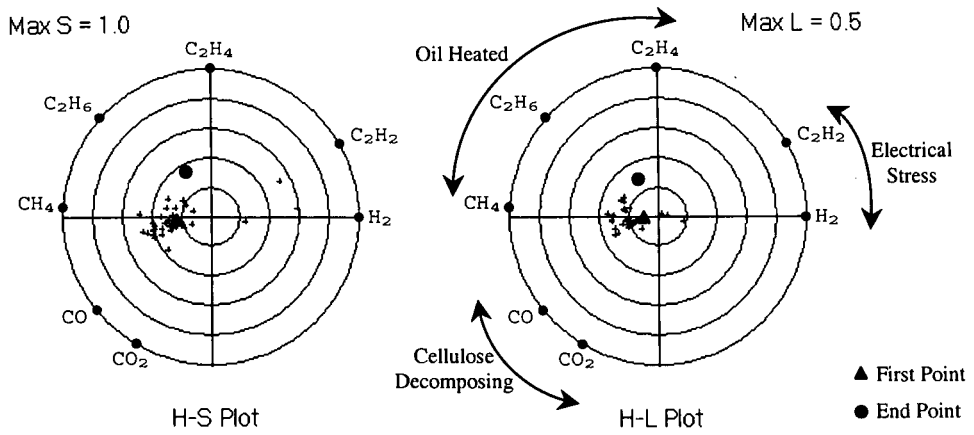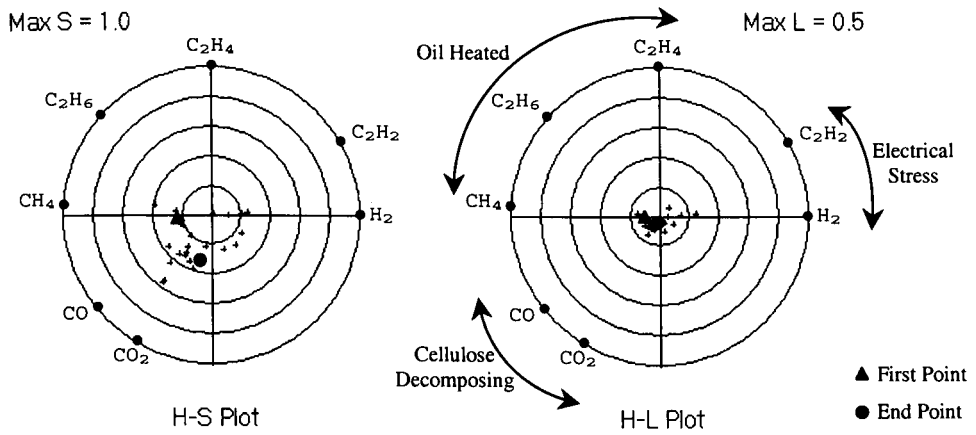(Sampled 20/07/1998 ~ 29/10/1999)

Max S = 1.0   Max L = 0.5

Oil Heated   Electrical Stress

Cellulose Decomposing

▲ First Point
● End Point

H-S Plot   H-L Plot

Figure B.30 DGA chromatic map of transformer WALX2Bmtb
(Sampled 13/02/1987 ~ 09/09/1999)

Max S = 1.0   Max L = 0.5

Oil Heated   Electrical Stress

Cellulose Decomposing

▲ First Point
● End Point

H-S Plot   H-L Plot

Figure B.31 DGA chromatic map of transformer WYLF2mtb
(Sampled 15/06/1979 ~ 29/06/1999)

Max S = 1.0   Max L = 0.5

Oil Heated   Electrical Stress

Cellulose Decomposing

▲ First Point
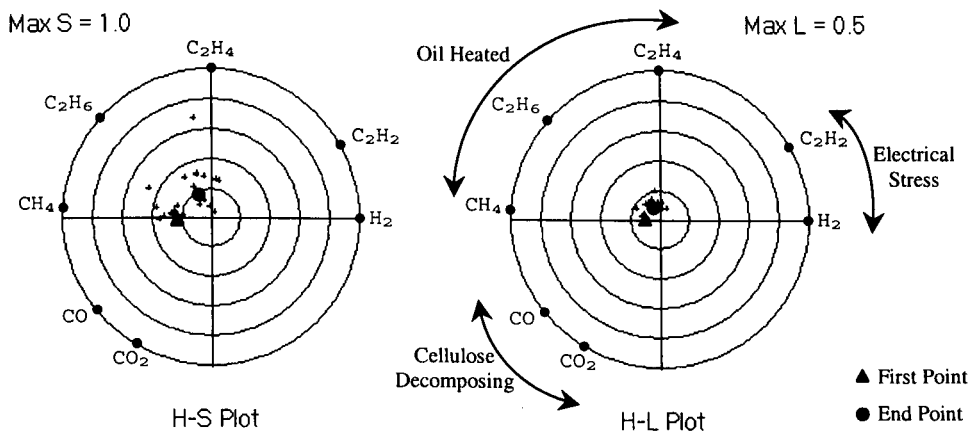● End Point

H-S Plot   H-L Plot

Figure B.32 DGA chromatic map of transformer WYLF4mtb
(Sampled 05/10/1979 ~ 29/06/1999)

Appendix C. Chromatic Results for Additional UMIST RF Signals

Figure C.1 HLS result for UMIST RF signal "May 25 02, 15-27-36"
(a), (b) & (c) Raw time-varying signal for channels 2, 3 & 4
(d), (e) & (f) HLS results for channels 2, 3 & 4

Figure C.2 HLS Result for UMIST RF signal "May 25 02, 15-31-08"
(a), (b) & (c) Raw time-varying signal for channels 2, 3 & 4
(d), (e) & (f) HLS results for channels 2, 3 & 4

Figure C.3 HLS Result for UMIST RF signal "May 25 02, 15-39-58"
(a), (b) & (c) Raw time-varying signal for channels 2, 3 & 4
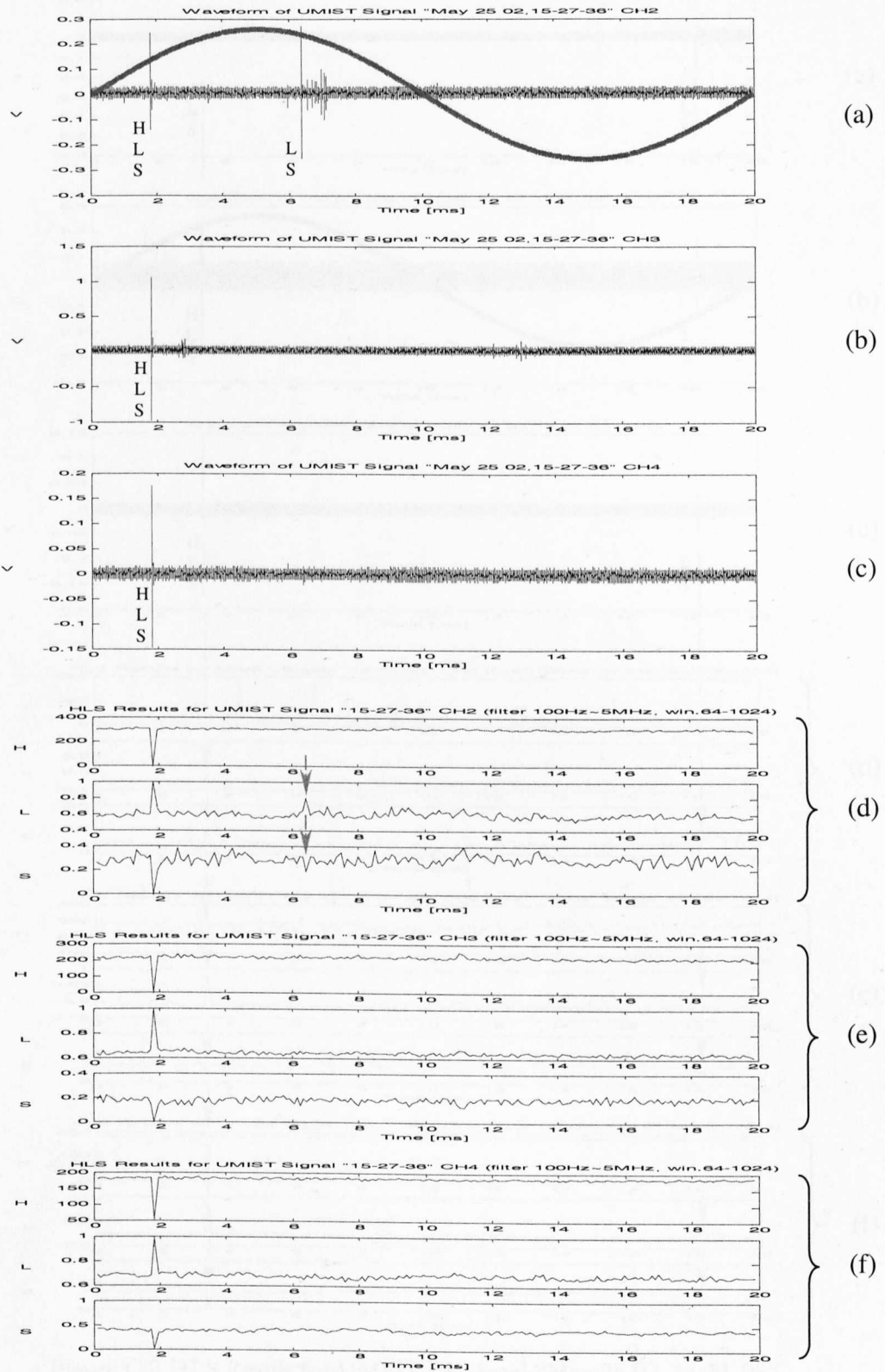(d), (e) & (f) HLS results for channels 2, 3 & 4

Figure C.4 HLS Result for UMIST RF signal "May 25 02, 15-33-26"
(a), (b) & (c) Raw time-varying signal for channels 2, 3 & 4
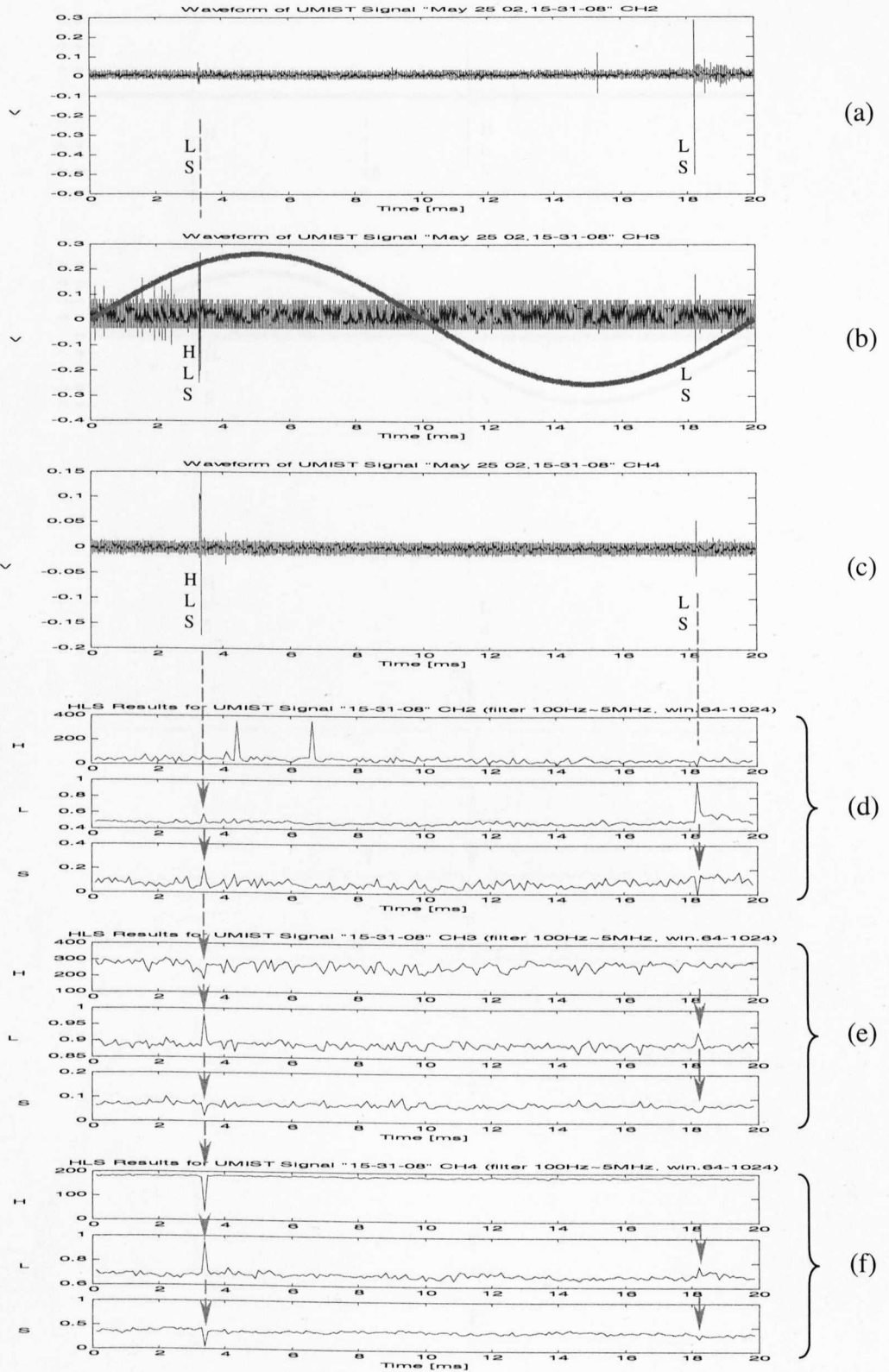(d), (e) & (f) HLS results for channels 2, 3 & 4
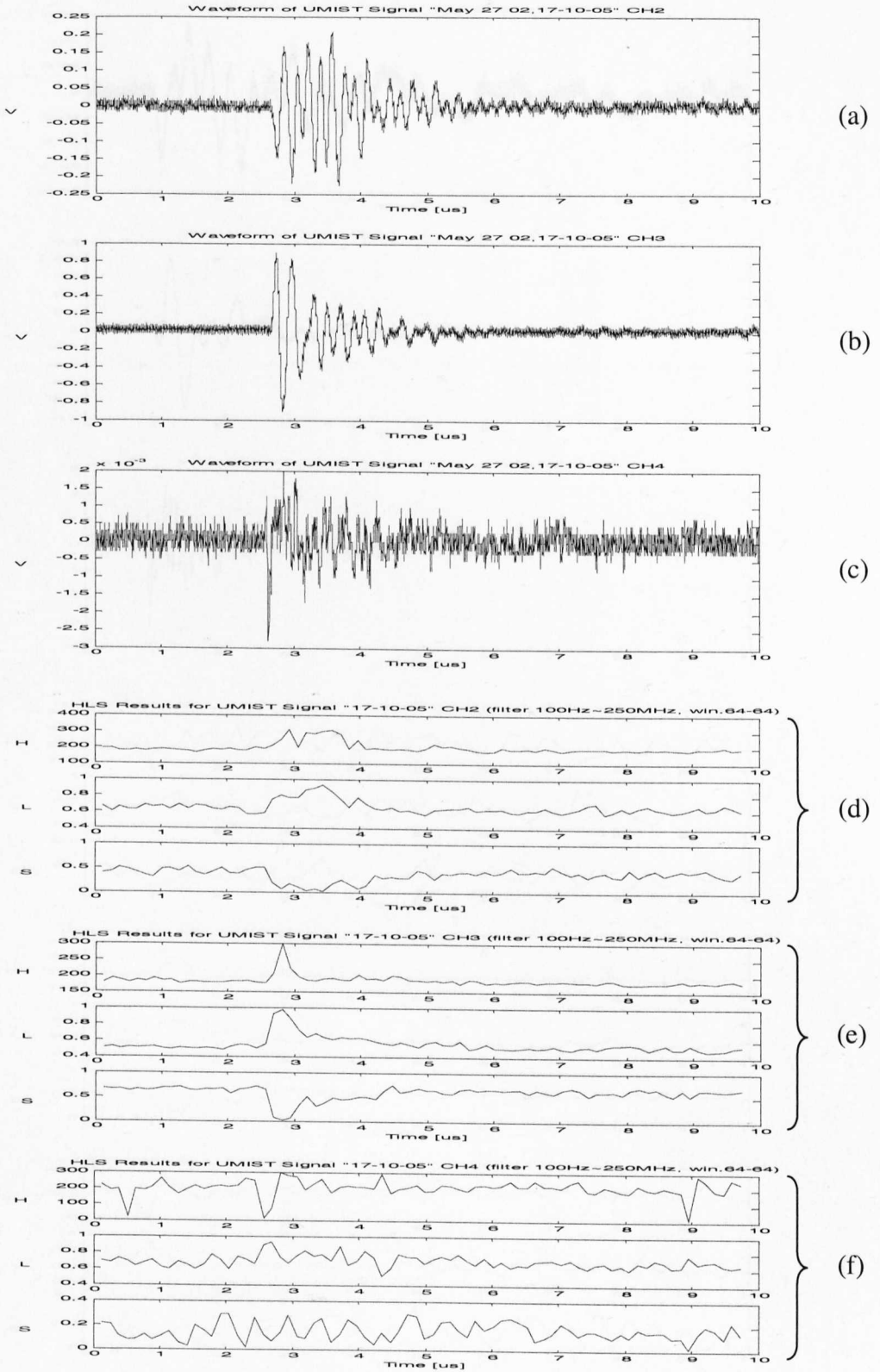
Figure C.5 HLS Result for UMIST RF signal "May 27 02, 17-10-05"
(a), (b) & (c) Raw time-varying signal for channels 2, 3 & 4
(d), (e) & (f) HLS results for channels 2, 3 & 4
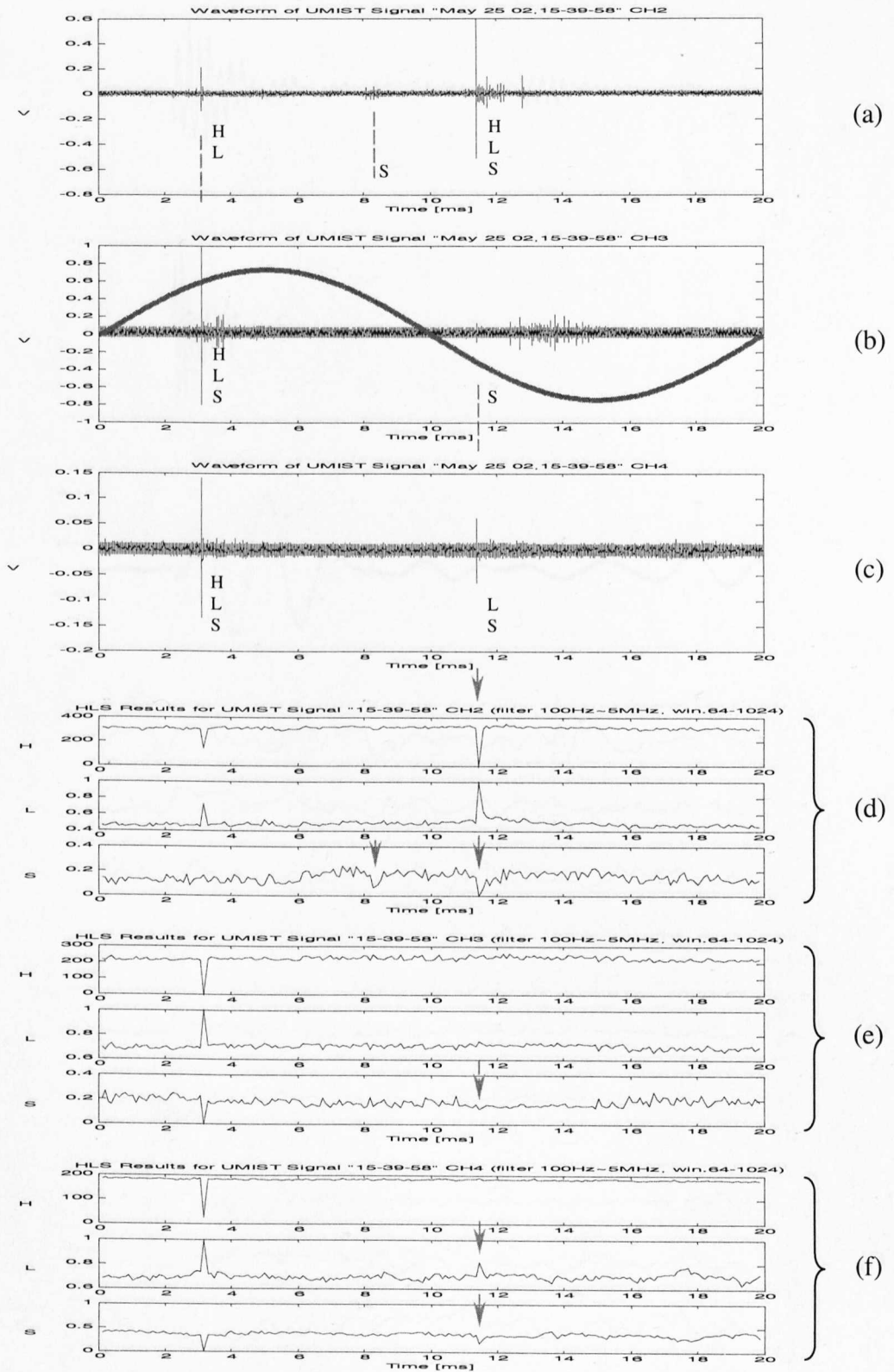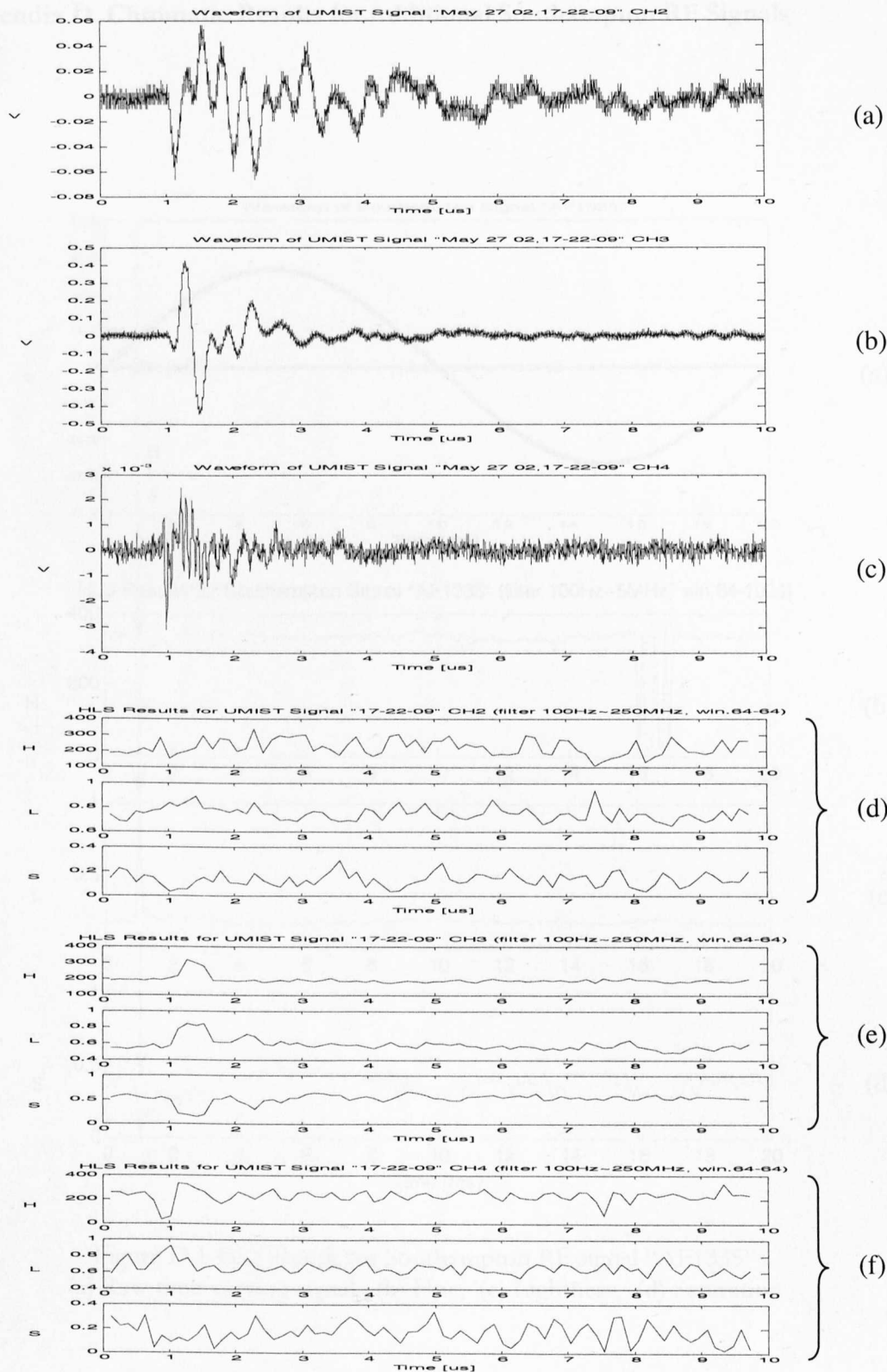
Figure C.6 HLS Result for UMIST RF signal "May 27 02, 17-22-09"
(a), (b) & (c) Raw time-varying signal for channels 2, 3 & 4
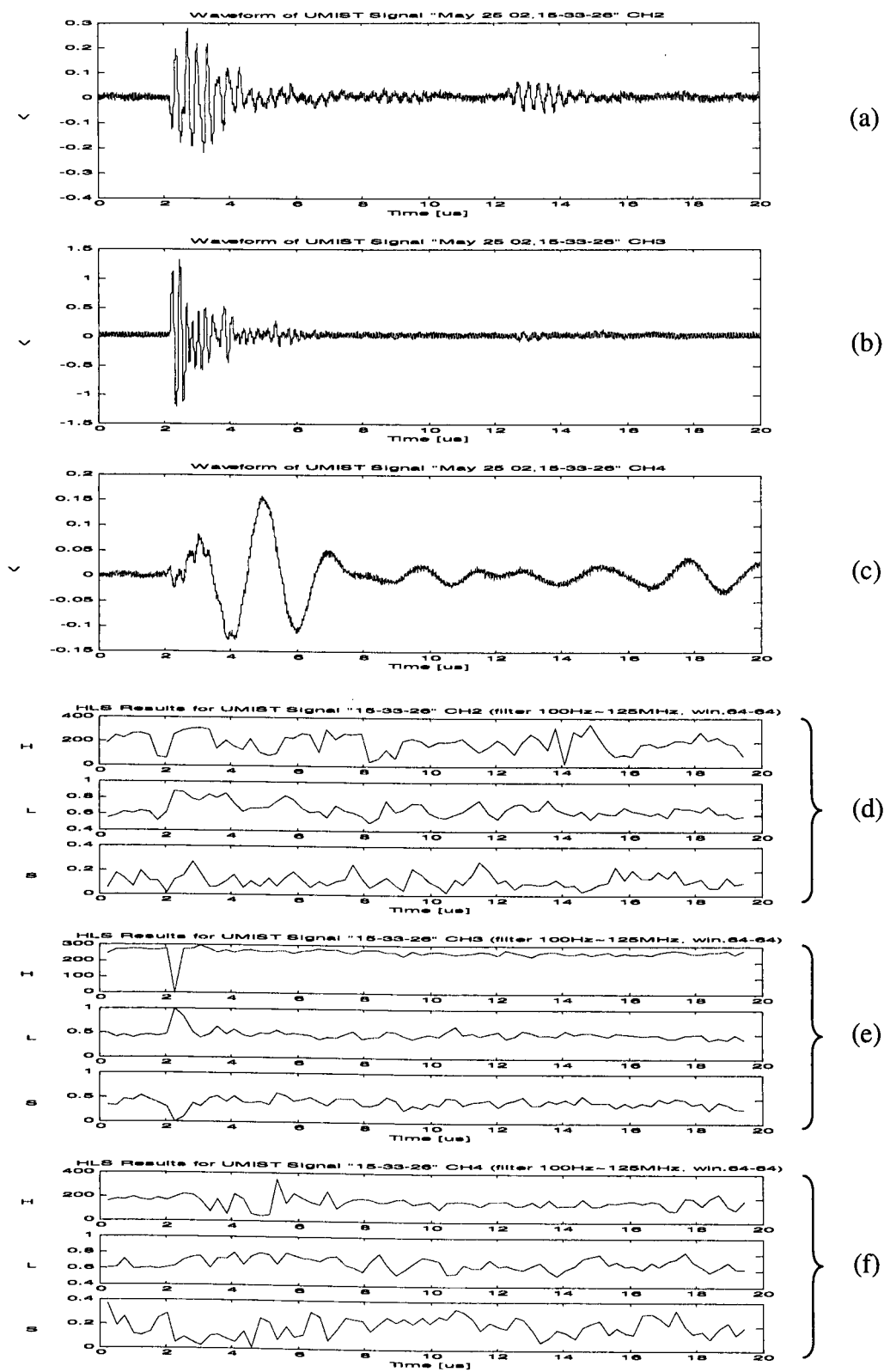(d), (e) & (f) HLS results for channels 2, 3 & 4

Appendix D. Chromatic Results for Additional Southampton RF Signals
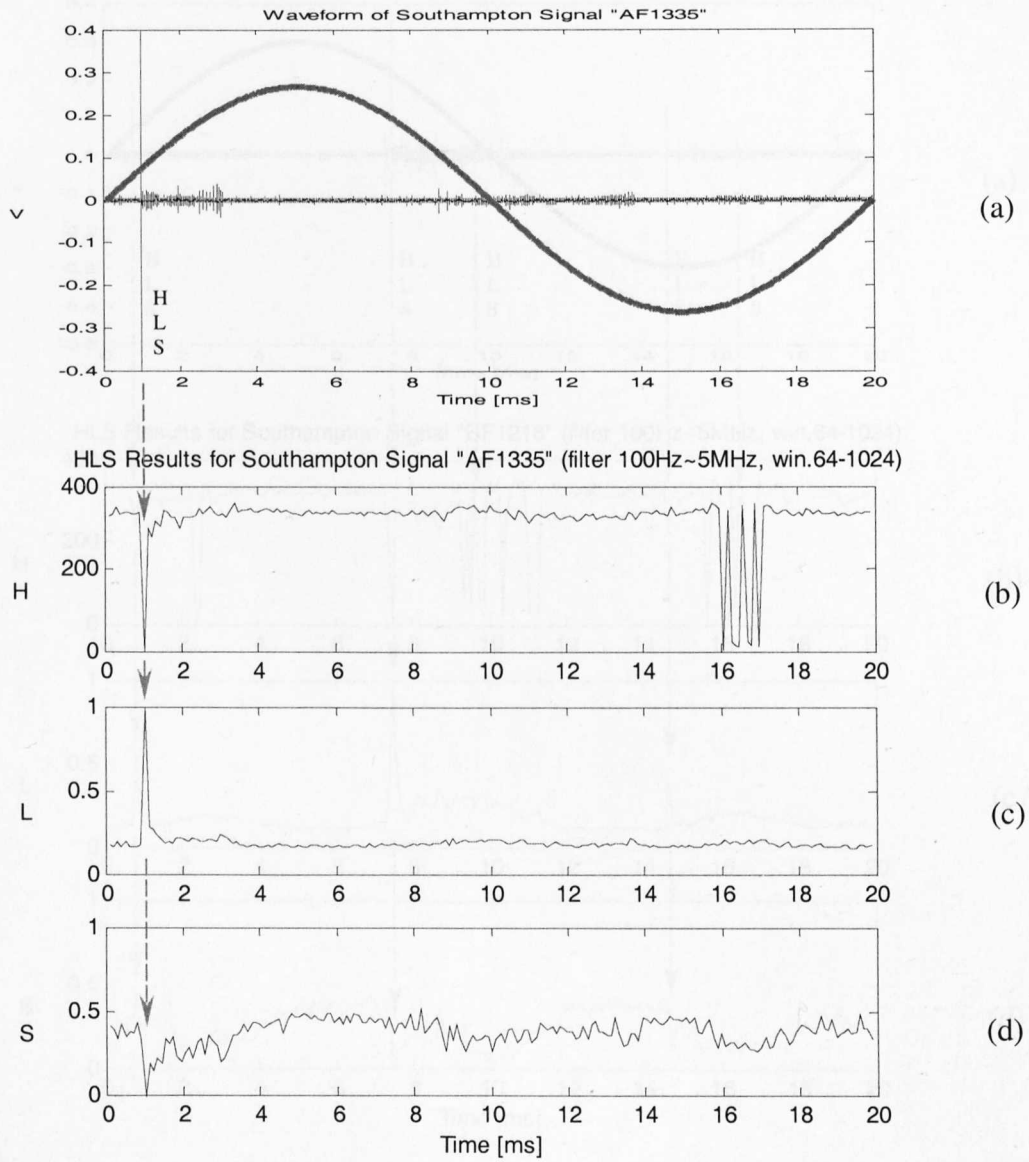
Figure D.1 HLS Result for Southampton RF signal "AF1335"
(a) Raw time-varying signal, (b) Hue, (c) Lightness, (d) Saturation
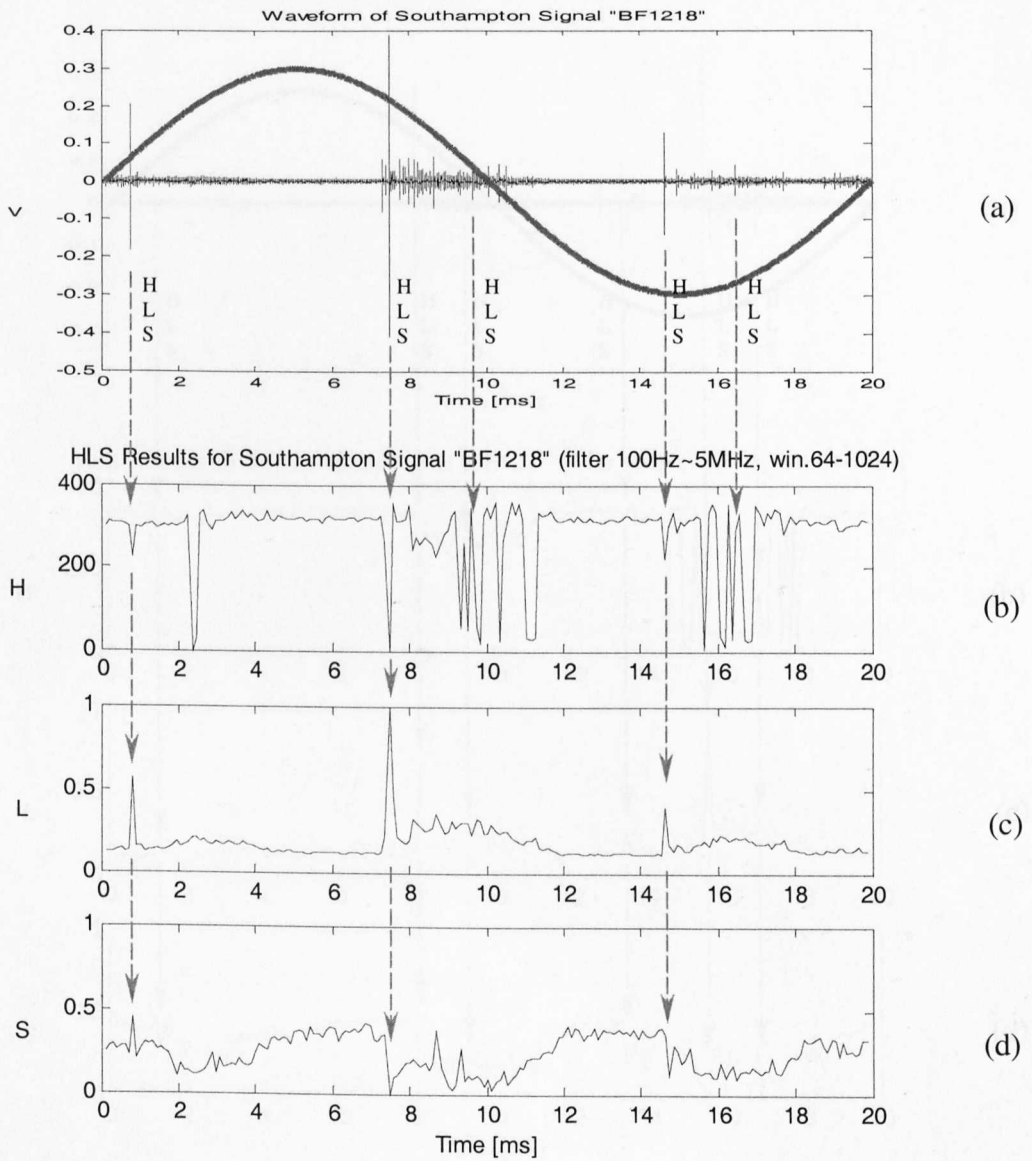
Figure D.2 HLS Result for Southampton RF signal "BF1218"
(a) Raw time-varying signal, (b) Hue, (c) Lightness, (d) Saturation

Figure D.3 HLS Result for Southampton RF signal "CF1237"
(a) Raw time-varying signal, (b) Hue, (c) Lightness, (d) Saturation

Appendix E. Chromatic Results for Additional Acoustic Simulation Signals
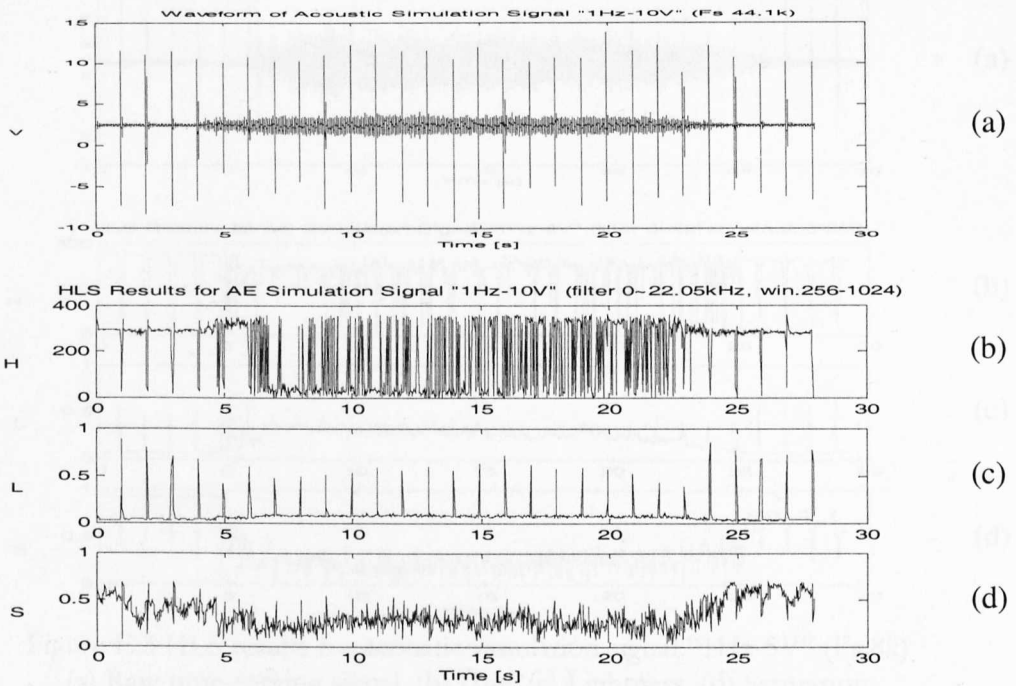
Figure E.1 HLS results for acoustic simulation signal "1Hz-10V" (Fs 44.1k)
(a) Raw time-varying signal, (b) Hue, (c) Lightness, (d) Saturation
Pulse: 1Hz, 10V; Sample rate: 44100Hz
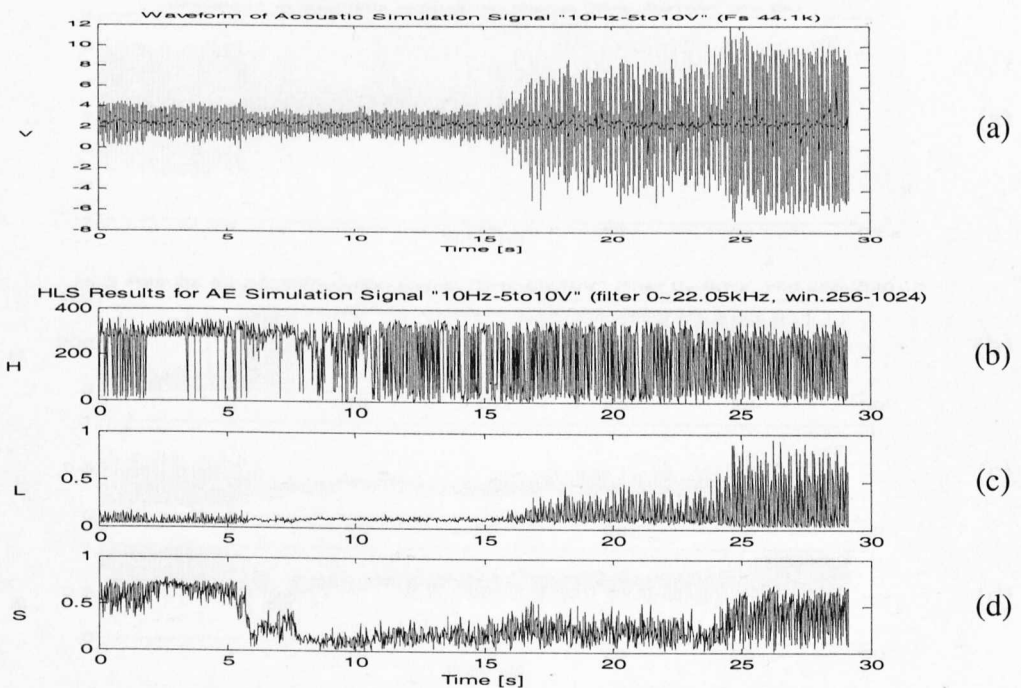
Figure E.2 HLS results for acoustic simulation signal "10Hz-5to10V" (Fs 44.1k)
(a) Raw time-varying signal, (b) Hue, (c) Lightness, (d) Saturation
Pulse: 10Hz, 5~10V; Sample rate: 44100Hz
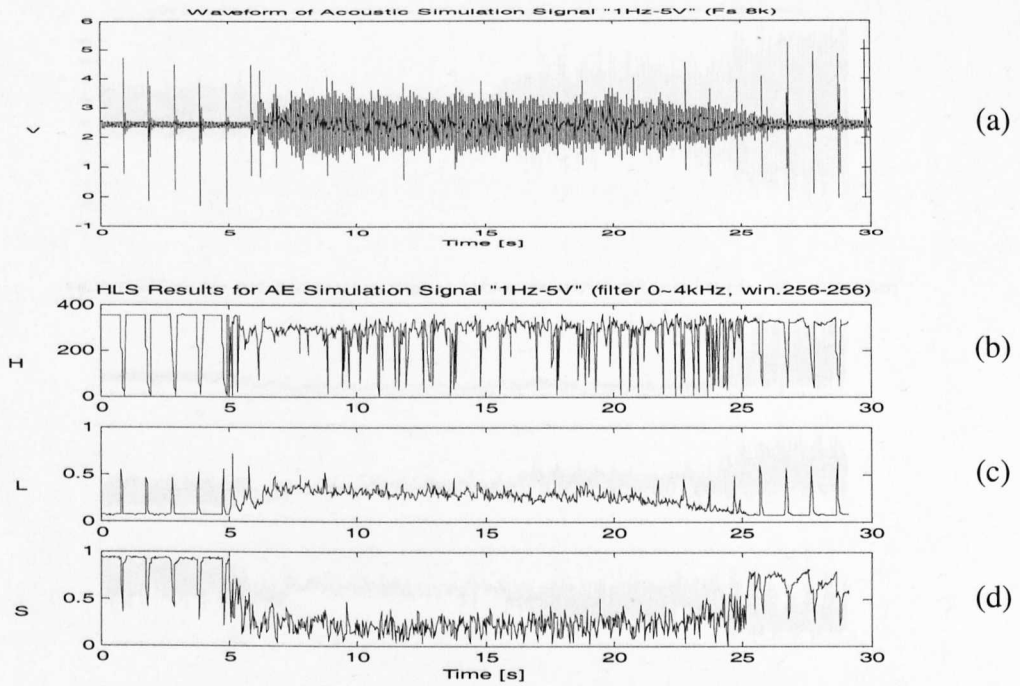
Figure E.3 HLS results for acoustic simulation signal "1Hz-5V" (Fs 8k)
(a) Raw time-varying signal, (b) Hue, (c) Lightness, (d) Saturation
Pulse: 1Hz, 5V; Sample rate: 8kHz
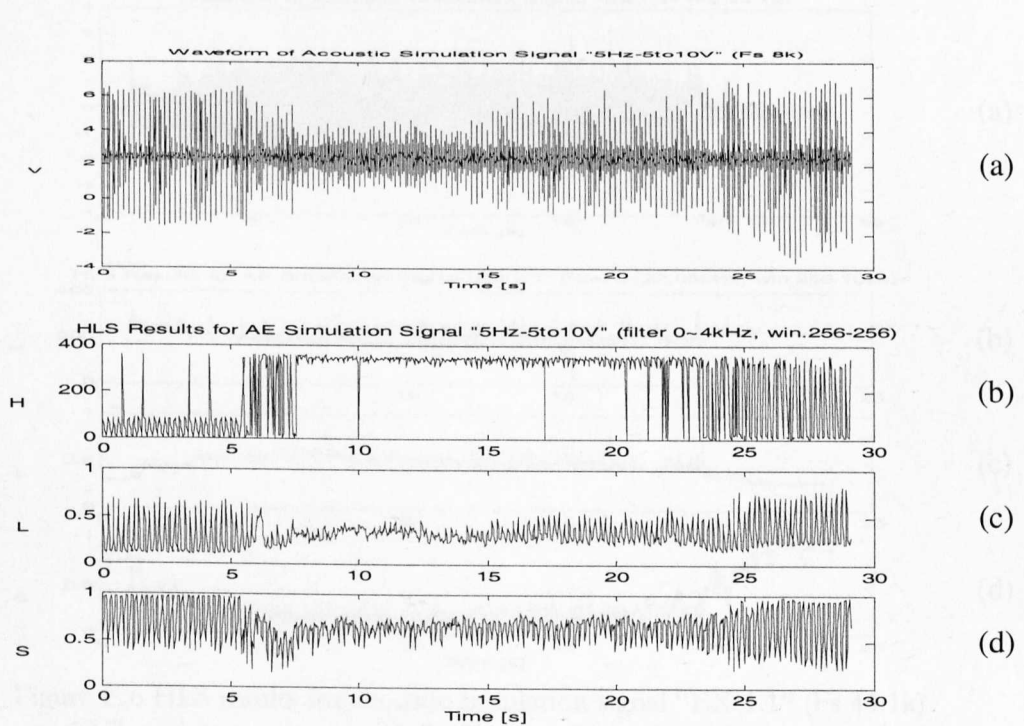
Figure E.4 HLS results for acoustic simulation signal "5Hz-5to10V" (Fs 8k)
(a) Raw time-varying signal, (b) Hue, (c) Lightness, (d) Saturation
Pulse: 5Hz, 5~10V; Sample rate: 8kHz
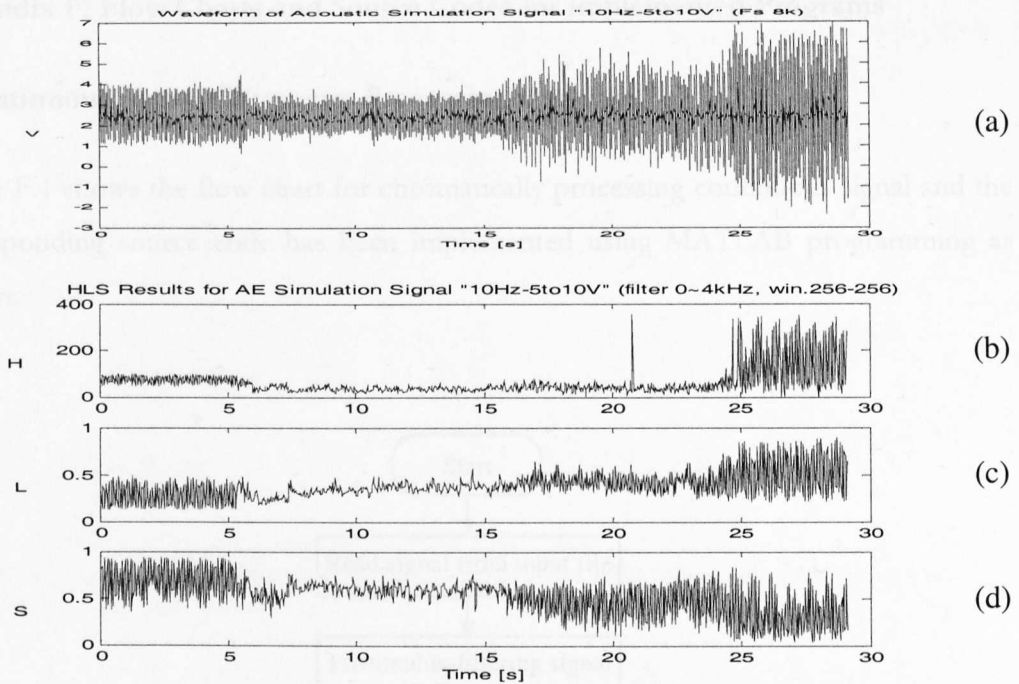
Figure E.5 HLS results for acoustic simulation signal "10Hz-5to10V" (Fs 8k)
(a) Raw time-varying signal, (b) Hue, (c) Lightness, (d) Saturation
Pulse: 10Hz, 5~10V; Sample rate: 8kHz
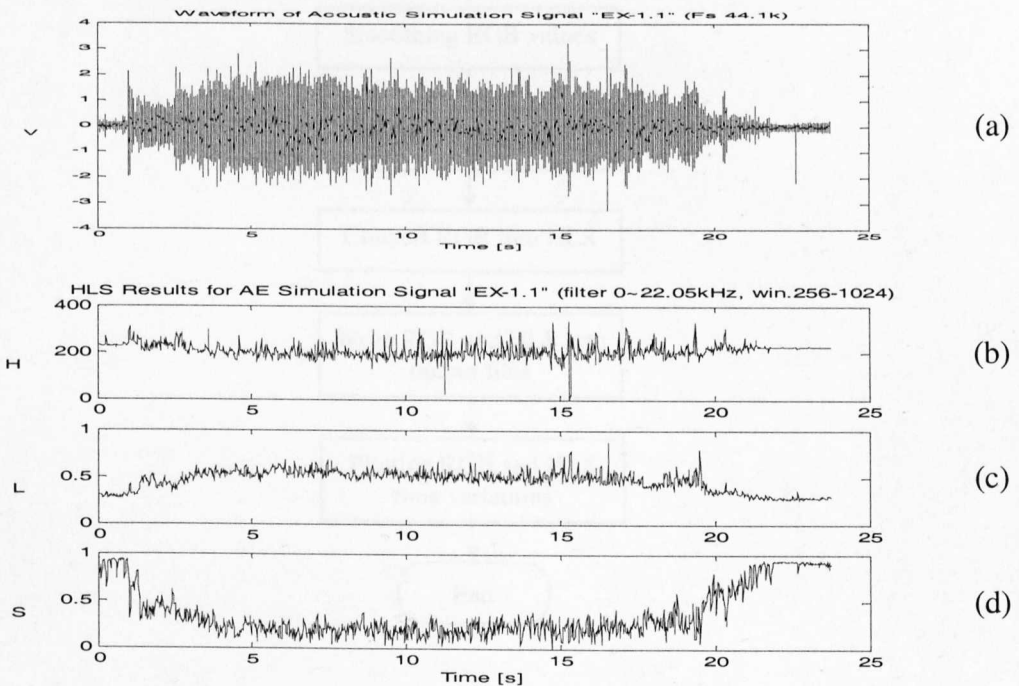
Figure E.6 HLS results for acoustic simulation signal "EX-1.1" (Fs 44.1k)
(a) Raw time-varying signal, (b) Hue, (c) Lightness, (d) Saturation
Original water flow (without pulse); Sample rate: 44100Hz

Appendix F. Flow Charts and Source Codes for implemented Programs

1. Continuous Signal Chromatic Processing Program

Figure F.1 shows the flow chart for chromatically processing continuous signal and the corresponding source code has been implemented using MATLAB programming as follows.
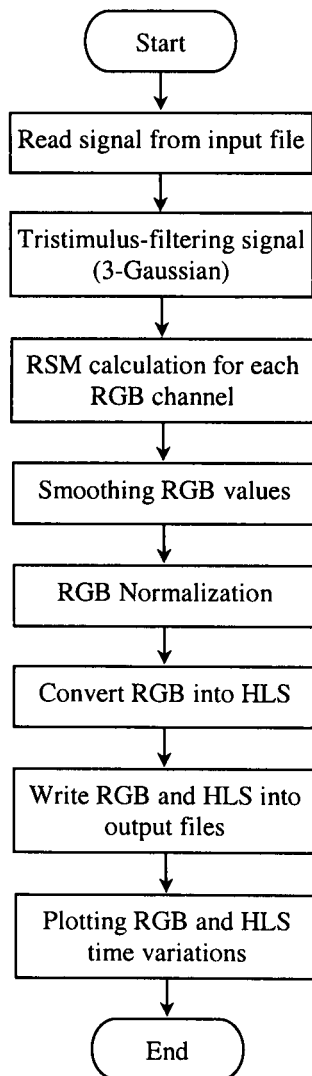
Figure F.1 Flow chart for continuous signal chromatic processing program

```
%CONTINUOUSPRO using tristimulus filters chromatically process
%      continuous signal in terms of three chromatic parameters HLS.
%
%      Input is a continuous signal from a text file.
%          (1 or 2 columns [time, signal])
%      Output is a text file containing 3-column HLS values.
%          Hue is within [0,360).
%          Lightness is within [0,1].
%          Saturation is within [0,1].

%      Code by Jinghua Zhang, 18 Jun 2001.
%      Copyright © 1997-2003 CIMS, The University of Liverpool,
%      All Rights Reserved.
%      $Revision: Zhang1.6 $  $Date: 01 Oct 2003 18:00:00 $

clear all
close all


%%%%%%%%%%%%%%%%%%%%%%%%%%%%%%%%%%%%%%%%%%%%%%%%%%%%%%%%%%%%%%%%%%%%%%%%
% Reading signal from input file

disp(' ')
numColumn=input('Inputing signal file, how many columns? [1 or 2]');
if numColumn==1
    Fs=input('What is the sample rate (Hz) ?');
    [signal,count,path,infname]=fileip(numColumn);
    tDuration=count/Fs;
    tScale=0:1/Fs:tDuration;
    tScale=tScale(1:count)';
elseif numColumn==2
    [signal,count,path,infname]=fileip(numColumn);
    tScale=signal(:,1);
    tDuration=tScale(end)-tScale(1);
    Fs=count/2/tDuration;
    signal=signal(:,2);
else
    return
end


%%%%%%%%%%%%%%%%%%%%%%%%%%%%%%%%%%%%%%%%%%%%%%%%%%%%%%%%%%%%%%%%%%%%%%%%
% Filtering raw signal

[r,g,b]=triFilter(signal); % Code by Ellis Dean,
%CIMS, Dept of EEE, University of Liverpool, Liverpool L69 3GJ, UK.


%%%%%%%%%%%%%%%%%%%%%%%%%%%%%%%%%%%%%%%%%%%%%%%%%%%%%%%%%%%%%%%%%%%%%%%%
% RMS values calculation for each RGB channel

rmsWin=input('Window size for RMS calculations?   ');
s=ones(1,rmsWin); % Convolution kernel

% Square values
rmsR=r.^2;
rmsG=g.^2;
rmsB=b.^2;
```

```
% Mean squares
rmsR=conv(rmsR,s)./rmsWin;
rmsG=conv(rmsG,s)./rmsWin;
rmsB=conv(rmsB,s)./rmsWin;

% Trim invalid convolution products
trim=rmsWin-1;
[row col]=size(rmsR);
rmsR=rmsR(trim:row-trim);
rmsG=rmsG(trim:row-trim);
rmsB=rmsB(trim:row-trim);

% Root mean squares
rmsR=sqrt(rmsR);
rmsG=sqrt(rmsG);
rmsB=sqrt(rmsB);
rgb=[rmsR rmsG rmsB];


%%%%%%%%%%%%%%%%%%%%%%%%%%%%%%%%%%%%%%%%%%%%%%%%%%%%%%%%%%%%%%%%%%%%%%%
% Smoothing RGB values

smooth=input('Smoothing window size for RGB and HLS?   ');
[row col]=size(rgb);

numSamp=round(row./smooth);
RGB=zeros(numSamp-1,3);

for i=1:numSamp-1;
    first=(1+(i-1)*smooth);
    last=(i*smooth);
    RGB(i,:)=mean(rgb(first:last,:));
end


%%%%%%%%%%%%%%%%%%%%%%%%%%%%%%%%%%%%%%%%%%%%%%%%%%%%%%%%%%%%%%%%%%%%%%%
% Normalization of RGB values based on Rmax, Gmax, Bmax separately

Rmax=max(RGB(:,1));
Gmax=max(RGB(:,2));
Bmax=max(RGB(:,3));

RGB(:,1)=RGB(:,1)./Rmax;
RGB(:,2)=RGB(:,2)./Gmax;
RGB(:,3)=RGB(:,3)./Bmax;


%%%%%%%%%%%%%%%%%%%%%%%%%%%%%%%%%%%%%%%%%%%%%%%%%%%%%%%%%%%%%%%%%%%%%%%
% Converting RGB into HLS

HLS=rgb2hls_zhang(RGB);


%%%%%%%%%%%%%%%%%%%%%%%%%%%%%%%%%%%%%%%%%%%%%%%%%%%%%%%%%%%%%%%%%%%%%%%
% Time vector for final RGB & HLS variations

[row col]=size(HLS);
i=1:row;
```

```
i=i';
tPlot(i,1)=i./(Fs/smooth);


%%%%%%%%%%%%%%%%%%%%%%%%%%%%%%%%%%%%%%%%%%%%%%%%%%%%%%%%%%%%%%%%%%%%%%%%%%%%
% Writing RGB and HLS values into output files

frgb=([path, infname(1:end-3), 'rgb']);
fileop(RGB,frgb);

fhls=([path, infname(1:end-3), 'hls']);
fileop(HLS,fhls);


%%%%%%%%%%%%%%%%%%%%%%%%%%%%%%%%%%%%%%%%%%%%%%%%%%%%%%%%%%%%%%%%%%%%%%%%%%%%
% Plotting Results

setScale=input('Which time scale do u want for plots [us, ms or s]?
','s');

if setScale=='us'
    tPlot=tPlot.*10^6;
    label='Time [us]';
elseif setScale=='ms'
    tPlot=tPlot.*10^3;
    label='Time [ms]';
else
    tPlot=tPlot;
    label='Time [s]';
end

figure
subplot(3,1,1); plot(tPlot,RGB(:,1),'r-')
title('RGB Time Variations')
ylabel('R');
subplot(3,1,2); plot(tPlot,RGB(:,2),'g-')
ylabel('G');
subplot(3,1,3); plot(tPlot,RGB(:,3),'b-')
ylabel('B');
xlabel(label);

figure
subplot(3,1,1); plot(tPlot,HLS(:,1))
title('HLS Results for the Signal')
ylabel('H');
subplot(3,1,2); plot(tPlot,HLS(:,2))
ylabel('L');
subplot(3,1,3); plot(tPlot,HLS(:,3))
ylabel('S');
xlabel(label);

disp(' ')
disp('********************** FINISHED **********************')
disp(' ')
disp(' ')
%%%%%%%%%%%%%%%%%%%%%%%%%%%%%%%%%% END %%%%%%%%%%%%%%%%%%%%%%%%%%%%%%%%%%%%%
```

2. Discrete Data Chromatic Analysis Program

Figure F.2 shows the flow chart for chromatically analysing discrete data and the corresponding source code has been implemented using MATLAB programming as follows.

```
                    ┌─────────────┐
                    (    Start    )
                    └──────┬──────┘
                           │
              ┌────────────▼────────────┐
              │ Read data from input file│
              └────────────┬────────────┘
                           │
              ┌────────────▼────────────┐
              │ Tristimulus-filtering data│
              │        (3-triangle)      │
              └────────────┬────────────┘
                           │
              ┌────────────▼────────────┐
              │    RGB Normalization     │
              └────────────┬────────────┘
                           │
              ┌────────────▼────────────┐
              │   Convert RGB into HLS   │
              └────────────┬────────────┘
                           │
              ┌────────────▼────────────┐
              │  Write RGB and HLS into  │
              │      output files        │
              └────────────┬────────────┘
                           │
                    ┌──────▼──────┐
                    (     End     )
                    └─────────────┘
```
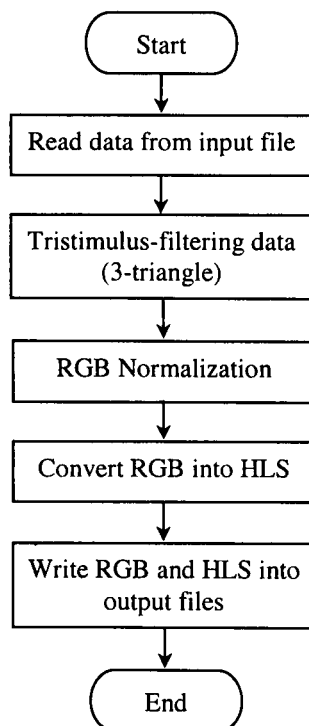
Figure F.2 Flow chart for discrete data chromatic analysis program

```
%DISCRETEPRO using tristimulus filters chromatically process
%       discrete data sets in terms of three chromatic parameters HLS.
%
%       Input is raw discrete data (e.g. DGA records) from a text file
%               (3 or 10 columns).
%       text file row-by-row layout:
%               (use space or tab to separate values/columns)
%
%               maximum1    max2     max3 ...
%               minimum1    min2     min3 ...
%               DataRec1o1  D2o1     D3o1 ...
%               DataRec1o2  D2o2     D3o2 ...
%               DataRec1o3  D2o3     D3o3 ...
%               ...
%
%       Output is a text file containing 3-column HLS values.
%               Hue is within [0,360).
%               Lightness is within [0,1].
%               Saturation is within [0,1].

%       Code by Jinghua Zhang, 18 Jun 2001.
%       Copyright (c) 1997-2003 CIMS, The University of Liverpool,
%       All Rights Reserved.
%       $Revision: Zhang1.2 $  $Date: 01 Oct 2003 18:18:18 $

clear all
close all


%%%%%%%%%%%%%%%%%%%%%%%%%%%%%%%%%%%%%%%%%%%%%%%%%%%%%%%%%%%%%%%%%%%%%%%
% Reading data from input file

disp(' ')
noSensors=input('Inputing signal file, how many components?   ');
[data,count,path,infname]=fileip(noSensors);
maxi=data(1,:);
mini=data(2,:);
data=data(3:end,:);


%%%%%%%%%%%%%%%%%%%%%%%%%%%%%%%%%%%%%%%%%%%%%%%%%%%%%%%%%%%%%%%%%%%%%%%
% Filtering raw data

noRec=count/noSensors-2
for i=1:noRec
    data(i,:)=data(i,:)-mini;
    data(i,:)=data(i,:)./maxi;
end

i=1;
red=zeros(noRec,1);
green=zeros(noRec,1);
blue=zeros(noRec,1);

rInc=0.00001;
gInc=0.00001;
bInc=1.0;
stepInc=0.9/noSensors; % 0.1 to 1
```

```
while i<=noSensors

    red=red+data(:,i)*rInc;
    green=green+data(:,i)*gInc;
    blue=blue+data(:,i)*bInc;

    if i<(noSensors/2)
        rInc=0.00001;
    else
        rInc=rInc+(2*stepInc);
    end

    bInc=bInc-2*stepInc;
    if bInc<0
        bInc=0.00001; % set min value
    end

    if i<(noSensors/2)
        gInc=gInc+stepInc*2;
    else
        gInc=gInc-stepInc*2;
    end
    i=i+1;
end


%%%%%%%%%%%%%%%%%%%%%%%%%%%%%%%%%%%%%%%%%%%%%%%%%%%%%%%%%%%%%%%%%%%%%%%%%
% Normalization of RGB values

L_max=(noSensors/2+1); % Arbitrary at moment
red=red./L_max;
green=green./L_max;
blue=blue./L_max;


%%%%%%%%%%%%%%%%%%%%%%%%%%%%%%%%%%%%%%%%%%%%%%%%%%%%%%%%%%%%%%%%%%%%%%%%%
% Converting RGB into HLS

HLS=rgb2hls_zhang([red green blue]);


%%%%%%%%%%%%%%%%%%%%%%%%%%%%%%%%%%%%%%%%%%%%%%%%%%%%%%%%%%%%%%%%%%%%%%%%%
% Writing RGB and HLS values into output files

frgb=([path, infname(1:end-3), 'rgb']);
fileop([red green blue],frgb);

fhls=([path, infname(1:end-3), 'hls']);
fileop(HLS,fhls);

disp(' ')
disp('*********************** FINISHED ***********************')
disp(' ')
disp(' ')
%%%%%%%%%%%%%%%%%%%%%%%%%%%%%%%%%%%%% END %%%%%%%%%%%%%%%%%%%%%%%%%%%%%%%%
```

3. RGB to HLS Conversion Subroutine

```
function [hls]=rgb2hls_zhang(rgb)
%RGB2HLS converts red-green-blue colour inputs to
%      hue-lightness-saturation outputs.
%
%
%      Input is an nx3 matrix of RGB normalized values, within [0,1].
%      Output is an n rows x 3 columns matrix of HLS values.
%            Hue progresses from 0 (red) through 120 (green) through
%            240 (blue) to 360 (red); Lightness is within [0,1];
%            Saturation is within [0,1], has two formulas
%            depended on Lightness (L<=0.5 or L>0.5).

%      Algorithm is from
%      H. Levkowitz & G.T. Herman (1993)
%      "GLHS: a generalized lightness, hue, and saturation
%      color model", CVGIP-Graphical Models and Image Processing,
%      vol.55, no.4, pp.271-285.
%      &
%      K.J. Brazier, A.G. Deakin, R.D. Cooke, P.C. Russell &
%      G.R. Jones (2001)
%      "Colour space mining for industrial monitoring" in D. Braha
%      (ed.), Data Mining for Design and Manufacturing, pp.371-400.
%      Kluwer Academic Publishers, Netherlands.

%      Code by Jinghua Zhang, 18 Jan 2001
%      Copyright (c) 1997-2003 CIMS, The University of Liverpool,
%      All Rights Reserved.
%      $Revision: Zhang1.8 $  $Date: 18 Oct 2003 18:00:00 $

[row,col]=size(rgb);

for i=1:row
    R=rgb(i,1);                  %Red values from the input matrix
    G=rgb(i,2);                  %Green values from the input matrix
    B=rgb(i,3);                  %Blue values from the input matrix
    maxi=max(rgb(i,:));
    mini=min(rgb(i,:));

    if ((R==G)&(R==B)) H=-1; L=maxi; S=0; %Set hue to -1 (undefined)
    else
        %Hue calculation
        if R==maxi H=60*(G-B)/(maxi-mini); end
        if G==maxi H=60*(2+(B-R)/(maxi-mini)); end
        if B==maxi H=60*(4+(R-G)/(maxi-mini)); end
        if H<0 H=H+360; end

        L=(maxi+mini)/2; %Lightness calculation

        %Saturation calculation
        if L<=0.5 S=(maxi-mini)/(maxi+mini); %i.e. S=(L-mini)/L
        else S=(maxi-mini)/(2-maxi-mini);    %i.e. S=(maxi-L)/(1-L)
        end
    end

    hls(i,1)=H;    hls(i,2)=L;    hls(i,3)=S;
end
```

4. File I/O Subroutines

```
function [data,count,fPath,fName]=fileip(column)
%[data,count,fPath,fName]=FILEIP(column) reads a matrix from a file.
%
%      Input is the column count of the text file,
%              which contains an "n x 1 to 10" matrix;
%      Output is a matrix for Matlab program further processing.


[name path]=uigetfile('*.txt','reading file, max 10 columns');
file=[path name]
fid=fopen(file,'r');

switch column
case 1
   [Din,count]=fscanf(fid,'%f',[1,inf]);
case 2
   [Din,count]=fscanf(fid,'%f %f',[2,inf]);
case 3
   [Din,count]=fscanf(fid,'%f %f %f',[3,inf]);
case 4
   [Din,count]=fscanf(fid,'%f %f %f %f',[4,inf]);
case 5
   [Din,count]=fscanf(fid,'%f %f %f %f %f',[5,inf]);
case 6
   [Din,count]=fscanf(fid,'%f %f %f %f %f %f',[6,inf]);
case 7
   [Din,count]=fscanf(fid,'%f %f %f %f %f %f %f',[7,inf]);
case 8
   [Din,count]=fscanf(fid,'%f %f %f %f %f %f %f %f',[8,inf]);
case 9
   [Din,count]=fscanf(fid,'%f %f %f %f %f %f %f %f %f',[9,inf]);
case 10
   [Din,count]=fscanf(fid,'%f %f %f %f %f %f %f %f %f %f',[10,inf]);
otherwise
   disp('Columns count exceeds 10. File input unsuccessful!')
   fclose(fid);
   return
end

fclose(fid);
data=Din';
fPath=path;
fName=name;
```

```
function[]=fileop(data,file);
%FILEOP(data,file) writes a matrix of data into a text file
%
%      Input can be an "n x 1 to 10" matrix;
%      Output is a text file in disc; path can be sepecified.

[row column]=size(data);      Dout=data';

if nargin==1
    [name,path]=uiputfile('*.txt','writing file, max 10 columns');
    file=([path name])
end
fid=fopen(file,'w');

switch column
case 1
    for i=1:row; fprintf(fid,'%f\n',Dout(i));
    end
case 2
    for i=1:row;
        fprintf(fid,'%f %f\n',Dout(:,i));
    end
case 3
    for i=1:row;
        fprintf(fid,'%f %f %f\n',Dout(:,i));
    end
case 4
    for i=1:row;
        fprintf(fid,'%f %f %f %f\n',Dout(:,i));
    end
case 5
    for i=1:row;
        fprintf(fid,'%f %f %f %f %f\n',Dout(:,i));
    end
case 6
    for i=1:row;
        fprintf(fid,'%f %f %f %f %f %f\n',Dout(:,i));
    end
case 7
    for i=1:row;
        fprintf(fid,'%f %f %f %f %f %f %f\n',Dout(:,i));
    end
case 8
    for i=1:row;
        fprintf(fid,'%f %f %f %f %f %f %f %f\n',Dout(:,i));
    end
case 9
    for i=1:row;
        fprintf(fid,'%f %f %f %f %f %f %f %f %f\n',Dout(:,i));
    end
case 10
    for i=1:row;
        fprintf(fid,'%f %f %f %f %f %f %f %f %f %f\n',Dout(:,i));
    end
otherwise
    disp('Columns count exceeds 10. File output unsuccessful!')
end
fclose(fid);
```